

IMPERIAL COLLEGE OF SCIENCE, TECHNOLOGY
AND MEDICINE

University of London

**METHODS FOR UPDATING NUMERICAL
MODELS IN STRUCTURAL DYNAMICS**

by

Saeed Ziaei Rad

A thesis submitted to the University of London
for the Degree of Doctor of Philosophy and
for the Diploma of Imperial College

Department of Mechanical Engineering
Imperial College of Science, Technology and Medicine
London SW7

June, 1997

Abstract

This thesis investigates several methods for updating numerical models in structural dynamics with a view to identify and develop the most suitable algorithms. To achieve this objective, the work initially focused on reviewing existing updating techniques in a broad sense. The constrained eigenstructure assignment method, often used in control applications, was identified as a possible updating route. The basic algorithm was modified so that it could deal with the updating of large-order systems and its formulation was made compatible with more conventional updating techniques such as the response function and the inverse eigensensitivity methods.

Model updating based on forced vibration testing was introduced next. Its formulation and the computational aspects of the technique were described in detail. Satisfactory results were obtained, even in the case of noisy and incomplete experimental data. The effects of including damping were also addressed and some recommendations for an appropriate choice of frequency points were made.

Different regularisation techniques for the solution of ill-posed problems were investigated and presented in a unified notation. Such techniques were applied to incomplete and noisy measured FRF data sets and the results obtained were considered to be superior to those computed using conventional updating methods.

The use generic elements in both FE modelling and updating was considered in the later part of the work as their internal formulation allows a certain amount of solution adaptivity. The findings showed that generic elements could deal with both physical parameter errors and discretisation errors. A generic element family for rectangular plates was introduced and used successfully in the case of a uniform square

plate. A similar route was also followed for exact elements but the results looked less encouraging in this latter case.

In parallel with updating methods, a number of fundamental questions were also addressed. The required experimental accuracy that must be attained when updating finite element models using measured vibration test data was determined via a matrix norm solution. It was shown that a well-defined relationship, that can be expressed as a characteristic function, exists between the system's properties, the correction matrices and the actual amount of experimental noise. The formulation was then applied to the standard response function updating formulation and it was shown that the updating algorithm was dependent on a number of conditions which arose from two distinct cases: one convergent and the other divergent.

Finally, the use of physical parameters in model updating is implemented and then verified by experimental case studies on two configurations of a rectangular plate. Some recommendations for further work in this area were also forwarded.

Acknowledgements

The author is most grateful to his supervisor, Dr. M. Imregun, for his encouragement, interest, stimulus and guidance throughout this project. It was due to his initiatives that the project was possible in the first place, and his unwavering enthusiasm that helped to keep it going.

Thanks are due to the Head of Dynamics Section, Prof. D. J. Ewins, for his valuable advice on various issues. I would also like to thank past and present colleagues at Dynamics Section who provided insight into the related fields of interest and an enjoyable working environment. I would particularly like to mention J.V. Ferreira, M.R. Ashory and Y.H. Chong.

I wish to express my gratitude to my true friends and colleagues, M.D. Emami, S. Mansoorzadeh, Dr. A. Pischevar, J. Parvizian and M.A. Sadri who shared my successes and disappointments over these years.

Special thanks are due to my wife and my parents for all their love and support during the course of this work. Without them this thesis would not have been completed.

Finally, the author is indebted to the Ministry of Culture and Higher Education of Iran and the Committee of Vice-Chancellors and Principals (CVCP) of Imperial College for providing the financial support needed for this research.

Nomenclature

Basic Terms, Dimensions and Subscripts

i, j, k, l	integers
i	$\sqrt{-1}$
J	Number of load cases/Optimisation function
L	Number of elements in Finite Element Model
m	Number of measured modes
n	Number of measured set of degrees of freedom
N	Total number of degrees of freedom/co-ordinates
N_f	Number of selected frequencies in the measurement spectrum
r	Number of rigid body modes/ Number of modes used to form transformation matrix
s	Number of slave set of degrees of freedom
x, y, z	Translational degrees of freedom/co-ordinates
$\theta_x, \theta_y, \theta_z$	Rotational degrees of freedom/co-ordinates
δ	Kronecker delta function
σ	Uniformly-distributed noise

Matrices, Vectors and Scalars

[]	Matrix
{ }	Column vector

$[]^T; \{ \}^T$	Transpose of a matrix; vector
$[]^{-1}$	Inverse of a matrix
$[]^*$	Complex conjugate of a matrix
$()^\dagger$	Generalised/Pseudo inverse of a matrix
$Re(), ()_R$	Real part of a matrix; vector
$Im(), ()_I$	Imaginary part of a matrix; vector
$[^{Red}]$	Reduced matrix
$\ \ $	Frobenious norm of a matrix/vector
$Cond[]$	Condition number of a matrix
$Range[]$	Range of a matrix
$Diag[]$	Diagonal matrix
$Trace[]$	Trace of a matrix
$[I]$	Identity matrix
$[U], [V]$	Matrices of left and right singular values
$[\Sigma]$	Rectangular matrix of singular values
$[S]$	Sensitivity matrix
$[T]$	Transformation Matrix
$[\epsilon]$	Error matrix

Spatial and Modelling Properties

N_k	Total number of mass elements
N_m	Total number of stiffness elements
N_c	Total number of viscous damping elements
N_d	Total number of hysteretic damping elements
$[K]$	Stiffness matrix
$[M]$	Mass matrix
$[C]$	Viscous damping matrix
$[D]$	Hysteretic damping matrix

$[\Delta K], [\bar{K}]$	Stiffness correction matrix
$[\Delta M], [\bar{M}]$	Mass correction matrix
$[\Delta D], [\bar{D}]$	Hysteretic damping correction matrix
$[K^e]$	Element stiffness matrix
$[M^e]$	Element mass matrix
$[Z_A]$	Analytical dynamic stiffness matrix
$[\Delta Z_A]$	Dynamic stiffness correction matrix
$[\Delta Z]$	Difference between analytical and experimental dynamic stiffness matrices
$[H_X]$	Experimental receptance matrix
$[H_A]$	Analytical receptance matrix
$\{f\}$	Force vector
$\{p\}$	Vector of design variables
$\{X\}$	Displacement vector
p_i^m	i-th correction factor for mass matrix
p_i^k	i-th correction factor for stiffness matrix
p_i^c	i-th correction factor for viscous damping matrix
p_i^d	i-th correction factor for hysteretic damping matrix

Modal and Frequency Response Properties

ω_r	r-th natural Frequency
$[\Lambda]$	Eigenvalue matrix
$[\Psi]$	Unit-normalised mode shape/eigenvector matrix
$[\Phi]$	Mass-normalised mode shape/eigenvector matrix
$\{\phi_r\}$	r-th mode shape
$(\phi_X)_{ir}$	i-th element of r-th experimental mode shape

Standard Abbreviations

DOF(s)	Degree(s) of freedom
FE	Finite element
FRF	Frequency response function
MAC	Modal assurance criterion
COMAC	Co-ordinate modal assurance criterion
SVD	Singular value decomposition
RFM	Response function method
IESM	Inverse eigen sensitivity method
CEAM	Constrained eigenstructure assignment method

Contents

Chapter 1. Introduction	21
1.1 Background	21
1.2 The Finite Element Method	23
1.3 Modal Testing	25
1.4 Model Updating	26
1.5 Objective of Thesis	27
1.6 Overview of Thesis	28
Chapter 2. Literature Survey	31
2.1 Introduction	31
2.2 Correlation Methods	31
2.2.1 Direct Natural Frequency Correlation	32
2.2.2 Direct Mode Shape Correlation	33
2.2.3 The Modal Assurance Criterion (MAC)	33
2.2.4 The Coordinate Modal Assurance Criterion (COMAC)	34
2.2.5 Orthogonality Methods	34
2.2.6 Energy Comparison and Force Balance	36
2.2.7 Frequency Response Function Correlation	37
2.3 Dealing with Complex Mode Shapes	38
2.3.1 Realisation Methods	38
2.3.2 Force Appropriation Methods	44

2.4	Reduction Techniques	48
2.4.1	Introduction	48
2.4.2	Reduction of System Matrices	48
2.4.3	Guyan Reduction	49
2.4.4	Improved Reduced System Technique (IRS)	50
2.4.5	Dynamic Reduction	51
2.4.6	System Equivalent Reduction expansion Process (SEREP)	52
2.5	Coordinate expansion	53
2.5.1	Guyan/Irons Expansion	54
2.5.2	IRS Expansion	54
2.5.3	Dynamic expansion	55
2.5.4	Gysin Modified Dynamic Expansion	55
2.5.5	SEREP Expansion	56
2.5.6	SEREPa Expansion	57
2.5.7	Test Analysis Model Expansion	57
2.6	Model Updating Methods Using Modal Data	58
2.7	Direct Methods using Modal Data	58
2.7.1	Lagrange Multiplier Methods	59
2.7.2	Matrix Mixing Methods	63
2.7.3	Error Matrix Method	64
2.7.4	The Eigenstructure Assignment Methods	66
2.8	Iterative Methods Using Modal Data	68
2.8.1	Penalty Function Methods	69
2.8.2	Minimum Variance Methods	72
2.8.3	Updating Methods Using Frequency Response Data	73
2.8.4	Equation Error Methods	73
2.8.5	Output Error Methods	76
2.9	Regularisation Technique	76

2.9.1	Tikhonov Regularisation	77
2.9.2	Iterative Methods	78
2.9.3	Truncated Singular Value Decomposition (TSVD)	79
2.9.4	Total Least Square Method	80
2.9.5	The Maximum Entropy Method	80
2.10	Concluding Remarks	81
Chapter 3. FRF Based Model Updating		83
3.1	Introduction	83
3.2	Theory	84
3.2.1	Background	84
3.2.2	Incomplete Data and Dynamic Reduction	86
3.2.3	Formulation of FRF Based Model Updating	87
3.2.4	Error Modelling	91
3.3	Case 1: 10 Degree-of-Freedom System	93
3.3.1	Updating Using Complete Experimental Data	94
3.3.2	Using Incomplete Experimental Data	95
3.3.3	Using FRF Data Polluted by Noise	97
3.4	Case 2: 3D Bay Structure	98
3.4.1	Noise-free Experimental Data - FE1 Vs X1	101
3.4.2	Noisy Experimental Data - FE1 vs X1	102
3.4.3	Updating of FE2 vs X1	103
3.4.4	Updating of FE1 vs X2	103
3.5	Computational Aspects of the Method	104
3.5.1	Frequency Range Considerations	104
3.5.2	Noise Sensitivity Reduction	107
3.5.3	Choice of the Damping Matrix	110
3.5.4	Case 3: Complex FRF Data	113

3.5.5	The Selection of Frequency Points	117
3.5.6	An Improved Formulation for the Iterative Calculation of p-values	119
3.6	Concluding Remarks	121
Chapter 4. Regularisation Techniques		123
4.1	Introduction	123
4.2	Least-Squares Solution via SVD	123
4.3	Tikhonov Regularisation Technique	125
4.4	Truncated Singular Value Decomposition (TSVD)	126
4.5	Total-Least-Squares Method	128
4.6	The Maximum Entropy Method	131
4.7	Some Case Studies Using Regularisation Technique	133
4.7.1	10 DOF System - Incomplete Experimental Model	134
4.7.2	Frame Example - Incomplete Experimental Model	138
4.7.3	A Comparison of Regularisation Methods	139
4.8	Concluding Remarks	141
Chapter 5. On The Accuracy Required of Experimental Data For Finite Element Model Updating		142
5.1	Overview	142
5.2	Introduction	143
5.3	Determination of The Required Experimental Accuracy	146
5.4	Application to the p-Value Formulation	149
5.5	Case Study	156
5.6	Concluding Remarks	163
Chapter 6. A Modified Eigenstructure Assignment Technique For Finite Element Model Updating		165
6.1	Introduction	165

6.2	Review of the CEAM Formulation	167
6.3	Formulation of a Quadratic Solution Procedure	171
6.4	Numerical Study	175
6.4.1	CEAM Case Studies	175
6.4.2	A Comparison with the Response Function Method	185
6.5	Concluding Remarks	187
Chapter 7. Model Updating Using Generic Elements		189
7.1	Introduction	189
7.2	Basic Theory	190
7.3	Rod Elements	193
7.4	Beam Elements	195
7.5	Plate Elements	197
7.6	Model Updating	199
7.7	Case Studies	201
7.7.1	Uniform Rod	201
7.7.2	Uniform Beam	202
7.7.3	Uniform Plate	204
7.7.4	Computational Considerations	208
7.8	Concluding Remarks	209
Chapter 8. Model Updating based on Physical Parameters		211
8.1	Introduction	211
8.2	Three Dimensional Beam Element	211
8.3	Case Study	215
8.4	Plate Element	216
8.5	Case Study	219
8.6	Updating of Exact elements Using Design Parameters	221
8.6.1	Introduction	221

8.6.2	Spatial Vibration of a Prismatic Bar	222
8.7	Case Study	225
8.8	Concluding Remarks	227
Chapter 9. Experimental Case Study		229
9.1	The Two Plate Structures	229
9.2	Experimental Data	231
9.3	The FE Models	233
9.4	Correlation of Experimental and Predicted Results for Structure A	234
9.5	Model Updating for Structure A	238
9.6	Correlation of Experimental and Predicted Results for Structure B	241
9.7	Model Updating for Structure B	244
9.7.1	Updating Using Simulated Experimental Data	244
9.7.2	Updating Using Measured FRF Data	246
9.8	Concluding Remarks	249
Chapter 10. Conclusions and Recommendations for Further Work		250
10.1	Conclusions	250
10.2	Suggestions for Further Work	254
10.3	Summary of Contributions of Present Work	255
10.4	Closure	255
Appendix A. Derivatives of the Sensitivity Matrices with Respect to the Updating Parameters		257
A.1	3D Beam Element	257
A.2	2D Plate Element	259
A.3	Exact 3D Beam Element	261

List of Figures

1.1	Overview of the work presented in this thesis	30
3.1	The 10 DOF system	93
3.2	Receptance FRF, α_{55} , obtained from the experimental and analytical models of 10 DOF system	93
3.3	Receptance FRF, α_{55} , obtained from the experimental and updated analytical models of 10 DOF system (complete experimental model)	94
3.4	Receptance FRF, α_{55} , obtained from the experimental, analytical and updated analytical models of 10 DOF system (incomplete experimental model)	95
3.5	Convergence toward unique solution	96
3.6	Receptance FRF, α_{55} , obtained from the experimental and updated analytical models of 10 DOF system (complete experimental model with 10% noise)	98
3.7	Model FE1	99
3.8	Model FE2	99
3.9	Receptance FRF, α_{33} , obtained from experimental (X1) and analytical (FE1) models	100
3.10	p-values for the case of 10 measured coordinates	101
3.11	Receptance FRF, α_{33} , obtained from experimental and updated models with .5% and 1% noise levels	103
3.12	Component Z_{33} of the dynamic stiffness matrix of model FE1	105
3.13	Component Z_{33}^{red} of the reduced dynamic stiffness matrix of model FE1	106

3.14	Variable of the cost function J_2 for $p_1^k \in [-.9, .9]$ and $p_8^k \in [-.9, .9]$. . .	108
3.15	Cost function J_2	109
3.16	The plate model	113
3.17	Receptance FRF, α_{33} , obtained from experimental model of uniform plate	114
3.18	Incomplete data and 0% noise	115
3.19	Incomplete data and 2% noise	116
3.20	Three different updating frequencies for experimental model X1 . . .	118
4.1	The linear least-squares solution	128
4.2	The total linear least-squares solution	130
4.3	Receptance FRF, α_{55} , obtained from the experimental and updated analytical models of the 10 DOF system (different TSVD levels) . .	134
4.4	Receptance FRF, α_{55} , obtained from the experimental and updated analytical models of the 10 DOF system (different ϵ values)	135
4.5	Receptance FRF, α_{55} , obtained from the experimental and updated analytical models of the 10 DOF system (different regularisation techniques)	136
4.6	Receptance FRF, α_{55} , obtained from the experimental and updated analytical models of 10 DOF system using maximum entropy regularisation	137
4.7	Receptance FRF, α_{33} , obtained from experimental and updated models with different TSVD levels	138
4.8	Comparison of TLSQ and TSVD with LLS	140
5.1	A non-injective operator H	144
5.2	Characteristic log function for 0.1%, 0.5%, 1.0%, 5.0% and 10% noise	158
5.3	Error component $\log(\ \epsilon\)$ and the system component $\log(\ [\Delta Z]\ /\ [Z + \Delta Z]\ ^2)$ of the characteristic log function	159
5.4	Characteristic log function at optimum frequency points	160

5.5	p-values for different amount of noise	161
5.6	p-values for the 0.5% noise case - 10 frequency points Optimum (darker bar) vs. random selection of the excitation frequency points	162
5.7	p-values for the 0.5% noise case - 30 frequency points Optimum (darker bar) vs. random selection of the excitation frequency points	163
6.1	Computed p-values for Case1 (CEAM)	177
6.2	Initial, target and updated responses for Case1 (CEAM) The updated and target responses are identical	177
6.3	Computed p-values for Case2 (CEAM)	178
6.4	Computed p-values for Case3 (CEAM)	179
6.5	Initial, target and updated responses for Case1 (CEAM) The updated and target responses are identical	179
6.6	Effect of increasing the number of assigned modes - Case4 (CEAM) .	181
6.7	Computed p-values for Case5 (CEAM)	181
6.8	Initial, target and updated responses for Case5 (CEAM)	182
6.9	Target and Initial Models belong to the same domain	183
6.10	Target and Initial Models do not belong to the same domain	183
6.11	Initial, target and two updated responses for Case6 (Two-stage CEAM)	184
6.12	Computed p-values for Case4 (CEAM)	186
6.13	Computed p-values for Case4 (RFM)	186
7.1	Uniform rod	201
7.2	Initial, target and updated FRFs Rod example	202
7.3	Uniform Beam	202
7.4	Initial, target and updated FRFs Beam example - case A	203
7.5	Initial, target and updated FRFs Beam example - case B	204
7.6	A four-node rectangular 2D plate element	205
7.7	The two mesh configurations for the plate example	205

7.8	Initial, target and updated FRFs Plate example - Case A	206
7.9	Initial, target and updated FRFs Plate example - Case B	207
7.10	Initial, target and updated FRFs Plate example - Case C	208
8.1	Spatial coordinates of beam element	212
8.2	Error location for structure FE2	215
8.3	Comparison of the measured, analytical and updated receptance FRF, α_{1z1z}	220
8.4	Comparison of the measured, analytical and updated receptance FRF, α_{1z1z}	226
9.1	Structure A	230
9.2	Structure B	230
9.3	Experimental set-up	231
9.4	Measurement points for Structure A	232
9.5	Measurement points for Structure B	232
9.6	The FE model for both Structures A and B	233
9.7	Experimental and analytical receptance FRFs, α_{1z1z} - Structure A	234
9.8	45 Degree lines for natural frequencies of Structure A	236
9.9	MAC values for Structure A	236
9.10	COMAC values for Structure A	237
9.11	45 degree plots for selected mode shapes	237
9.12	Measured and synthesised receptance FRF α_{1z1z} - Structure A	238
9.13	Convergence of the physical parameters - Structure A	239
9.14	Experimental, initially-predicted and updated receptance FRF α_{1z1z} - Structure A	240
9.15	Experimental and initially-predicted receptance FRF α_{1z1z} - Structure B	242
9.16	COMAC values between experimental and FE data - Structure B	243

9.17	Experimental, initially-predicted and updated receptance FRF α_{1z1z} - Structure B	245
9.18	Experimental and synthesised FRF α_{1z1z} - Structure B	246
9.19	Measured FRF α_{1z9z} - Structure B	247
9.20	Experimental, initially-predicted and updated FRF α_{1z1z} - Structure B	249

List of Tables

5.1	Summary of Direct and Inverse Problems	143
6.1	The target and initial FE Models of the Frame Structure	175
6.2	Computational effort for RFM and CEAM updating	185
7.1	Computational effort for generic element and p-value formulations . .	209
8.1	Computational effort for macro elements	221
8.2	Details of the errors in the analytical model	225
9.1	Measured and predicted natural frequencies of Structure A	235
9.2	Measured, initially-predicted and updated natural frequencies of Structure A	241
9.3	Comparison of experimental model with initially-predicted model - Structure B	243
9.4	Measured, initially-predicted and updated natural frequencies of Structure B	248

Chapter 1

Introduction

1.1 Background

The dynamic analysis of engineering assemblies is becoming increasingly complex, and it will continue to do so in order to meet the challenges and demands of the 21st century. Interest in the vibration properties arises because nearly all structures are subject to vibration of one form or another, which is usually undesirable. For example, unwanted vibration effects include noise, decrease in fatigue strength of machines and equipment and lost precision in measuring instruments and machine tools. Sometimes, however, vibration is desirable, as in vibratory conveyors, friction dampers, the delimitation and consolidation of materials and so on. Because of devastating effects that vibration can have on machines and structures, vibration analysis and testing have become a standard procedure in the design and development of most engineering systems.

The subject of dynamics and vibration has probably started with the work of Galileo (1564-1642) who examined the oscillations of a simple pendulum. He was the first to discover the relationship between the frequency of a simple pendulum and its length. At the age of 26, Galileo established the law of falling bodies and wrote the first treatise on modern dynamics. In 1636 he disclosed the idea of the pendulum clock which

was later constructed by Huygens in 1656. Based on Galileo's work, Sir Isaac Newton (1642-1727) formulated the laws of motion in which the relationship between force, mass, and momentum is established. In particular, Newton's second law has been a fundamental tool for formulating the dynamic equation of motion of a vibratory system. Later, French mathematician Jean le Rond d'Alembert's (1717-1783) expressed Newton's second law in a different form in which the inertia forces are treated in the same way as the applied forces. Based on d'Alembert's principle, Joseph Louis Lagrange (1736-1813) developed his well-known equations. Unlike Newton's second law which uses vector quantities, Lagrange's equations can be used to formulate the differential equations of dynamic systems using scalar energy expressions. The Lagrangian approach, compared to the Newtonian approach, lends itself more easily to formulating the dynamic equations of multi-degree of freedom systems.

Another significant contribution to the theory of vibration was made by Robert Hooke (1635-1703) who was first to announce, in 1676, the relationship between the stress and strain in elastic bodies. Hooke's law for deformable bodies states that the stress at any point on a deformable body is proportional to the strain at that point. Based on Hooke's law of elasticity, Leonhard Euler (1707-1783) in 1744 and Daniel Bernoulli (1700-1782) in 1751 derived the differential equation that governs the vibration of beams and obtained the solution in the case of small deformations.

Towards the end of the 19th century, however, high speed machinery introduced many new problems including the phenomena now associated with mechanical vibration. Baron William Strutt and Lord Rayleigh (1842-1919), developed the theory of mechanical vibration to its current form. Rayleigh developed a method for finding the natural frequency of vibration for mechanical systems and made a correction to the existing beam theory by considering the effect of rotary inertia of the cross section of the beam. Later, in 1921, Stephen Timoshenko (1878-1972) presented an improved theory, known as Timoshenko beam theory, for the vibrations of the beams. In modern times, there have been many workers who contributed to theoretical dynamics and the subject matter has expanded enormously. Special reference can be made to the work of J. P. den Hartog who was a pioneer in studying industrial vibration

problems.

Today, for the dynamic design and analysis of complex structures, it is necessary to have reliable dynamic mathematical models. This is especially true for structures whose operation, integrity, safety and control critically depend on the structure's dynamic characteristics. The study of a structure's dynamic behaviour can be categorised into two distinct activities, namely analytical modelling and vibration tests. Due to different limitations and assumptions, each approach has its advantages and disadvantages. These will be briefly discussed below:

1.2 The Finite Element Method

The finite element method is a numerical analysis technique for obtaining approximate solutions to a wide variety of engineering problems. Because of its diversity and flexibility as an analysis tool, it became a well established procedure in industry.

Finite element method originated in the field of structural analysis and was widely developed and exploited in the aerospace industry during the 50s and 60s. Information on this and other advanced topics may be found in Zienkiewicz (1971), Desai & Abel (1972), Nath (1974), Bathe (1982) and Zienkiewicz & Taylor (1989).

The finite element method involves dividing the actual physical system into small subregions or elements. Each element is a simple unit, the behaviour of which can readily be analysed using approximation of displacement or stress fields by second or third-order shape functions. Once the elements and their interpolation functions have been chosen, the matrix equations, expressing the properties of individual elements, must be determined. For this task, one of the following four approaches may be used: the direct approach, the variational approach, the weighted variational approach, or the energy balance approach. The next step is to assemble all the element properties. The resulting model is composed of mass and stiffness matrices of dimension N , N being the number of degrees of freedom in the model. The choice of N is arbitrary and it should be large enough to minimise discretisation errors. The number of degrees of

freedom and the mass and stiffness matrices of a structure can vary from one analyst to another, and from one FE code to another. In any case, an accurate representation of damping matrices is not yet possible, the most common way being a proportional damping matrix which is based on experimentally-derived modal damping factors.

The resulting mathematical model is simply a set of differential equations that may or may not accurately represent the actual structure. The inaccuracies or uncertainties that may be present in finite element models can be divided into two broad categories:

- (i) those which are inherent to the finite element technique, and
- (ii) those which are introduced by the analyst.

The first category includes inevitable errors that arise because of employing numerical techniques. The most critical one is the discretisation error which is due to approximating a continuous structure by a finite number of individual elements. The magnitude of this error depends on the mesh quality and on the efficiency of the elemental shape functions. Discretisation errors can be subdivided into approximation errors and interpolation errors, where the first type manifest themselves as global errors and the second as elemental ones (Fletcher, 1984). Errors in this first category also include inaccuracies due to integration, truncation, round-off and eigen parameter extraction techniques.

The second category consists of modelling errors due to the assumptions made by the analyst: choice of elements to represent a given geometry, omission of unimportant details, uncertainties associated with the boundary conditions, etc. Although some of these errors will primarily manifest themselves at an elemental (i.e. local) level, others will contribute significantly to the global eigen parameters. From an error location viewpoint, these global errors may pose major problems since, in general, there are no elements that are directly associated with them.

1.3 Modal Testing

Due to lack of confidence in analytical models, actual dynamic testing of structures has become a classical procedure to verify an existing finite element models or adjust them to match test results. Over the past thirty years, modal analysis has been a fast developing technique in the experimental evaluation of the dynamic properties. The data from a modal analysis has several uses:

- to verify finite element or other mathematical models,
- to predict the effects of a design change by structural coupling,
- to provide a basis for model updating.

The modal testing basically consists of two steps: Data acquisition and data analysis for the extraction of modal parameters such as natural frequencies, mode shapes and damping ratios.

There are two main methods for exciting a structure. The structure can be either hit by an instrumented hammer or excited by a shaker which is connected to the structure through a push rod. Sometimes more than one shaker may be used to excite the structure, a technique called multi-point excitation.

Transducers, which made from piezoelectric materials, are generally used to measure both the response and the excitation force on the structure. The response can be measured at one or more points, usually by accelerometers, which are connected to a data acquisition device.

After measurements have been performed, a modal analysis or modal identification is carried out to find the modal properties of the system. This area has been extensively developed and various techniques for identifying modal models from FRF data have been proposed. Further details of the theoretical and practical aspects of vibration measurement techniques are given by Zaveri (1984), Ewins (1984) and Snoeys *et al.* (1987). As for the analytical modelling, modal testing has also a number of problems:

- The maximum number of measurement locations is limited and the size of the experimental model is always less than that of the analytical model.
- With the present technology, it is not possible to measure some degrees of freedom, such as rotational and internal ones.
- The number of identified modes is limited by the frequency range.
- The modal analysis usually yields complex mode shapes while the theoretical analysis is usually based on the normal mode theory.
- Measured data are contaminated by a certain level of noise.
- Some modes of the structure may not be excited during the test or, even if excited, some modes may not be identified.
- The clamped boundary conditions are very difficult to achieve while free-free boundary conditions are subject to suspension effects.
- The test structure may exhibit significant nonlinearities while analytical model assumes linearity.

1.4 Model Updating

Because of the different limitations and assumptions in the two approaches, the finite element model and the experimental modal model have different advantages and disadvantages. The finite element model provides information on dynamical behaviour of the structure while the experimentally-derived model contains information from actual structure.

Generally, it is believed that more confidence can be placed on experimental modal data than on the finite element model. Therefore, in order to determine the spatial properties of the structure which can reproduce the whole characteristics of the

test structures (measured or unmeasured), reconciliation processes including model correlation and model updating, must be performed.

Model updating can be defined as the adjustment of an existing analytical model in the light of measured vibration test. After adjustment, the updated model is expected to represent the dynamic behaviour of the structure more accurately.

There are two model updating philosophies (Nobari *et al.*, 1994). The first one states that model updating consists of two distinct stages, namely error localisation and error correction. The first stage being a pre-requisite for the second stage. It is inherently assumed that the mathematical model possesses a number of discrete errors which cause the observed discrepancies between predictions and measurements. The updated model is based on the correction of locatable errors, hopefully associated with a physical meaning. The second philosophy advocates a global correction of the finite element model which may or may not contain discernible errors in the first place. Hence, corrections must be made in a curve-fitting sense in order to minimise a number of pre-set criteria. The corrections do not, in general, correspond to specific modelling errors and hence there are several such updated models.

1.5 Objective of Thesis

Over the last fifteen years, a significant number of model updating techniques have been proposed. However, no reliable and generally-applicable procedures have been formulated so far. As there is an obvious need to a robust and practical updating strategy for industrial problems, this work is an attempt:

- to critically review the existing techniques and find out the advantages and disadvantages of various methods.
- to identify new techniques and to develop them further in order to be able to cope with industrial problems.

- to find the required experimental accuracy that must be attained for successful model updating.

1.6 Overview of Thesis

Chapter 2 reviews the methods that are currently used for the correlation of the experimental and analytical models. It also contains a comprehensive review of normal mode extraction technique from measured complex response functions. A literature survey of the available reduction and expansion techniques is also presented. Finally, a survey of finite element model updating technique is given in a unified notation, followed by a brief discussion of different regularisation techniques for ill-posed problems.

Chapter 3 deals with the updating of finite element models using FRF data. It outlines the formulation used in this thesis and discusses the advantages and shortcomings of the approach. Additionally, a series of examples has been considered to demonstrate the capability of the technique when dealing with different problems. Computational considerations, a strategy for the selection of updating frequency points and an initial guess procedure for the damping matrix are also discussed.

Chapter 4 introduces some popular regularisation techniques for ill-posed problems. A comparative study has been conducted to show the effectiveness of such techniques on noisy FRF data.

Chapter 5 deals with the determination of the required experimental accuracy that must be attained when updating finite element models using measured vibration test data. It is shown that a well-defined relationship, that can be expressed as a characteristic function, exists between the system's properties, the correction matrices and the actual amount of experimental noise. The findings are illustrated in the case of a 3D space frame and the efficiency of the proposed characteristic function is discussed in some detail. Finally, a way of selecting the optimum excitation frequency values is presented as a means of relaxing the minimum experimental accuracy.

Chapter 6 examines the method of constrained eigenstructure assignment in some detail. The existing approach is modified to handle the effect of hysteretic damping and the non-linear optimisation of the original formulation is changed to a quadratic optimisation which not only converges faster but also enables the solution for large-size problems. Cases with polluted FRF data are investigated and the results show that a small amount of noise can be tolerated by the algorithm.

Chapter 7 deals with the theory and application of a relatively new model updating technique which is based on the use of generic finite elements. In this particular approach, the element mass and stiffness matrices are allowed to change dynamically while retaining their full physical meaning and mathematical properties by virtue of belonging to a same consistent family of such matrices. The existing formulation is extended to include some 2D and 3D finite elements and a number of case studies are presented to investigate the effect of various modelling errors as well as experimental noise. The performance of the generic element method is compared to the other popular updating methods, namely RFM and IESM.

Chapter 8 explains the use of physical parameters in model updating. A number of case studies involving 3D beam elements and 2D plate elements are presented in order to show the advantages of using physical parameters in model updating.

Chapter 9 is devoted to experimental case studies on two different configurations of a rectangular plate. A comparison of the measured and predicted modal properties for both structures is carried out to find the degree of correlation between the initially-predicted results and the experimental data. The advantages and shortcomings of the proposed physical parameters approach is then investigated in some detail using true experimental data.

Chapter 10 concludes the discussions of the previous chapters and includes recommendations for further work in the area of model updating.

An overview of the thesis is given in Fig. (1.1).

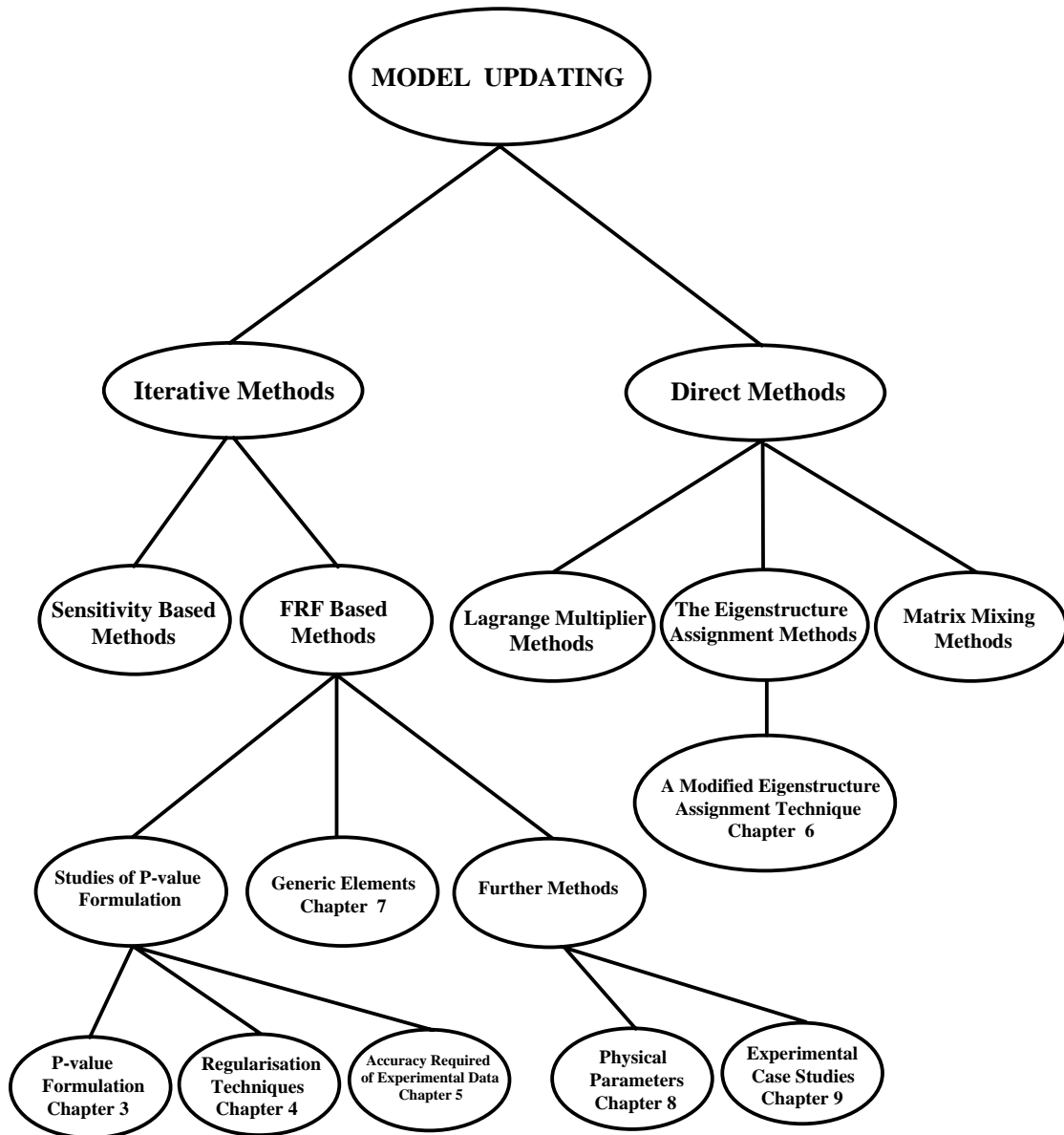


Figure 1.1: Overview of the work presented in this thesis

Chapter 2

Literature Survey

2.1 Introduction

In spite of extensive research over the past fifteen years, the state-of-the-art in finite element model updating is far from maturing and no reliable and generally applicable procedures have been formulated so far. Literature reviews which have been published by Ibrahim & Saafan (1987), Caesar (1987), Heylen & Sas (1987), Natke (1988), Imregun & Visser (1991), Mottershead & Friswell (1993) and Friswell & Mottershead (1995) compare various techniques but fall short of agreeing on methods or practices.

Given the extensive list of publications in model updating, the aim of this chapter is to review the latest developments only and to present a number of state-of-the-art of model updating techniques in a consistent and unified notation.

2.2 Correlation Methods

Correlation can be defined as the initial step to assess the quality of the analytical model. Test data are considered to be more accurate and thus used as reference to assess the quality of the available finite element model. If the difference between

the analytical and experimental data is within some pre-set tolerances, the analytical model can be judged to be accurate and no updating is necessary. If larger than acceptable differences exist but there is reasonable overall agreement, updating may still be possible.

In almost all cases, the experimental data set is incomplete as the measurements are taken at selected locations in selected coordinate directions. The lack of measured degrees of freedom can be solved in two ways, either by reducing the FE model to the size of experimental one or by expanding the experimental data to include the unmeasured degrees of freedom in the FE model. Another problem is the absence of damping in the FE model. So the complex mode shapes are usually identified from modal analysis while the FE model are based on normal modes. Hence, a number of methods concerned with the realisation of normal modes from complex measured modes were proposed. These issues will be reviewed below in Sections (2.2.1) to (2.3.2).

2.2.1 Direct Natural Frequency Correlation

The most common and simplest approach to correlate two modal models is the direct comparison of the natural frequencies. If a plot of the experimental values against analytical ones lies on a straight line of slope 1, the data are perfectly correlated. A percentage difference can also be defined as:

$$\epsilon_{\omega_i} = \frac{|\omega_{A_i} - \omega_{X_i}|}{\omega_{A_i}} \times 100 \quad (2.1)$$

and an overall frequency scatter indicator may be used as:

$$\epsilon_{\omega} = \left[\frac{\sum_{i=1}^L (\omega_{A_i} - \omega_{X_i})^2}{\sum_{i=1}^L \omega_{A_i}^2} \right]^{1/2} \times 100 \quad (2.2)$$

where L is the number of measured natural frequencies or mode shapes in the frequency range of interest.

2.2.2 Direct Mode Shape Correlation

Mode shapes can also be compared by plotting the analytical ones against experimental ones. As before, for a perfect correlation the resulting curve should lie on a straight line of slope one. The slope of the best straight line through the data points of two correlated mode can be defined as the modal scale factor (MSF) (Allemang & Brown, 1982):

$$MSF(\phi_A, \phi_X) = \frac{\{\phi_A\}^T \{\phi_X\}^*}{\{\phi_A\}^T \{\phi_A\}^*} \quad (2.3)$$

The modal scale factor (MSF) also provides a means of normalising all estimates of the same modal vector. Since the mass distribution of the finite element model and that of the actual structure may be different, the experimental and analytical mode shapes should be scaled correctly. When two modal vectors are scaled similarly, elements of each vector can be averaged, differenced, or sorted to provide a better estimate of the modal vector or to provide an indication of the type of error vector superimposed on the modal vector.

2.2.3 The Modal Assurance Criterion (MAC)

Mode pairing is one of the most critical tasks when the updating is based on modal data. The matching of modes can be a very difficult task especially for structures with high modal densities. The modal assurance criterion (MAC) (Allemang & Brown, 1982) is often used in pairing and comparing mode shapes. A matrix of MAC coefficients is computed from:

$$MAC_{ij} = \frac{\left(\{\phi_A\}_i^T \{\phi_X\}_j^*\right)^2}{\{\phi_A\}_i^T \{\phi_A\}_i^* \{\phi_X\}_j^T \{\phi_X\}_j^*} \quad (2.4)$$

A MAC value close to 1 suggests that the two modes are well correlated. An overall mode shape error indicator may be calculated from:

$$\epsilon_\Phi = \left[1 - \frac{1}{L} \sqrt{\sum_{i=1}^L (MAC)_i^2} \right] \times 100 \quad (2.5)$$

2.2.4 The Coordinate Modal Assurance Criterion (COMAC)

The coordinate MAC (COMAC) was developed by Lieven & Ewins (1988) from the original MAC concept in such a way that the correlation is now related to the degrees of freedom of the structure rather than to mode numbers. Having first constructed the set of L mode pairs via MAC, COMAC calculates the amount of correlation at each coordinate over all correlated mode pairs as:

$$COMAC_i = \frac{\sum_{r=1}^L |(\phi_A)_{ir} (\phi_X)_{ir}^*|^2}{\sum_{r=1}^L (\phi_A)_{ir}^2 \sum_{r=1}^L (\phi_X)_{ir}^2} \quad (2.6)$$

Again, to have a good coordinate correlation the COMAC value should be near to 1.

2.2.5 Orthogonality Methods

The self compatibility of a set of measured vibration modes is usually checked by the mass orthogonality check (MOC) which can be defined as (Targoff, 1976):

$$[\epsilon] = [\Phi_X]^T [M_A] [\Phi_X] \quad (2.7)$$

A commonly-accepted goal is to keep the off-diagonal terms of $[\epsilon]$ to .1 or less and to have diagonal elements greater than .9 (Chu & DeBroy, 1989). Since the order of the mass matrix is generally greater than the number of test coordinates, the mass matrix is usually reduced before the mass orthogonality check. The error introduced by this condensation process can exceed the difference between the analytical and experimental modal vectors. However, Parker & Ujihara (1982) proposed an improved procedure by expanding the size of the test data.

Another approach is the cross orthogonality method (COM) which uses a mixture of analytical and experimental eigenvectors:

$$[\epsilon] = [\Phi_A]^T [M_A] [\Phi_X] \quad (2.8)$$

Avitabile & O'Callahan (1988) proposed a method called Pseudo Orthogonality Check (POC) which uses SEREP to reduce the mass matrix down to the set of test DOF such that the effects of condensation on the mass matrix are minimised. Alternatively, they also used the transformation matrix developed by the SEREP reduction technique (Section 2.4.6) to expand the measured modal vector back to the full set of analytical DOFs of the system and found an improved analytical mass matrix. In addition, a general normalisation of either the analytical or the experimental vector was used to adjust the vector sets. Therefore, at either the measured or the full analytical DOFs, the following four pseudo orthogonality checks can be made:

$$\begin{aligned} [\epsilon_1] &= [\Psi_X]^T [M_A] [\Psi_A] \\ [\epsilon_2] &= [\Psi_X]^T [M_I] [\Psi_A] \\ [\epsilon_3] &= [\Phi_X]^T [M_A] [\Phi_A] \\ [\epsilon_4] &= [\Phi_X]^T [M_I] [\Phi_A] \end{aligned} \quad (2.9)$$

where $[\Psi_X]$ and $[\Phi_X]$ are set of experimental and normalised set of experimental modal vectors respectively and:

$$\begin{aligned}
[M_I] &= [M_A] + [V_g]^T ([I] - [\Phi_X]^T [M_A] [\Phi_X]) [V_g] \\
[V_g] &= ([\Phi_X]^T [M_A] [\Phi_X])^{-1} [\Phi_X]^T [M_A]
\end{aligned}
\tag{2.10}$$

The first and third equations of (2.9) have a bias on the analytical set of vectors since the mass matrix is directly related to the analytical vectors while the second and fourth equations have a bias on the experimental vectors since the mass matrix is improved by the help of experimental vectors.

Recently, O'Callahan (1995) proposed a general pseudo orthogonality correlation where a weighting matrix is used to scale and normalise the vector sets in a more consistent fashion. Again, the SEREP procedure was used to show that the POC calculation in the full and reduced spaces are equivalent and that the expansion and the full space POC need not be performed. Therefore, the reduced POC is computationally efficient and does not require any system mass matrix.

A different form of orthogonality, that between the experimentally-derived mode shapes and their reciprocal modal vectors, was proposed by He & Imregun (1995) as a criterion for the quality of modal analysis. The method is based on the use of measured FRFs and the corresponding modal vectors. Thus, a spatial description of the system is not required. Imregun & Ewins (1996) developed the previous method by including structural damping, and applied it to the analysis of a large industrial structure.

2.2.6 Energy Comparison and Force Balance

Bugeat & Lallement (1976) proposed a method for comparing the kinetic and potential energies for each mode of the experimental and analytical models:

$$\begin{aligned}
\epsilon_P &= \frac{1}{2} \{\phi_X\}_i^T [M_A] \{\phi_X\}_i - \frac{1}{2} \{\phi_A\}_i^T [M_A] \{\phi_A\}_i \\
\epsilon_K &= \frac{1}{2} \{\phi_X\}_i^T [K_A] \{\phi_X\}_i - \frac{1}{2} \{\phi_A\}_i^T [K_A] \{\phi_A\}_i
\end{aligned}
\tag{2.11}$$

where the index i denotes the mode number.

A static force balance for i^{th} measured and analytical mode shapes is proposed by Wada (1980) as:

$$\begin{aligned} \{F_X\}_i &= [K_A]\{\phi_X\}_i \\ \{F_A\}_i &= [K_A]\{\phi_A\}_i \end{aligned} \quad (2.12)$$

Fisette & Ibrahim (1988) developed a procedure based on a simple force balance approach by defining a force vector:

$$\{F\}_i = ([K_A] - \omega_{X_i}^2[M_A])\{\phi_X\}_i \quad (2.13)$$

where high unbalance forces indicate coordinates that need updating.

2.2.7 Frequency Response Function Correlation

To compare analytical and experimental transfer functions, a visual inspection is usually sufficient to determine agreement. In addition, an error indicator may be computed using the Euclidean norm of the frequency response function vectors measured at discrete frequencies as (Ibrahim, 1993):

$$\epsilon_{H_{ij}} = \frac{\| (H_A)_{ij} - (H_X)_{ij} \|}{\| (H_A)_{ij} \|} \quad (2.14)$$

Based on MAC technique, and on the concept of frequency shifting Pascual *et al.* (1996) proposed to measure the closeness between measured and analytical FRF by using the following criterion:

$$FDAC(\omega_A, \omega_X, j) = \frac{\left(\{H_A(\omega_A)\}_j^T \{H_X(\omega_X)\} \right)^2}{\left(\{H_A(\omega_A)\}_j^T \{H_A(\omega_A)\}_j \right) \left(\{H_X(\omega_X)\}_j^T \{H_X(\omega_X)\}_j \right)} \quad (2.15)$$

Where j corresponds to the measured column of $[H]$. ω_A corresponds to the frequency at which $\{H_A\}$ is calculated and ω_X corresponds to the frequency at which the FRF was measured experimentally. The frequency Domain Assurance Criterion (FDAC) can be regarded as equivalent to MAC in the FRF domain. As for MAC, values of FDAS are limited between 0 and 1. A value of 1 means perfect correlation while 0 means no correlation at all.

2.3 Dealing with Complex Mode Shapes

2.3.1 Realisation Methods

Normal modes are those with modal vectors consisting of real elements. Such modes exist for structures with no or proportional damping. Unlike normal modes, complex modes may possess any phase angle distribution, each element of modal vector being described by a complex number. The normal mode approximation is the simplest and the most frequently used approach to the complex modes:

$$|\phi_R| = \sqrt{|\operatorname{Re}\{\phi_C\}|^2 + |\operatorname{Im}\{\phi_C\}|^2} \quad (2.16)$$

The sign of the element is determined by the sign of the cosine of its phase angle and this technique works reasonably well for lightly damped structures.

Ibrahim (1983a) proposed a method for estimating the matrix $[M]^{-1}[K]$. Having calculated the matrix $[M]^{-1}[K]$, the normal modes can be obtained according to the eigenvalue equation:

$$[M]^{-1}[K]\{\Phi\} = \omega^2\{\Phi\} \quad (2.17)$$

In this approach, the equation of motion for a N degree-of-freedom system with viscous damping can be written as:

$$\begin{Bmatrix} \{\dot{x}(t)\} \\ \{\ddot{x}(t)\} \end{Bmatrix} = \begin{bmatrix} 0 & [I] \\ -[M]^{-1}[K] & -[M]^{-1}[C] \end{bmatrix} \begin{Bmatrix} \{x(t)\} \\ \{\dot{x}(t)\} \end{Bmatrix} \quad (2.18)$$

or compact form:

$$\{\dot{y}\} = [A]\{y\} \quad (2.19)$$

where $\{y\}$ is the system's state vector containing the displacements and velocities responses. By repeating equation (2.19) for $2n$ time instants, the following equation can be formed:

$$[\dot{Y}] = [A][Y] \quad (2.20)$$

where $[\dot{Y}]$ and $[Y]$ contain responses measured at the $2n$ time instants. From equation (2.20) the matrix $[A]$ can be identified as:

$$[A] = [\dot{Y}][Y]^{-1} \quad (2.21)$$

By computing the matrix $[A]$, the $[M]^{-1}[K]$ matrix give normal modes according to (2.17).

Another approach which was proposed by the same author (Ibrahim, 1983b), assumed that the structure under consideration is linear and the measured modal parameters satisfy the following equation:

$$\begin{bmatrix} [M]^{-1}[K] & [M]^{-1}[C] \end{bmatrix} \begin{Bmatrix} \{\phi_X\}_i \\ \lambda_{Xi} \{\phi_X\}_i \end{Bmatrix} = \begin{Bmatrix} -\lambda_{Xi}^2 \{\phi_X\}_i \\ \{\phi_X\}_i \end{Bmatrix} \quad i = 1, \dots, m \quad (2.22)$$

Equation (2.22) represents $N \times m$ complex equation or $2N \times m$ real equations where

m and N are the number of measured modes which are assumed to be complete and the number of measured DOFs respectively.

Since no information is available beyond the measured frequency range of interest, the analytical modes can be used to fill in for the missing measured modes:

$$\left[\begin{array}{cc} [M]^{-1}[K] & [M]^{-1}[C] \end{array} \right] \left\{ \begin{array}{c} \{\phi_A\}_i \\ \lambda_{Ai} \{\phi_A\}_i \end{array} \right\} = \left\{ \begin{array}{c} -\lambda_{Ai}^2 \{\phi_A\}_i \\ \end{array} \right\} \quad i = m + 1, \dots, N \quad (2.23)$$

Combining equation (2.22) and equation (2.23), the $2N^2$ linear equations can be solved and the corresponding normal modes can be computed from the undamped eigenproblem.

Wei *et al.* (1987) and Wei & Zhang (1987) studied the use of a transformation matrix to express the incomplete physical coordinates in modal coordinates and thus deal with a reduced but complete system. The method is iterative since it is based on assuming an initial transformation matrix which is updated till convergence is achieved. Ibrahim & Fullekrug (1990) presented a method for computing a non-iterative transformation matrix from the decomposition of the complex eigenvector matrix. Sestieri & Ibrahim (1993) analysed the errors introduced by such transformation matrices and showed that the errors can be quite significant when the system is incomplete and highly damped. Finally, Ibrahim & Sestieri (1995) concluded that using normal modes obtained through such transformations can lead to an erroneous updating of the analytical model since erroneous experimental modes are being matched.

A frequency domain technique to determine the real eigenvalues and eigenvectors of the undamped system from the identified modes was suggested by Zhang & Lallement (1985). The method assumed that the identified complex eigenvectors could be represented by a linear combination of the corresponding eigenvectors of the associated undamped system. Lembregts & Brughmans (1989) and Lembregts *et al.* (1989) also proposed a frequency-domain algorithm, theirs being based on a state-space for-

mulation and on extracting the normal modes by direct parameter estimation. The measurement data were described by a second-order linear model with real-valued constant matrices. The state transition matrix was then estimated in a global least square sense. The normal modes were identified by removing the mass-modified damping matrix from the second order eigenvalue problem.

Hsu & Tsuei (1993) and Chen & Tsuei (1993) proposed a relationship between the frequency response function (FRF) of the complex and the normal modes. For a structure with viscous damping, the equation of motion in the frequency domain is:

$$([K] - \omega^2[M]) \{X_C(\omega)\} + i\omega [C] \{X_C(\omega)\} = \{f(\omega)\} \quad (2.24)$$

Since the first term in the left hand side of the above equation represent the inverse of normal FRF matrix, equation (2.24) can be written as:

$$[H_R]^{-1} \{X_C(\omega)\} + i\omega [C] \{X_C(\omega)\} = \{f(\omega)\} \quad (2.25)$$

where subscripts C and R refer to complex and realised modes respectively and $[H_R]$ is the frequency response function matrix generated from the normal modes. Equation (2.25) can be rearranged as:

$$\{X_C(\omega)\} = ([I] + i[G(\omega)])^{-1} [H_R(\omega)] \{f(\omega)\} \quad (2.26)$$

where $[G(\omega)] = \omega[H_R(\omega)] [C]$. On the other hand, the complex frequency response function equation can also be represented as:

$$\{X_C(\omega)\} = [H_C(\omega)] \{f(\omega)\} \quad (2.27)$$

Comparing equation (2.26) and (2.27), the relationship between the FRFs of Complex modes and normal modes can be written as:

$$[H_R(\omega)] = ([I] + i[G(\omega)]) [H_C(\omega)] \quad (2.28)$$

By separating $[H_C(\omega)]$ into its real and imaginary parts and by denoting that the left hand side of equation (2.28) is real, one can get:

$$[H_R(\omega)] = Re[H_C(\omega)] + Im[H_C(\omega)] Re[H_C(\omega)]^\dagger Im[H_C(\omega)] \quad (2.29)$$

Noting that $\{X_R(\omega)\} = [H_R(\omega)]\{f(\omega)\}$, equation (2.26) yields:

$$\{X_R(\omega)\} = ([I] + i[G(\omega)]) \{X_C(\omega)\} \quad (2.30)$$

When the excitation frequency is equal to the i^{th} natural frequency, the displacement vector represents the i^{th} mode shape of the structure:

$$\{\phi_R(\omega_i)\} = ([I] + i[G(\omega_i)]) \{\phi_C(\omega_i)\} \quad (2.31)$$

separating the complex mode shape into its real and imaginary parts and using the fact that the left hand side of the above equation is real:

$$\{\phi_R(\omega_i)\} = ([I] + Im[H_C(\omega)]^2 Re[H_C(\omega)]^{\dagger 2}) \{\phi_C(\omega_i)\} \quad (2.32)$$

It should be noted that the magnitude and phase of FRFs are required at resonance only.

A technique by Niedbal (1984) involves the use of a complex transformation given by:

$$[\Phi_R] = [\Phi_C] [T] \quad (2.33)$$

Separating (2.33) into its real and imaginary parts, it can be shown that $[\Phi_R]$ can be expressed in terms of $[\Phi_C]$ and of $Re([T])$. Assuming that the latter can be approximated into a unit matrix, the realised mode shape matrix can be written as:

$$[\Phi_R] = Re[\Phi_C] + Im[\Phi_C] \left(Re[\Phi_C]^T Re[\Phi_C] \right)^{-1} Re[\Phi_C]^T Im[\Phi_C] \quad (2.34)$$

Imregun & Ewins (1993) proposed to use the MAC value to assess the degree of success between the complex modes and extracting real modes in the realisation methods. They also maximised this correlation by assuming that a better approximation of the realised mode shape can be written as:

$$\{\phi'_R\} = \{\phi_R\} + \kappa \{\gamma\}$$

where $\{\gamma\}$ is an arbitrary vector and κ is a tuning parameter. The MAC value between the complex mode shape $\{\phi_C\}$ and the corrected vector $\{\phi'_R\}$ can be written as:

$$MAC = \frac{A + B\kappa + C\kappa^2}{D + E\kappa + F\kappa^2}$$

where

$$\begin{aligned} A &= \{\phi_C\}^{*T} \{\phi_R\} \{\phi_R\}^T \{\phi_C\}^* \\ B &= \{\phi_C\}^{*T} (\{\gamma\} \{\phi_R\}^T + \{\phi_R\} \{\gamma\}^T) \{\phi_C\}^* \\ C &= \{\phi_C\}^{*T} \{\gamma\} \{\gamma\}^T \{\phi_C\}^* \\ D &= \{\phi_R\}^T \{\phi_R\}^T \{\phi_C\}^T \{\phi_C\}^* \\ E &= (\{\gamma\} \{\phi_R\}^T + \{\phi_R\} \{\gamma\}^T) \{\phi_C\}^T \{\phi_C\}^* \\ F &= \{\gamma\}^T \{\gamma\} \{\phi_C\}^T \{\phi_C\}^* \end{aligned}$$

Since the objective is to obtain maximum correlation between the complex and the normal modes, the partial derivative of MAC with respect to κ must vanish. After

some manipulation, the following equation yields:

$$(CE - BF) \kappa^2 + 2(CD - AF) \kappa + (BD - AE) = 0$$

and the roots of this equation make the correlation between $\{\phi_C\}$ and $\{\phi_R\}$ maximum.

Ahmadian & Gladwell (1995) presented a generalisation of the above method. They showed analytically that the realised mode and the real part of the initial complex mode should correlated most, when the complex mode is rotated properly. However, it is not possible to find such a rotation without identifying the damping in the system.

Ozguven & Imregun (1991) investigated complex modes arising from linear identification of non-linear systems. They showed that nonlinearities in the system may be falsely identified as complex linear modes and investigated some of the consequences of applying linear modal parameter extraction techniques to non-linear systems. They concluded that even a small nonlinearity in a system may influence the modal parameter identified. The most affected parameter is the phase of modal constant which makes the identified modes to be significantly complex. Imregun & Ewins (1995) studied various cases that lead to complex modes, such as non-linear structure behaviour, non-proportional damping, aerodynamic damping, gyroscopic effects and experimental noise. They also introduced two indicators, called modal complexity factors, to assess the amount of modal complexity.

2.3.2 Force Appropriation Methods

The aim of force appropriation methods is to provide an estimate for the force pattern required in order to excite a "pure" normal mode using multiple exciters. For instance, in aerospace industry, it is common practice to try to measure undamped natural frequencies and the corresponding mode shapes. In many cases, a single or a pair of symmetric or antisymmetric forces may be adequate but a true multi-point excitation approach may be needed where the modes are close in frequency. A "pure" mode is

excited when all responses are in monophasic and in quadrature with the sinusoidal excitation. A number of methods have been developed to determine the force vector required to excite normal modes. These methods can be classified into iterative and direct methods. Iterative methods are those in which the force distribution is progressively adjusted until some cost criterion is satisfied. On the other hand, direct methods use the measured FRF matrix relating a selected number of responses to the excitation positions and then generally use some eigenproperties of that matrix to yield the necessary force distribution. In the following, only the direct methods are discussed.

Consider a structure with m modes and n measurement transducer locations:

$$\{x\} = (Re[H(\omega)] + i Im[H(\omega)]) \{f\} \quad (2.35)$$

where $\{f\}$ is the monophasic excitation force vector defined at e locations. A pure mode is excited when response and excitation are in quadrature or when the real part of the response is zero, i.e.:

$$Re[H(\omega)]\{f\} = 0 \quad (2.36)$$

For a square $Re[H]$ matrix ($n = e$), a non-trivial solution for (2.36) is possible only if its determinant is zero:

$$|Re[H(\omega)]| = 0 \quad (2.37)$$

There are several methods for obtaining the solution of (2.37). The Asher method finds the roots of determinant $|Re[H(\omega)]|$ to obtain the natural frequencies and then solves equation (2.36) to find the appropriated force vector by using the adjoint matrix of $Re[H(\omega)]$, or by Gauss-Sidel method. The modified Asher approach (Alexiou & Wright, 1985) tries to solve the following eigenvalue problem:

$$Re[H(\omega)]\{f\} = \lambda\{f\} \quad (2.38)$$

The natural frequencies are found when one of the eigenvalues of equation (2.38) is zero. The appropriated force vectors are the eigenvectors of the system at the corresponding frequencies. The Traill-Nash method (Alexiou & Wright, 1987) considers the following equation:

$$Re[H(\omega)]\{f\} = \mu Im[H(\omega)]\{f\} \quad (2.39)$$

Again, the natural frequencies and force patterns can be found in a similar fashion to the modified Asher method.

When the FRF matrix is not square ($n > e$), the problem can still be solved approximately by minimising the real parts of the response in some way. The extended Asher method was used by Ibanez & Blakely (1984) with the following cost function:

$$\sum_{i=1}^n |Re(x_i)|^2 \quad (2.40)$$

It can be shown that the above equation is equivalent to the following eigenvalue problem:

$$Re[H(\omega)]^T Re[H(\omega)]\{f\} = \alpha\{f\} \quad (2.41)$$

Finally, the multivariate mode indicator function (MMIF) minimises a cost function in the form of (Williams & Crowley, 1986):

$$\frac{\sum_{i=1}^n |Re(x_i)|^2}{\sum_{i=1}^n |x_i|^2} \quad (2.42)$$

When no weighting is employed, the minimisation reduces to the solution of the following eigenvalue problem:

$$Re[H(\omega)]^T Re[H(\omega)]^T \{f\} = \beta \left(Re[H(\omega)]^T Re[H(\omega)] + Im[H(\omega)]^T Im[H(\omega)] \right) \{f\} \quad (2.43)$$

In this case, the natural frequencies correspond to minima in the eigenvalues α and β and the eigenvectors give the force patterns as before. Alternatively, Nash (1991) defined a variant cost function of the MMIF:

$$\frac{\sum_{i=1}^n |Im(x_i)|^2}{\sum_{i=1}^n |x_i|^2} \quad (2.44)$$

He also overcame the difficulty associated with a large number of exciting forces by using the principal force vectors.

One major problem is the selection of the right number of exciters and their correct locations. Some methods become ill-conditioned if more excitation positions than the required maximum are selected. Juang & Wright (1991) proposed a method based on SVD to eliminate the ill-conditioning in the evaluation of the appropriated force vectors. Cooper & Wright (1992) used the experimental FRFs of a rectangular perspex plate with close modes to find the appropriated force vectors. With the use of 24 accelerometers and 2 exciters, it was possible to identify the close modes. Only the SVD method and the MMIF technique using the principal force vectors were able to realise the pair, when four exciters were used. Otte (1993) reduced the order of FRF matrix $[H]$ by retaining the most significant singular values and the corresponding singular vectors from the decomposition of $[H]$. A transformation matrix, constructed by the retained singular vectors and the appropriated force vectors, was obtained from the reduced FRF matrix. Holmes & Cooper (1996) presented a criterion for the prediction of optimum exciter locations in normal mode testing using an a priori

mathematical dynamic model of the test structure. The criterion was successfully tested on the rectangular perspex plate and a representative aircraft structure by the help of a genetic algorithm.

2.4 Reduction Techniques

2.4.1 Introduction

The reduction (or expansion) of experimental modal vectors is a necessary process in the comparison, correlation, error localisation and model updating stage of structural modelling.

Due to the large size mismatch between the analytical and experimental degrees of freedom, substantial effort has been devoted to the investigation of the effects of model reduction and the most popular technique being the static condensation of Guyan (1965). Other important techniques are: Dynamic Reduction, Improved Reduction System (IRS), System Equivalent Reduction Expansion Process (SEREP).

2.4.2 Reduction of System Matrices

In all reduction techniques, there exists a relation between the measured (or master) 'n' degrees of freedom and the unmeasured (or slave) 's' degrees of freedom:

$$\{x_N\} = \begin{Bmatrix} \{x_n\} \\ \{x_s\} \end{Bmatrix} = [T] \{x_n\} \quad (2.45)$$

where

$\{x\}$ is the physical displacement,
 $[T]$ is the transformation matrix,
 N is the total number of FEM DOFs,

The reduced mass and stiffness matrices can be written as:

$$\begin{aligned}
 [M_n] &= [T]^T [M_N] [T] \\
 [K_n] &= [T]^T [K_N] [T]
 \end{aligned}$$

2.4.3 Guyan Reduction

Guyan reduction (1965) has been used for many years as one of the most common tools for the reduction of large analytical models.

Starting from the time domain equation of motion, one can write:

$$[M] \{\ddot{x}\} + [K] \{x\} = \{f\} \quad (2.46)$$

Partitioning the matrices into measured (or master) 'n' and slave 's' DOFs and neglecting inertia terms, one obtains:

$$\begin{bmatrix} [K_{nn}] & [K_{ns}] \\ [K_{sn}] & [K_{ss}] \end{bmatrix} \begin{Bmatrix} \{x_n\} \\ \{x_s\} \end{Bmatrix} = \begin{Bmatrix} \{f_n\} \\ \{f_s\} \end{Bmatrix} \quad (2.47)$$

Using the lower set of equations in (2.47) leads to:

$$\{x_s\} = -[K_{ss}]^{-1} [K_{sn}] \{x_n\} + [K_{ss}]^{-1} \{f_s\} \quad (2.48)$$

Assuming that there are no external forces at the slave DOFs, the Guyan reduction

transformation matrix will be obtained as:

$$[T_1] = \begin{bmatrix} [I] \\ -[K_{ss}]^{-1} [K_{sn}] \end{bmatrix} \quad (2.49)$$

Since the inertia terms are neglected, this technique is also called static reduction. The Guyan reduction depends heavily on the selection of the master degrees of freedom, a poor selection yielding inaccurate models.

2.4.4 Improved Reduced System Technique (IRS)

The Improved Reduced System (IRS) was developed by O'Callahan (1989) to compensate for the mass misappropriation of the Guyan reduction process, especially when the selection of measured DOF is not optimum. It improves the accuracy over the static condensation technique by approximating the second term in equation (2.48) as:

$$[K_{ss}]^{-1} \{f_s\} = \left[[K_{ss}]^{-1} [M_{sn}] - [K_{ss}]^{-1} [M_{ss}] [K_{ss}]^{-1} [K_{sn}] \right] [M_R]^{-1} [K_R] \{x_n\} \quad (2.50)$$

where $[M_R]$ and $[K_R]$ are the Guyan reduced mass and stiffness matrices given by:

$$\begin{aligned} [M_R] &= [T_1]^T [M] [T_1] \\ [K_R] &= [T_1]^T [K] [T_1] \end{aligned}$$

Substituting (2.50) into (2.48) and comparing the terms related to the transformation matrix, yields:

$$[T_2] = [T_1] + [T_2'] \quad (2.51)$$

where

$$\begin{aligned}
 [T'_2] &= [S] [M] [T_1] [M_R]^{-1} [K_R] \\
 [S] &= \begin{bmatrix} 0 & 0 \\ 0 & [K_{ss}]^{-1} \end{bmatrix}
 \end{aligned} \tag{2.52}$$

2.4.5 Dynamic Reduction

An extension of Guyan reduction can be introduced by considering the inertia terms in equation (2.46). The procedure is almost identical to Guyan reduction except that the transformation is based on the dynamic stiffness matrix $[Z]$ instead of stiffness matrix $[K]$. In this case, the transformation matrix is given by:

$$[T_3] = \begin{bmatrix} [I] \\ -([K_{ss}] - \omega^2 [M_{ss}])^{-1} ([K_{sn}] - \omega^2 [M_{sn}]) \end{bmatrix} \tag{2.53}$$

The selection of the best frequency point for a exact response of the system is of particular importance, the centre frequency point being recommended by Paz (1984).

It can be seen that the inversion of dynamic stiffness matrix in equation (2.53) is computationally expensive. The procedure not only involves the inversion of $[Z_{ss}] = [K_{ss}] - \omega^2 [M_{ss}]$ matrix but the transformation matrix has also to be calculated for each mode. A number of approximate techniques based on series expansion and spectral decomposition have been proposed by various authors to obtain a computationally efficient inversion of $[Z_{ss}]$.

Kidder (1973) used the geometric series to expand the inverse of $[Z_{ss}]$.

$$\begin{aligned}
 ([K_{ss}] - \omega^2 [M_{ss}])^{-1} &= [K_{ss}]^{-1} [I - \omega^2 [M_{ss}] [K_{ss}]^{-1}]^{-1} \\
 &= [K_{ss}]^{-1} ([I] + \omega^2 [M_{ss}] [K_{ss}]^{-1} + \\
 &\quad \omega^4 [M_{ss}] [K_{ss}]^{-1} [M_{ss}] [K_{ss}]^{-1} + \dots)
 \end{aligned} \tag{2.54}$$

Substituting equation (2.54) into equation (2.53):

$$[T_3] = \begin{bmatrix} [I] \\ -[K_{ss}]^{-1}[K_{sn}] + \omega^2 ([K_{ss}]^{-1} ([M_{sn}] - [M_{ss}][K_{ss}]^{-1}[K_{sn}])) + \\ \omega^4 ([K_{ss}]^{-1}[M_{ss}][K_{ss}]^{-1} ([M_{sn}] - [M_{ss}][K_{ss}]^{-1}[K_{sn}])) + \dots \end{bmatrix} \quad (2.55)$$

By neglecting the ω^2 terms, (2.55) reverts back to (2.49) which is for static Guyan reduction. If terms up to ω^2 are included, the result is identical to the IRS formulation.

Petersman (1984) calculated the inverse of $[Z_{ss}]$ using the eigensolution of the eigenproblem associated with $[Z_{ss}]$:

$$[Z_{ss}]^{-1} = [\Phi] ([\Lambda] - \omega^2 [I])^{-1} \Phi^T \quad (2.56)$$

where $[\Phi]$ and $[\Lambda]$ are the mass-normalised modal and spectral matrices related to the slave DOFs respectively. It can be seen from equation (2.56) that only the diagonal matrix $([\Lambda] - \omega^2 [I])^{-1}$ is frequency dependent. Thus, its inversion is simpler than that of the corresponding dynamic stiffness matrix. It is also obvious that element $(\lambda_i - \omega^2)^{-1}$ will tend to zero for $\lambda_i \gg \omega^2$. Therefore, the problem can be further simplified by ignoring of those elements of spectral matrix with $\lambda \gg \lambda_i$. The number of terms used depends on the actual natural frequency and on the eigenvalues of the slave-only system. However, a large number of modes may well have to be included in order to increase the accuracy of the reduced system.

2.4.6 System Equivalent Reduction expansion Process (SEREP)

This method was originally introduced by O'Callahan *et al.* (1986) who suggested that the rotational degrees of freedom for the experimental model could be derived from those analytical counterparts. Since then, SEREP has been found to provide

improved accuracy in applications such as cross orthogonality checks between analytical and experimental modal vectors, linear and non-linear forced response studies, and analytical model improvement.

Using a collection of modes that are to be preserved in the reduction process, a transformation matrix can be developed using a generalised inverse of the modal matrix:

$$[T_4] = \begin{bmatrix} [\Phi_{nr}] \\ [\Phi_{sr}] \end{bmatrix} [\Phi_{nr}]^\dagger \quad (2.57)$$

where \dagger denotes pseudo-inverse and r is the number of modes used to form the transformation matrix. Using a generalised inverse, which carries information pertaining to the selected modes at the selected set of 'n' DOFs, the formulation allows the reduction process to preserve the dynamics of the full system in a reduced set of matrices, a feature which not possible by Guyan or IRS reduction techniques.

2.5 Coordinate expansion

An alternative approach to reducing the finite element model is to expand the measured mode shapes by estimating the unmeasured degrees of freedom. In general more confidence can be placed in the expanded results by increasing the number of measurement points. It is noticeable that any reduction method can also be used for expansion.

All expansion methods use a transformation matrix that relates the experimental modal vectors $[\Phi]_X$ to the full space vectors $[\Phi]$:

$$[\Phi_{Nr}] = \begin{bmatrix} [\Phi_{nr}] \\ [\Phi_{sr}] \end{bmatrix} = [T]_{Nr} [\Phi_X]_{nr} \quad (2.58)$$

where N, n, r represent the number of FE model DOFs, the number of measured DOFs and the number of measured modes respectively. In the following, the derivation of the transformation matrix for various expansion methods will be explained.

2.5.1 Guyan/Irons Expansion

This expansion technique is effectively the inverse of the static condensation process described in Section (2.4.3) and it is based on the partitioned eigenvalue equation:

$$\left[\begin{array}{cc} [K_{nn}] & [K_{ns}] \\ [K_{sn}] & [K_{ss}] \end{array} \right] - \lambda_i \left[\begin{array}{cc} [M_{nn}] & [M_{ns}] \\ [M_{sn}] & [M_{ss}] \end{array} \right] \begin{Bmatrix} \{\phi_n\}_i \\ \{\phi_s\}_i \end{Bmatrix} = 0 \quad (2.59)$$

Using the same procedure as Guyan reduction technique, one can easily obtain the transformation matrix $[T_1]$ as:

$$[T_1] = \begin{bmatrix} [I] \\ -[K_{ss}]^{-1} [K_{sn}] \end{bmatrix} \quad (2.60)$$

The Guyan expansion can be interpreted as the determination of an expanded mode shape $\{\phi_i\}$ which minimise the total strain energy of mode i such that its elements are the same as the test values at measured DOFs. (Levine-West & Kissil, 1994)

2.5.2 IRS Expansion

The IRS expansion is a modified version of the Guyan expansion. Instead of minimising the strain energy, the method minimise both the strain energy and the potential energy of applied forces.

The transformation matrix for the IRS expansion is given by:

$$[T_2] = [T_1] + [S] [M] [T_1] [M_R]^{-1} [K_R] \quad (2.61)$$

where $[S]$, $[M_R]$ and $[K_R]$ are defined by (2.52).

2.5.3 Dynamic expansion

The dynamic expansion process is based on the frequency domain equation of motion written at a single frequency. Relating the measured and slave DOFs through the second set equations in (2.59), the transformation matrix of dynamic expansion becomes:

$$[T_3] = \begin{bmatrix} [I] \\ -([K_{ss}] - \lambda_i [M_{ss}])^{-1} ([K_{sn}] - \lambda_i [M_{sn}]) \end{bmatrix} \quad (2.62)$$

where λ_i is i^{th} eigenvalue of the system. Another approach is to calculate $\{\phi_{s_i}\}$ by using the upper part of (2.59). Since the number of measured DOFs are almost always less than the number of unmeasured DOFs, this latter approach usually gives poor results.

2.5.4 Gysin Modified Dynamic Expansion

Gysin (1990) modified the dynamic expansion process to include all the DOFs in the inverse processing. By considering both the upper and lower sets in (2.59):

$$\begin{bmatrix} [K_{nm}] - \lambda_i [M_{nm}] \\ [K_{sn}] - \lambda_i [M_{sn}] \end{bmatrix} \begin{Bmatrix} \{\phi\}_n \\ \{\phi\}_s \end{Bmatrix} + \begin{bmatrix} [K_{ns}] - \lambda_i [M_{ns}] \\ [K_{ss}] - \lambda_i [M_{ss}] \end{bmatrix} \begin{Bmatrix} \{\phi\}_n \\ \{\phi\}_s \end{Bmatrix} = 0 \quad (2.63)$$

Solving for the generalised inverse of (2.63) and comparing terms for the transformation matrix, a transformation matrix is obtained as:

$$[T_4] = \left[- \left(\begin{bmatrix} [K_{ns}] \\ [K_{ss}] \end{bmatrix} - \lambda_i \begin{bmatrix} [M_{ns}] \\ [M_{ss}] \end{bmatrix} \right)^{\dagger} \begin{bmatrix} [I] \\ \left(\begin{bmatrix} [K_{nn}] \\ [K_{sn}] \end{bmatrix} - \lambda_i \begin{bmatrix} [M_{nn}] \\ [M_{sn}] \end{bmatrix} \right) \end{bmatrix} \right] \quad (2.64)$$

2.5.5 SEREP Expansion

The concept of SEREP was first developed as equivalent Reduction (ER) by O'Callahan *et al.* (1986). The collection of the analytical modes used in the SEREP process will control the expansion. The system matrices are not used directly in the formation of transformation matrix as they are in all other techniques.

The SEREP method assumes that a full-space eigensolution has been obtained and that the modal equation from the physical full space to the modal space is:

$$\{x_N\} = [\Phi_{Nr}] \{P_r\} \quad (2.65)$$

where $\{x_N\}$ is the displacement vector in the physical full space, $[\Phi_{Nr}]$ the modal matrix obtained from the finite element mass and stiffness matrices and $\{P_r\}$ is the displacement modal vector. Partitioning equation (2.65) into measured and slave DOFs yields:

$$\begin{Bmatrix} \{x_n\} \\ \{x_s\} \end{Bmatrix} = \begin{bmatrix} [\Phi_{nr}] \\ [\Phi_{sr}] \end{bmatrix} \{P_r\} \quad (2.66)$$

Consider the upper equation set, we obtain:

$$\{x_n\} = [\Phi_{nr}] \{P_r\} \quad (2.67)$$

Solving the above equation by performing a generalised inverse:

$$\{P_r\} = [\Phi_{nr}]^\dagger \{x_n\} \quad (2.68)$$

Substituting (2.68) into (2.65) and comparing terms related to the transformation matrix, produces the SEREP transformation matrix as:

$$[T_5] = \begin{bmatrix} [\Phi_{nr}] \\ [\Phi_{sr}] \end{bmatrix} [\Phi_{nr}]^\dagger \quad (2.69)$$

2.5.6 SEREPa Expansion

To prevent the SEREP process from modifying the test data in the expansion process, a non-smoothing version, SEREPa was proposed by O'Callahan & Li (1990). The consistency of the SEREP is maintained and the measured DOFs are not modified. It is assumed that the number of measured modes 'r' in the SEREP transformation are equal to the number of measured DOFs 'n'. By applying this additional condition to the SEREP process, the SEREPa transformation matrix becomes:

$$[T_6] = \begin{bmatrix} [I_{nn}] \\ [\Phi_{sn}] [\Phi_{nn}]^{-1} \end{bmatrix} \quad (2.70)$$

2.5.7 Test Analysis Model Expansion

The TAM approach is similar to SEREP and SEREPa except that the transformation for the measured DOFs is fixed during the expansion process (Kammer, 1987). The transformation matrix for the TAM is defined as:

$$[T_7] = \begin{bmatrix} [I_{nn}] \\ [\Phi_{sn}] [\Phi_{nn}]^\dagger \end{bmatrix} \quad (2.71)$$

The hybrid TAM (Kammer, 1991) which is a mixture of TAM and Guyan expansion, combines the accuracy of the TAM with the robustness of the static Guyan reduction. An oblique projection is formed using the FE mode shapes, the transformation matrix of 2.71, and the FE mass matrix as:

$$[Q] = [\Phi][\Phi]^T[T_7]^T[M][T_7] \quad (2.72)$$

The final transformation matrix for the hybrid TAM is a combination of the transformation matrices for Guyan reduction and modal TAM methods:

$$[T_8] = [T_1] + ([T_7] - [T_1])[Q]$$

2.6 Model Updating Methods Using Modal Data

This section is a review of existing model updating techniques using modal data. Two categories, namely direct and iterative methods, will be considered.

2.7 Direct Methods using Modal Data

The updated model is expected to match some reference data, usually consisting of an incomplete set of eigenvalues and eigenvectors derived from measurements. Such approaches are called direct or representation models (Zhang & Lallement, 1987).

The main advantages of direct methods are:

- assured convergence, since the method do not need any iterations.
- the CPU time is usually less than that required by the iterative methods.

- the methods try to produce the reference data set exactly.

However, there are also disadvantages:

- high quality measurements and accurate modal analysis are needed.
- the mode shapes must be expanded to the size of finite element model.
- the methods are usually unable to keep the connectivity of the structure and the updated matrices are usually fully populated.
- there is no guarantee for the positive definiteness of the updated mass and stiffness matrices.

2.7.1 Lagrange Multiplier Methods

All Lagrange multiplier methods try to minimise an objective function subject to some constraints on the independent variables.

Such a method was proposed by Baruch & Bar Itzhac (1978) who assumed that the mass matrix was correct and found a matrix $[\Phi_U]$ that minimised the weighted Euclidean norm:

$$J = \| [M_A]^{1/2} ([\Phi_U] - [\Phi_X]) \| \quad (2.73)$$

and satisfied the weighted orthogonality condition:

$$[\Phi_U]^T [M_A] [\Phi_U] = [I] \quad (2.74)$$

The final result may be expressed as:

$$[\Phi_U] = [\Phi_X]([\Phi_X]^T[M_A][\Phi_X])^{-1/2} \quad (2.75)$$

Baruch (1978) proposed another method in which the mass matrix was correct and updated the stiffness matrix by minimising:

$$J_K = \| [M_A]^{-1/2} ([K_U] - [K_A]) [M_A]^{-1/2} \| \quad (2.76)$$

subject to the following constraints:

$$[K_U] = [K_U]^T \quad (2.77)$$

$$[K_U][\Phi_X] = [M_U][\Phi_X][\omega_X^2]$$

which enforce the symmetry of stiffness matrix and the equation of motion respectively. The updated stiffness matrix can then be obtained as:

$$\begin{aligned} [K_U] = & [K_A] - [K_A][\Phi_X][\Phi_X]^T[M_A] - [M_A][\Phi_X][\Phi_X]^T[K_A] + \\ & [M_A][\Phi_X][\Phi_X]^T[K_A][\Phi_X][\Phi_X]^T[M_A] + [M_A][\Phi_X][\omega_X^2][\Phi_X]^T[M_A] \end{aligned}$$

Berman (1979) and Baruch (1982) assumed that the measured modes were correct and tried to update the mass matrix. Berman & Nagy (1983) used the same assumptions and updated the mass and stiffness matrices sequentially. They defined the problem as the minimisation of:

$$J_M = \| [M_A]^{-1/2} ([M_U] - [M_A]) [M_A]^{-1/2} \| \quad (2.78)$$

subject to:

$$[\Phi_X]^T [M_U] [\Phi_X] = [I] \quad (2.79)$$

The minimisation procedure results in the following expression for the updated mass matrix:

$$[M_U] = [M_A] + [M_A] [\Phi_X] [m_A]^{-1} ([I] - [m_A]) [m_A]^{-1} [\Phi_X]^T [M_A] \quad (2.80)$$

where $[m_A] = [\Phi_X]^T [M_A] [\Phi_X]$.

After the computation of $[M_U]$, the stiffness matrix can be calculated by the minimising:

$$J_K = \| [M_A]^{-1/2} ([K_U] - [K_A]) [M_A]^{-1/2} \| \quad (2.81)$$

subject to three constraints:

$$[K_U] = [K_U]^T$$

$$[\Phi_X]^T [K_U] [\Phi_X] = [\omega^2] \quad (2.82)$$

$$[K_U] [\Phi_X] = [M_A] [\Phi_X] [\omega_X^2]$$

which enforce the stiffness symmetry, the orthogonality condition and the equation of motion. The result is:

$$[K_U] = [K_A] + ([\Delta] + [\Delta]^T) \quad (2.83)$$

where

$$[\Delta] = \frac{1}{2} [M_A] [\Phi_X] ([\Phi_X]^T [K_A] [\Phi_X] + [\omega_X^2]) [\Phi_X]^T [M_A] - [K_A] [\Phi_X] [\Phi_X]^T [M_A]$$

Caesar (1986) suggested a range of methods that updated the mass and the stiffness matrices using different cost functions and constraints. To improve the physical meaning of the updated results, he also introduced additional constraints from rigid-body considerations, such as the position of the centre of gravity, total mass and moments of inertia.

Wei (1990) updated the mass and stiffness matrices simultaneously using the measured eigenvectors and a cost function of the form:

$$J = \| [M_A]^{-1/2} ([K_U] - [K_A]) [M_A]^{-1/2} \| + \| [M_A]^{-1/2} ([M_U] - [M_A]) [M_A]^{-1/2} \| \quad (2.84)$$

He used the usual constraints of mass orthogonality, the equation of motion and the symmetry of the updated matrices. The corrected mass and stiffness matrices which satisfy the above requirement are:

$$\begin{aligned} [M_U] &= [M_A] - [M_0] + ([I] - [P][\Phi_X]^T)[S][Y] + [Y]^T[S]^T([I] - [\Phi_X][P]^T) \\ [K_U] &= [K_0] + [P]([\Phi_X]^T[K_A][\Phi_X] + [\omega^2])[P]^T - [U][\Phi_X][P]^T - [P][\Phi_X]^T[U]^T \end{aligned} \quad (2.85)$$

where

$$\begin{aligned}
[M_0] &= [M_A][\Phi_X][Q]^{-1}([Q] - [I])[Q]^{-1}[\Phi_X]^T[M_A] \\
[K_0] &= [K_A] - [K_A][\Phi_X][P]^T - [P][\Phi_X]^T[K_A] + [U]^T + [U] \\
[P] &= [M_A][\Phi_X][Q]^{-1} \\
[Q] &= [\Phi_X]^T[M_A][\Phi_X] \\
[S] &= [K_A][\Phi_X]([Q] + [\omega^2][Q][\omega^2]) \\
[U] &= [P][\omega^2][Q][\omega^2][S]^T \\
[Y] &= [\omega^2][\Phi_X]^T[M_A]
\end{aligned}$$

Fuh & Chen (1984) developed a reference basis method for representational updating of structural system with non-proportional damping. A detailed review of methods based on Lagrange multiplier is given by Heylen & Sas (1987).

2.7.2 Matrix Mixing Methods

The matrix mixing method is due to Ross (1971) and Thoren (1972) and further development are introduced by Caesar (1987) and Link *et al.* (1987). If one can assume that all vibration modes are measured at all degrees of freedom, one can construct the mass and stiffness matrices directly. If we assume the eigenvectors are mass normalised then:

$$\begin{aligned}
[M_U]^{-1} &= [\Phi_X] [\Phi_X]^T = \sum_{i=1}^N \{\phi_X\}_i \{\phi_X\}_i^T \\
[K_U]^{-1} &= [\Phi_X] [\omega_{X_i}^2] [\Phi_X]^T = \sum_{i=1}^N \frac{\{\phi_X\}_i \{\phi_X\}_i^T}{\omega_{X_i}^2}
\end{aligned} \tag{2.86}$$

There are two main difficulties with the above approach. First, the number of measured modes is usually much less than the number of degrees of freedom. Second, the response of the structure can only be measured at a limited number of coordinates. However, the second difficulty may be partly overcome by expanding the experimental

mode shapes to full size by using mass and stiffness matrices from the finite element model.

In early work, Ross (1971) added some linearly independent vectors to the modal matrix to make it square and invertible. Sometimes the number of measurement locations is less than the number of measured modes. In this case Thoren (1972) limited the number of degrees of freedom to be equal to the number of measured modes while Luk (1987) applied a pseudo inverse to incomplete modal matrix.

Caesar (1987) and Link *et al.* (1987) assumed that the measured mode shapes were expanded to analytical degrees of freedom. Also, they used the data from the corresponding finite element model to fill the non-measured modes. Under such assumptions, the mass and stiffness matrices can be written as:

$$\begin{aligned}
 [M_U]^{-1} &= \sum_{i=1}^m \{\phi_X\}_i \{\phi_X\}_i^T + \sum_{i=m+1}^N \{\phi_A\}_i \{\phi_A\}_i^T \\
 [K_U]^{-1} &= \sum_{i=1}^m \frac{\{\phi_X\}_i \{\phi_X\}_i^T}{\omega_{X_i}^2} + \sum_{i=m+1}^N \frac{\{\phi_A\}_i \{\phi_A\}_i^T}{\omega_{A_i}^2}
 \end{aligned} \tag{2.87}$$

where m and N are the number of measured modes and the number of total degrees of freedom respectively. If the number of measured modes is much less than the total number of modes in the finite element model, equations (2.87) becomes:

$$\begin{aligned}
 [M_U]^{-1} &= [M_A]^{-1} + \sum_{i=1}^m \{\phi_X\}_i \{\phi_X\}_i^T - \sum_{i=1}^m \{\phi_A\}_i \{\phi_A\}_i^T \\
 [K_U]^{-1} &= [K_A]^{-1} + \sum_{i=1}^m \frac{\{\phi_X\}_i \{\phi_X\}_i^T}{\omega_{X_i}^2} - \sum_{i=1}^m \frac{\{\phi_A\}_i \{\phi_A\}_i^T}{\omega_{A_i}^2}
 \end{aligned} \tag{2.88}$$

2.7.3 Error Matrix Method

Error matrix methods are a group of techniques that directly estimate the error in the mass and stiffness matrices by assuming that the error is very small. One of

the earliest papers in this subject is due to Sidhu & Ewins (1984) who defined an expression for the error matrix as:

$$[\Delta K] = [K_X] - [K_A] \quad (2.89)$$

Due to the incompleteness of the experimental data, the error matrix cannot be obtained from the above equation directly. Sidhu & Ewins (1984) rearranged equation (2.89) and expanded the flexibility matrix $[K_X]^{-1}$ by a geometric series. The error matrix can then be approximated by considering the first order terms of the expansion as:

$$[\Delta K] \cong [K_A]([K_A]^{-1} - [K_X]^{-1})[K_A] \quad (2.90)$$

A similar approach can also be applied to the mass matrix. Gysin (1986) has expressed the two pseudo-flexibility matrices , $[K_A]^{-1}$ and $[K_X]^{-1}$, in (2.90) by using modal data:

$$\begin{aligned} [\Delta K] &\cong [K_A] \left([\Phi_A] \left[\frac{1}{\omega_A^2} \right] [\Phi_A]^T - [\Phi_X] \left[\frac{1}{\omega_X^2} \right] [\Phi_X]^T \right) [K_A] \\ [\Delta M] &\cong [M_A] \left([\Phi_A] [\Phi_A]^T - [\Phi_X] [\Phi_X]^T \right) [M_A] \end{aligned} \quad (2.91)$$

Further work has been carried out on this technique by He & Ewins (1986) who applied the error matrix method to investigate the damping properties of a simulated vibration system. Lawrence (1987) carried out a number of case studies, including a practical example. Zhang & Lallement (1987) expanded the flexibility matrix to include some of the second order terms. Park & Lee (1988) used the weighted error matrix method to search the damage area using stiffness changes smaller than measurement errors. Lieven & Ewins (1990) proposed a modified version of the error matrix method by using the singular value decomposition (Maia, 1989). They defined the stiffness error matrix in equation (2.90) as:

$$[\Delta K] = \left([\Phi_X][\omega_X^2][\Phi_X]^T\right)^\dagger - \left([\Phi_A][\omega_A^2][\Phi_A]^T\right)^\dagger \quad (2.92)$$

The advantage of this approach is that the analytical system matrices are no longer required. Lieven & Ewins (1992) discussed the effect of incompleteness and noise on the quality of the results obtained from the error matrix method.

2.7.4 The Eigenstructure Assignment Methods

The basic approach is adapted from the control theory and the updated model is expected to reproduce a number of measured modes exactly. If only the eigenvalues are used, then the method is called pole placement (Porter & Crossley, 1972). Using state feedback Moore (1976) formulated the necessary and sufficient conditions for simultaneous eigenvalue and eigenvector assignment for the case of distinct eigenvalues. Srinathkumar (1978) addressed the problem of pole-assignment in linear time-invariant multi-variable systems using output feedback. Andry & Chung (1983) were among the first to apply the technique to a linear mechanical system for the purpose of parameter identification.

Consider the equation of motion for a system containing N degrees of freedom:

$$[M_A] \{\ddot{X}\} + [C_A] \{\dot{X}\} + [K_A] \{X\} = [B_0] \{U\} \quad (2.93)$$

where $\{U\}$ is the input force vector and the matrix $[B_0]$ determines the location of forces on the structure.

An arbitrary output $\{Y\}$ can be a combination of displacements and velocities:

$$\{Y\} = [D_0] \{X\} + [D_1] \{\dot{X}\} \quad (2.94)$$

In control applications, the problem is usually to find the feedback matrix, $[G]$, such

that:

$$\{U\} = [G] \{Y\} \quad (2.95)$$

which ensures that the closed loop system has the desired eigenvalues and eigenvectors. Combining the above equations, the result for the updated stiffness and damping matrices is:

$$[K_U] = [K_A] - [B_0] [G] [D_0] \quad (2.96)$$

$$[C_U] = [C_A] - [B_0] [G] [D_1]$$

where the matrix $[B_0]$ can be chosen arbitrary. The matrices $[D_0]$ and $[D_1]$ must be chosen such that $[D_1] [\Phi_X] [\Lambda_X] + [D_0] [\Phi_X]$ is invertible. The matrices $[\Lambda_X]$ and $[\Phi_X]$ are the experimentally-derived eigenvalues and eigenvectors that are to be assigned to the initial structural model.

Minas & Inman (1988) and Inman & Minas (1990) used expanded mode shapes and determined the matrix $[G]$ as:

$$[G] = \frac{([M_A][B_0])^\dagger ([\Phi_X] [\Lambda_X^2] + [M_A]^{-1} [C_A] [\Phi_X] [\Lambda_X] + [M_A]^{-1} [K_A] [\Phi_X])}{([D_1] [\Phi_X] [\Lambda_X] + [D_0] [\Phi_X])^\dagger} \quad (2.97)$$

In general, the updated stiffness and damping matrices are not symmetric unless constraint equations are used. Inman & Minas (1990) proposed an iterative scheme to ensure symmetry of the updated matrices.

Zimmerman & Widengren (1990) used a modified algorithm that allowed a symmetric eigenstructure assignment when correcting the damping and stiffness matrices. Their method required the solution of a general algebraic Riccati matrix equation, the size

of which depended on the number of assigned modes, thus requiring very considerable CPU power for large order systems.

Recently, Shulz & Inman (1994) used the eigenstructure assignment technique with a number of constraints that could be related to the physical properties of the system to be updated. The constraints were built into a non-linear optimisation procedure that preserved the desired properties of updated model. They considered small-order system that were symmetric, banded and bounded.

Ziaei Rad & Imregun (1996a) modified the Shulz and Inman formulation to accommodate large systems by developing a quadratic linear optimisation procedure which is unconditionally stable. They also considered the updating of damping matrices.

2.8 Iterative Methods Using Modal Data

The basic approach of iterative updating methods using modal data is to improve the correlation between the experimental and analytical models via a penalty function. Because of the general nature of penalty functions, the problem has to be linearised and thus optimised iteratively. Since the penalty function is usually non-linear, the iterations may not converge. In any case, iterative methods have two main advantages. First, a wide range of parameters can be updated simultaneously and second, both measured and analytical data can be weighted, a feature which can accommodate engineering intuition.

On the other hand, there are three major problems with the use of iterative methods:

- the experimental and theoretical modes must be paired from the outset. Though the modal assurance criteria (MAC) is a useful tool, there is no guarantee that all modes will be matched.
- since the mass distribution of the finite element model and that of the actual structure may be different, the experimental and analytical mode shapes should

be scaled correctly. This problem can be solved by using modal scale factor (MSF).

- in the absence of damping in the theoretical model, either a real mode shape should be extracted from measured complex FRF data or the updating algorithm must be able to cope such disparities (Section 2.3).

2.8.1 Penalty Function Methods

The methods are generally based on the use of a Taylor series of the modal data expanded as a function of the unknown updating parameters. This series is often truncated to produce a linear approximation of the form:

$$\{\Delta w^i\} = [S^i] \{\Delta p^i\} \quad (2.98)$$

where the superscript i is the iteration index, $\{\Delta p^i\}$ is the unknown vector of design parameters, and $\{\delta w^i\}$ represents the difference between the measured and estimated modal data, via:

$$\{\Delta w^i\} = \{\{\Delta \phi_1^i\}^T, \dots, \{\Delta \phi_m^i\}^T, \{\Delta \lambda_1^i, \dots, \Delta \lambda_m^i\}^T\}^T \quad (2.99)$$

$[S^i]$ in (2.98) is the sensitivity matrix and contains the first derivatives of the eigenvalues and eigenvectors with respect to the design parameters. Equation (2.98) is solved for $\{\Delta p^i\}$ which is then used to obtain the updated mass and stiffness matrices at the i^{th} iteration. The process is repeated until convergence is achieved within a specified tolerance.

The sensitivity methods differ in the choice of design parameters and the definition of optimisation constraints. Design parameters such as individual elements of the mass and stiffness matrices, sub-matrices, geometric or material properties can be defined. Constraints are usually imposed on natural frequencies and mode shapes.

Fox & Kapoor (1968) calculated the first derivatives of the eigenvalues with respect to the design parameters. The result for the derivative of the r^{th} eigenvalue, λ_r , with respect to the s^{th} design parameter p_s is:

$$\frac{\partial \lambda_r}{\partial p_s} = \phi_r^T \left(\frac{\partial [K]}{\partial p_s} - \lambda_r \frac{\partial [M]}{\partial p_s} \right) \phi_r \quad (2.100)$$

They have also suggested two methods for calculating the first derivative of the eigenvectors. Lim (1987) suggested an approximate method for calculating the first derivative of the eigenvectors which is only valid for the low frequency modes. Other methods for calculating mode shapes derivatives have been suggested by Chu & Rudisill (1975), Ojalvo (1987) and Tan & Andrew (1989).

Usually, the number of design parameters and that of measurements are not equal and hence the matrix $[S^i]$ in (2.98) is not square. The case in which there are more design parameters than measurements was considered by Chen & Garba (1980). They found the solution to the problem by seeking a set of design parameters by minimising the norm as an additional constraint equation:

$$Q = \sum_s \Delta p_s^2 \quad (2.101)$$

Similarly, the SVD technique was used by Hart & Yao (1977) and Ojalvo *et al.* (1989) for a case with less design parameters than measurements. The solution of (2.98) can be calculated by minimising the penalty function:

$$J(\{\Delta p^i\}) = (\{\Delta w^i\} - [S^i] \{\Delta p^i\})^T (\{\Delta w^i\} - [S^i] \{\Delta p^i\}) \quad (2.102)$$

Differentiating J with respect to $\{\Delta p^i\}$ and setting the result equal to zero, it can be shown that the solution is given by:

$$\{\Delta p^i\} = ([S^i]^T [S^i])^{-1} [S^i]^T \{\Delta w^i\} \quad (2.103)$$

and an updated estimate of the unknown design parameter vector is obtained by:

$$\{p^{i+1}\} = \{p^i\} + \{\Delta p^i\} \quad (2.104)$$

In practical situations, all measured data do not have the same accuracy. Usually, mode shape data are less accurate than natural frequency data. The accuracy of measured data can be incorporated into the updating process by including a positive definite weighting matrix $[V_{ee}]$. Equation (2.102) becomes:

$$J(\{\Delta p^i\}) = (\{\Delta w^i\} - [S^i] \{\Delta p^i\})^T [V_{ee}] (\{\Delta w^i\} - [S^i] \{\Delta p^i\}) \quad (2.105)$$

The minimisation of (2.105) yields:

$$\{\Delta p^i\} = ([S^i]^T [V_{ee}] [S^i])^{-1} [S^i]^T [V_{ee}] \{\Delta w^i\} \quad (2.106)$$

Another approach (Natke, 1988) is to add an extra term to minimise the change of the design parameters. The extended weighted penalty function can be expressed as:

$$J(\{\Delta p^i\}) = (\{\Delta w^i\} - [S^i] \{\Delta p^i\})^T [V_{ee}] (\{\Delta w^i\} - [S^i] \{\Delta p^i\}) + \{\Delta p^i\}^T [V_{PP}] \{\Delta p^i\}$$

where $[V_{PP}]$ is a weighted matrix which estimates the variance of the current parameters. The solution of $\{\Delta p^i\}$ is given by:

$$\{\Delta p^i\} = ([S^i]^T [V_{ee}] [S^i] + [V_{PP}])^{-1} [S^i]^T [V_{ee}] \{\Delta w^i\} \quad (2.107)$$

Many researchers have used this method with different sets of unknown parameters. Thomas (1986) and Dascotte & Vanhonacker (1989) used the approach to update the elements of the mass and stiffness matrices. Dascotte (1990) demonstrated and

discussed the relative merit of combining analytical and experimental modal data on a practical application. Physical parameters were also chosen by many authors. Such parameters allows an easier interpretation of the updated model. Wei (1989) selected moments of inertia as design parameters to update a simple 3D beam structure. They compared the results with that of using p-values whereby each elemental matrix is corrected on a non-physical basis. Dascotte (1992) updated a composite structure selecting the material constant as design parameters.

A second-order sensitivity method has been tried by Kuo & Wada (1987) who produced correction terms to improve the convergence properties compared to that of the linearised algorithm. Ojalvo & Pilon (1991) used second-order natural frequency sensitivities to update the system mass and stiffness matrices.

2.8.2 Minimum Variance Methods

These methods can be regarded as penalty function methods in which the weight matrices change from one iteration to the next. They are also based on the assumption that both the measured data and the initial model have errors which can be expressed in terms of variance matrices.

Collins & Young (1972) introduced the minimum variance method by assuming that that the measured data and the initial model are statistically independent, a feature which is only true in the first iteration. In subsequent iterations, the measured data will have been used to predict the unknown parameters and hence the two are correlated.

Friswell (1989) calculated the correlation matrix between the measurements and the updated data at each iteration. This matrix was then used to calculate the next estimate of the unknown parameters, thus addressing the above shortcoming.

2.8.3 Updating Methods Using Frequency Response Data

This family of methods uses the measured FRF data directly and optimises a penalty function which is some difference between the initial and target values.

The penalty functions can be defined in terms of two types of error function, namely equation error and output error.

2.8.4 Equation Error Methods

Consider the equation of motion for a viscously damped system:

$$(-\omega^2 [M_A] + i \omega [C_A] + [K_A]) \{X(\omega)\} = \{f(\omega)\} \quad (2.108)$$

where $[M_A]$, $[C_A]$ and $[K_A]$ are the initial mass, viscous damping and stiffness matrices respectively. The above equation can be rewritten in terms of the dynamic stiffness matrix as:

$$[Z_A(\omega)] \{X_A(\omega)\} = \{f_A(\omega)\} \quad (2.109)$$

The equation error method minimises the difference between the measured and calculated forces in the form of :

$$\{\epsilon_{EE}\} = \{f_X(\omega)\} - [Z_A(\omega)] \{X_A(\omega)\} \quad (2.110)$$

A more detailed discussion can be found in papers by Cottin *et al.* (1984), Fritzen (1986), Natke (1988) and Fritzen & Zhu (1991). Assuming that equation error is a nonlinear function of updating parameters $\{p\}$, a penalty function can be defined as:

$$J(\{p\}) = \|\{\epsilon_{EE}\}\|^2 + \sum_{i=1}^N \sum_{j=1}^{N_f} \left| \{f_X(\omega_j)\}_i - [Z_A(\{p\}, \omega)] \{X_A(\omega_j)\}_i \right|^2 \quad (2.111)$$

where N is the total number degrees of freedom and N_f is the number of frequencies in the measurement spectrum.

Let us assume that all degrees of freedom are measured and that the dynamic stiffness matrix can be written as a linear combination of the design parameters:

$$[Z_A(\{p\})] = [Z_A^0] + [Z_A^1] p_1 + [Z_A^2] p_2 + \dots + [Z_A^N] p_N \quad (2.112)$$

In this case, minimising J is equivalent to :

$$[A] \{p\} = \{b\} \quad (2.113)$$

where

$$[A] = \begin{bmatrix} [Z_A^1(\omega_1)] \{X_A(\omega_1)\} & [Z_A^2(\omega_1)] \{X_A(\omega_1)\} & \dots & [Z_A^N(\omega_1)] \{X_A(\omega_1)\} \\ [Z_A^1(\omega_2)] \{X_A(\omega_2)\} & [Z_A^2(\omega_2)] \{X_A(\omega_2)\} & \dots & [Z_A^N(\omega_2)] \{X_A(\omega_2)\} \\ \vdots & \vdots & \vdots & \vdots \\ [Z_A^1(\omega_{N_f})] \{X_A(\omega_{N_f})\} & [Z_A^2(\omega_{N_f})] \{X_A(\omega_{N_f})\} & \dots & [Z_A^N(\omega_{N_f})] \{X_A(\omega_{N_f})\} \end{bmatrix}$$

and

$$\{b\} = \left\{ \begin{array}{l} \{f_X(\omega_1)\} - [Z_A^0(\omega_1)] \{X_A(\omega_1)\} \\ \{f_X(\omega_2)\} - [Z_A^0(\omega_2)] \{X_A(\omega_2)\} \\ \vdots \\ \{f_X(\omega_{N_f})\} - [Z_A^0(\omega_{N_f})] \{X_A(\omega_{N_f})\} \end{array} \right\}$$

The SVD technique can be applied for the solution of (2.113). The major advantage of the equation error method is that the error is a linear function of the spatial parameters so that a rapid convergence can be achieved. The major disadvantages of the method are that all degrees of freedom should be measured and that the parameters are biased due to the presence of measurement noise. However, model reduction may be used to overcome the first problem while unbiased estimates may be obtained by using instrumental variable approach.

Foster & Mottershead (1990) and Link (1990) used static and dynamic reduction to condense the system matrices and to evaluate the equation error. Friswell & Penny (1990) used modal truncation to reduce the state space system matrices and then minimised an equation-error based penalty function.

Cottin *et al.* (1984) showed that with significant amount of noise, results from an equation-error formulation are more biased than those from an output-error formulation. Fritzen (1986) suggested the use of instrumentation variable to eliminate the bias problem by pre-multiplying the equation-error function by a matrix which is uncorrelated with measurement noise. The details of such an unbiased estimate method have been investigated further by Eykhoff (1980) and Ljung (1987) where the choice of the instrument matrix is also discussed. Mottershead & Lees (1987) performed a non-linear optimisation based on a recursive frequency domain filter to update the structural parameters. Mottershead (1988) further developed the technique to include an instrumental variable filter to eliminate bias. Mottershead (1990) and Mottershead & Foster (1991) modified the linear filtering method by using the SVD to find a minimum norm solution.

Larsson & Sas (1991) used a Taylor series for the expansion of the dynamic stiffness matrix, the so-called modified equation approach. They used an exact reduction to overcome the size incompatibility. They introduced an algorithm (Larsson & Sas, 1992b) which was stable up to a cut-off frequency for both large variations in design parameters and for incomplete measured data.

2.8.5 Output Error Methods

For the output error method, the penalty function can be defined as :

$$J(\{p\}) = \|\epsilon_{OE}\|^2 \quad (2.114)$$

where

$$\{\epsilon_{OE}\} = [H_A(\omega)] \{f_A(\omega)\} - \{X_X(\omega)\} \quad (2.115)$$

For this case, a non-linear penalty function should be solved which is prone to convergence problems and may require significant CPU effort.

Lin & Ewins (1990) presented a method that express changes in the receptance matrix as linear functions of the design parameters in the case of complete measured data. They recommended to use the elements of the analytical receptance matrix for missing measured receptances. However, when the measured data are incomplete, their method can be shown to revert to a weight-equation error. Mottershead & Shao (1991) expressed the output error as a first order series in the design parameters. Imregun & Visser (1991) and Imregun *et al.* (1993) generated a set of linear equation in terms of the design parameters based on the experimental and analytical receptance matrices. The use of more frequency points was shown to be useful in improving the condition of the problem.

2.9 Regularisation Technique

The basic idea of a method of regularisation is to replace an ill-posed equation by a nearby well-posed one. Since there is a huge amount of literature on methods for approximate solutions of inverse problems, it is not possible to review all such techniques here. Only a few main themes will be discussed in this section.

2.9.1 Tikhonov Regularisation

Consider an ill-posed equation of the form:

$$[A] \{p\} = \{b\} \quad (2.116)$$

where $[A]$ is a linear, ill-posed operator. A generalised solution to the above equation can be found from:

$$([A]^* [A]) \{p\} = [A]^* \{b\} \quad (2.117)$$

which yields:

$$\{p\} = ([A]^* [A])^{-1} [A]^* \{b\} \quad (2.118)$$

where $[A]^*$ is the adjoint of $[A]$. Since the problem is ill-posed, $([A]^* [A])^{-1}$ is near to singular. Tikhonov's approximation considers the following well-posed problem:

$$\{p\} = ([A]^* [A] + \alpha [I])^{-1} [A]^* \{b\} \quad (2.119)$$

where α is a positive number. Equation (2.119) reverts back to (2.118) for $\alpha = 0$.

Tikhonov's paper, published in 1963, has been seminal for further development of the theory of approximation. Many authors have discussed the optimum choice of the regularisation parameter, α , see for instance Heinz & Neubauer (1987).

2.9.2 Iterative Methods

Iterative methods for solving sets of linear equations are popular because they use relatively simple operations which are performed repeatedly. There are many iterative methods that can be applied to ill-posed problems. One of the simplest on is Landweber-Fridman iteration (Landweber, 1951).

Consider the equation:

$$([A]^* [A]) \{p\} - [A]^* \{b\} = 0 \quad (2.120)$$

The Landweber-Fridman method suggests an iterative solution of the form:

$$\{p_{n+1}\} = \{p_n\} + \beta ([A]^* \{b\} - [A]^* [A]\{p_n\}) \quad (2.121)$$

where β is a positive number. It can be shown that if $0 < \beta < \frac{2}{\lambda_1}$ where λ_1 is the largest eigenvalue of $([A]^* [A])$, then the iteration will converge. The major drawback of the method is its slow convergence. Zhou & Rushforth (1991) and King (1992) applied multigrid ideas adopted from the CFD field to accelerate the convergence. Some applications of the method can be found in Abbiss (1983). In any case, (2.121) can be written as:

$$\{p_{n+1}\} = Q_n([A]^* [A]) [A]^* \{b\} \quad (2.122)$$

where Q_n is an arbitrary polynomial of degree n which must be chosen in order to optimise the iteration. One approach would be to construct a polynomial so that the residual:

$$\| [A] \{p_{n+1}\} - \{b\} \|^2 \quad (2.123)$$

is as small as possible, the solution technique being called the conjugate gradient method. King (1989) provided an in-depth discussion of this particular technique while Kammerer & Nashed (1972), Brakhage (1987) and Louis (1987) discussed its convergence in some detail.

2.9.3 Truncated Singular Value Decomposition (TSVD)

A straightforward approach to computing $\{p\} = [A]^\dagger \{b\}$ is to truncate the corresponding singular decomposition of $[A]$. Therefore the truncation yields a solution for $\{p\}$:

$$\{p\} = \sum_{i=1}^{n_t} \sigma_i^{-1} (\{u_i\}^T \{b\}) \{v_i\} \quad (2.124)$$

where n_t is truncation level and σ_i , $\{u_i\}$ and $\{v_i\}$ are singular values and the orthonormal set of basis vectors from singular value decomposition of $[A]$ respectively. As with any regularisation method for ill-posed problems, the choice of the truncation level in the TSVD method is a delicate matter. Hansen (1987) investigated the TSVD as a means of regularisation and compared it with Tikhonov's work. The truncated SVD method, with the level of truncation chosen by generalised cross validation method, was investigated by Vogel (1986) for data contaminated by white noise error. The convergence rate for the expected value of the square error was obtained under certain assumption on the decay rates of the singular values.

Fregolent (1996) presented an updated model based on the use of the input residual. In order to treat the ill-conditioning, they used a TSVD, the truncation being based on response minimisation. They claimed that such a criterion yielded more reliable results than other truncation selectors, irrespective of the distance between the theoretical and experimental models.

2.9.4 Total Least Square Method

The total least square (TLS) is a method of solving over-determined sets of linear equations of the form:

$$[A]\{p\} = \{b\} \quad (2.125)$$

where both the observation vector $\{b\}$ and the data matrix $[A]$ contain errors. The technique has been discussed by several authors: Madansky (1959) and Golub & Vanloan (1979). In their further work Golub & Vanloan (1980) used a singular value decomposition and obtained a solution by fitting a best subspace to $[[A], \{b\}]$. They also explored the sensitivity of the TLS method as well as its relationship to ordinary least-squares regression. Van Huffel & Vandewalle (1985) presented a geometrical interpretation of the TLS method. They showed that TLS was superior to ordinary LS in system identification and parameter estimation when the measured data were contaminated by noise.

2.9.5 The Maximum Entropy Method

The origin of the maximum entropy method for estimating solution to inverse problems can be traced back to the fundamental work of Boltzmann on statistical mechanics (Boltzmann, 1910). Recently, the maximum entropy idea has been used to regularise solutions of integral equations of the first kind. As in Tikhonov regularisation, the idea is to seek a function which combines the features of a least-squares solution with the regularity of an additional constraint by minimising an augmented least-squares functional.

There is a huge amount of literature on maximum entropy method. Klaus & Smith (1988) showed that for certain Fredholm integral equations of the first kind, the maximum entropy method is stable. Amato & Hughes (1991) compared the results for the Fredholm integral equation obtained both from the maximum entropy method and

from the Tikhonov's regularisation. They showed that, under most circumstances, the maximum entropy method is regular in the sense of Tikhonov. The convergence rate for the entropy-regularised approximation of a Fredholm integral equation of the first kind was addressed by Engl & Landl (1991).

2.10 Concluding Remarks

- In spite of extensive research over the past fifteen years, the state-of-the-art in finite element model is far from maturing and no reliable and generally applicable procedure have been formulated so far.
- While many researchers have reported successful results for different updating algorithms, there are no robust techniques which can handle industrial problems routinely.
- The uniqueness and existence aspects of the updating problems are vital and should be investigated further. In most case studies the solution seems to depend on the selected parameters and constraints as well as the employed updating technique.
- In general, all expansion methods produce reasonable results as long as the measured set of DOFs remains spatially distributed. The Guyan and IRS yield inaccurate results for a poor selection of master DOFs. SEREP expansion produces consistently good results for different distributions of master DOFs. SEREPa, which uses over-expansion, is very sensitive to the selection of the master DOFs but produces better results than SEREP when a good selection of masters is achieved. The relative ranking of the expansion methods is given by O'Callahan & Li (1995) as SEREP, SEREPa, TAM, Dynamic, IRS and Guyan expansion.
- In analytical model validation, it is common practice to convert the complex measured mode shapes into a set of real mode shapes. For significantly-complex

modes, the use of a global transformation matrix can introduce misleading results. However, further improvements can be obtained by tuning the realised modes.

- It seems that sensitivity and FRF-based methods are the most promising updating techniques. Both methods depend largely on the reduction and expansion technique used.
- Many researchers use simulated experimental data to assess their proposed method. Such data are not necessarily a true reflection of the actual situation. However, this avoids additional difficulties which are present in true experimental data, such as experimental and modal analysis errors, the effect of damping and modal complexity.
- In principle, regularisation techniques can be used when the experimental data are contaminated by noise so that a solution which is close enough to an acceptable solution can be obtained. However, many numerical difficulties exist and such techniques should be used with caution.

Chapter 3

FRF Based Model Updating

3.1 Introduction

The use of frequency response functions instead of modal parameters for model updating is relatively recent (Lin & Ewins, 1990; Larsson & Sas, 1992b; Lammens, 1993; Nalitolela, 1993). The approach presents some advantages. Since the FRF is a measured quantity, errors due to modal parameter extraction are avoided. Furthermore, a large amount of data can be used to improve the stability of the updating equations. In other words, the problem can be made overdetermined due to the availability of FRF data at a large number of frequency points, although it is not possible to write down as many independent equations as there are frequency points.

In this Chapter the response function method (RFM), an updating technique using frequency response function data, is investigated. A modified version of this updating technique was recently presented by Larsson & Sas (1992b), the basic algorithm being reviewed in Chapter 2. This approach has two important advantages: FRF approximation for large parameter variation and incomplete measurement data. The effects of some regularisation techniques, such as truncated SVD, total least square solution and minimum entropy regularisation on the accuracy of the results will be addressed in the next chapter.

3.2 Theory

3.2.1 Background

A fundamental difference between various methods of model updating is related to the definition of the residual terms. Some methods define the residual as the difference between the experimental and analytical displacements when the structure is excited by the same harmonic force:

$$\{\epsilon_1(\{p\})\} = \{X_X\} - \{X_A(\{p\})\} \quad (3.1)$$

where $\{p\}$ is the vector of updating parameters. For the analytical system:

$$\{X_A\} = [H_A(\omega)] \{f_A\} \quad (3.2)$$

where $[H_A(\omega)]$ is the receptance FRF matrix. On the other hand, applying a unit force at the j^{th} experimental degree of freedom yields :

$$\{X_X\} = \{H_X\}_j \quad (3.3)$$

where $\{H_X\}_j$ is the j^{th} column of experimental receptance FRF matrix. Substituting (3.3) and (3.2) into (3.1):

$$\{\epsilon_1(\{p\})\} = \{H_X\}_j - [H_A(\{p\})] \{I\}_j = \{H_X\}_j - \{H_A(\{p\})\}_j \quad (3.4)$$

The approach results in a complex-valued residual vector $\{\epsilon_1\}$. For a good correlation at a given frequency point ω , the residual vector $\{\epsilon_1\}$ should be less than a set tolerance or the sum of $\|\{\epsilon_1\}\|$ over a number of frequency points should be a minimum.

Although equation (3.4) is very straightforward, its application is limited by the fact that the elements of matrix $[H_A]$ do not vary smoothly for changes in parameters p_i at any given frequency. In addition, $[H_A]$ is discontinuous near resonances particularly for low damping system.

The above remarks lead us to a different way of formulating the problem. The residual instead of being the difference between the experimental and analytical displacements, can also be defined as the difference between the forces acting on the real structure, $\{f_X\}$, and those predicted by the analytical model at the same frequency:

$$\{\epsilon_2(\{p\})\} = \{f_X\} - \{f_A(\{p\})\} \quad (3.5)$$

Since $\{f_A\} = [Z_A]\{X_A\}$ then:

$$\{\epsilon_2(\{p\})\} = \{f_X\} - [Z_A(\{p\})]\{X_A\} \quad (3.6)$$

where

$$[Z_A] = [K_A] + i[D_A] + i\omega[C_A] - \omega^2[M_A]$$

$[K_A]$, $[D_A]$, $[C_A]$ and $[M_A]$ being the stiffness, structural damping, viscous damping and mass matrices respectively.

By applying a unit load at j^{th} degree of freedom and using equation (3.3):

$$\{\epsilon_2(\{p\})\} = \{I\}_j - [Z_A(\{p\})]\{H_X\}_j \quad (3.7)$$

Equation (3.7) represents a set of non-linear equations, whose solution for $\{p\} = \{p_1, p_2, \dots\}^T$ may or may not exist. Assuming that the solution exists and the

components of matrix $[Z_A]$ behave in an almost linear fashion, matrix $[Z_A]$ can be linearised by a truncated Taylor series:

$$[Z_A(\{p\})] = [Z_A^0] + \sum_i \frac{\partial[Z_A]}{\partial p_i} \Delta p_i + O(\Delta p_i)^2 \quad (3.8)$$

By substituting equation (3.8) into equation (3.7) and setting the residual vector $\{\epsilon_2\}$ to null vector, one obtains:

$$\{I\}_j - [Z_A^0]\{H_X\}_j = \left(\sum_i \frac{\partial[Z_A]}{\partial p_i} \Delta p_i\right) \{H_X\}_j \quad (3.9)$$

3.2.2 Incomplete Data and Dynamic Reduction

The quantity $\{H_X\}$ appears on both sides of equation (3.9). On the left hand side, the incompleteness of $\{H_X\}$ is not a problem but a full vector of $\{H_X\}$ is required on the right hand side. One way of dealing with incompleteness is the expansion of measured data. Many attempts have been made for the expansion of measured data but experience shows that none have been particularly satisfactory.

An alternative is to reduce the size of analytical model by using a matrix condensation technique, many such techniques being discussed in Chapter 2. An exact dynamic condensation will be considered here. The proposed algorithm is effective provided that the components of the reduced impedance matrix, $[Z_A^{Red}]$, are well approximated by linear functions of the updating parameters.

Starting with the following identity:

$$[Z][H] = [I] \quad (3.10)$$

and partitioning the matrices $[Z]$ and $[H]$ into measured, n , and unmeasured, s , degrees of freedom, one obtains:

$$\begin{bmatrix} [Z_{nn}] & [Z_{ns}] \\ [Z_{sn}] & [Z_{ss}] \end{bmatrix} \begin{bmatrix} [H_{nn}] & [H_{ns}] \\ [H_{sn}] & [H_{ss}] \end{bmatrix} = \begin{bmatrix} [I_{nn}] & 0 \\ 0 & [I_{ss}] \end{bmatrix} \quad (3.11)$$

The first column of (3.11) can be written explicitly as:

$$\begin{aligned} [Z_{nn}] [H_{nn}] + [Z_{ns}] [H_{sn}] &= [I_{nn}] \\ [Z_{sn}] [H_{nn}] + [Z_{ss}] [H_{sn}] &= 0 \end{aligned} \quad (3.12)$$

By eliminating $[H_{sn}]$ from (3.12), one obtains:

$$\left([Z_{nn}] - [Z_{ns}] [Z_{ss}]^{-1} [Z_{sn}] \right) [H_{nn}] = [I_{nn}] \quad (3.13)$$

Post-multiplying (3.13) by $[H_{nn}]^{-1}$:

$$[H_{nn}]^{-1} = [Z_{nn}] - [Z_{ns}] [Z_{ss}]^{-1} [Z_{sn}]$$

If we define $[Z_A^{Red}]$ as the inverse of H_{nn} , then:

$$[Z_A^{Red}] = [Z_{nn}] - [Z_{ns}] [Z_{ss}]^{-1} [Z_{sn}] \quad (3.14)$$

3.2.3 Formulation of FRF Based Model Updating

Based on the exact dynamically-reduced dynamic stiffness matrix, it is possible to avoid the introduction of additional approximations which detract from the solution of the updating equations. The approach here is based on the following observations:

- (i) The dynamically-reduced system is exact in the sense that it has identical dynamic properties as the original system.

- (ii) The reduced model contains the information in terms of the reduced degrees of freedom only.
- (iii) The problem can be defined in terms of a well-behaved mathematical function.

Starting with (3.7), a new formulation can be expressed as (Chargin & Miura, 1993):

$$\{\epsilon_2(\{p\})\} = \{I\}_j - [Z_A^{Red}(\{p\})] \{H_X\}_j \quad (3.15)$$

By expanding $[Z_A^{Red}]$ in (3.15) via a Taylor series and setting the residual vector $\{\epsilon_2\}$ to the null vector:

$$\{I\}_j - [Z_A^{Red}]^0 \{H_X\}_j = \left(\sum_i \frac{\partial [Z_A^{Red}]}{\partial p_i} \Delta p_i \right) \{H_X\}_j \quad (3.16)$$

Now, the aim is to find a relationship between the derivatives of matrices $[Z]$ and $[H]$, as well as those of $[Z^{Red}]$ and $[H^{Red}]$. By considering the identity $[H_A] [Z_A] = [I]$ and calculating its partial derivative with respect to p_i , one can get:

$$\frac{\partial [H_A]}{\partial p_i} [Z_A] + [H_A] \frac{\partial [Z_A]}{\partial p_i} = 0$$

or

$$\frac{\partial [H_A]}{\partial p_i} = -[H_A] \frac{\partial [Z_A]}{\partial p_i} [H_A] \quad (3.17)$$

Similarly for the derivative of $[Z]$:

$$\frac{\partial [Z_A]}{\partial p_i} = -[Z_A] \frac{\partial [H_A]}{\partial p_i} [Z_A] \quad (3.18)$$

Using equations (3.17) and (3.18) for $[Z_A^{Red}]$, the following exact expression for the derivative of $[Z_A^{Red}]$ with respect to p_i can be obtained (Larsson & Sas, 1992b):

$$\frac{\partial[Z_A^{Red}]}{\partial p_i} = [Z_A^{Red}] \left[[H_A] \frac{\partial[Z_A]}{\partial p_i} [H_A] \right]^{Red} [Z_A^{Red}] \quad (3.19)$$

inserting equation (3.19) into equation (3.16), one obtains:

$$\left(\sum_i [Z_A^{Red}] \left[[H_A] \frac{\partial[Z_A]}{\partial p_i} [H_A] \right]^{Red} [Z_A^{Red}] \Delta p_i \right) \{H_X\}_j = \{I\}_j - [Z_A^{Red}]^0 \{H_X\}_j \quad j = 1, \dots, n \quad (3.20)$$

where

$$[Z_A] = ([K_A] + i[D_A]) + i\omega[C_A] - \omega^2[M_A]$$

and $[D_A]$ and $[C_A]$ are analytical matrices of structural and viscous damping respectively, thus:

$$\frac{\partial[Z_A]}{\partial p_i} = \frac{\partial[K_A]}{\partial p_i} + i \frac{\partial[D_A]}{\partial p_i} + i\omega \frac{\partial[C_A]}{\partial p_i} - \omega^2 \frac{\partial[M_A]}{\partial p_i}$$

If we assume that the total number of unknown parameters is Q , then equation (3.20) can be rewritten in matrix form as:

$$\begin{bmatrix} \frac{\partial[Z_A^{Red}]}{\partial p_1} \{H_X\}_1 & \frac{\partial[Z_A^{Red}]}{\partial p_2} \{H_X\}_1 & \dots & \frac{\partial[Z_A^{Red}]}{\partial p_Q} \{H_X\}_1 \\ \frac{\partial[Z_A^{Red}]}{\partial p_1} \{H_X\}_2 & \frac{\partial[Z_A^{Red}]}{\partial p_2} \{H_X\}_2 & \dots & \frac{\partial[Z_A^{Red}]}{\partial p_Q} \{H_X\}_2 \\ \vdots & \vdots & \vdots & \vdots \\ \frac{\partial[Z_A^{Red}]}{\partial p_1} \{H_X\}_J & \frac{\partial[Z_A^{Red}]}{\partial p_2} \{H_X\}_J & \dots & \frac{\partial[Z_A^{Red}]}{\partial p_Q} \{H_X\}_J \end{bmatrix} \begin{Bmatrix} \Delta p_1 \\ \Delta p_2 \\ \vdots \\ \Delta p_Q \end{Bmatrix} =$$

$$\left\{ \begin{array}{l} \{I\}_1 - [Z_A^{Red}]^0 \{H_X\}_1 \\ \{I\}_2 - [Z_A^{Red}]^0 \{H_X\}_2 \\ \vdots \\ \{I\}_J - [Z_A^{Red}]^0 \{H_X\}_J \end{array} \right\} \quad (3.21)$$

Where J is the number of load cases. It should be mentioned that the number of independent load cases, J , is a subset of number of degrees of freedom of which the n FRFs are measured (Chargin & Miura, 1993).

Taking an undamped structure modelled with N degrees of freedom yields a maximum of $N(N + 1)$ unknowns when both the mass and stiffness matrices are symmetrical. Assuming that a **full** column of the FRF matrix can be measured for each of the J load cases, the number of equations at each frequency point becomes $N \times J$. If N_f defines the number of frequency points, then the total number of equations is equal to $N \times J \times N_f$. Hence, the minimum requirement for the solution is the knowledge of any column of the FRF matrix at $\frac{N+1}{J}$ frequency points since there are $N(N + 1)$ unknowns. It should also be noted that the problem can be made overdetermined since, in general, there are many frequency points within the range of interest.

Although many frequency points are available within the frequency range of interest, it does not mean that it is possible to write down as many independent equations as frequency points. It seems that the updating frequencies that produce independent equations and their actual position are case dependent, the number of measured modes in the frequency range being the most important factor.

In reality, FRFs are measured at n degrees of freedom only, such that $n \ll N$. Therefore, the total number of responses available will be $n \times J \times N_f$. So, the minimum requirement for the solution becomes the knowledge of any column of the FRF matrix at $\frac{N \times (N+1)}{n \times J \times N_f}$ frequency points.

3.2.4 Error Modelling

In the case of coordinate incompleteness, the solution of the updating equations is non-unique. Additional constraints, taking into account physical connectivities, can be introduced. For instance, forcing the zero elements to remain zero in order to limit the number of possible solutions is an obvious route to take.

Further constraints can be introduced by considering the mass, stiffness and damping matrices of individual finite elements. Let us assume that modelling errors can be expressed as linear combination of the individual element mass, stiffness and damping matrices:

$$\begin{aligned}
 [M_A] &= \sum_{i=1}^{N_m} (1 + p_i^m) [M^e]_i \\
 [K_A] &= \sum_{i=1}^{N_k} (1 + p_i^k) [K^e]_i \\
 [C_A] &= \sum_{i=1}^{N_c} (1 + p_i^c) [C^e]_i \\
 [D_A] &= \sum_{i=1}^{N_d} (1 + p_i^d) [D^e]_i
 \end{aligned} \tag{3.22}$$

Referring to equation (3.21), the p-values derivatives of the receptance matrix and of the reduced receptance matrix can be calculated as:

$$\begin{aligned}
 \frac{\partial [Z_A]}{\partial p_i^m} &= -\omega^2 [M^e]_i & i = 1, \dots, N_m \\
 \frac{\partial [Z_A]}{\partial p_i^k} &= [K^e]_i & i = 1, \dots, N_k \\
 \frac{\partial [Z_A]}{\partial p_i^c} &= i \omega [C^e]_i & i = 1, \dots, N_c \\
 \frac{\partial [Z_A]}{\partial p_i^d} &= i [D^e]_i & i = 1, \dots, N_d
 \end{aligned} \tag{3.23}$$

$$\begin{aligned}
\frac{\partial [Z_A^{Red}]}{\partial p_i^m} &= -\omega^2 [Z_A^{Red}] ([H_A][M^e]_i[H_A])^{Red} [Z_A^{Red}] & i = 1, \dots, N_m \\
\frac{\partial [Z_A^{Red}]}{\partial p_i^k} &= [Z_A^{Red}] ([H_A][K^e]_i[H_A])^{Red} [Z_A^{Red}] & i = 1, \dots, N_k \\
\frac{\partial [Z_A^{Red}]}{\partial p_i^c} &= i\omega [Z_A^{Red}] ([H_A][C^e]_i[H_A])^{Red} [Z_A^{Red}] & i = 1, \dots, N_c \\
\frac{\partial [Z_A^{Red}]}{\partial p_i^d} &= i [Z_A^{Red}] ([H_A][D^e]_i[H_A])^{Red} [Z_A^{Red}] & i = 1, \dots, N_d
\end{aligned} \tag{3.24}$$

Thus, for linear modelling errors, one can write equation (3.21) as:

$$[R(\omega)]_{(n \times J \times N_f) \times (N_m + N_k + N_c + N_d)} \{p\}_{(N_m + N_k + N_c + N_d) \times 1} = \{q\}_{(n \times J \times N_f) \times 1} \tag{3.25}$$

where $\{p\} = \{p_1^m, \dots, p_{N_m}^m, p_1^k, \dots, p_{N_k}^k, p_1^c, \dots, p_{N_c}^c, p_1^d, \dots, p_{N_d}^d\}$. As the p-values are always real, equation (3.25) can be separated into its real and imaginary parts and the resulting equation re-arranged as:

$$\begin{bmatrix} Re[R(\omega)] \\ Im[R(\omega)] \end{bmatrix} \{p\} = \begin{Bmatrix} Re\{q\} \\ Im\{q\} \end{Bmatrix}$$

or in short form as:

$$[A(\omega)]_{(2 \times n \times J \times N_f) \times (N_m + N_k + N_c + N_d)} \{p\}_{(N_m + N_k + N_c + N_d) \times 1} = \{b\}_{(2 \times n \times J \times N_f) \times 1} \tag{3.26}$$

The matrix equation (3.26) is inverted by SVD to calculate the unknown vector $\{p\}$ so as to obtain an updated estimate of the stiffness, mass and damping matrices for the next iteration. The process continues until the convergence of vector $\{p\}$.

3.3 Case 1: 10 Degree-of-Freedom System

A 10-DOF lumped parameter system, shown in Fig. (3.1), was employed to investigate the use of the reduced dynamic stiffness matrix technique of previous section.

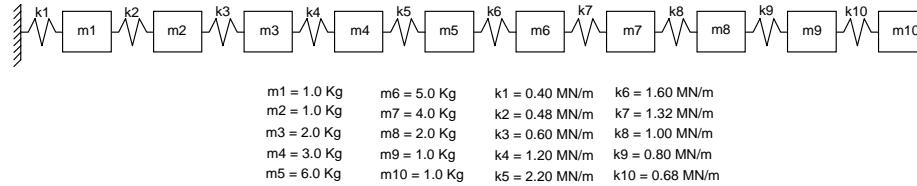


Figure 3.1: The 10 DOF system

The experimental model was provided by a version of the basic system in which there was 10% and 25% decrease in the values of m_1 and m_4 and 15%, 10%, 30% and 10% increase in those of m_7 , k_3 , k_5 and k_9 respectively. A typical receptance FRF, α_{55} , computed for both models over the 20-200 Hz frequency range is plotted in Fig. (3.2).

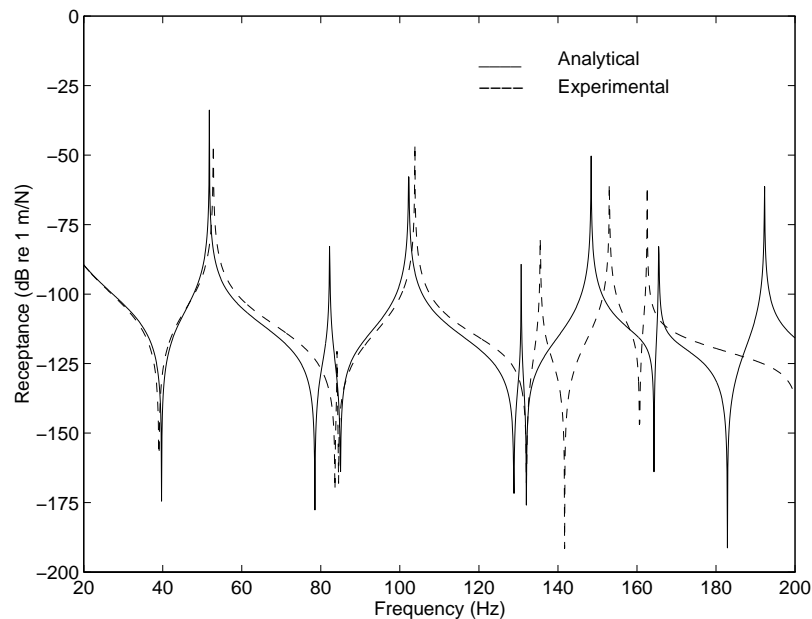


Figure 3.2: Receptance FRF, α_{55} , obtained from the experimental and analytical models of 10 DOF system

3.3.1 Updating Using Complete Experimental Data

At first it was assumed that all required FRFs were measured. One load case and ten frequency points were selected in the range of 20-200 Hz, namely 20, 30, 60, 80, 90, 110, 120, 150, 170 and 180 Hz. The selection of the frequency points is a very important step: if a point is selected in the immediate vicinity of a resonance, the inversion of matrix $[A]$ becomes prone to ill-conditioning. In this first case, the frequency response functions were updated correctly in the sense that they matched those of experimental model. The receptance FRF, α_{55} , obtained from the updated analytical model is shown in Fig. (3.3) together with the measured receptance. Both curves are seen to be identical within the frequency range of interest and beyond.

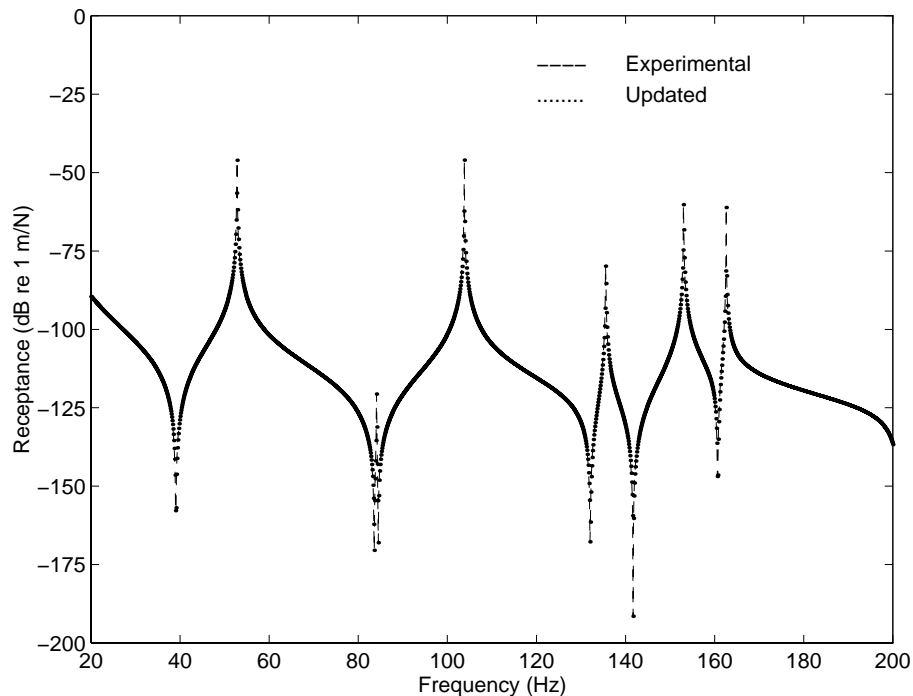


Figure 3.3: Receptance FRF, α_{55} , obtained from the experimental and updated analytical models of 10 DOF system (complete experimental model)

3.3.2 Using Incomplete Experimental Data

The incomplete experimental model consisted of 5 FRFs only, these being measured at coordinates 1, 4, 6, 7 and 10. Ten points were selected from the frequency range 20-80 Hz. The convergence criterion was defined as $\|\{p\}\| < 10^{-4}$ and convergence was obtained after 11 iterations. The solution path was also examined by selecting different sets of frequency points from the same range. In all cases, the FRFs of the updated system were found to be identical to the experimental ones (Fig. 3.4).

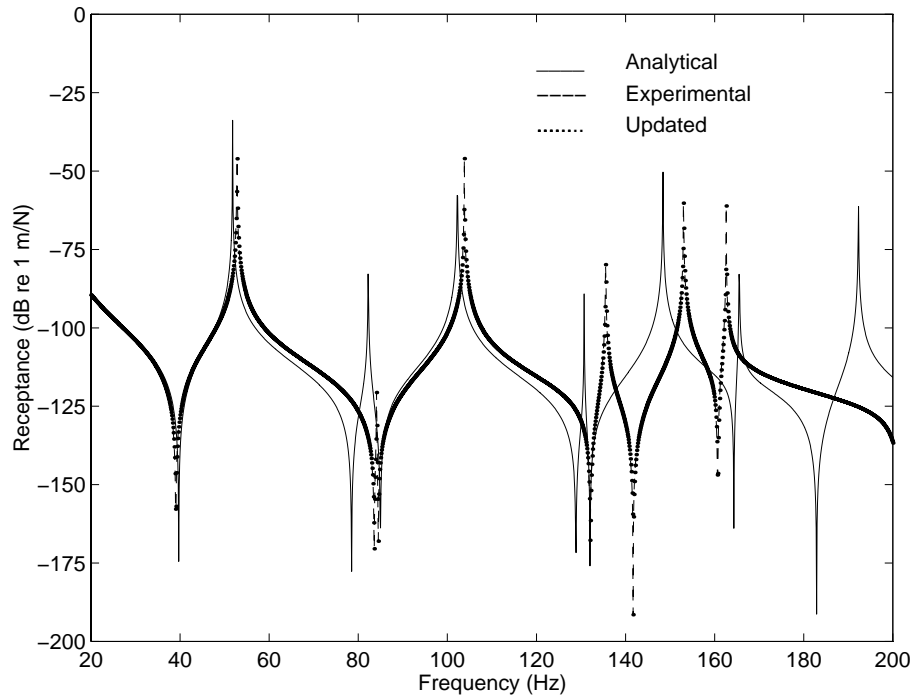
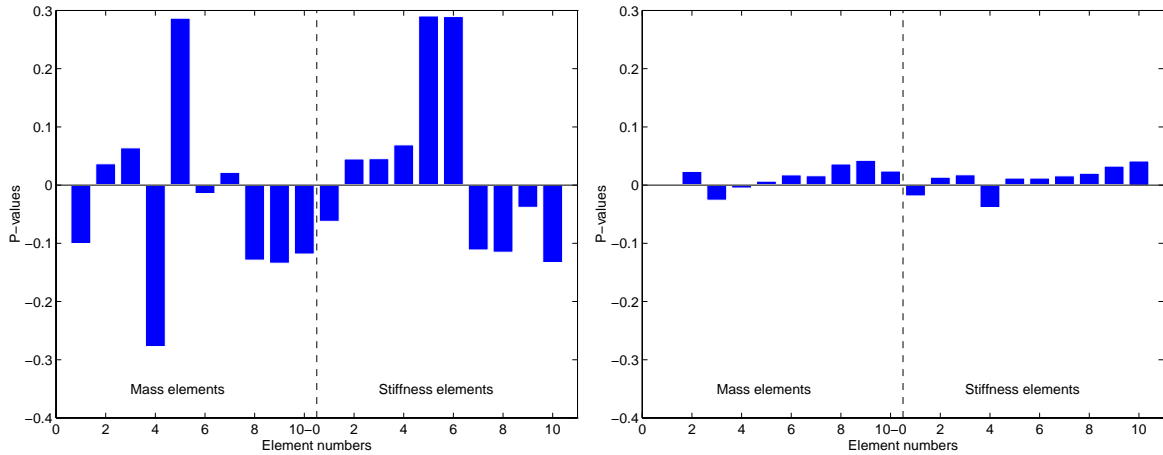


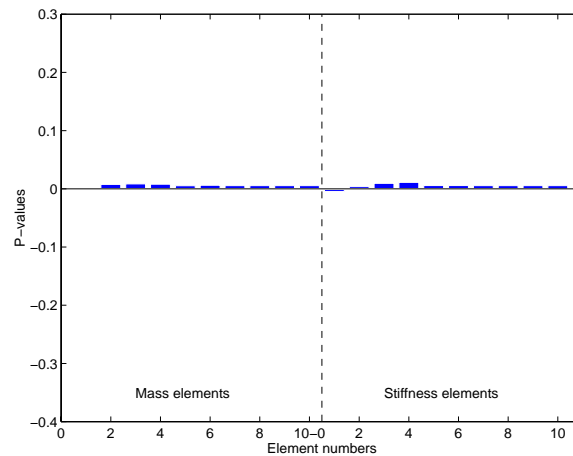
Figure 3.4: Receptance FRF, α_{55} , obtained from the experimental, analytical and updated analytical models of 10 DOF system (incomplete experimental model)

Although incomplete measured data were used, the solution seemed to be unique. Figs (3.5-a), (3.5-b) and (3.5-c) show convergence towards this unique solution after 1, 2 and 3 iterations respectively. This reduced dynamic stiffness matrix algorithm seems to be more stable than the method used by Visser (1992) in a similar study.



(a) p-values after 1 iteration

(b) p-values after 2 iterations



(c) p-values after 3 iterations

Figure 3.5: Convergence toward unique solution
(All plots have the same scale)

3.3.3 Using FRF Data Polluted by Noise

At this stage, it should be noted that there are no realistic models for the introduction of simulated experimental noise into analytically-generated data. Basically, experimental noise consists of correlated and uncorrelated noise, the former comprising errors arising from signal conditioning, transduction, signal-processing and the interaction of the measurement system with the structure. The latter includes errors due to thermal noise in electronic circuits as well as those due to external disturbances.

In the absence of a more realistic representation, a simple frequency-domain model with uniformly-distributed noise will be used here:

$$H'_{ij} = (1 + \sigma\%) H_{ij} \quad (3.27)$$

where H and H' are the noise-free and polluted values of the FRF. σ is a random number that varies between zero and maximum expected error, typically 2% – 5% depending on the type of structure that is being tested. The experimental data in Section (3.3.2) were polluted by adding noise between 1% to 10%. The number of frequency points was increased to 25 to compensate for the expected adverse effects of random noise. The calculations were repeated with different set of frequency points in order to check the repeatability of the solution. Although, good agreement was reached at the FRF level, it was observed that the updated model was not unique. Fig. (3.6) shows the receptance, α_{55} , computed for analytical, measured and updated models when there is 10% noise in the experimental data.

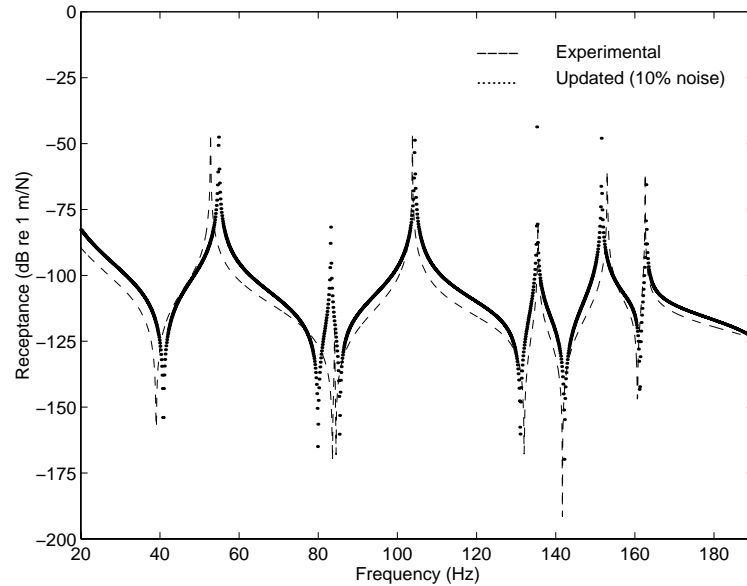


Figure 3.6: Receptance FRF, α_{55} , obtained from the experimental and updated analytical models of 10 DOF system (Incomplete experimental model with 10% noise)

3.4 Case 2: 3D Bay Structure

The second example was based on a three dimensional free-free frame structure which is called 3D Bay structure. The structure was chosen to be representative but simple. It was modelled using twenty 12-DOF 3D beam elements. The material properties were modulus elasticity of $207 \times 10^9 \text{ N/m}^2$ and mass density of 7850 Kg/m^3 . All beams have a rectangular cross section with a width of 10cm and height of 1cm. Four models were created:

- 1- Model FE1 has 10 elements for which the Young's modulus was increased by 8 %.
- 2- Model FE2 has 8 elements for which the X and Y moments of inertia were increased by 30%.

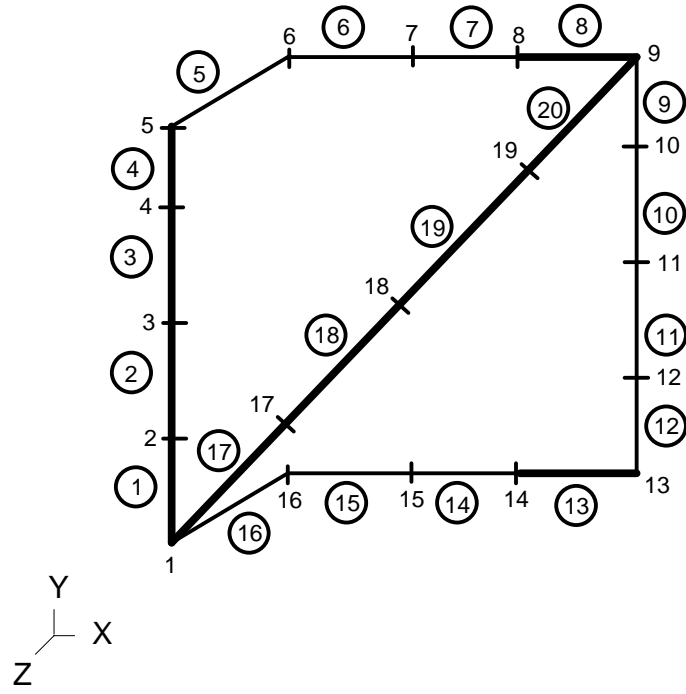


Figure 3.7: Model FE1

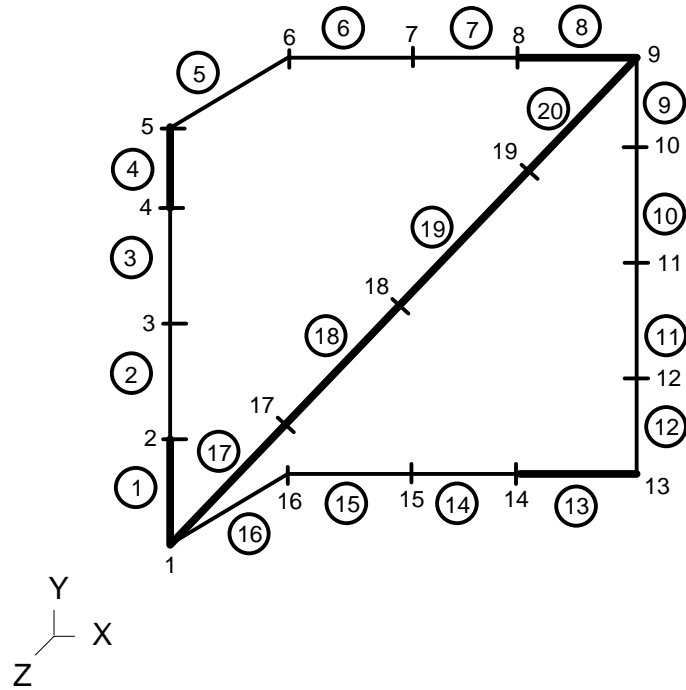


Figure 3.8: Model FE2

3- Model X1 contains no errors and was used to generate the simulated experimental data.

4- Model X2 is the same as model X1 but its mesh is double in size.

Models FE1 and FE2 are shown in Figs. (3.7) and (3.8), the bold lines indicating those elements that contain the errors.

A typical FRF, exemplified here by receptance α_{33} , is plotted in Fig. (3.9) for models FE1 and X1.

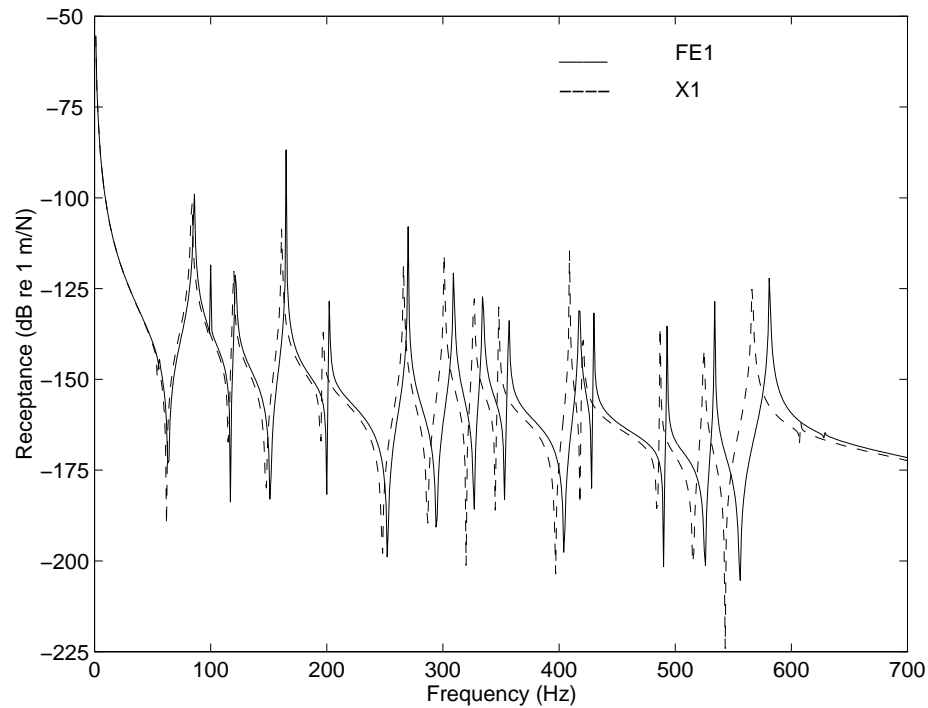


Figure 3.9: Receptance FRF, α_{33} , obtained from experimental (X1) and analytical (FE1) models

3.4.1 Noise-free Experimental Data - FE1 Vs X1

Two initial cases were carried out using noise-free data. In the first case, all elements of the receptance vector (rotations as well as translations) were assumed to be known while in the second case it was assumed that measurement were made only in X, Y and Z directions at node 1 plus in the Z direction at nodes 5, 7, 9, 11, 13, 15 and 18. For this second case the correspondence factor, or the ratio of the number of measured DOFs to the total number of DOFs is 8.7%.

By using 10 frequency points in the range of interest and 10 measured coordinates, the number of rows in matrix $[A]$ is 100, while the number of unknowns is 40 since there are 2 unknowns per element. The first case converged in 2 iterations only while the second one required 5 iterations for convergence. The p-values for the second case are shown in Fig. (3.10).

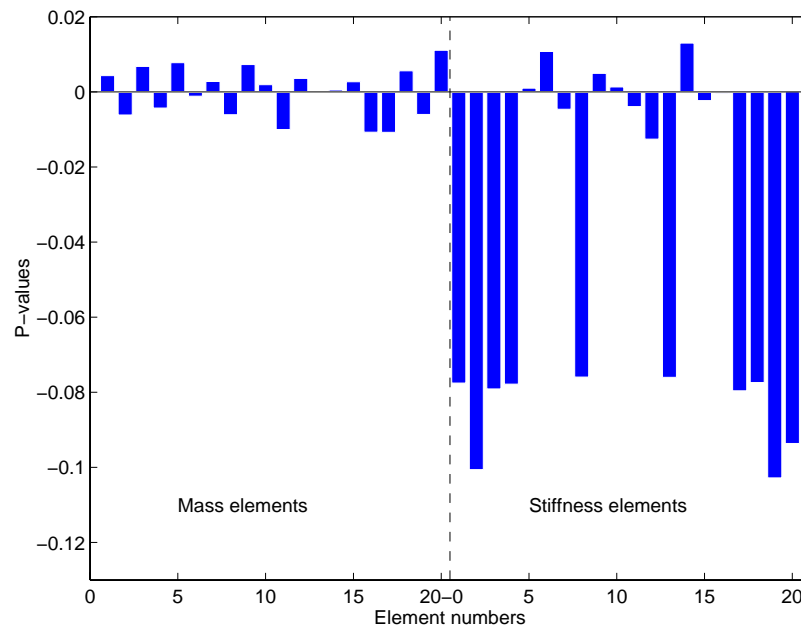


Figure 3.10: p-values for the case of 10 measured coordinates

Since the errors are linear combinations of individual finite elements, the dynamic stiff-

ness matrix is a linear function of p-values for the complete measured data. Therefore, it is expected to have a unique solution in the first case. In the second case only 9 out of 114 DOFs were known. Thus, the reduced dynamic stiffness matrix is not a linear function of p-values anymore and the uniqueness of the solution cannot be guaranteed. It is also noticeable that in the second case the model was corrected using a receptance column for excitation in Z direction as well as X and Y directions. In this example, no improvement were achieved for excitation in just Z direction because in a simple beam model the axial and lateral variation are decoupled.

3.4.2 Noisy Experimental Data - FE1 vs X1

In the case of incomplete FRF data with added noise, the solution is not unique and different sets of p-values can be obtained for different sets of frequency points. The adverse effects of coordinate incompleteness and noise can be partly offset by choosing more frequency points than the required minimum. However, there is a cut-off frequency above which the linear approximation in equation (3.16) is not valid anymore and causes the divergence of the solution. Also by adding more frequency points, the CPU time for each run will increase. Nevertheless, updated models obtained from FRF data with .5% and 1% random noise showed a marked improvement over the original model (Fig. 3.11). Noise levels of more than 1% led to the instability of the updating algorithm and no solution was found. This matter will be discussed in some detail in Chapter 5.

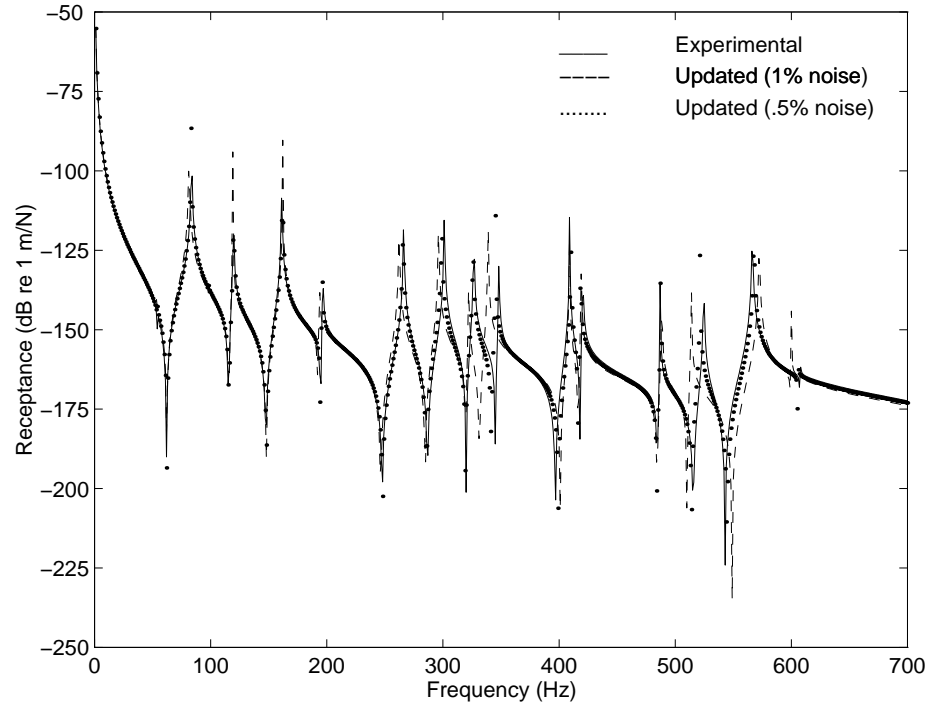


Figure 3.11: Receptance FRF, α_{33} , obtained from experimental and updated models with .5% and 1% noise levels

3.4.3 Updating of FE2 vs X1

In this model, the X and Y moments of inertia for eight elements were increased by 30%. These changes affect both the mass and stiffness matrices and the errors are no longer linear combinations of the individual finite elements. Consequently, the updating solution was not unique and different for each frequency points set. Another reason for non-uniqueness is due to the fact that the amount of error for each element is large (30%) so that a first-order approximation is not accurate enough.

3.4.4 Updating of FE1 vs X2

In the previous case studies, it was assumed that there was a one-to-one correspondence between the theoretical and experimental models, a feature which cannot be

achieved in practice. In other words, the fact that models FE1, FE2 and X1 were discretised using the same mesh not only simplifies the problem of model updating significantly, but also the situation is not all representative of the real engineering problem where the errors are not explicitly present in the model. After some deliberation, it was decided to update Model FE1 using Model X2 which has double the mesh size of X1. In spite of using the complete FRF vector obtained from X2 (target model), the solution diverged and no improvements were obtained in this case. During the first few iterations, p-values of -1.0 were obtained, implying that the corresponding element should be deleted from the updated matrices, resulting in numerical instability and divergence. The problem could not be cured by selecting different sets of frequency points, a fact which indicates that the discretisation errors cannot be expressed as linear combinations of the individual element mass, stiffness matrices. This observation has far reaching implications in FE model updating as it is unlikely that discretisation differences between the two models will ever be resolved.

3.5 Computational Aspects of the Method

3.5.1 Frequency Range Considerations

As mentioned before, the force-based residual is a function of $[Z_A(\{p\})]$ or $[Z_A(\{p\})]^{Red}$, the former for complete and the latter for incomplete systems respectively. The analytical dynamic stiffness matrix for an undamped structure at a particular frequency ω , can be written as:

$$[Z_A(\{p\})] = [K_A(\{p\})] - \omega^2 [M_A(\{p\})] \quad (3.28)$$

where the vector $\{p\}$ contains the updating parameters. In most cases, the elements of $[Z_A]$ are smooth functions of the updating parameters. For instance, Fig. (3.12) shows a typical element, here Z_{33} , of the dynamic stiffness matrix for model FE1

of the Bay structure. Fig. (3.12b) shows the variation of many such curves with a typical design variable, here the change in the stiffness of element 13.

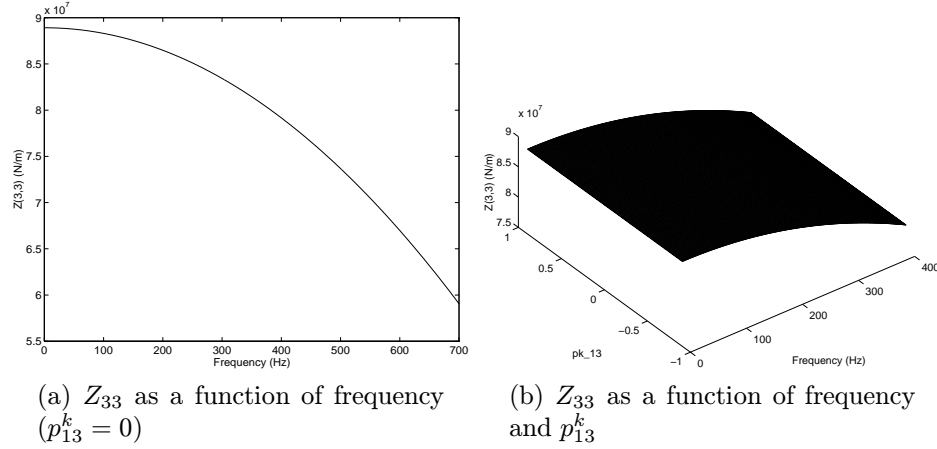


Figure 3.12: Component Z_{33} of the dynamic stiffness matrix of model FE1

As expected, the elements of the dynamic stiffness matrix are smooth functions of frequency for a particular vector $\{p\}$ of updating variables. As long as the changes in these parameters remain physically acceptable, the elements will keep their smooth behaviour, a feature that justifies the linearisation of equation (3.8). The same justification is also necessary for the reduced dynamic stiffness matrix. Fig. (3.13) shows element Z_{33} in the same format as Fig. (3.12), but this time for the reduced dynamic stiffness matrix resulting from incomplete measurements, the reduction being that of Section (3.4.1). In this case, the co-ordinate reduction ratio is 10/114 and significant discontinuities are apparent from Fig. (3.13).

If the stiffness, damping and mass matrices are smooth functions of the updating parameters, the only singularities will be due to $[Z_{ss}]^{-1}$ in (3.14). Matrix $[Z_{ss}]$ can be viewed as the impedance matrix of a structure which is obtained by grounding all n measured degrees of freedom of the main structure. Assuming that the structure is undamped, the natural frequencies of this partially-grounded structure can be found as, $\omega_{R_1}, \omega_{R_2}, \dots, \omega_{R_s}$. A typical element of matrix $[Z_{ss}]^{-1}$ can then be written as:

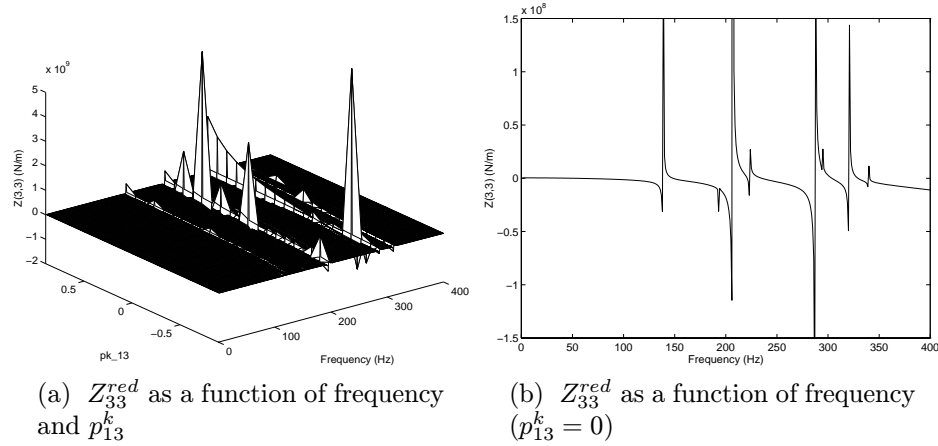


Figure 3.13: Component Z_{33}^{red} of the reduced dynamic stiffness matrix of model FE1

$$(\alpha_{ss})_{ij} = \frac{A(\omega)}{(\omega_{R_1}^2 - \omega^2)(\omega_{R_2}^2 - \omega^2) \cdots (\omega_{R_s}^2 - \omega^2)} \quad (3.29)$$

From equation (3.29), it is obvious that the reduced impedance matrix is singular when the excitation frequency ω is near one of the natural frequencies of the partially grounded structure. In other words, in such situations the partially grounded structure cannot be assumed to yield a smooth $[Z^{Red}]$.

The above discussion is important when selecting the range of the updating frequencies. Larsson & Sas (1992b) suggest using the first natural frequency of the partially grounded structure as the upper bound. However, this criterion is too restrictive and may prevent the consideration of practical uses. The useful range of excitation frequencies is not necessarily limited by the first frequency of the partially-grounded structure, but it is difficult to draw any general conclusions for finding a reduced impedance matrix whose elements are smooth functions of both the excitation frequencies and the updating parameters. Further research is recommended to establish guidelines for the calculation of a cut-off frequency or for the avoidance of discontinuities.

3.5.2 Noise Sensitivity Reduction

Two types residuals will be used for reducing the sensitivity of the updating formulation to experimental noise:

(i) Receptance residue

$$\{\epsilon_1(\{p\}, \omega)\} = \{H_X(\omega)\}_j - \{H_A(\{p\}, \omega)\}_j \quad (3.30)$$

The receptance residue is based on minimising the distance between the experimental and analytical receptance values at selected frequencies. The corresponding cost function, denoted by $J_1(\{p\})$ can be written as:

$$\text{Min } J_1(\{p\}) = \sum_{i=1}^{N_f} \left(\frac{\|\{\epsilon_1(\{p\}, \omega_i)\}\|^2}{\|\{H_X(\omega_i)\}\|^2} \right) \quad (3.31)$$

The minimisation of the receptance residue is one of the most straightforward ways to use the experimental data directly. However, as discussed earlier, the disadvantages are the non-smoothness of analytical receptances as a functions of the updating parameters and the excitation-frequency. Thus, the linearisation assumption of (3.8) is not always applicable and the algorithm may become unstable. Convergence towards local minima and/or divergence are very likely to happen during the minimisation process.

(ii) Force-balance residue

$$\{\epsilon_2(\{p\}, \omega)\} = \{I\}_j - [Z_A(\{p\}, \omega)]^{Red} \{H_X(\omega)\}_j \quad (3.32)$$

The minimisation of the force balance residue is not as direct as that of the receptance residue. The corresponding cost function, denoted by $J_2(\{p\})$ can be written as:

$$\text{Min } J_2(\{p\}) = \sum_{i=1}^{N_f} \left(\frac{\|\{\epsilon_2(\{p\}, \omega_i)\}\|^2}{\|\{H_X(\omega_i)\}\|^2} \right) \quad (3.33)$$

This minimisation is more likely to be stable. However, convergence cannot be guaranteed and divergence and/or convergence towards local minima is still possible. Fig. (3.14) shows typical values of the cost function J_2 which are obtained by varying two out of forty p_i parameters, namely the stiffness of the first and 8th elements (p_1^k and p_8^k) in the second example of Section (3.4.1).

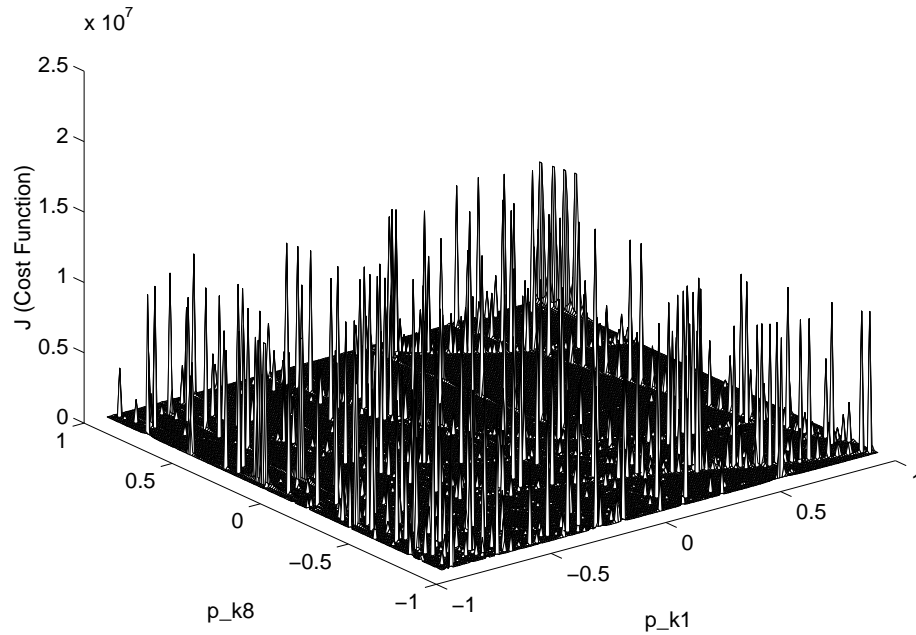
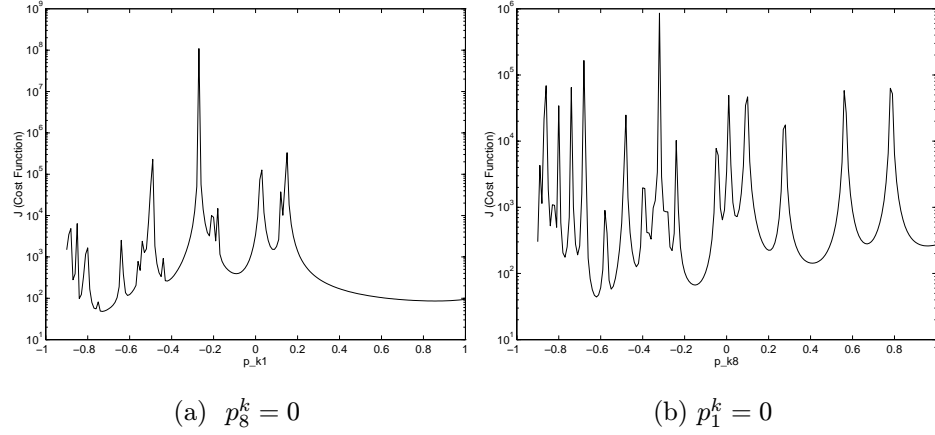


Figure 3.14: Variable of the cost function J_2 for $p_1^k \in [-.9, .9]$ and $p_8^k \in [-.9, .9]$

The importance of this observation is that, around resonance, a small change in the updating parameters can lead to very large amplitude differences between the measured and predicted receptances. It is also evident that the radius of convergence based on (3.33) is usually very small and perhaps even unstable for some applications. Figs. (3.15a & b), which illustrate the behaviour of J_2 for a specific test case, show this point clearly.

Figure 3.15: Cost function J_2

The minimisation of the force-balance residue is also prone to numerical problems since equation (3.32) is inherently ill-conditioned. $\{\epsilon_2(\{p\}, \omega)\}$ is a vector of small-valued elements. As a consequence, the J_2 cost function is very sensitive to measurement errors in $\{H_X\}_j$ and leads to biased parameters. Thus, it is recommended to weight $\{\epsilon_2(\{p\}, \omega)\}$ by pre-multiplying it by the dynamic flexibility matrix of the analytical model:

$$\{\tilde{\epsilon}_2\} = [H_A^0]^{Red} \{\epsilon_2\} \quad (3.34)$$

or

$$\{\tilde{\epsilon}_2\} = \{H_A^0\}_j - [H_A^0]^{Red} [Z_A]^{Red} \{H_X\}_j \quad (3.35)$$

Expanding $[Z_A]^{Red}$ using Taylor series yields:

$$\{\tilde{\epsilon}_2\} = \{H_A^0\}_j - [H_A^0]^{Red} \left([Z_A^0] + \sum_i \frac{\partial [Z_A]^{Red}}{\partial p_i} \Delta p_i \right) \{H_X\}_j \quad (3.36)$$

For maximum correlation at a given frequency point, the residue should be equal to zero:

$$\left([H_A^0] \sum_i \frac{\partial [Z_A]^{Red}}{\partial p_i} \Delta p_i \right) \{H_X\}_j = \{H_A^0\}_j - \{H_X\}_j \quad (3.37)$$

Equation (3.37) is better conditioned than equation (3.32). It can be seen from equation (3.35) that if one puts $[H_A^0] = [H_A]$, the new force residue will be the same as the receptance residue. So, in this final form, the minimisation of the new receptance residue leads to the minimisation of the receptance residue. However, for most selection of updating parameters, this minimisation is more stable.

3.5.3 Choice of the Damping Matrix

Experimental FRFs contain information about the damping behaviour of the structure while the FE model describes this behaviour in a very approximate way or neglects it altogether. Model updating procedures which use experimental FRFs must somehow deal with such a discrepancy or their applicability is limited to structures with low damping. Different approaches to include damping in the FE models will be described here. Most methods use experimentally-identified damping ratios to construct a viscous damping matrix $[C]$ or a structural damping matrix $[D]$. Although damping is the least accurate of the identified modal parameters, such a route is an accepted way of incorporating realistic damping values into a finite element model.

Viscous Damping

In most cases, the finite element model is undamped and hence the individual element damping matrices are not available. Nevertheless, a form of proportional damping can be assumed as a starting point:

$$[C_i^e] = \alpha_i [K_i^e] \quad (3.38)$$

This form of proportional damping also allows for variations in damping values over parts of the structure. For a more refined description of damping, a linear combination of the elemental mass and stiffness matrices can be considered:

$$[C_i^e] = \alpha_i [K_i^e] + \beta_i [M_i^e] \quad (3.39)$$

In such case, there will be two additional updating parameters associated with each finite element. This route will increase the number of unknowns and the benefit of the finer description of the damping may be lost in some cases. However, using (3.39) and discretising the structure into N finite elements:

$$[C] = \sum_{i=1}^N \alpha_i [K_i^e] + \beta_i [M_i^e] \quad (3.40)$$

The coefficients α_i and β_i are initially estimated and then corrected by an appropriate updating procedure. The main difficulties are the initial estimation of the $[C]$ matrix and the physical significance of the damping parameters. For the initial approximation, the structure is assumed to be homogenous and isotropic, i.e.:

$$[C] = \alpha [K] + \beta [M] \quad (3.41)$$

where $[M]$ and $[K]$ are the global mass and stiffness matrices. One approach is to determine α and β from the experimental damping ratios by assuming SDOF behaviour around resonances. The damping ratio for a single degree of freedom system is:

$$\xi_r = \frac{c/m}{2\omega_r} \quad r = 1, \dots, N \quad (3.42)$$

Since $c = \alpha k + \beta m$:

$$\xi_r = \frac{\alpha\omega_r^2 + \beta}{2\omega_r} \quad r = 1, \dots, N \quad (3.43)$$

Having obtained ξ_r and ω_r from experimental modal analysis, values of α and β can be determined through a least square solution and used as initial guesses in (3.40).

Modal Damping

The modal damping approach defines a viscous damping matrix of the form:

$$[C] = \sum_{r=1}^N 2\omega_r \xi_r \{\phi_X\}_r \{\phi_X\}_r^T \quad (3.44)$$

where $\{\phi_X\}_r$ is the r^{th} mass-normalised measured mode shape. The coefficients ξ_r are initially estimated by the modal damping ratios and then corrected by the updating procedure. In this case, there is only one additional updating parameters per each finite element.

Structural Damping

A structural damping matrix, $[D]$, can be defined in a similar manner to the viscous damping matrix of equation (3.38):

$$[D_i^e] = \eta_i [K_i^e] \quad (3.45)$$

or

$$[D] = \sum_{i=1}^N \eta_i [K_i^e] \quad (3.46)$$

As a first approximation, one can assume that all η_i are equal to some averaged value η given by:

$$\eta = \frac{2}{m} \sum_{r=1}^m \xi_r \quad (3.47)$$

3.5.4 Case 3: Complex FRF Data

A free-free rectangular plate was used as an example to carry out model updating using complex FRF data. The dimensions of the plate were $0.25m \times 0.45m \times .001m$ with a mass density of $7860 \text{ Kg}/m^3$. (Fig. 3.16)

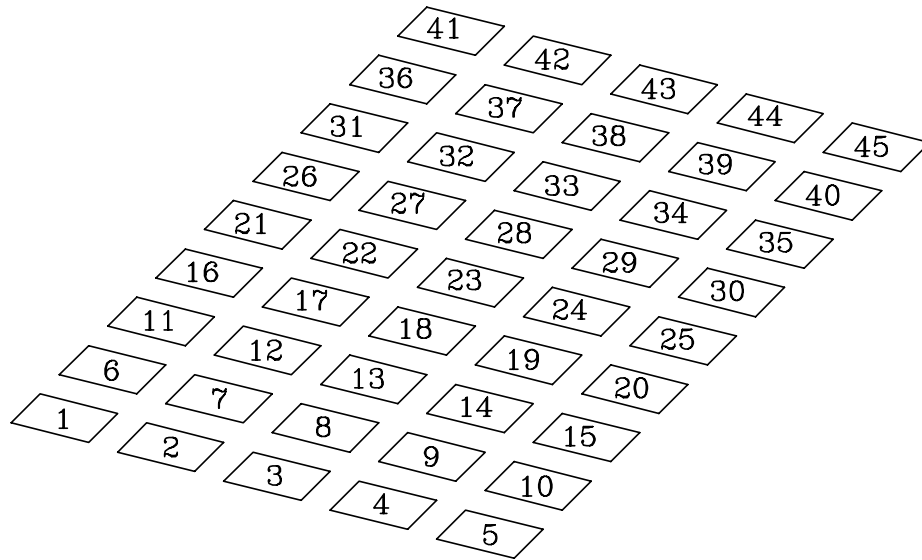


Figure 3.16: The plate model

The plate was divided into 45 three dimensional plate elements on a mesh of 6×10 . The total number of DOFs was therefore $60 \times 6 = 360$. The elemental mass and stiffness matrices were taken from the FE code ANSYS. Since the finite element model was undamped, the individual element damping matrices were formed using proportional damping in the form of:

$$[D^e] = \eta [K^e]$$

where η was taken as 1% initially. The experimental data were simulated using a uniform plate model with 1% structural damping and the FRF data for this damped plate consisted of all Z direction receptances obtained for a Z direction excitation at node 1. The analytical model contains errors in the form of 10% increase in the mass matrix of elements 1, 6, 11, 16, 21, 26, 31, 36 and 41 and 10% increase in the stiffness matrix of elements 3, 8, 13, 18, 23, 28, 33, 38 and 43. Nine known errors of 10% were also introduced to damping matrices of elements 5, 10, 15, 20, 25, 30, 35, 40 and 45.

A typical FRF, here α_{33} , computed from the experimental model is depicted in Fig. (3.17).

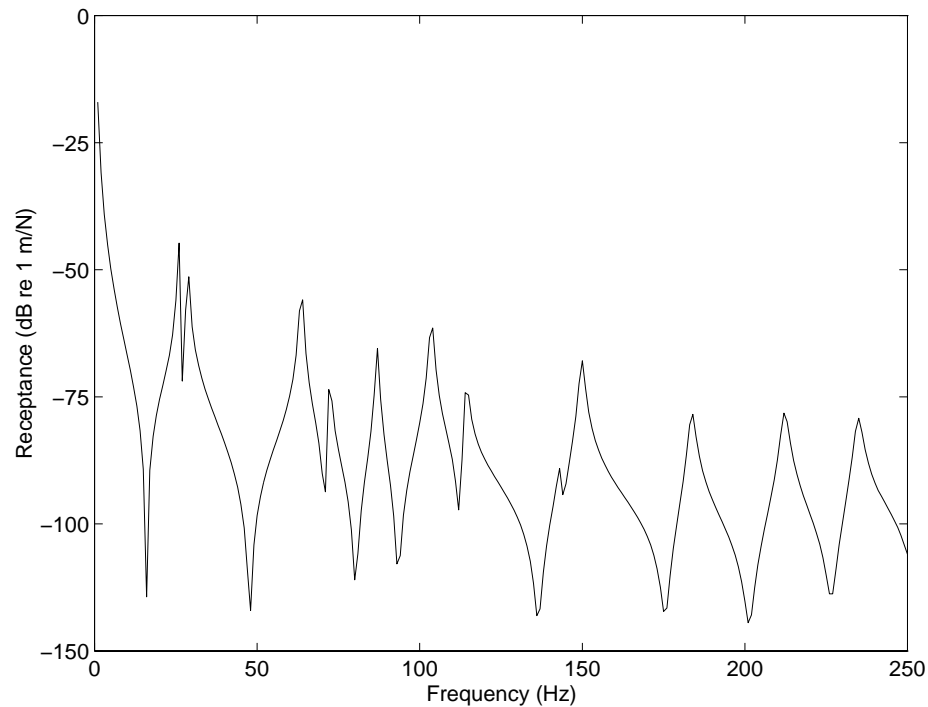


Figure 3.17: Receptance FRF, α_{33} , obtained from experimental model of uniform plate

Two case studies were considered at this stage. In the first one, the experimental FRFs were generated with 0% random noise for 60 out of the 360 known coordinates. Several runs, each with a different set of frequency points, were considered. Convergence was obtained within a few iterations and both the location and the size of errors were correctly identified in spite of model incompleteness (Fig. 3.18).

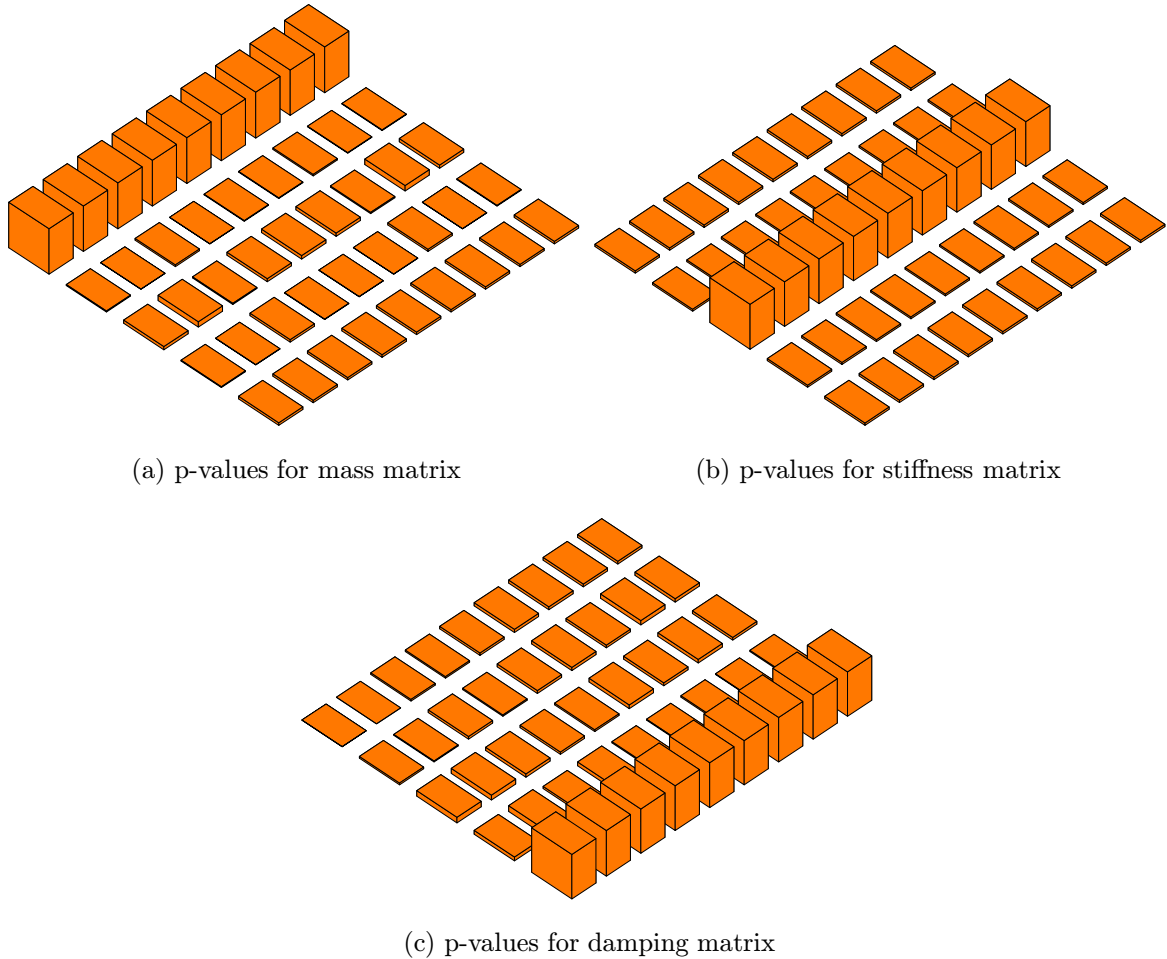


Figure 3.18: Incomplete data and 0% noise

In the second case, the incomplete experimental data were polluted with 2% noise. Although the convergence of the p-values required more iterations than the first case, the solution was again satisfactory. Fig. (3.19) shows the location and magnitude of the errors in the mass, stiffness and damping matrices.

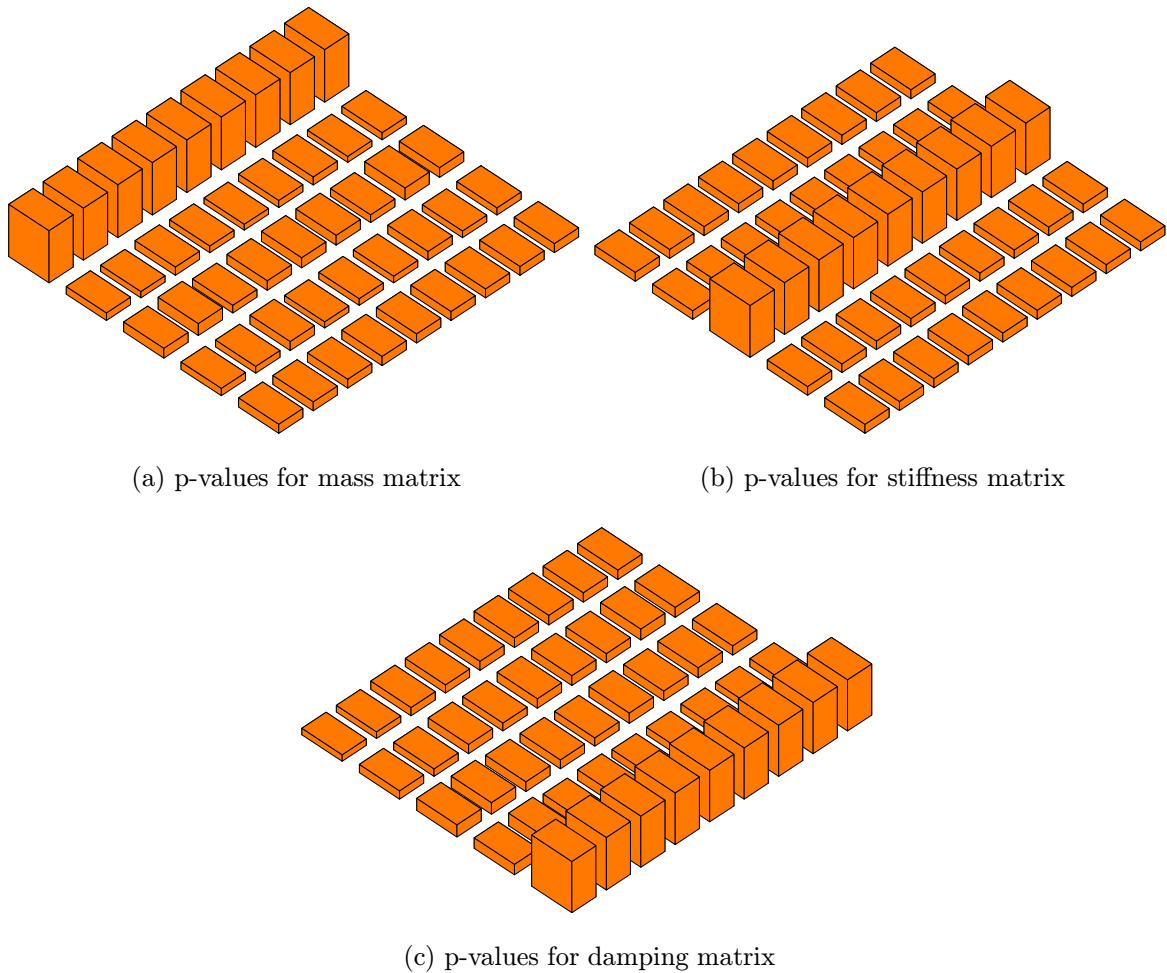


Figure 3.19: Incomplete data and 2% noise

The results indicate that complex FRF data with or without noise make the convergence process numerically more stable. This can be explained by the fact that damping makes the FRF data more smooth near the resonance and anti-resonance points.

3.5.5 The Selection of Frequency Points

Experimental FRFs consist of data acquired at a large number of frequency points in a given frequency range. Using all available data in an updating procedure needs a significant amount of CPU time. Moreover, there is a lot of redundant information in the measured FRFs. As a consequence, a small number of optimum frequency points should be used. However, the minimum number and their position in the frequency range of interest are case dependent. Nevertheless, some general considerations will be pursued here.

A set of selected frequency points should contain all information that is given by the experimental data. It means that the number of frequency points should be equal to, or greater than, the number of modes in the measured frequency range. In order to reduce the effect of noise, this number is usually more than twice the number of measured modes.

The position of the frequency points is obtained by a rule of thumb which states that at least one frequency point needs to be selected between two consecutive resonances. The quality of the selection can later be checked by a singular value decomposition of the FRF matrix using the selected points only:

$$[H_X^{sel}]_j = \left[\{H_X(\omega_1)\}_j \quad \{H_X(\omega_2)\}_j \quad \dots \quad \{H_X(\omega_{N_f})\}_j \right] \quad (3.48)$$

As mentioned before, matrix $[H_X^{sel}]_j$ should contain all the information which is present in the full set of experimental receptances. To do so, the rank of the matrix $[H_X^{sel}]_j$ should be at least equal to the number of modes, m , in the experimental frequency range. Also the ratio of the first and the m^{th} singular values, $\frac{\sigma_1}{\sigma_m}$, should not be too large.

The accuracy of the experimental data may vary from point to point. Due to the influence of noise, the FRF data close to anti-resonances are not very accurate. The data near the resonance frequencies are biased by measurement errors like leakage.

Thus, it is recommended to avoid choosing the frequency points near such areas. The coherence data can also give some information about possible errors.

Another important point in the selection of frequency points is the stability of the updating technique (see Section 3.5.1). As was pointed out previously, the stability of the updating procedure is independent of the updating frequencies when these are chosen below the first natural frequency of the grounded structure. However, some numerical considerations must still be made. The solid line curve in Fig. (3.20) shows the experimental model X1 for the Bay structure while the dash line shows the corresponding analytical model FE1.

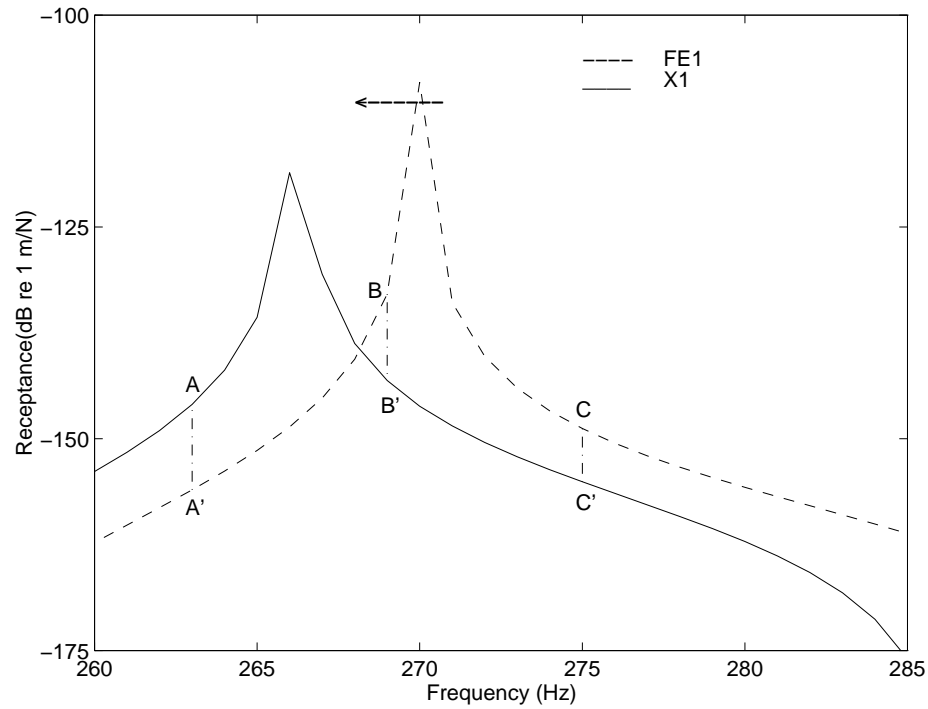


Figure 3.20: Three different updating frequencies for experimental model X1

The natural frequencies of the experimental and analytical models are 265.8 and 270 Hz respectively. Three updating frequencies were selected in the 200 Hz-285 Hz frequency range:

- (1) below the experimental natural frequency. (point A)
- (2) between the experimental and analytical natural frequencies. (point B)
- (3) above the analytical natural frequency. (point C)

The vertical lines $A - A'$, $B - B'$ and $C - C'$ show the differences between the experimental and the analytical receptances at these updating frequencies. The aim of the updating procedure is to minimise these differences. However, during the iteration, when the analytical natural frequency shifts to a value close to an updating frequency (here point B), the analytical receptance at that updating frequency becomes very large. Such a large increment in the receptance difference can cause numerical problems and instability. As a result, the selection of an updating frequency between analytical and experimental resonances should be avoided whenever possible.

3.5.6 An Improved Formulation for the Iterative Calculation of p-values

Most researchers suggest the following expression for the calculation of consecutive p-values:

$$\{p\}_{new} = \{p\}_{old} + \{\Delta p\} \quad (3.49)$$

or

$$\{p\}^i = \{1\} + \{\Delta p\}^1 + \{\Delta p\}^2 + \dots + \{\Delta p\}^i$$

where i is the iteration number and $\{p\}^0$ is the initial guess vector, usually assumed to be one. At each iteration, the original mass and stiffness matrices are multiplied by the corresponding elements of $\{p\}^i$ and the new global mass and stiffness matrices are assembled. This scheme is employed until the difference between the predicted and the analytical models is within a predefined tolerance.

An alternative route will be investigated here. The updated elemental stiffness matrix j at iteration i for instance is:

$$\begin{aligned}
 [K_j^e]^1 &= [K_j^e]^0 (1 + \Delta p_j^1) \\
 [K_j^e]^2 &= [K_j^e]^1 (1 + \Delta p_j^2) = [K_j^e]^0 (1 + \Delta p_j^1) (1 + \Delta p_j^2) \\
 \vdots &= \vdots = \vdots \\
 [K_j^e]^i &= [K_j^e]^{i-1} (1 + \Delta p_j^{i-1}) = [K_j^e]^0 (1 + \Delta p_j^1) (1 + \Delta p_j^2) \dots (1 + \Delta p_j^i)
 \end{aligned} \tag{3.50}$$

Using this approach, the final correction factor associated with the initial stiffness matrix $[K_j]^0$ of element j is:

$$\begin{aligned}
 p_j^i &= (1 + \Delta p_j^1)(1 + \Delta p_j^2) \dots (1 + \Delta p_j^i) \\
 p_j^i &= (1 + \Delta p_j^1 + \Delta p_j^2 + \dots + \Delta p_j^i + \Delta p_j^1 \Delta p_j^2 + \dots + \Delta p_j^1 \Delta p_j^2 \Delta p_j^3 + \dots)
 \end{aligned} \tag{3.51}$$

The above equation is a special case of the usual approach in which the higher terms are neglected. By using this new form, the stability of the algorithm was improved considerably. It was also found that the speed of convergence was affected favourably. This can be explained as follows. The updating optimisation problem is non-linear function of the correction factors and hence it must be solved iteratively. The iteration for the j^{th} unknown parameter can be written in the following general form:

$$p_j^i = p_j^{i-1} + \lambda_j^i \Delta p_j^i \tag{3.52}$$

where i denotes the iteration step number. The new parameter is dictated by the search direction Δp_j^i and the step length λ_j^i . In that form, the old and the new form of the final correction factors can be written as:

$$\text{Old Formulation:} \quad p_j^i = p_j^{i-1} + \Delta p_j^i$$

$$\text{New Formulation:} \quad p_j^i = p_j^{i-1} + p_j^{i-1} \Delta p_j^i$$

In the old form the step length is assumed to be unity while in the new form the step length $\lambda_j^i = p_j^{i-1}$. This may explain the faster convergence and stability of the new formulation. It should be mentioned that neither of the above form give an optimal value for λ_j^i . However, the optimal step length λ_j^i in the i^{th} search direction Δp_j^i can be determined via a uni-directional line search.

3.6 Concluding Remarks

- The response function method based on forced vibration testing was introduced in this chapter. It has been shown that the elements of the reduced dynamic stiffness matrix are smooth functions of the updating parameters and of the excitation frequency, provided that the upper limit of the updating range is the first natural frequency of the partially-grounded system of the measurement points. However, this limit is a sufficient but not necessary condition and the updating range may be increased, subject to other considerations.
- The use of the method was investigated in some detail on a number of case studies: a 10 DOF lumped parameter model, a free-free 3D Bay structure and a damped 3D plate, all with known modelling errors. Satisfactory results were obtained even in the case of noisy incomplete experimental data.
- The problem of discretisation errors was investigated by doubling the mesh for the 3D Bay structure. It was found that the discretisation errors could not be corrected as they cannot be expressed as a linear combination of individual finite elements. Therefore, only approximate solutions can be found in such case.

-
- When the experimental data are incomplete and contaminated by noise, the solution is not unique. However, the incompleteness problem of the experimental model can be overcome by introducing an exact reduction technique albeit by reducing the updating frequency range.
 - It should be noted that the minimum number of updating frequencies that is needed and the position of them in the available frequency range are case dependent. However, some general criteria were presented.
 - A new p-value formulation was introduced and implemented in the RFM algorithm. The results show that by using this new formulation, the algorithm is more stable and converges faster.
 - Different approaches to include damping in the FE models were described. Moreover, the effect of damping (complex FRFs) on the solution stability was investigated. It is shown that the damping makes the convergence process numerically more stable.
 - A strategy for the selection of updating frequency points was introduced. The quality of the selection can later be checked by a singular value decomposition of the FRF matrix formed by the selected points only.
 - A treatment to avoid ill-conditioning in the minimisation of force balance residue was made by pre-multiplying the residue vector by the dynamic flexibility matrix of the analytical model. This can reduce the sensitivity of the method to measurement errors.

Chapter 4

Regularisation Techniques

4.1 Introduction

As it was mentioned, non-uniqueness may arise under several conditions such as incomplete models and noisy measurement data. In such cases, the problem may also become ill-conditioned, which results in rank deficiency of matrix $[A]$ in equation (3.26). If it happens, then serious errors may occur in the estimated parameters $\{p\}$.

There is a growing literature on findings approximate solutions to ill-conditioned problems but only two main themes will be discussed in this section.

4.2 Least-Squares Solution via SVD

Model updating formulations yield a set of overdetermined algebraic equations of the form $[A]\{p\} = \{b\}$, where vector $\{p\}$ contains the unknowns. A least-squares solution can be obtained using the generalised inverse or the singular value decomposition (SVD).

The SVD, applied to structural dynamics problems in the last fifteen years, is one of the most important tools in numerical analysis (Frosythe *et al.*, 1977; Golub &

Van Loan, 1983).

The SVD of a $n \times m$ matrix $[A]$ is defined by:

$$[A]_{n \times m} = [U]_{n \times n} [\Sigma]_{n \times m} [V]_{m \times m}^T \quad (4.1)$$

where $[U]$ and $[V]$ are orthogonal matrices, i.e.:

$$\begin{aligned} [U]^T [U] &= [U] [U]^T = [I] \\ [V]^T [V] &= [V] [V]^T = [I] \end{aligned} \quad (4.2)$$

The columns of $[U]$ and $[V]$ are called the left and right singular vectors, respectively. $[\Sigma]$ is a real matrix with the following form:

$$[\Sigma] = \begin{bmatrix} S & 0 \\ 0 & 0 \end{bmatrix} \quad (4.3)$$

where

$$S = \text{Diag}(\sigma_1, \sigma_2, \dots, \sigma_r) \quad r \leq \min(n, m) \quad (4.4)$$

with $\sigma_1 \geq \sigma_2 \geq \dots \geq \sigma_r > 0$. The rank of a matrix is given by the number of independent rows (or columns) of the matrix. If a matrix $[A]$ is nearly rank deficient, it is said to be ill-conditioned, meaning that the solution of a linear system of equations, $[A]\{p\} = \{b\}$ is very sensitive to small variations in $\{b\}$ and not much confidence can be placed in the solutions. A measure of $[A]$'s rank is given by r , the number of non-zero singular values of $[A]$. The ratio of the largest singular value, σ_1 , to the smallest non-zero one, σ_r , can be an indicator for ill-conditioning. The so-called condition number is defined as $\text{Cond}[A] = \sigma_1/\sigma_r$. If $\text{Cond}[A]$ is small, a small change in $\{b\}$ cannot produce a large relative change in $\{p\}$ and the problem is

said to be well-conditioned. Conversely, if $Cond[A]$ has a large value, a large change in $\{p\}$ may result from a small perturbation in $\{b\}$. If ill-conditioning is caused by round-off errors, the singular values tend to separate into two groups, one large- and one small-valued.

In the case of incomplete and noisy vibration test data, the separation of large- and small-valued singular values does not occur and the singular values spread over a wide range (Link, 1985; Foster & Mottershead, 1990). So, some techniques should be used to improve the conditioning of least-squares problem for incomplete and noisy data. Such issues will be addressed in the next sections.

4.3 Tikhonov Regularisation Technique

The idea of the method of regularisation is to replace an ill-conditioned problem by a well-conditioned one which has an almost identical, albeit different, solution. Consider equation (3.26) where $[A]$ is a linear operator from one Hilbert space into another one. We have seen that the equation does not generally have a unique solution. Therefore, we seek a particular generalised solution, namely the least-squares solution of minimum norm.

$$[A]^T [A]\{p\} = [A]^T \{b\} \quad (4.5)$$

The product $[A]^T [A]$, which is quadratic, has non-negative eigenvalues and therefore, for any positive number α , the quantity $[A]^T [A] + \alpha [I]$, where $[I]$ is the identity matrix, has positive eigenvalues. Of particular interest, $[A]^T [A] + \alpha [I]$ is guaranteed to have an inverse, that is to say equation:

$$([A]^T [A] + \alpha [I])\{p_\alpha\} = [A]^T \{b\} \quad (4.6)$$

is well-posed. Equation (4.6) is a regularised form of equation (4.5) and has a unique

solution of the form:

$$\{p_\alpha\} = ([A]^T [A] + \alpha [I])^{-1} [A]^T \{b\} \quad (4.7)$$

which is called the Tikhonov approximation to $[A]^\dagger$ or the minimum norm solution of equation (4.5). It can be shown that:

$$\lim_{\alpha \rightarrow 0} \{p_\alpha\} = [A]^\dagger \{b\} \quad (4.8)$$

This method can be viewed as a variant of least square problem:

$$\begin{pmatrix} [A] \\ \alpha [I] \end{pmatrix} \{p\} = \begin{pmatrix} \{b\} \\ \alpha [I] \{x^*\} \end{pmatrix}$$

where x^* is an initial estimate.

Many attempts have been carried out to find an optimum value for the parameter α (Vogel, 1986). Although some theoretical results are formulated, it seems that a case-dependent regularisation parameter, which is calculated on the basis of the actual computations would be more effective in practice. A related approach is the so-called L-curve technique which is a plot of $\|\{p\}\|$ versus $\|[A]\{p\} - \{b\}\|$ parametrised by α . The log-log plot presents an L-corner where the value of α is optimum (Hansen, 1992).

4.4 Truncated Singular Value Decomposition (TSVD)

Another approach to computing $[A]^\dagger \{b\}$ is to truncate the singular value decomposition of $[A]^\dagger$. This technique is called truncated singular value decomposition or TSVD.

Using (4.1), one can re-write (3.26) as:

$$[U][\Sigma][V]^T \{p\} = \sum_{i=1}^n \sigma_i (\{v\}_i^T \{p\}) \{u\}_i = \{b\} \quad (4.9)$$

Using the orthogonal properties of matrices $[U]$ and $[V]$, the solution of (4.9) can be sought as:

$$\{p\} = [U]^T [\Sigma^{-1}] [V] \{b\} = \sum_{i=1}^n \sigma_i^{-1} (\{u\}_i^T \{b\}) \{v\}_i \quad (4.10)$$

If we suppose that the first r singular values are not zero, the upper limit of summation in equations (4.9) and (4.10) will change from n to r .

The terms corresponding to zero singular values do not contribute to the summation in equation (4.9). However, in ill-conditioned problems, the singular values of the second group i.e. $i = r + 1, \dots, n$ (see Section 4.1) are not exactly zero and not necessarily very small compared to the first group. Such values have a small contribution to the summation of (4.9) which becomes very large in the inverse equation (4.10). In any case, in updating problems errors contained in the FRF data affect all terms in the summation but the highest effect is on those which correspond to the smallest singular values. One way of dealing with this problem is using TSVD by considering the following series:

$$\{p\} = \sum_{i=1}^{n_t} \sigma_i^{-1} (\{u\}_i^T \{b\}) \{v\}_i \quad (4.11)$$

where n_t is the truncation level, the choice of which has been the subject of many research papers (Engl & Gfrerer, 1988; Vogel, 1986). Pickard's condition (Hansen, 1990) can be used to decide where the summation (4.10) has to be truncated. By comparing the decay rate of $|\{u_i\}^T \{b\}|$ with the corresponding singular values, the subsequent singular values can be excluded as they will not be able to filter out the error contained in the data.

4.5 Total-Least-Squares Method

In the previous methods, it was assumed that the measurement uncertainty was associated with the vector $\{b\}$ and that the matrix $[A]$ was completely free of noise. In many of model updating problems using FRF data, both $[A]$ and $\{b\}$ contain noise. The total linear least-squares (TLSQ) approach can be applied to such cases as it possesses noise rejection properties.

Assume that there are more equations n than unknowns m . The classical linear least-squares problem $[A] \{p\} = \{b\}$ try to find a best approximation $\{\hat{b}\}$ to the vector $\{b\}$ such that $[A] \{p\} = \{\hat{b}\}$ is not contradictory. If the equation $[A] \{p\} = \{b\}$ has no solution, this implies that the m dimensional subspace $Range([A])$, which has been generated by the columns of matrix $[A]$, does not contain the vector $\{b\}$. In the linear least-squares method, the solution is obtained by projecting the vector $\{b\}$ orthogonally onto $Range([A])$ and solving $[A] \{p\} = \{\hat{b}\}$ (Fig. 4.1).

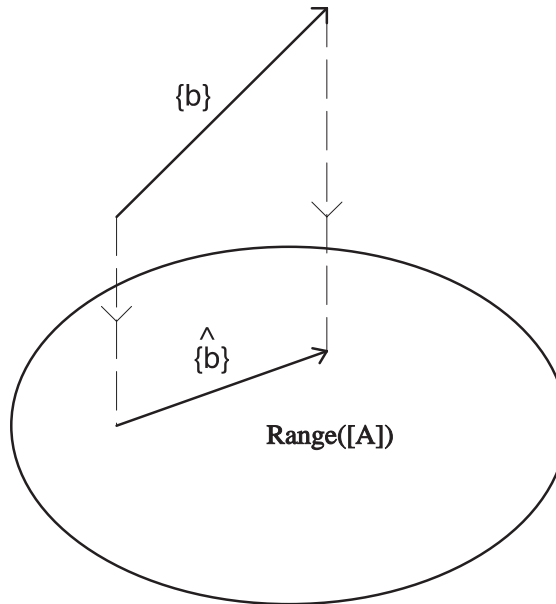


Figure 4.1: The linear least-squares solution

To put in another way, one is looking for a vector $\{r\}$ which satisfies the following conditions:

$$\| [D] \{r\} \|_2 \text{ is minimum subject to } \{\hat{b}\} = \{b\} + \{r\} \in \text{Range}([A]) \quad (4.12)$$

where $[D]$ is a weighting matrix.

The total-least-squares solution is then:

Define matrix $[E]$ as:

$$[E] = [\hat{A}] - [A] \quad (4.13)$$

Given two non-singular weighting matrices for n equations and m unknowns:

$$\begin{aligned} [D] &= \text{diag}(d_1, d_2, \dots, d_n) \\ [T] &= \text{diag}(t_1, t_2, \dots, t_{m+1}) \end{aligned} \quad (4.14)$$

One seeks to find vector $\{r\}$ and matrix $[E]$ such that :

$$\| [D] [[E], \{r\}] [T] \|_F \text{ is minimum subject to } \{\hat{b}\} \in \text{Range}([\hat{A}]) \quad (4.15)$$

where F stands for the Frobenius norm of matrix. Geometrically the TLSQ bends $\{b\}$ and $[A]$ towards each other to find a new set of equations such that the relation (4.15) is satisfied (Fig. 4.2).

In other words, The TLSQ method is equivalent to solving a nearest compatible LLS problem, $\min \| [\hat{A}] \{p\} - \{\hat{b}\} \|_2$, where nearness is measured by the weighted Frobenius norm above.

TLSQ algorithms for the solution of $[A] \{p\} = \{b\}$ can be found in Golub & Vanloan (1980) and Van Huffel & Vandewalle (1985). A summary is given below:

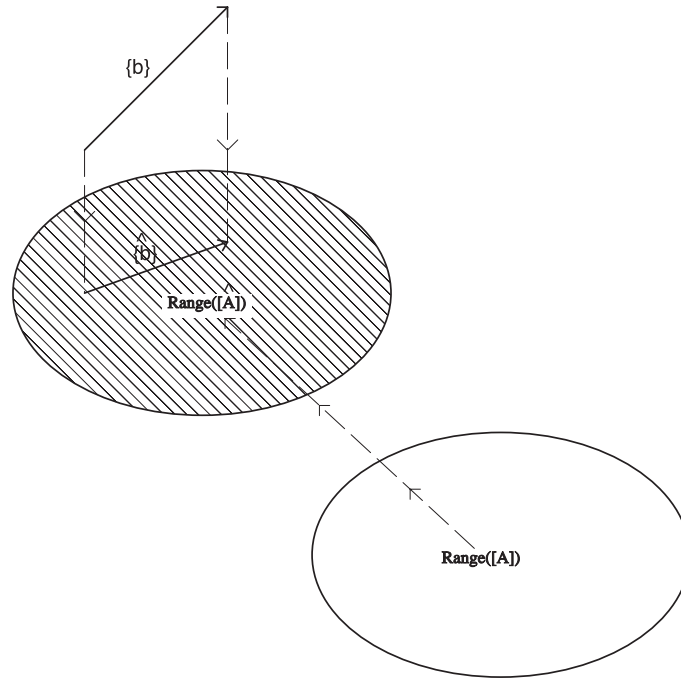


Figure 4.2: The total linear least-squares solution

Step 1 : Compute the SVD of products $[D][[A] \{b\}][T]$:

$$[U]^T [D] [[A], \{b\}] [T] [V] = \text{diag}(\sigma_1, \dots, \sigma_{m+1}) \quad (4.16)$$

Step 2 : Determine the rank r of $[[A], \{b\}]$:

$$\sigma_1^2 \geq \dots \geq \sigma_r^2 \geq 2 \max(n, m) \sigma_v^2 \geq \sigma_{r+1}^2 \geq \dots \geq \sigma_{n+1}^2 \quad (4.17)$$

where σ_v^2 is the noise variance

Step 3 : If $r < m$ compute a Householder matrix $[Q]$ such that

$$[v_{r+1}, \dots, v_{m+1}] [Q] = \begin{bmatrix} \bullet & \bullet & \dots & \bullet & y_1 \\ \bullet & \bullet & \dots & \bullet & y_2 \\ \vdots & \vdots & \ddots & \vdots & \vdots \\ \bullet & \bullet & \dots & \bullet & y_m \\ 0 & 0 & \dots & 0 & \alpha \end{bmatrix} \quad (4.18)$$

Step 4 : If $|\alpha| < \epsilon$, lower the rank with multiplicity of σ_r . Go back to step3. Otherwise $\{p\} = -\frac{1}{\alpha} \{y\}$.

It is expected that the method and algorithm will be useful in linear problems where both the matrix and the observation vector are polluted with errors. The main advantage of TLSQ over LLS is that a solution can be found with a smaller changes of data in $[A]$ and $\{b\}$. So, for a comparable amount of computational efforts TLSQ is likely to yield more accurate result than LLS.

4.6 The Maximum Entropy Method

The origin of the maximum entropy method for estimating the inverse problem can be traced back to the fundamental work of Boltzmann (1910) on statistical mechanics. Boltzmann analysed a large number N of gas molecules by subdividing the phase space into s cells. The statistical state of such a system is then given by partitioning $(N_1, N_2, \dots, N_k, \dots, N_s)$ where:

$$N_1 + N_2 + \dots + N_k + \dots + N_s = N \quad (4.19)$$

N_k being the number of molecules in the k^{th} cell.

It can be shown that the entropy of the probability distribution (p_1, p_2, \dots, p_s) is (Smith & Grandy, 1985):

$$H = - \sum_{k=1}^s p_k \ln(p_k) \quad (4.20)$$

where $p_k = \frac{N_k}{N}$ represents the probability that a molecules occupies the k^{th} cell in the phase space.

In general, the entropy function of a probability distribution measures the degree of uncertainty involved in guessing the exact state of a system having this distribution.

It should be mentioned that the entropy function provides a meaningful measure of the disorder of a system, or equivalently, the uncertainty involved in choosing a given state for a system. The maximum entropy method for inverse problems exploits this idea by invoking a kind of principle of parsimony in trying to reconstruct a solution of the problem. Namely, if the solution is known to be non-negative, and hence may be normalised so that it is essentially a probability distribution, one chooses the distribution satisfying the given constraints which is maximally uncommitted with respect to the missing information. To put in another way, one chooses the distribution which satisfies the given constraints has maximum entropy.

Recently, the maximum entropy idea has been used to regularise solutions of integral equations of the first kind. To the author's best knowledge, nobody has yet applied the method to finite element model updating.

As in Tikhonov regularisation, the idea is to seek a function which combines the features of a least-squares solution with the regularity of an additional constraint by minimising an augmented least-squares functional. In Tikhonov's theory, the regularising term has the job of damping some norm of the solution, while in maximum entropy regularisation the goal is to choose an approximate solution that has large entropy, or equivalently, small negative entropy, i.e.:

$$v(\{p\}) = \sum_{k=1}^s p_k \ln(p_k) \quad (4.21)$$

So, in attempting to find an approximate non-negative maximum entropy solution of:

$$[A] \{p\} = \{b\} \quad (4.22)$$

one minimises the functional :

$$F(\{p\}) = \| [A] \{p\} - \{b\} \| + \alpha v(\{p\}) \quad (4.23)$$

where α is a regularisation parameter. A non-linear conjugate gradient algorithm, such as the Fletcher-Reeves method, can be used to compute the regularised solution

(Vanderplaats, 1984). Almost always to update the design parameters from iteration $i - 1$ to i , it is assumed that:

$$\{p\}^i = \{p\}^{i-1} + \{q\}^i \quad (4.24)$$

where $\{q\}^i$ is the search direction and determines the value of moving in this direction. The search direction in this method has the form of:

$$\{q\}^i = -\nabla F(\{p\}^{i-1}) + \beta_i \{q\}^{i-1} \quad (4.25)$$

where

$$\beta_i = \left\| \frac{\nabla F(\{q\}^{i-1})}{\nabla F(\{q\}^{i-2})} \right\| \quad (4.26)$$

The step-length parameter minimises $F(\{p\}^{i-1} + \{q\}^i)$ with the constraint that all elements of $\{p\}^{i-1} + \{q\}^i$ should be positive. The choice of β_i has the advantage that it gives automatic restart to the steepest descent direction in the case of slow convergence.

This is a much costlier procedure than the Tikhonov regularisation because the minimisation of this functional requires the solution of a non-linear problem while the algorithm remains linear in Tikhonov's approximation.

4.7 Some Case Studies Using Regularisation Technique

In the following numerical examples, different regularisation techniques have been applied to simple test cases, which already been presented in Chapter 3. Random noise with a Gaussian distribution was added to the simulated experimental receptance FRFs.

4.7.1 10 DOF System - Incomplete Experimental Model

The case of Section (3.3.3) will again be considered here. The simulated experimental data were polluted by adding 10% random noise with zero mean value. The same number of frequency points, 25 points, were selected in the range of 0-200 Hz. Fig. (4.3) illustrates the results of applying different truncation level when using the TSVD method. The reference solution, i.e. the target experimental FRF, is displayed as the solid line, the TSVD solutions with $n_t = 20$ and 17 are displayed as dashed and point lines respectively.

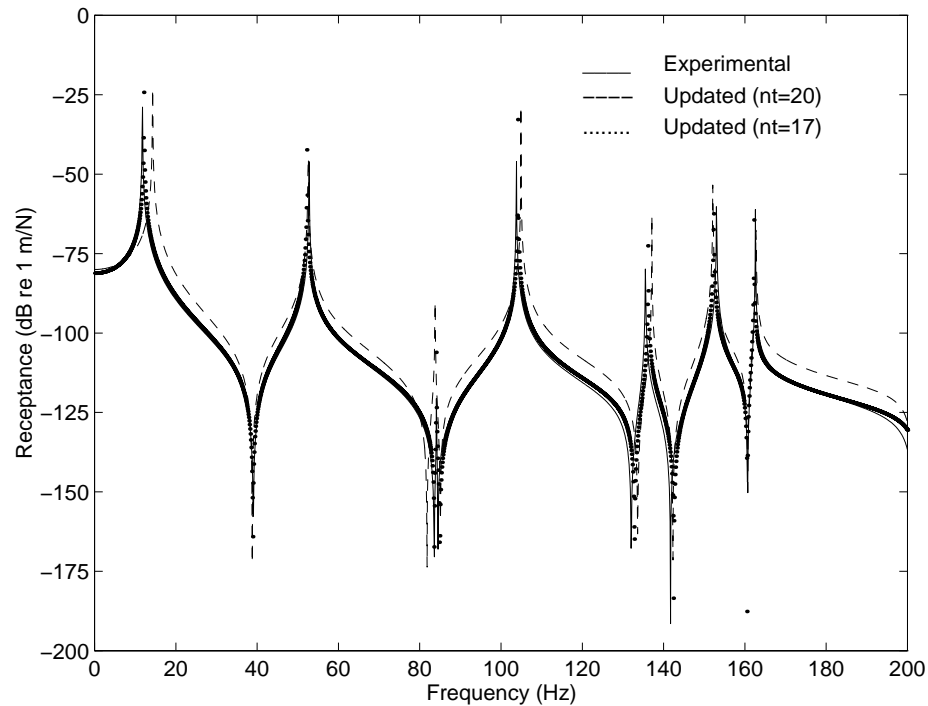


Figure 4.3: Receptance FRF, α_{55} , obtained from the experimental and updated analytical models of the 10 DOF system (different TSVD levels)

The results for $n_t = 17$ match the experimental ones almost perfectly. It was observed, by running the code with different values for n_t , that the best results were indeed those for $n_t = 17$, indicating that an optimum level had been achieved. It was observed

that the convergence of the updating algorithm was faster with the use of TSVD and that the number of iterations was also less.

The previous example was repeated again, this time using the total-least-squares technique. Fig. (4.4) illustrates the effect of ϵ on the results. As before, the reference data are plotted in solid line.

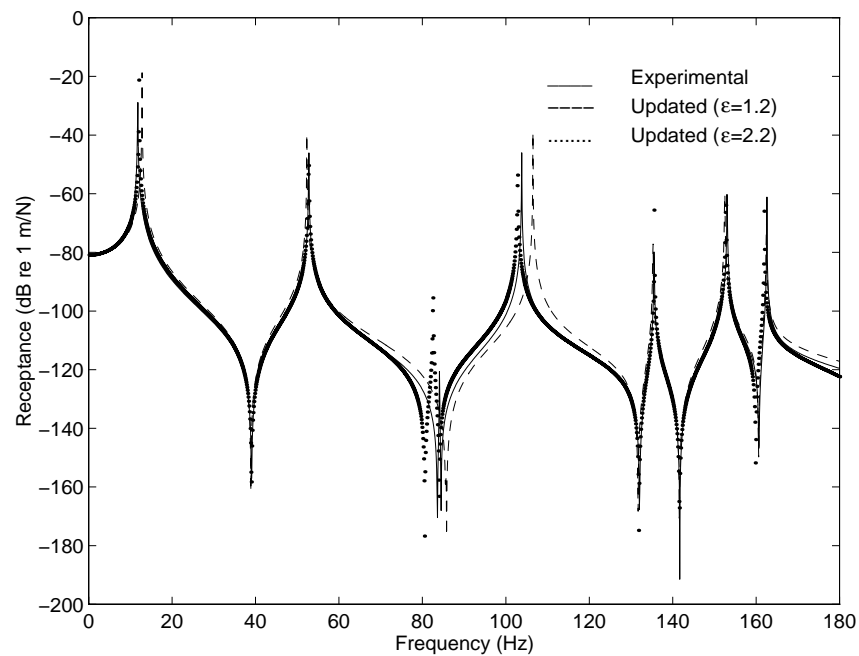


Figure 4.4: Receptance FRF, α_{55} , obtained from the experimental and updated analytical models of the 10 DOF system (different ϵ values)

It was again observed that there is an optimum value for ϵ , the choice of which is the single most important feature. This task is left to the analyst's judgement and experience, indicating once again the difficulty of dealing with inverse problems.

As mentioned before, the total-least-square method is useful in problems where both the coefficient matrix and the observation vector are contaminated by noise. Fig. (4.5) compares the updating results from the previous example for TSVD and TLSQ

techniques when the data were polluted by 15% noise. For a comparable amount of computations TLSQ seems to yield a more accurate result than TSVD, both being better than the standard LLS.

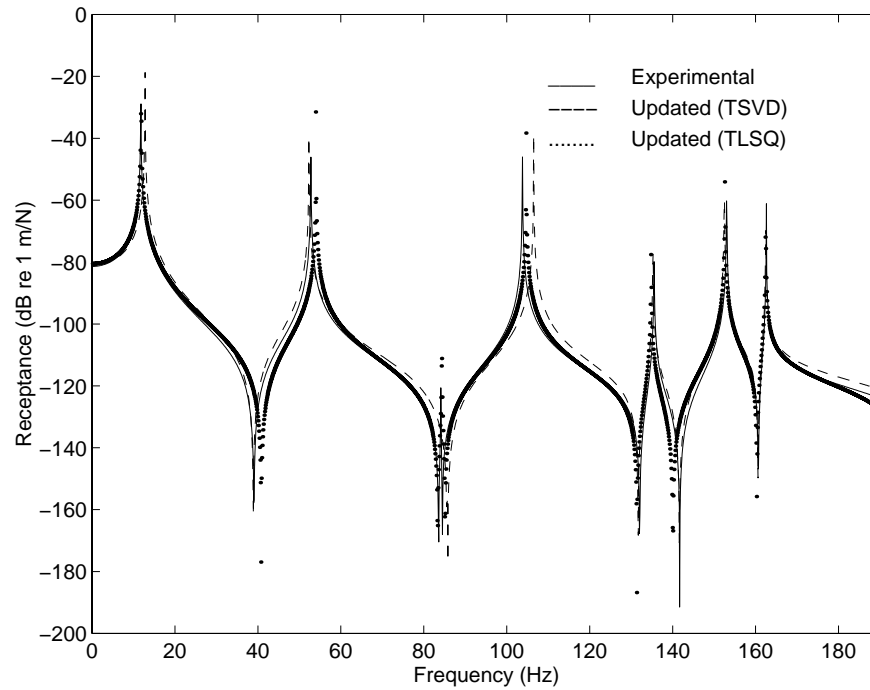


Figure 4.5: Receptance FRF, α_{55} , obtained from the experimental and updated analytical models of the 10 DOF system (different regularisation techniques)

Finally, it was decided to apply the maximum entropy regularisation technique, again to the same case. The non-linear conjugate gradient algorithm with inexact line search was used as part of the solution algorithm.

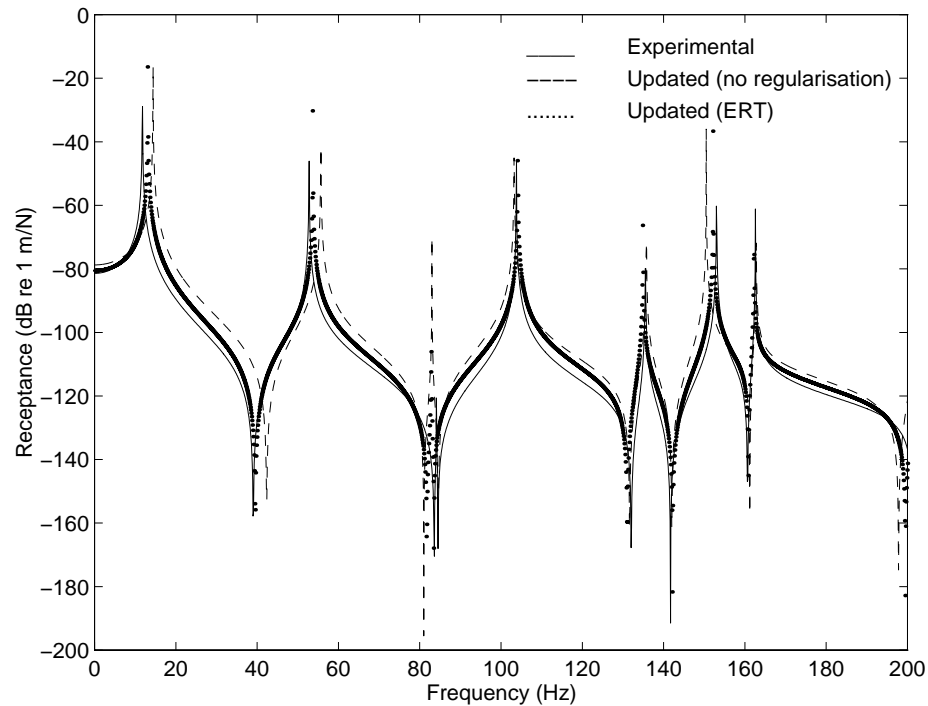


Figure 4.6: Receptance FRF, α_{55} , obtained from the experimental and updated analytical models of 10 DOF system using maximum entropy regularisation

Fig. (4.6) compares the results of updating obtained without regularisation (dashed line) and by applying the maximum entropy method for an optimal regularisation parameter α (dotted line). This technique is much costlier than the other two because the minimisation of this functional requires the solution of a non-linear set of equations. From an accuracy point of view, the additional effort seems unjustified as the updated FRF is not any closer to the reference one.

4.7.2 Frame Example - Incomplete Experimental Model

The second example was based on the three dimensional Bay structure of Section (3.4.2) shown in (Fig. 3.7). It was assumed that measurements were made in the Z direction at all nodes plus X and Y directions at node one only. Five frequency points were selected from the 0-200 Hz range and the FRF data were polluted by 1% using random noise with Gaussian distribution.

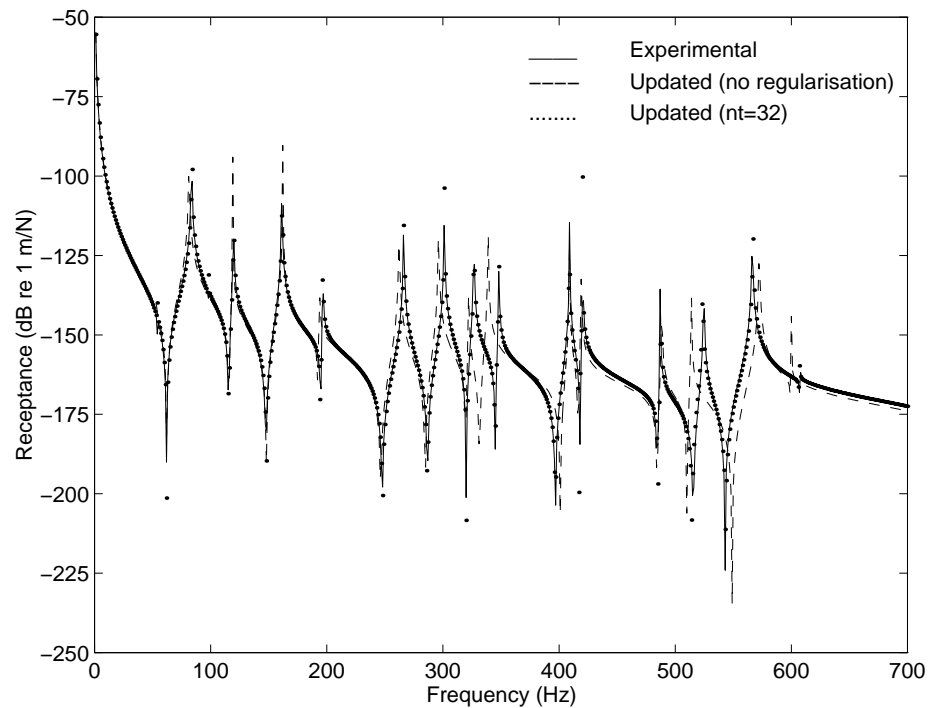


Figure 4.7: Receptance FRF, α_{33} , obtained from experimental and updated models with different TSVD levels

In the case of incomplete experimental model with added noise, the solution is not unique and different sets of p-values can be obtained by choosing different sets of frequency points. However, the adverse effects of coordinate incompleteness and noise can be partly offset by choosing more frequency points than the minimum required. This has been discussed in detail in Section (3.4.2).

The solution can also be improved by applying the TSVD technique. This is illustrated in Fig. (4.7) where the results for the case of 1% noise are displayed. The reference FRF is plotted as a solid line, the non-regularised solution is displayed as dashed lines and the TSVD solution with $n_t = 32$ is displayed in dotted line.

Very similar results were obtained by applying the different regularisation techniques, namely LLS, TLSQ and maximum entropy methods to this case and they are not given here.

4.7.3 A Comparison of Regularisation Methods

At this stage it was decided to carry out a set of numerical experiments in order to confirm if TLSQ would yield consistently better results in the presence of noise. We start with an overdetermined set of equations obtained from the Bay structure. The size of matrix $[A]$ is 105×40 and noise with zero mean and progressively large variances was added to the measured receptances. Both the matrix $[A]$ and the right hand side vector $\{b\}$ were polluted by noise. When there is no noise the solution is called 'reference' solution, $\{p_{ref}\}$. The noise variance, σ^2 , was changed between 0 and 1×10^{-3} . The relative error was defined as:

$$Relative\ Error = \frac{\|\{p\} - \{p_{ref}\}\|_f}{\|\{p_{ref}\}\|_f} \times 100$$

The optimum choice of the truncation level for the problem was found to be $n_t = 38$ and the optimum ϵ was determined as 0.05. Fig. (4.8) compares TSVD and TLSQ with optimum parameters with the standard linear least-squares approach. For each value of noise variance, 50 sets with random noise were created and the relative error was averaged and curve fitted over these sets.

It is obvious that the relative error will increase steadily if the variance of noise is increased. From the graph, one can see that, as the noise variance increases the difference between the relative errors also increases. It is also noticeable that TLSQ

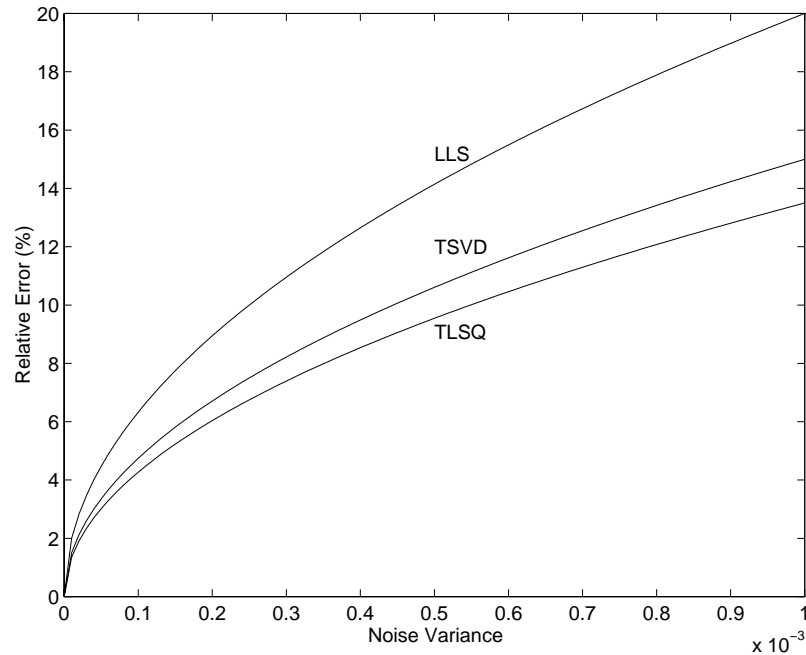


Figure 4.8: Comparison of TLSQ and TSVD with LLS

shows its superiority over LLS and TSVD when the noise variance is large. However, this is unlikely to happen in updating cases, since most updating procedures can tolerate a small amount of error. For instance, referring to the examples of the previous sections, the solutions will diverge when the noise variance is more than 1×10^{-4} . As a result, the difference between the results of LLS, TSVD and TLSQ is not all that significant within the radius of convergence.

The number of equations, n , plays an important role in the TSVD and TLSQ methods. If n increases ($n > m$) the subspace $R([A])$ spanned by the columns of $[A]$ gets *thinner and thinner* with respect to R^n . Hence, noise becomes more important in the subspace of $R([A])$. As the effects of noise on each subspace is inversely proportional to the corresponding singular value (Parlett, 1980), noise will mostly affect the smallest singular values and their corresponding vectors. These are the singular values which are removed by the TSVD or TLSQ algorithms. Thus, by increasing n , the accuracy of TSVD or TLSQ solutions will improve faster than that of LLS. From a practical view point, the application of TLSQ is more attractive since it is much easier to

increase the number of measurements than to increase the measurement accuracy. This topic will be discussed in Chapter 5.

4.8 Concluding Remarks

- As expected, noise on the FRF data has an adverse effect on updating results: convergence becomes slow and often numerically unstable. However, an acceptable and potentially more accurate solution can be found by using regularisation techniques.
- Three different methods of regularisation are presented and compared with each other. The results show that, in the case of updating problems, the TLSQ method can handle noise better than the other methods.
- The numerical experiments have shown that the difference between the solutions from TLSQ and LLS is quite substantial for large noise variance. However, this is unlikely to be the case for updating problems.
- By increasing the number of equations, the accuracy of TSVD and TLSQ solutions increase faster than that for LLS.
- The maximum entropy method was applied to the solution of the updating equations. The results showed that the method required significantly more computational effort without any increased accuracy.

Chapter 5

On The Accuracy Required of Experimental Data For Finite Element Model Updating ¹

5.1 Overview

This Chapter deals with the determination of the required experimental accuracy that must be attained when updating finite element models using measured vibration test data. A theoretical basis is developed for FRF-based updating techniques as these use measured data directly. It is shown that a well-defined relationship, that can be expressed as a characteristic function, exists between the system's properties, the correction matrices and the actual amount of experimental noise. The formulation is then applied to the standard response function updating formulation where the element mass and stiffness matrices are corrected using a single multiplier, the so-called p-value. In the presence of noise, the convergence of the updating algorithm is shown to be dependent on a number of conditions which arise from two distinct cases: one convergent and the other divergent. The findings are illustrated in the case of a

¹published on *Journal of Sound and Vibration*, Vol. 196, No. 3, Sept. 1996, pp323-336

Table 5.1: Summary of Direct and Inverse Problems

Problem Type	Knowns	Unknowns
Direct	F, H	X
Inverse 1st Kind: Force Identification	X, H	F
Inverse 2nd Kind: Model Updating	F, X	H

3D space frame and the efficacy the proposed characteristic function is discussed in some detail. Finally, a way of selecting the optimum excitation frequency values is presented as a means of relaxing the minimum experimental accuracy.

5.2 Introduction

In spite of extensive research over the past fifteen years, the state-of-the-art in finite element model updating is far from maturing and no reliable and generally-applicable procedures have been formulated so far. Several review articles reveal a wealth of updating algorithms but the success seems to remain case dependent and the applicability bounded by the skill of the analyst in choosing a correct updating procedure (Natke, 1988; Imregun & Visser, 1991; Mottershead & Friswell, 1993). A review of the case studies reported in the literature unveils a fundamental problem: a particular solution is usually non-unique and a generated solution does not necessarily represent a true physical meaning (Imregun, 1995).

Given a model (or operator) H , which relates the input F to the output X via the relationship $X = H * F$, it is possible to define direct and inverse problems which are commonly encountered in structural dynamics. These are listed in Table (5.1) and illustrated schematically in Fig. (5.1).

Let us now define the inverse, the domain and the range of the operator H .

- The inverse of H is a transformation such that the multiplication of its result with H yields the identity operator.
- The range of H is a set of all values resulting from its application as an operator.
- The domain of H is the set of all values for which operator H is defined.
- An operator H is called injective if it produces distinct outputs for distinct inputs.

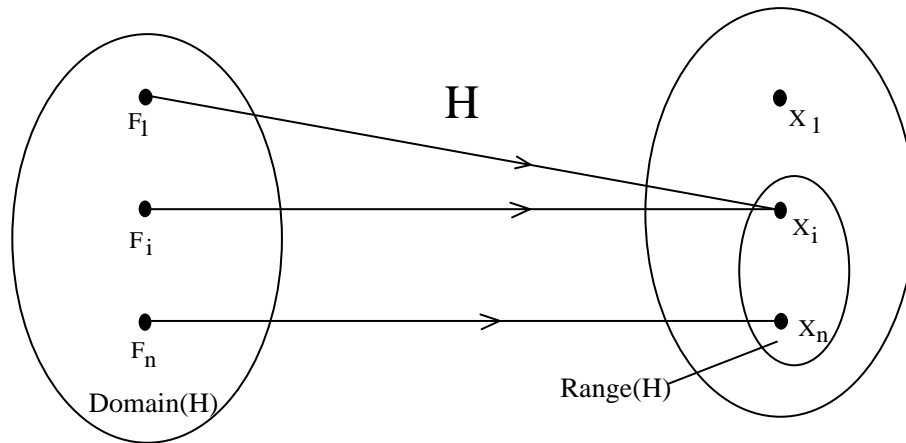


Figure 5.1: A non-injective operator H

A discussion of the force identification (or force updating) inverse problem is outside the scope of this thesis and we shall focus on the model updating inverse problem. From the outset, one can envisage four distinct possibilities while seeking a solution.

(a) Non-convergence. If the output X does not belong to the range of H , then the inverse problem has no solutions. In such cases, numerical behaviour can be random divergence or it can exhibit oscillations about some arbitrary mean value.

(b) Non-uniqueness. If H is not injective, then its inverse does not exist. In this case, even if X belongs to the range of H , the inverse problem will have several solutions.

(c) Instability. If the inverse of H exists but it is not continuous on X , then the solution will depend on the condition of the inverse operator.

(d) Existence. If the inverse of H exists and is continuous on X , then a unique solution will exist.

The difficulties associated with model updating are self-evident since Case (d) has very stringent requirements, a feature that probably explains the lack of consistency and success in many studies reported so far. However, even when one can satisfy the conditions imposed by Case (d), the determination of an updated model cannot be guaranteed in situations when the output X is polluted by noise. As it is not possible to eliminate experimental errors altogether, the fundamental question becomes the determination of the required experimental accuracy for model updating studies.

Another important issue is the reliability of specimen consistency when reference test data are acquired for updating purposes. Let us assume that we are given several nominally- identical specimens, all of which are represented by a single finite element model. For simplicity, let us further assume that there are no measurement errors at all. As we cannot guarantee that all specimens will exhibit identical dynamic behaviour, we can see that the previous problem of measurement error has now been transformed into one of manufacturing consistency. Therefore, a manufacturing consistency threshold, analogous to measurement error threshold, will exist as a limiting factor for model updating. We will assume that there is only one reference specimen and hence it will focus on measurement errors only. However, the findings are equally applicable to the variability between the nominally-identical specimens.

A review of the reported cases using experimental data seems to suggest that the required measurement accuracy is determined by trial-and-error. The main objective of the present Chapter is to present a more systematic treatment and to provide general guidelines. To this end, it is proposed to use the response function method as its direct handling of measured data will provide a suitable vehicle for such a study. A second objective is to develop a methodology for the selection of optimum excitation frequencies that must be used during the updating process.

5.3 Determination of The Required Experimental Accuracy

The response function method for finite element model updating is based on the following identity (Cottin *et al.*, 1984; Lin & Ewins, 1990; Visser & Imregun, 1991):

$$[I] - [Z_A][H_X] = [\Delta Z][H_X] \quad (5.1)$$

where $[I]$, $[Z_A]$ and $[H_X]$ are the identity, analytical impedance and experimental receptance matrices respectively, $[\Delta Z]$ being the unknown dynamic stiffness correction matrix. Given the number of recent publications on the subject, no detailed derivation will be given here. If the experimental data are free of noise and if there is a one-to-one correspondence between the discrepancies and the analytical model, the experimental response function matrix can be written as:

$$[H_X] = ([Z_A] + [\Delta Z_A])^{-1} \quad (5.2)$$

From the outset, it should be noted that the assumption above is not a realistic proposition for the purposes of conducting model updating investigations. However, our sole concern here is the determination of experimental error bounds for an otherwise well-posed problem.

In this case, it can easily be shown that:

$$[\Delta Z] = [\Delta Z_A] \quad (5.3)$$

which is the expected result since equation (5.1) is an identity. It has been assumed that the experimental and analytical models are have been made compatible in size by reduction or expansion.

Let us now assume that the experimental FRF matrix $[H_X]$ contains measurement errors which can be due to noise, transduction, signal processing, shaker-structure interaction, non-linear behaviour of the test structure, loss of digital accuracy, etc. With the addition of such an error matrix $[\epsilon]$, equation (5.2) becomes:

$$[H_X] = ([Z_A + [\Delta Z_A]]^{-1} + [\epsilon]) \quad (5.4)$$

Remembering that $[\Delta Z] = [H_X]^{-1} - [Z_A]$ we obtain:

$$\begin{aligned} [\Delta Z] &= ([Z_A + \Delta Z_A]^{-1} + [\epsilon])^{-1} - [Z_A] \\ &= \left([Z_A + \Delta Z_A]^{-1} ([I] + [Z_A + \Delta Z_A][\epsilon]) \right)^{-1} - [Z_A] \\ &= \left([I] + [Z_A + \Delta Z_A][\epsilon] \right)^{-1} [Z_A + \Delta Z_A] - [Z_A] \end{aligned} \quad (5.5)$$

Let us impose the following constraint on the spectral radius ρ of $[Z_A + \Delta Z_A][\epsilon]$:

$$\rho([Z_A + \Delta Z_A][\epsilon]) = \text{MAX} \{ | \text{Eigenvalue of } [Z_A + \Delta Z_A][\epsilon] | \} < 1 \quad (5.6)$$

In this case, $[\Delta Z]$ can be computed by expanding the first term in the right hand side of equation (5.5):

$$[\Delta Z] = \left([I] - [Z_A + \Delta Z_A][\epsilon] + ([Z_A + \Delta Z_A][\epsilon])^2 - \dots \right) [Z_A + \Delta Z_A] - [Z_A] \quad (5.7)$$

After some manipulation, equation (5.7) becomes:

$$\begin{aligned} [\Delta Z] &= [\Delta Z_A] - [Z_A + \Delta Z_A][\epsilon][Z_A + \Delta Z_A] \\ &\quad + [Z_A + \Delta Z_A][\epsilon][Z_A + \Delta Z_A][\epsilon][Z_A + \Delta Z_A] - \dots \end{aligned} \quad (5.8)$$

Since the correction is to be applied to the analytical model, the norm of $[\Delta Z]$ must be equal (or very close) to that of $[\Delta Z_A]$. In order to satisfy this condition, we must have:

$$\| [Z_A + \Delta Z_A][\epsilon][Z_A + \Delta Z_A] \| \ll \| [\Delta Z_A] \| \quad (5.9)$$

Because of the norm property $\|ABC\| \leq \|A\| \|B\| \|C\|$, the LHS of (5.9) must satisfy:

$$\| [Z_A + \Delta Z_A][\epsilon][Z_A + \Delta Z_A] \| \leq \| [Z_A + \Delta Z_A] \| \| [\epsilon] \| \| [Z_A + \Delta Z_A] \| \quad (5.10)$$

Considering (5.9) and (5.10) together, one can impose a more stringent criterion:

$$\| [Z_A + \Delta Z_A] \| \| [\epsilon] \| \| [Z_A + \Delta Z_A] \| \ll \| [\Delta Z_A] \| \quad (5.11)$$

Equation (5.11) can be re-arranged to give:

$$\| [\epsilon] \| \ll \frac{\| [\Delta Z_A] \|}{\| [Z_A + \Delta Z_A] \|^2} \quad (5.12)$$

Equation (5.12) is an important relationship between the maximum allowable experimental error (or discrepancy between nominally identical specimens), the initial model and the correction that needs to be applied. It also highlights the case-dependent nature of the updating process: for a given structure and testing conditions, the norm of the left hand side experimental error matrix is likely to remain constant while the matrix norms of the right hand side will depend on the actual mathematical model that is being used.

An alternative way of looking at equation (5.12) is to write equation (5.4) as:

$$\| [H_X] - [\epsilon] \| = \| ([Z_A] + [\Delta Z_A])^{-1} \| \quad (5.13)$$

It can than be shown that:

$$\| [Z_A] + [\Delta Z_A] \| \geq \frac{1}{\| [H_X] - [\epsilon] \|} \quad (5.14)$$

Multiplying both sides by $\|[\epsilon]\|$ and using equation (5.12) gives:

$$\frac{\|[\epsilon]\|}{\| [H_X] - [\epsilon] \|} \leq \|[\epsilon]\| \| [Z_A] + [\Delta Z_A] \| \ll \frac{\|[\Delta Z_A]\|}{\| [Z_A] + [\Delta Z_A] \|} \quad (5.15)$$

In this form, equation (5.15) can be related to what is intuitively known already: the relative measurement error (first term) must be much smaller than the relative modelling error (last term).

5.4 Application to the p-Value Formulation

Next, let us consider the formulation discussed in Chapter 3 where the global errors can be expressed as a linear combination of individual elements:

$$\begin{aligned} [\Delta K] &= \sum_{i=1}^{n_k} p_i^K [K_i] \\ [\Delta M] &= \sum_{i=1}^{n_m} p_i^M [M_i] \end{aligned} \quad (5.16)$$

where the design parameters p_i , the so-called p-values, will be zero if there are no errors. In order to simplify the algebra of the following analysis, it will be assumed that $n_m = n_k = n$, n_m and n_k denoting the number of individual design parameters for the mass and stiffness matrices. This simplification brings no loss of generality and it is in line with a number of updating methods that consider one correction factor per individual finite element matrix.

The initial and updated dynamic stiffness matrices can now be written as:

$$[Z] = \sum_{i=1}^n [Z_i] \quad (5.17)$$

where $[Z_i] = [K_i] - \omega^2 [M_i]$

and

$$[Z + \Delta Z_A] = \sum_{i=1}^n (1 + p_i^K) [K_i] - \omega^2 \sum_{i=1}^n (1 + p_i^M) [M_i] \quad (5.18)$$

Substituting equations (5.16) and (5.18) into equation (5.1):

$$[I] - \left[\left([K_1 - \omega^2 [M_1]] [H_X] + \dots + [K_n - \omega^2 [M_n]] [H_X] \right) = \right. \\ \left. \left[p_1^K [K_1] + \dots + p_n^K [K_n] - \omega^2 \left(p_1^M [M_1] + \dots + p_n^M [M_n] \right) \right] [H_X] \right] \quad (5.19)$$

In the general case, for a given column of the FRF matrix in equation (5.19), there will be more unknowns (i.e. p-values) than there are equations available. The accepted way of dealing with this problem is to write equation (5.19) at a number of excitation frequencies, the so-called frequency points, and to form an over-determined set of equations. However, one of the main difficulties of such an approach is the determination of suitable frequency points as no rigorous guidelines exist when dealing with measured FRF data. However, a technique for optimal selection will be discussed later in Section (5.5).

Let us consider the j^{th} column of equation (5.19) written s times at each of the s frequency points:

$$\begin{bmatrix} [K_1][H_X]_j & \dots & [K_n][H_X]_j & \dots & -\omega_1^2[M_1][H_X]_j & \dots & -\omega_1^2[M_n][H_X]_j \\ \vdots & \ddots & \vdots & \ddots & \vdots & \ddots & \vdots \\ [K_1][H_X]_j & \dots & [K_n][H_X]_j & \dots & -\omega_s^2[M_1][H_X]_j & \dots & -\omega_s^2[M_n][H_X]_j \end{bmatrix} \begin{Bmatrix} p_1^K \\ \vdots \\ p_n^K \\ p_1^M \\ \vdots \\ p_n^M \end{Bmatrix} =$$

$$\begin{Bmatrix} \{I\}_j - ([K_1] + \dots + [K_n] - \omega_1^2([M_1] + \dots + [M_n]))\{H_X\}_j \\ \vdots \\ \{I\}_j - ([K_1] + \dots + [K_n] - \omega_s^2([M_1] + \dots + [M_n]))\{H_X\}_j \end{Bmatrix}$$

In compact form:

$$[A]\{p\} = \{b\} \quad (5.20)$$

If we introduce some error $\{\epsilon\}_j$ into the experimental FRF vector $\{H_X\}_j$, equation (5.20) becomes:

$$\begin{bmatrix} [K_1](\{H_X\}_j + \{\epsilon\}_j) & \dots & \dots & -\omega_1^2[M_n](\{H_X\}_j + \{\epsilon\}_j) \\ \vdots & \ddots & \ddots & \vdots \\ [K_1](\{H_X\}_j + \{\epsilon\}_j) & \dots & \dots & -\omega_s^2[M_n](\{H_X\}_j + \{\epsilon\}_j) \end{bmatrix} \begin{Bmatrix} p_1^K \\ \vdots \\ p_n^K \\ p_1^M \\ \vdots \\ p_n^M \end{Bmatrix} =$$

$$\left\{ \begin{array}{c} \{I\}_j - ([K_1] + \dots + [K_n] - \omega_1^2([M_1 + \dots + [M_n])) (\{H_X\}_j + \{\epsilon\}_j) \\ \vdots \\ \{I\}_j - ([K_1] + \dots + [K_n] - \omega_s^2([M_1 + \dots + [M_n])) (\{H_X\}_j + \{\epsilon\}_j) \end{array} \right\} \quad (5.21)$$

It should be noted that $\{H_X\}_j$ and $\{\epsilon\}_j$ are functions of measured frequencies.

$$\begin{aligned} & \left(\begin{bmatrix} [K_1] \{H_X\}_j & \dots & [K_n] \{H_X\}_j & -\omega_1^2 [M_1] \{H_X\}_j & \dots & -\omega_1^2 [M_n] \{H_X\}_j \\ \vdots & \ddots & \vdots & \vdots & \ddots & \vdots \\ [K_1] \{H_X\}_j & \dots & [K_n] \{H_X\}_j & -\omega_s^2 [M_1] \{H_X\}_j & \dots & -\omega_s^2 [M_n] \{H_X\}_j \end{bmatrix} + \right. \\ & \left. \begin{bmatrix} [K_1] \{\epsilon\}_j & \dots & [K_n] \{\epsilon\}_j & -\omega_1^2 [M_1] \{\epsilon\}_j & \dots & -\omega_1^2 [M_n] \{\epsilon\}_j \\ \vdots & \ddots & \vdots & \vdots & \ddots & \vdots \\ [K_1] \{\epsilon\}_j & \dots & [K_n] \{\epsilon\}_j & -\omega_s^2 [M_1] \{\epsilon\}_j & \dots & -\omega_s^2 [M_n] \{\epsilon\}_j \end{bmatrix} \right) \begin{Bmatrix} p_1^K \\ \vdots \\ p_n^K \\ p_1^M \\ \vdots \\ p_n^M \end{Bmatrix} = \\ & \left\{ \begin{array}{c} \{I\}_j - ([K_1] + \dots + [K_n] - \omega_1^2([M_1 + \dots + [M_n])) \{H_X\}_j \\ \vdots \\ \{I\}_j - ([K_1] + \dots + [K_n] - \omega_s^2([M_1 + \dots + [M_n])) \{H_X\}_j \end{array} \right\} - \\ & \left\{ \begin{array}{c} ([K_1] + \dots + [K_n] - \omega_1^2([M_1 + \dots + [M_n])) \{\epsilon\}_j \\ \vdots \\ ([K_1] + \dots + [K_n] - \omega_s^2([M_1 + \dots + [M_n])) \{\epsilon\}_j \end{array} \right\} \quad (5.22) \end{aligned}$$

In compact form, equation (5.22) can be written as:

$$([A] + [A_\epsilon]) \{p'\} = \{b\} + \{b_\epsilon\} \quad (5.23)$$

where

$[A]$ Known matrix in terms of system's properties

$\{b\}$ Known vector in terms of system's properties

$\{p'\}$ Unknown vector of updating variables corresponding to the case where experimental data are polluted by noise,

$$[A_\epsilon] = \begin{bmatrix} [K_1]\{\epsilon\}_j & \dots & [K_n]\{\epsilon\}_j & -\omega_1^2[M_1]\{\epsilon\}_j & \dots & -\omega_1^2[M_n]\{\epsilon\}_j \\ \vdots & \ddots & \vdots & \vdots & \ddots & \vdots \\ [K_1]\{\epsilon\}_j & \dots & [K_n]\{\epsilon\}_j & -\omega_s^2[M_1]\{\epsilon\}_j & \dots & -\omega_s^2[M_n]\{\epsilon\}_j \end{bmatrix} \quad (5.24)$$

$$\{b_\epsilon\} = - \begin{Bmatrix} ([K_1] + \dots + [K_n] - \omega_1^2([M_1] + \dots + [M_n]))\{\epsilon\}_j \\ \vdots \\ ([K_1] + \dots + [K_n] - \omega_s^2([M_1] + \dots + [M_n]))\{\epsilon\}_j \end{Bmatrix}$$

Equation (5.23) can be solved using a pseudo-inverse, denoted by †.

$$\{p'\} = ([A] + [A_\epsilon])^\dagger (\{b\} + \{b_\epsilon\}) \quad (5.25)$$

Two possible cases will be discussed here. The first case is when the norm of matrix $[A_\epsilon]$ is much smaller than the norm of matrix $[A]$ while the situation is reversed in the second case.

Case 1: $\| [A]^\dagger \| \| [A_\epsilon] \| \ll 1$

In this case the norm of the error matrix is much smaller than that of system matrix, i.e.

$$\| [A_\epsilon] \| \ll \| [A] \|$$

If the following conditions are also satisfied:

$$\begin{aligned} \text{Range}([A_\epsilon]) &\subseteq \text{Range}([A]) \\ \text{Range}([A_\epsilon]^T) &\subseteq \text{Range}([A]^T) \end{aligned}$$

it can be shown that (Ben-Israel, 1974):

$$\{p'\} = ([I] + [A]^\dagger [A_\epsilon])^{-1} [A]^\dagger (\{b\} + \{b_\epsilon\}) \quad (5.26)$$

Assuming that matrix $[A]$ has full rank, the range conditions will automatically be satisfied. Expanding (5.26) as before:

$$\{p'\} = \{p\} - ([A]^\dagger [A_\epsilon]) (\{p\} - \{p_\epsilon\}) + ([A]^\dagger [A_\epsilon])^2 (\{p\} - \{p_\epsilon\}) - \dots \quad (5.27)$$

where $\{p_\epsilon\} = [A_\epsilon]^\dagger \{b_\epsilon\}$. From equation (5.27), it is evident that the noise-affected solution $\{p'\}$ will tend to the true solution as $\| [A_\epsilon] \| \rightarrow 0$. A solution is therefore possible for Case 1.

Case 2: $\| [A] \| \| [A_\epsilon]^\dagger \| \ll 1$

In this case the norm of the error matrix is much greater than the norm of the system matrix, i.e. $\| [A_\epsilon] \| \gg \| [A] \|$.

As before, it can be shown that:

$$\{p'\} = \left([I] + [A_\epsilon]^\dagger [A] \right)^{-1} [A_\epsilon]^\dagger (\{b\} + \{b_\epsilon\}) \quad (5.28)$$

Expanding, one obtains:

$$\{p'\} = \{p_\epsilon\} - \left([A_\epsilon]^\dagger [A] \right) (\{p_\epsilon\} - \{p\}) + \left([A_\epsilon]^\dagger [A] \right)^2 (\{p_\epsilon\} - \{p\}) - \dots \quad (5.29)$$

Remembering that $\{p_\epsilon\} = [A_\epsilon]^\dagger \{b_\epsilon\}$ and using equations (5.24), it can be shown that:

$$\{p_\epsilon\} = \{-1, -1, \dots, -1\}^T \quad (5.30)$$

In other words, the noise-affected solution $\{p'\}$ will tend to $\{p_\epsilon\}$ as $\| [A_\epsilon] \| \gg \| [A] \|$ and hence a meaningful solution is not possible. This finding is of significant practical importance as the $\{-1, -1, \dots, -1\}$ solution is often encountered in cases where p-value convergence cannot be obtained because of excessive noise. Such numerical behaviour simply indicates that the corrections and the initial model are of self cancelling nature. In this context, $\{-1, -1, \dots, -1\}$ is analogous to the trivial (zero) solution of a problem of the form: $[0]\{X\} = \{0\}$.

5.5 Case Study

From the outset, it must be stressed that the main purpose here is the determination of the required experimental accuracy for successful model updating. To this end, it is proposed to use a simple and artificial case so that the true difficulties of model updating are eliminated for the purposes of focusing on our objective. First, there is a one-to-one correspondence between the errors and the finite element model, so that error location becomes possible. Second, the design parameter is chosen to be the elemental Young's modulus, a feature that insures a further one-to-one correspondence between the unknowns (or p-values) and the design parameters. Third, although the measurement vector is incomplete, the updating technique used (Larsson & Sas, 1992b) ensures the existence of a unique solution up to a cut-off frequency by reducing equation (5.1) into the measurement co-ordinates only. In other words, the example under study concurs with Case (d) of Section (5.3), and there is little doubt that both the location and the correction of the Young's modulus errors will be successful for the noise-free case. Hence, the noise-free case has a unique reference solution and the objective of the case study is to investigate the relationship between the amount of experimental noise and the quality of the solution obtained. In other words, even with added noise, the solution will still remain unique but it will deviate from the reference one and we are seeking to quantify this deviation in terms of measurement accuracy. However, it should be noted that an understanding of the experimental error threshold does not guarantee that updating will be possible for the general case which includes several other factors.

Specifically, it is proposed to use the 19-node 3D space frame of Chapter 3 which is modelled using 20 12-DOF 3D beam elements. The analytical model contains errors in the form of 8% Young's modulus increase in 10 of its elements, as shown in Fig. (3.7). The experimental model, which contains no errors, consists of all 19Z direction receptances as well as 1X and 1Y direction receptances, both measured at node 1. The excitation is applied in the Z direction at node 1 and there are 15 modes within the frequency range of interest 0 Hz - 600 Hz. Therefore, we have 40 unknowns

corresponding to 2 p-values for each of the 20 finite elements and an incomplete measurement vector with 21 elements, the full size being $19 \times 6 = 114$ degrees of freedom.

A solution was obtained first for the noise-free case and, as expected, the p-values associated with the modified elements had a value of -0.08 while the remaining ones were found to be zero. Using equation (5.12), the maximum error threshold that would still produce the same result, albeit within acceptable error bounds, was investigated next.

As before, a simple frequency-domain model with uniformly-distributed noise will be used here:

$$H' = (1 + \sigma\%) H \quad (5.31)$$

where H and H' are the noise-free and polluted values of the FRF. σ is a random number that varies between maximum expected error, typically 2% – 5% depending on the type of structure that is being tested.

Using a frequency resolution of 1 Hz, equation (5.12) was evaluated for the 0 Hz -600 Hz frequency range and cases of 0.1%, 0.5%, 1%, 5% and 10% random added noise were considered. For convenience, the Frobenious norm was used throughout and equation (5.12) was expressed in the following format, referred to as the characteristic log function hereafter.

$$\log \left(\frac{\| [\epsilon] \|}{\frac{\| [\Delta Z_A] \|}{\| [Z_A + \Delta Z_A] \|^2}} \right) < 0 \quad (5.32)$$

Five such characteristic functions are plotted in Fig. (5.2), a close inspection of which reveals three important features.

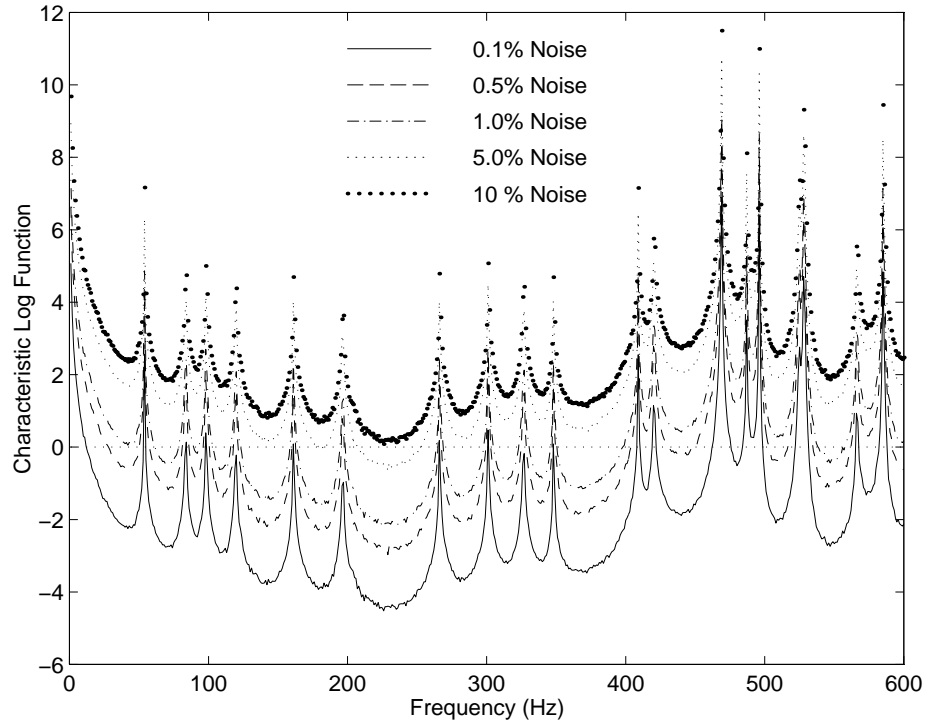


Figure 5.2: Characteristic log function for 0.1%, 0.5%, 1.0%, 5.0% and 10% noise

(i) Even for the 0.1% noise case, there is no guarantee that the model can be updated successfully since the corresponding log function is well above the zero line for some of the frequency range.

(ii) On the other hand, it is possible to eliminate this particular problem by some judicious choice of the excitation frequency values. In this example, most of the local minima of the characteristic log function will be suitable for this purpose.

(iii) Perhaps most importantly, for a given system, it is possible to determine the required experimental accuracy by plotting the characteristic log function, provided the norm of $\|\Delta Z\|$ can be estimated. In this particular example, it is unlikely that more than 1% error can be tolerated by the updating algorithm.

From Fig. (5.2), it can also be observed that the position of the best frequency points seems to be independent of the amount of noise. It was therefore decided to plot the error component ($\log \|\epsilon\|$) and the system component $\log \left(\frac{\|\Delta Z\|}{\|Z+\Delta Z\|^2} \right)$ separately, the

latter being the straight line-like curve within the 0 Hz - 350 Hz region and exhibiting several sharp drops thereafter (Fig. 5.3). This last format represents a convenient way of selecting the optimum excitation frequencies since it provides a direct means of quantifying the adverse effect of noise. In this particular example, it is clear that 5% and 10% noise cases have no chance of success since the error component is well above the system component. As expected, the best results will be obtained for 0.1% noise since this case corresponds to the maximum distance between the two components of the characteristic function.

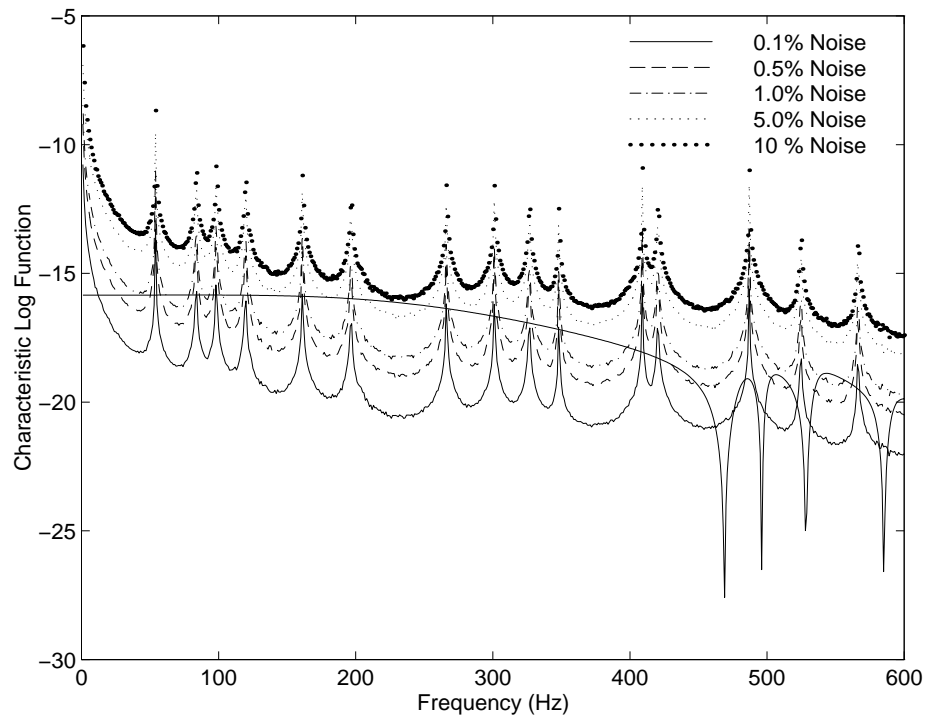


Figure 5.3: Error component $\log(\|\epsilon\|)$ and the system component $\log(\|\Delta Z_A\|/\|[Z_A + \Delta Z_A]\|^2)$ of the characteristic log function

To check the validity of the arguments above, it was decided to select 10 optimal frequency points (135 Hz, 155 Hz, 180 Hz, 210 Hz, 230 Hz, 257 Hz, 280 Hz, 300 Hz, 310 Hz, 325 Hz) and to update the FE model for 0.1%, 0.5% and 1.0% added noise cases. The characteristic log function is shown for these optimum points only in Fig. (5.4).

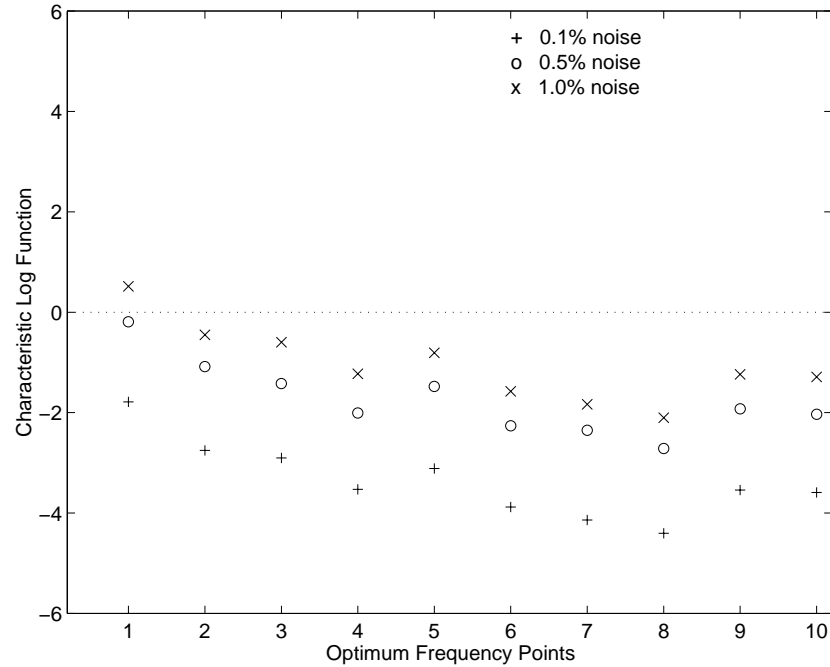
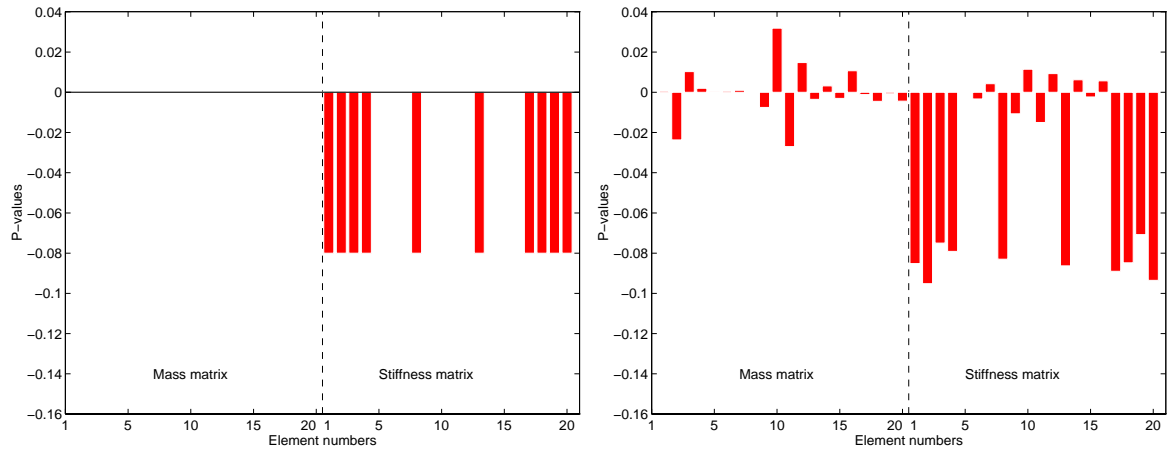


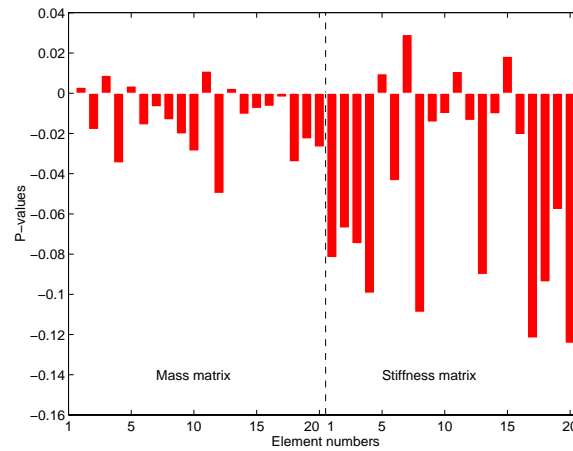
Figure 5.4: Characteristic log function at optimum frequency points

It is clear that the 1.0% noise case is very marginal since some values of the characteristic function are above acceptable levels. The computed p-values for the 0%, 0.1% and 0.5% noise cases are shown in Figs. (5.5a) to (5.5c), the pattern in 5a being the reference one and consisting of ten bars of -0.08 in the stiffness matrix (i.e. 10 individual elements, each with 8% change in the elastic modulus). Although the solution remains unique and well-conditioned for cases 5b and 5c, its heavy dependence on the amount of experimental noise is obvious. This is not a particularly encouraging result as a maximum error bound of even 0.5% may be rather difficult to achieve in practice. The p-values corresponding to the remaining three cases exhibit a totally random pattern and will not be shown here.



(a) 0% noise - Reference case

(b) 0.1% noise



(c) 0.5% noise

Figure 5.5: p-values for different amount of noise

Next, it was decided to compute the p-values of the 0.5% noise case, this time using randomly-chosen excitation frequency points but excluding obvious error zones such as the vicinity of resonances. The two sets of results are overlaid in Fig. (5.6) from which the positive effect of the optimum frequency selection is immediately seen: the randomly- selected set produce a very distorted pattern while the optimum set are somewhat reminiscent of the expected result.

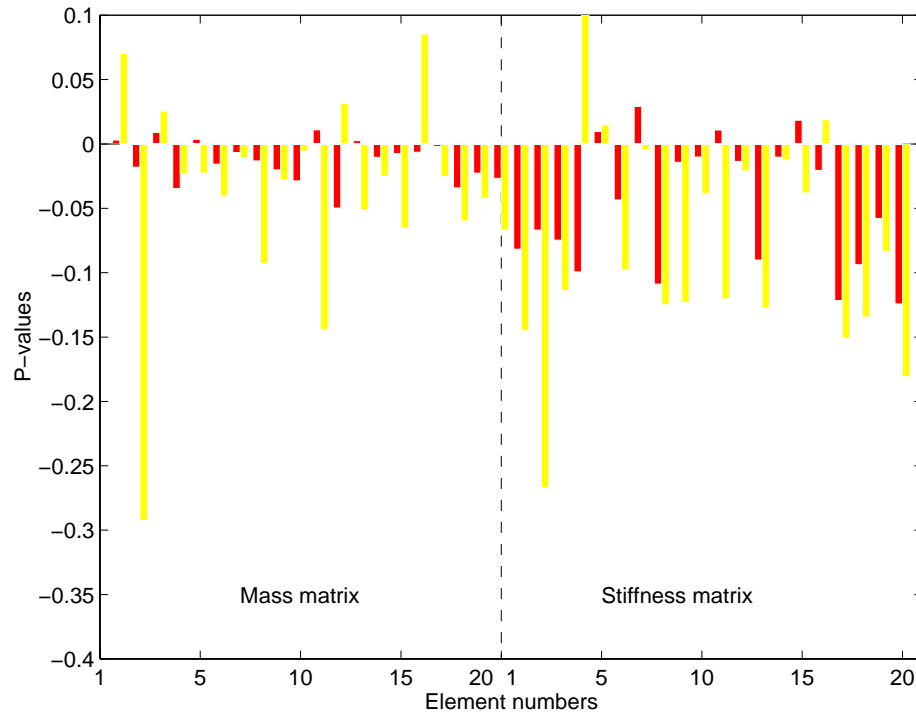


Figure 5.6: p-values for the 0.5% noise case - 10 frequency points
Optimum (darker bar) vs. random selection of the excitation frequency points

Finally, it was decided to repeat the case of 0.5% noise, this time choosing 30 frequency points in two sets: one optimum and one random selections. The two sets of results are plotted in Fig. (5.7) which exhibits a very similar pattern to that of the previous findings. The optimum set produces much better results than the randomly-selected one, though it is also seen that an increase in the number of frequency points is beneficiary to both cases.

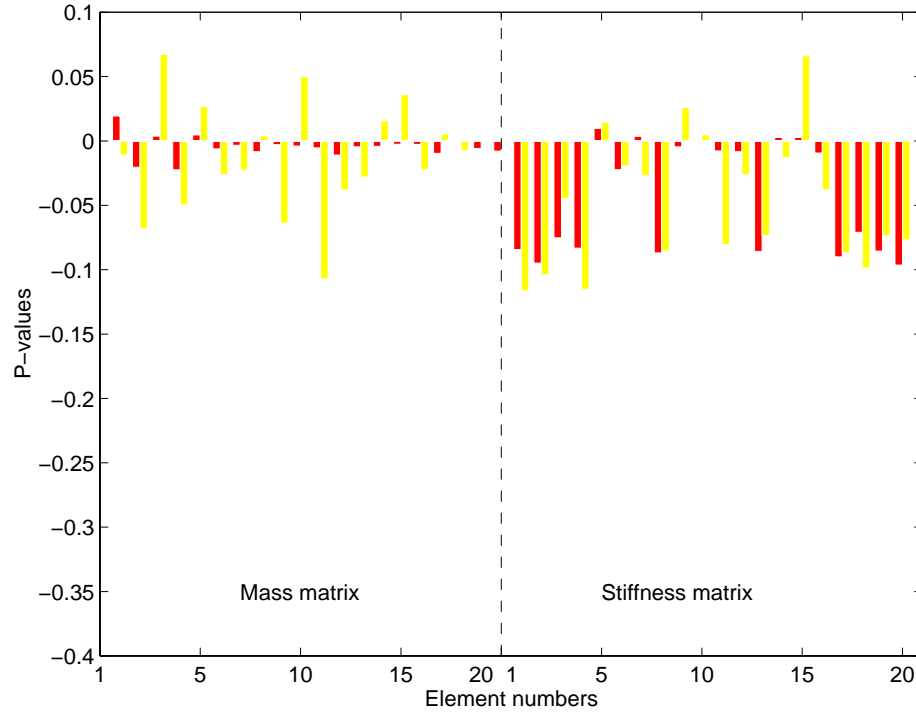


Figure 5.7: p-values for the 0.5% noise case - 30 frequency points
Optimum (darker bar) vs. random selection of the excitation frequency points

5.6 Concluding Remarks

- Starting from a response function based updating technique, it has been possible to develop a mathematical formulation in the form of a simple relationship between the system's properties, the correction matrices and the amount of experimental noise. However, it should be noted that the discussion is for a well-posed problem which is guaranteed to have a solution in all cases studied. Therefore, the results reported on the experimental error bounds should be considered as necessary but not sufficient conditions.

- It has been shown that the proposed formulation can be used to assess the threshold of maximum allowable experimental error. The most convenient way is probably to compute and plot the characteristic log function for a range of expected error bounds.
- A further use of the characteristic function lies in its ability to yield the optimum excitation frequency points that must be provided to the updating algorithm. This feature can be used for either relaxing the error threshold or for improving the numerical stability.
- The present calculations, as well as further numerical studies which are not reported here, suggest that the maximum allowable error is small, say within the 0.10% - 0.25% range. This finding is likely to have implications on the acquisition and processing of vibration test data which are going to be used in the updating of mathematical models.

Chapter 6

A Modified Eigenstructure Assignment Technique For Finite Element Model Updating ¹

6.1 Introduction

This Chapter deals with an extended application of the constrained eigenstructure assignment method (CEAM) to finite element model updating. The existing formulation is modified to accommodate larger systems by developing a quadratic linear optimisation procedure which is unconditionally stable. Further refinements include the updating of the mass matrix, a hysteretic damping model and the introduction of elemental correction factors. Six numerical test cases, dealing with effects of damping and measurement noise, mode shape incompleteness and discretisation differences, have been conducted in the case of a 3D frame model with 114 co-ordinates. The performance of the CEAM has been evaluated systematically both for the purpose of error location and the global correction of the initial model. The same cases have also been studied using another model updating approach, namely the response function

¹published on *Shock and Vibration*, Vol. 3, No. 4, 1996, pp247-258

method (RFM) of Chapter 3. It was found that the CEAM had a number of distinct advantages, such yielding a non-iterative direct solution, requiring much less computing power and providing acceptable results for cases that could not be handled using the RFM.

Eigenstructure assignment was first introduced in the field of control theory. Moore (1976) formulated the necessary and sufficient conditions for simultaneous eigenvalue and eigenvector assignment using state feedback for the case of distinct eigenvalues. Srinathkumar (1978) addressed the problem of pole-assignment in linear time-invariant multi-variable systems using output feedback. Andry & Chung (1983) applied the eigenstructure assignment technique for a linear mechanical system for parameter identification. Minas & Inman (1988), and Inman & Minas (1990) applied the constrained assignment technique for the correction of damping and stiffness matrices of a finite element model. They also used pole placement method for systems with unknown mode shapes. Zimmerman & Widengren (1990) used a modified algorithm that allowed a symmetric eigenstructure assignment when correcting the damping and stiffness matrices. Their method required the solution of a general algebraic Riccati matrix equation, the size of which depended on the number of assigned modes, thus requiring very considerable CPU power for large order systems. Finally, Shulz & Inman (1994) used the eigenstructure assignment technique with a number of constraints that were related to the physical properties of the system to be updated. They considered small-order systems that were symmetric, banded and bounded. The constraints were built into a non-linear optimisation procedure that preserved the desired properties of updated model.

The work presented in this Chapter is an extension of the work by Shulz & Inman (1994) and the following features are common to both studies. The correction of the finite element model is based on a subset of modes and frequencies, as would be in the case of measured data because of various practical limitations. The symmetry of the system matrices, the connectivity information and other conditions such as positive-definite mass matrix, the maximum allowable change in design variables, etc. are introduced in the form of constraints. Although the solution is bounded by

the limited variability of the design parameters, no formal functional constraints exist since the limits can only be expressed in terms of inequalities.

The primary purpose of this Chapter is to make the methodology applicable to large systems by both developing a quadratic linear optimisation procedure instead of the non-linear one and by reducing the number of unknowns via an error representation that involves one design parameter per individual finite element matrix. Although further variants of this latter feature, such as the allocation of design parameters to physical quantities, they will not be explored here. The main disadvantages of a non-linear optimisation procedure are the extensive CPU requirements and slow convergence. Further refinements embrace the inclusion of the mass matrix in the updating procedure and the use a hysteretic damping model as well as a viscous one.

A further objective is to compare the performance of the CEAM against the response function method (RFM) of Chapter 3.

6.2 Review of the CEAM Formulation

Although the formulation below is similar to that given by Shulz & Inman (1994), two differences can be noticed: (i) the mass matrix is included in the updating process, and (ii) a hysteretic damping model used instead of a viscous one.

Consider an N degree-of-freedom spatial model with structural damping:

$$[M]\{\ddot{X}\} + ([K] + i[D])\{X\} = 0 \quad (6.1)$$

where $[M]$, $[K]$, $[D]$ are the mass, stiffness and hysteretic damping matrices.

Let us assume that it is possible to find an updated system which satisfies the equation of motion:

$$\left[[M] + [\bar{M}] \right] \{\ddot{X}\} + \left[([K] + [\bar{K}]) + i([D] + [\bar{D}]) \right] \{X\} = 0 \quad (6.2)$$

where $[\bar{M}]$, $[\bar{K}]$, $[\bar{D}]$ denote the corrected mass, stiffness and hysteretic damping matrices. Two conditions will be imposed on the updated model.

(a) The updated matrices must remain real, symmetric and preserve the initial connectivity information.

(b) The initial and updated models must have the same m modes, characterised by natural frequencies and mode shapes $\{\phi_r\}$ where $r = 1, \dots, m$. At this stage, it will be assumed these are error-free and that they can be obtained from a modal analysis of the measured data.

Using equations (6.1), (6.2) and the two constraints above, we get:

$$\left([M] \omega_r^2 + [K] + i[D] \right) \{\phi_r\} + \left([\bar{M}] \omega_r^2 + [\bar{K}] + i[\bar{D}] \right) \{\phi_r\} = 0 \quad (6.3)$$

Equation (6.3) can be written as:

$$[\Gamma_r] \{\Psi_r\} = 0 \quad (6.4)$$

where

$$[\Gamma_r] = \left[[M] \omega_r^2 + [K] + i[D] \quad [I] \right]$$

and

$$\{\Psi_r\} = \left\{ \begin{array}{c} \{\phi_r\} \\ ([\bar{M}] \omega_r^2 + [\bar{K}] + i[\bar{D}]) \{\phi_r\} \end{array} \right\}$$

Using a QR decomposition, the vector $\{\Psi_r\}$ becomes:

$$\{\Psi_r\} = \begin{bmatrix} [V_r] \\ [\bar{V}_r] \end{bmatrix} \{e_r\} \quad (6.5)$$

where the vectors forming the columns of the $2N \times N$ matrix $\begin{bmatrix} [V_r] \\ [\bar{V}_r] \end{bmatrix}$ are the orthonormal basis for the null space of the matrix $[\Gamma_r]$ and $\{e_r\}$ is an $N \times 1$ vector of complex coefficients. Combining equations (6.4) and (6.5) we get:

$$\{\phi_r\} = [V_r] \{e_r\} \quad (6.6)$$

If all $N(> m)$ modes are measured:

$$\{e_r\} = [V_r]^{-1} \{\phi_r\} \quad (6.7)$$

However, if only $m < N$ mode shapes are available:

$$\{e_r\} = [V_r]^\dagger \{\phi_r\} \quad (6.8)$$

where \dagger denotes the pseudo-inverse of $[V_r]$.

Again, combining equations (6.4) and (6.5), one obtains:

$$\left([\bar{M}] \omega_r^2 + [\bar{K}] + i [\bar{D}] \right) \{\phi_r\} = [\bar{V}_r] \{e_r\} \quad (6.9)$$

Substituting equation (6.6) into equation (6.9) gives:

$$\left([\bar{M}] \omega_r^2 + [\bar{K}] + i [\bar{D}] \right) [V_r] \{e_r\} = [\bar{V}_r] \{e_r\} \quad (6.10)$$

Extending equation (6.10) into full matrix form yields:

$$[\bar{M}] [V] [E] [\Omega]^2 + ([\bar{K}] + i[\bar{D}]) [V] [E] = [\bar{V}] [E] \quad (6.11)$$

Rearranging equation (6.11) we get:

$$\begin{bmatrix} [\bar{M}] & [\bar{D}] & [\bar{K}] \end{bmatrix} \begin{bmatrix} [V] [E] [\Omega]^2 \\ i [V] [E] \\ [V] [E] \end{bmatrix} = [\bar{V}] [E] \quad (6.12)$$

where $\begin{bmatrix} [\bar{M}] & [\bar{D}] & [\bar{K}] \end{bmatrix}$ is $N \times 3N$, $\begin{bmatrix} [V][E][\Omega]^2 & [V][E] & i[V][E] \end{bmatrix}^T$ is $m \times 3N$ and $[\bar{V}] [E]$ is $N \times m$.

Separating equation (6.12) into its real and imaginary parts:

$$\begin{bmatrix} [\bar{M}] & [\bar{D}] & [\bar{K}] \end{bmatrix} \begin{bmatrix} ([V][E])_R([\Omega_R^2] - [\Omega_I^2]) - 2([V][E])_I[\Omega_R][\Omega_I] \\ -([V][E])_I \\ ([V][E])_R \end{bmatrix} \\ \begin{bmatrix} ([V][E])_I([\Omega_R^2] - [\Omega_I^2]) - 2([V][E])_R[\Omega_R][\Omega_I] \\ ([V][E])_R \\ ([V][E])_I \end{bmatrix} = \begin{bmatrix} ([\bar{V}][E])_R & ([\bar{V}][E])_I \end{bmatrix}$$

or

$$\begin{bmatrix} [\bar{M}] & [\bar{D}] & [\bar{K}] \end{bmatrix} [G] = [Q] \quad (6.13)$$

where the real-valued matrices $\begin{bmatrix} [\bar{M}] & [\bar{D}] & [\bar{K}] \end{bmatrix}$, $[G]$ and $[Q]$ are $N \times 3N$, $3N \times 2m$ and $N \times 2m$ respectively.

The uniqueness of the solution and the importance of imposing constraints is discussed in some detail by Shulz & Inman (1994). It is reported that, in the general case, an optimisation method will have to be used to solve equation (6.13), especially in cases such as finite element model updating when constraints are needed to preserve the form and connectivities of the mass, stiffness and damping matrices. The next section will deal with the derivation of such a solution procedure.

6.3 Formulation of a Quadratic Solution Procedure

A solution to equation (6.13) is sought by finding the minimum of:

$$J = \left\| \begin{bmatrix} [\bar{M}] & [\bar{D}] & [\bar{K}] \end{bmatrix} [G] - [Q] \right\|_f \quad (6.14)$$

subject to various constraints on matrices $[\bar{M}]$, $[\bar{D}]$ and $[\bar{K}]$ and $\|\cdot\|_f$ denoting the Frobenious norm of a matrix.

There are at least two ways of minimising J : the first one is to use a non-linear technique which results in an iterative scheme (Shulz & Inman, 1994); the second one, which will be developed here, is to use a quadratic formulation which has the added advantage of being unconditionally stable. Let us define J as:

$$J = \frac{1}{2} \{\Theta\}^T [A] \{\Theta\} + \{B\}^T \{\Theta\} \quad (6.15)$$

where $[A]$ is $3N^2 \times 3N^2$ matrix and $\{B\}$ is a $3N^2 \times 1$ vector. The partial derivatives are given by:

where δ is the Kronecker delta function.

The size of matrix $[A]$, $3N^2 \times 3N^2$, is prohibitive for any practical application to be considered. However, as in most updating studies, there is no particular need to update the individual elements of the global mass, stiffness and damping matrices. Common practice is to assign correction factors, the so-called p-values, to the individual finite element matrices and to compute those to obtain the required global changes. In other words, it is assumed that the errors are proportional to the elemental matrices:

$$\begin{aligned} [\bar{M}] &= \sum_{i=1}^L p_i^m [M_i] \\ [\bar{D}] &= \sum_{i=1}^L p_i^d [D_i] \\ [\bar{K}] &= \sum_{i=1}^L p_i^k [K_i] \end{aligned} \quad (6.21)$$

Referring to equation (6.13), let us define

$$[G] = \begin{bmatrix} [G_1] \\ [G_2] \\ [G_3] \end{bmatrix}$$

where $[G_1]$, $[G_2]$, $[G_3]$ are $N \times 2m$ matrices. Inserting equations (6.21) into equation (6.13), one obtains:

$$\left(\sum_{i=1}^L p_i^m [M_i] \right) [G_1] + \left(\sum_{i=1}^L p_i^d [D_i] \right) [G_2] + \left(\sum_{i=1}^L p_i^k [K_i] \right) [G_3] = [Q] \quad (6.22)$$

Equation (6.22) can explicitly be written as:

6.4 Numerical Study

6.4.1 CEAM Case Studies

It is now proposed to apply the CEAM to the case of the 3D frame, the Bay structure, which has already been used in Chapter 3. Four different models were created for the purposes of conducting parametric studies. Model FE1 had 20 elements, for 10 of which the Young's modulus was increased by 8%. Model FE2 had also 20 elements but this time 30% changes in the X and Y moments of inertia were introduced (Figs. 3.7 and 3.8). X1 and X2 were considered to be the reference models and hence they contained no errors, the latter being double the size of the former. The aim of the numerical studies was to correct models FE1 and FE2 using simulated experimental data obtained from models X1 and X2. The various models used are summarised in Table (6.1).

Table 6.1: The target and initial FE Models of the Frame Structure
(E: Young's modulus, I_x and I_y : moments of inertia)

Model	FE1 (initial)	FE2 (initial)	X1 (target)	X2 (target)
No of elts	20	20	20	40
Mesh size	19 nodes	19 nodes	19 nodes	39 nodes
No of DOFs	114	114	114	234
Errors	8% in E	30% in I_x and I_y	None	None

The main objective of the case study is to examine the performance of the CEAM from both numerical efficiency and updating quality viewpoints. The mass matrix was excluded from the updating process for all cases but the fifth one as its inclusion created numerical problems when there are no associated mass errors.

Case 1. Assigning Real and Complete Modes

The first case studied is a straightforward check of the formulation whereby the first 10 modes of model X1 are assigned to model FE1 without the presence of any damping or experimental noise. In this particular case, the p-values indicate the exact location of the error (Fig. 6.1) and the response obtained from the updated model is identical to that of the reference model X1 (Fig. 6.2). However, this is an expected result since:

- (i) the problem is over determined with 40 unknowns (mass and stiffness p-values for the 20 finite elements) and 10 complete modes, each containing 115 data items,
- (ii) the changes made are directly proportional to the correction factors and hence equations (21) are exact in this particular case, and
- (iii) the initial and target models have identical meshes and hence the discretisation errors cancel each other.

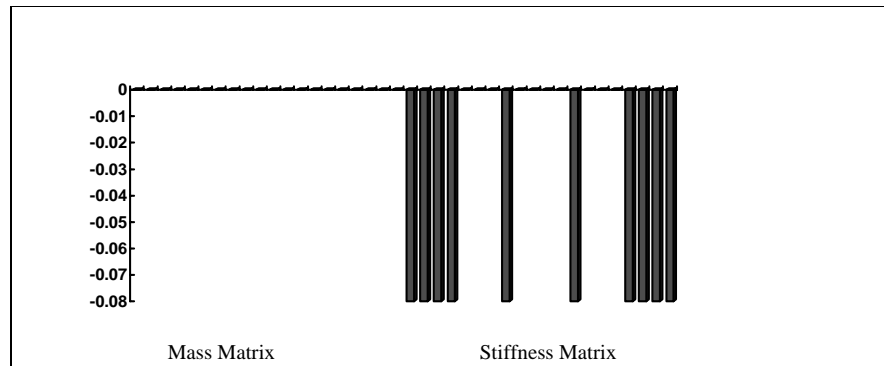


Figure 6.1: Computed p-values for Case1 (CEAM)

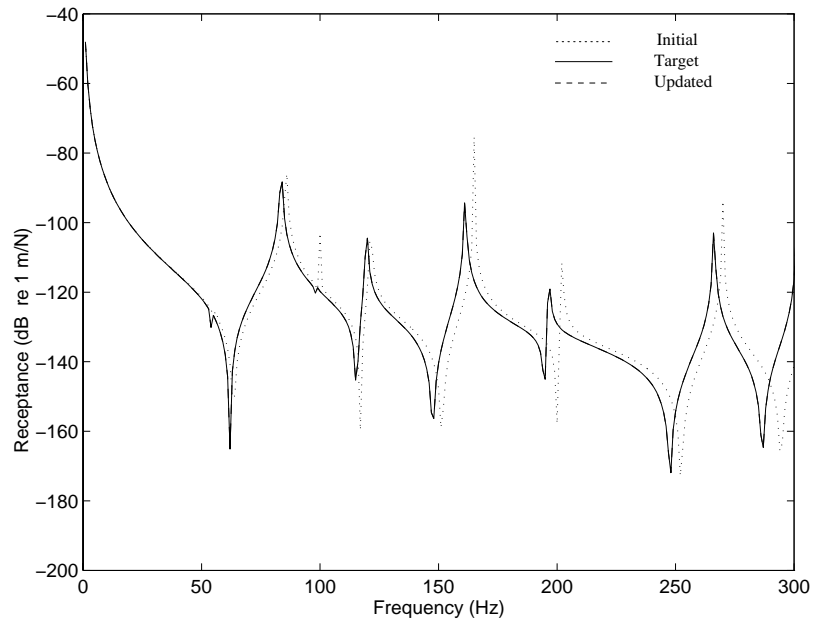


Figure 6.2: Initial, target and updated responses for Case1 (CEAM)
The updated and target responses are identical

Case 2. Effect of Damping

The same exercise was repeated by including 1% hysteretic damping in both models, i.e. FE1 and X1. The damping in model X1 was forced to be non-proportional by considering some of the elements only. The initial damping in FE1 was assumed to be proportional by allocating a damping matrix for each element. In this case the number of unknowns is $3 \times 20 = 60$ and the elements of the target mode shape vector are complex. Using again 10 complete modes, the errors were identified exactly, including those associated with the non-proportional damping (Fig. 6.3). As a direct consequence, the responses obtained from the reference and updated models were found to be identical. This result is somewhat encouraging because other updating approaches are known to be prone to numerical problems in similar cases (Imregun *et al.*, 1995b).

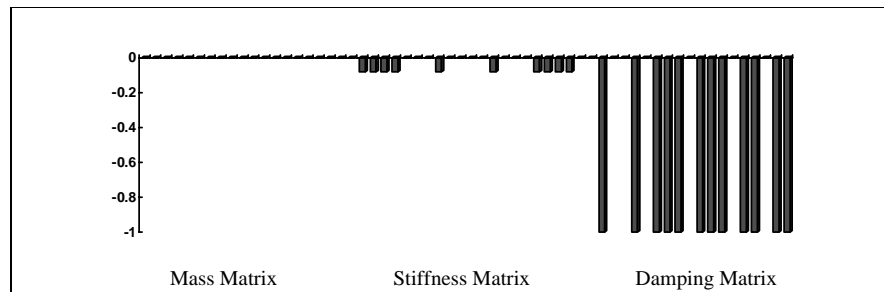


Figure 6.3: Computed p-values for Case2 (CEAM)

Case 3. Effect of Measurement Noise

The undamped and damped cases above were repeated for 5% random noise which was added to the simulated FRFs obtained from X1. The target eigenproperties were then obtained by applying a global rational fraction curve-fitting algorithm to the polluted FRFs. The computed p-values are shown in Fig. (6.4) and it is immediately seen that there is little correspondence between the actual errors and the proposed corrections. The responses obtained from the target (X1) initial (FE1) and updated

models are overlaid in Fig. (6.5). Although noise has an obvious detrimental effect on the updating quality, the updated model still shows a marked improvement over the initial one, indicating that the model has been corrected in some global sense without particular emphasis on the location or magnitude of the initial discrepancy. This finding is in line with those of many other studies that use a formulation similar to equation (6.21).

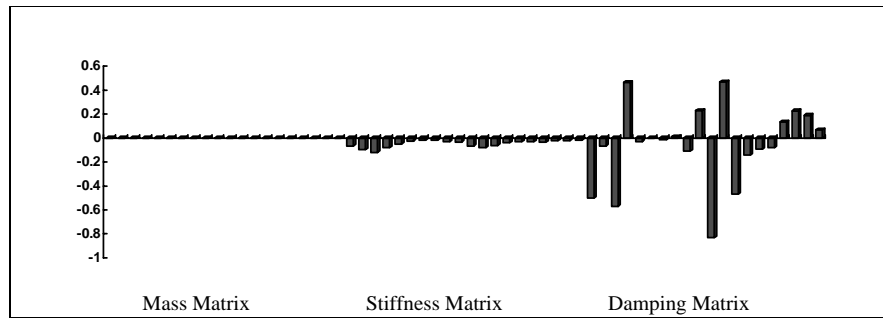


Figure 6.4: Computed p-values for Case3 (CEAM)

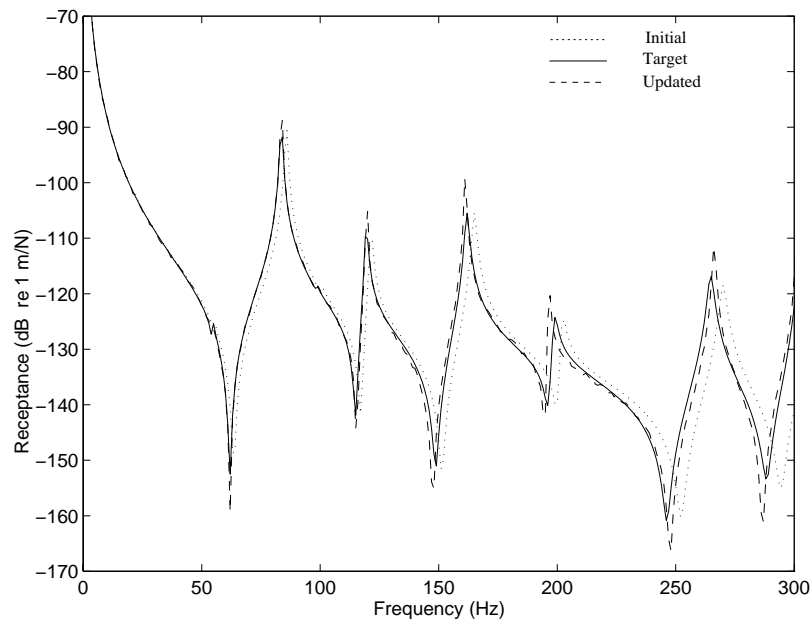


Figure 6.5: Initial, target and updated responses for Case1 (CEAM)
The updated and target responses are identical

Case 4. Effect of Mode Shape Incompleteness

One of the well-known problems in model updating is the size incompatibility between the experimental and theoretical models. The difficulties arise because of poor accessibility and due to the lack of reliable methods for measuring the rotational degrees of freedom. This latter situation is simulated here by removing the rotational co-ordinates from the target mode shapes. Three different sets of results, corresponding to 40-, 60- and 80-mode assignments, are shown in Fig. (6.6). The adverse effect of co-ordinate reduction is obvious and it can, to a certain extent, be compensated by using more and more modes in the assignment, though no updated model is able to match the target one exactly.

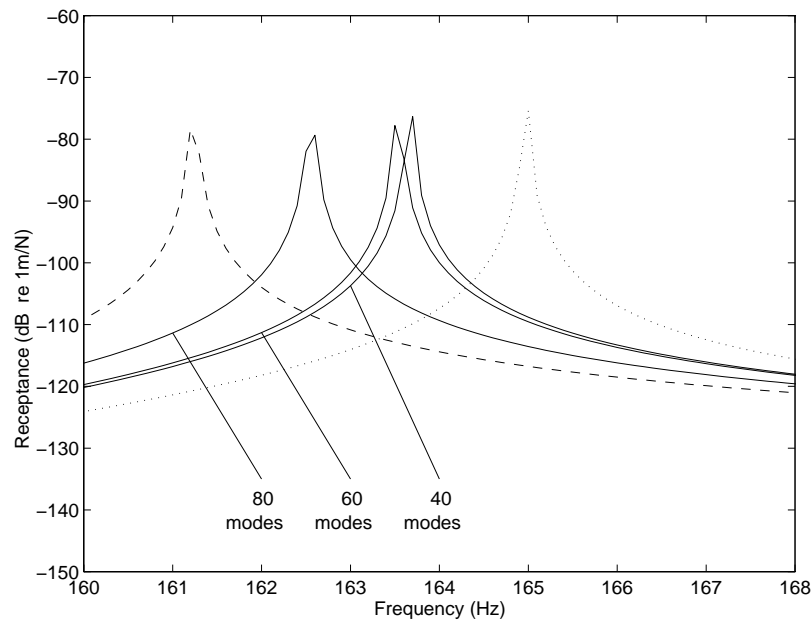


Figure 6.6: Effect of increasing the number of assigned modes - Case4 (CEAM)

Case 5. Effect of Localised Changes

Model FE2 was used to investigate the effect of localised changes. In this case, the discrepancies between X1 and FE2 are not directly proportional to the p-values and hence equations (6.21) are no longer exact in this particular case. In other words, the moment of inertia errors are not global in nature since the elements of the individual stiffness matrices are not all affected the same way. As the inertia errors are associated with the mass matrix, this was also included in the updating process. Initial calculations produced p-values which were not representative of the inertia discrepancies between the two models. More alarmingly, the resulting response model showed very poor agreement with the target one. After some deliberation it was decided to increase the number of modes to be assigned as this approach was observed to be a numerical cure in the previous case study. Given the practical limitations on the availability of higher experimental modes, 30 modes of the initial finite element FE2 were assigned to the updated model. The resulting p-values are shown in Fig. (6.7) and the FRFs obtained from the updated model are compared to the initially-predicted and target ones in Fig. (6.8). Although the error location is quite very poor, the performance of the updated model is acceptable at the response function level, a feature which again suggests that accurate error location is not necessarily a pre-requisite for updating.

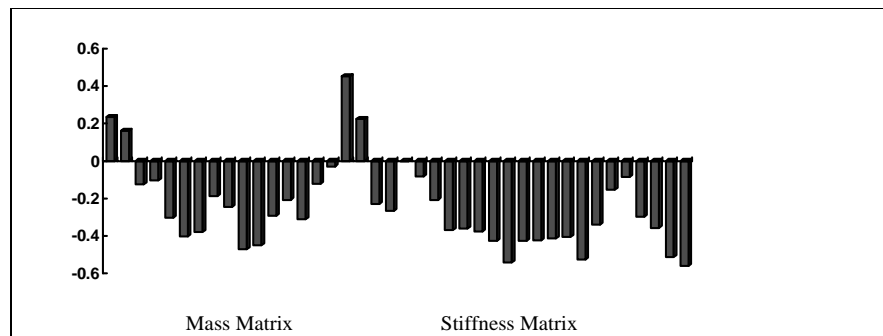


Figure 6.7: Computed p-values for Case5 (CEAM)

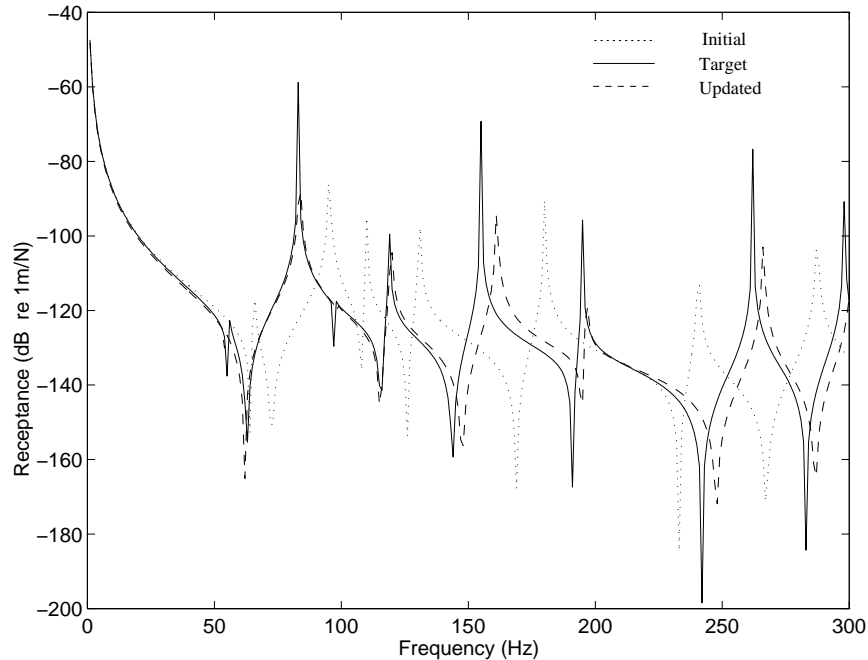


Figure 6.8: Initial, target and updated responses for Case5 (CEAM)

Case 6. Effect of Discretisation Differences

All cases studied so far are based on a one-to-one correspondence between the theoretical and experimental models, a feature that cannot be achieved in practice. The fact that models FE1, FE2 and X1 have been discretised using the same mesh not only simplifies the problem of model updating significantly, but is also unrepresentative of the real engineering problem where the discrepancies between the experimental and theoretical models not explicitly present in the theoretical model in the form of directly correctable parameters. It was therefore decided to update Model FE1 using Model X2, the mesh of which is double in size. Initially, it was attempted to assign the modal properties of model X2 to model FE1 directly. However, after few attempts, it was noticed that p -values were all approaching the value of -1, indicating that only the trivial solution could be found. The explanation for such behaviour is relatively straightforward. As shown in Figs. (6.9) and (6.10), the assignment can only succeed if the target and initial sets belong to the same eigen domain. If the two sets are not

in the same domain, it is not possible to find mass and stiffness correction matrices so that the initial and updated models span the same set of eigenvalues and eigenvectors for a given frequency range and hence no updated model can be guaranteed until the closeness of the two sets is improved. Such an approach will be adopted here in the form of a two-stage assignment.

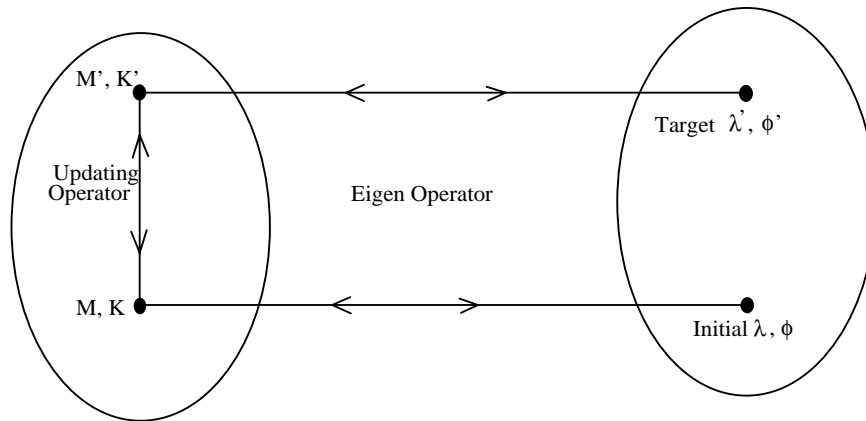


Figure 6.9: Target and Initial Models belong to the same domain

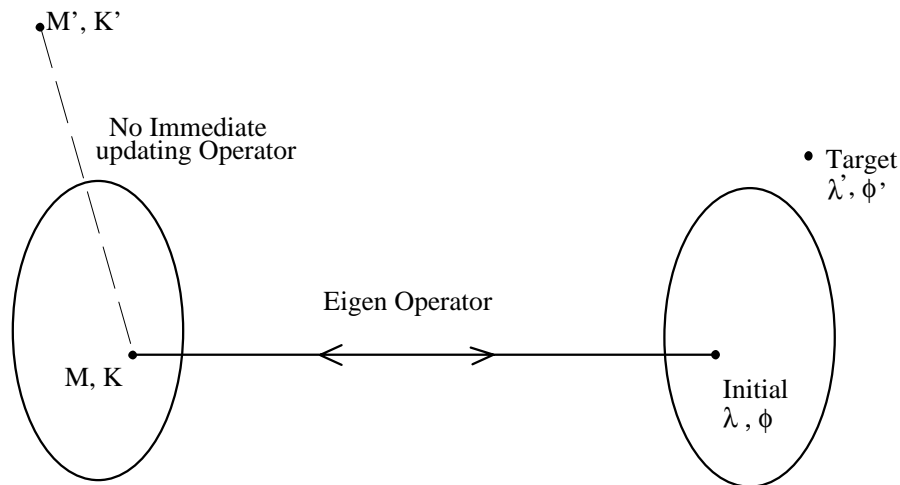


Figure 6.10: Target and Initial Models do not belong to the same domain

After some deliberation, it was decided to assign the first 10 eigenvalues (but not eigenvectors) of model X2 to model FE1 and to keep the eigenvectors of FE1 un-

changed. This approach is equivalent to changing the global material properties of the system, say as density and Young's modulus, since such a modification will produce shifts in natural frequencies only. Once an updated model was obtained, a further assignment was made by using the first 10 eigenvalues and eigenvectors of X2. To force model closeness, a further 60 modes (both eigenvalues and eigenvectors) of model FE1 were self-assigned. The results of this two-stage assignment are plotted in Fig. (6.11) in the form of initial, target and updated FRFs. It is interesting to note that the first mode is not particularly well corrected but the remaining part of the response shows a marked improvement. The problem is, once again, in the closeness of the initial and target models. For the two given sets, it was not possible to find a modification that could correct the first mode.

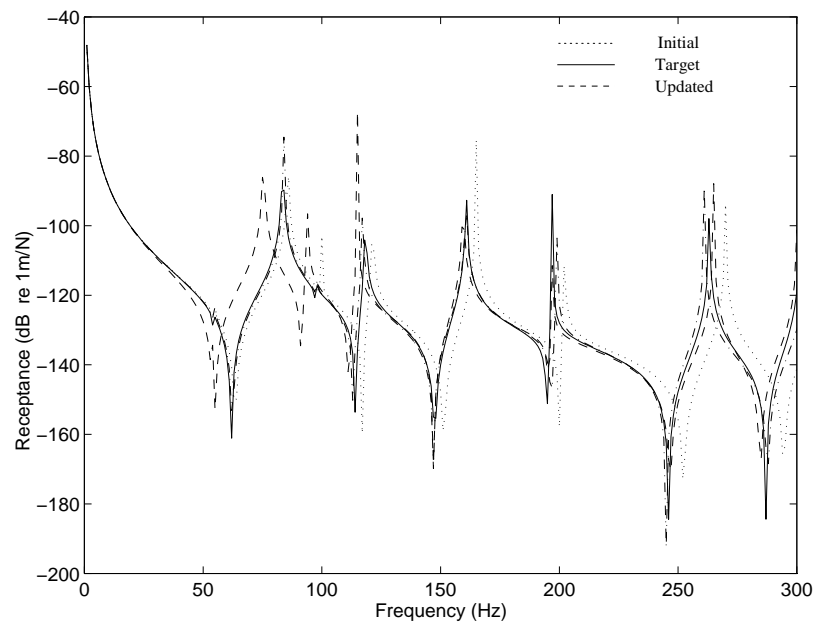


Figure 6.11: Initial, target and two updated responses for Case6 (Two-stage CEAM)

6.4.2 A Comparison with the Response Function Method

It is now proposed to compare the performance of the response function and eigenstructure assignment methods by repeating the six cases above using the former technique. From the outset, it must be stressed the RFM is an iterative method where the convergence of the p-values cannot be guaranteed. On the other hand, the CEAM is based on the direct solution of an over-determined set of linear equations and the optimisation algorithm is unconditionally stable by virtue of being quadratic. Although both methods will yield identical results for noise-free and complete modal information cases, very significant differences can be seen in other situations. The results are listed in Table (6.2).

Table 6.2: Computational effort for RFM and CEAM updating.
All CPU seconds normalised with respect to Case 1 - CEAM solution

Case	Description	CEAM Seconds	RFM	
			Seconds/iter	No of iters
1	FE1 vs X1, 10 complete modes no damping, no noise	100	284	3
2	FE1 vs X1, 10 complete modes 1% damping, no noise	106	431	4
3	FE1 vs X1, 10 complete modes 1% damping, 5% noise	359	No. conv.	-
4	FE1 vs X1, 60 incomplete modes no damping, no noise	471	170	12
5	FE2 vs X1, 50 complete modes no damping no noise	746	207	20
6	FE1 vs X2, 70 complete modes no damping, no noise	881	No. conv.	-

For the first two cases, both methods produced identical answers but the CEAM is seen to be about an order of magnitude faster, as the RFM needs 3-4 iterations for convergence. For the third case, where the measured FRF data are polluted by noise, the RFM fails to converge while the CEAM produces an updated model, the

response from which is in good agreement with the target one. The fourth case, where incomplete mode shapes are used, is handled better by the RFM in the sense that both the discrepancies are identified and the agreement at the response level is good. However, it should be noted that relatively small errors still appear in the mass matrix. A comparison of the p-values computed using the two methods is given in Figs. (6.12) and (6.13). The performance of the two methods is about the same for the fifth case for which the changes are in the moments of inertia. The last case, for which there is no one-to-one correspondence between the target and the initial models, can only be dealt with the CEAM and the agreement of the target and updated models at the response level is acceptable, except in the vicinity of the first mode.



Figure 6.12: Computed p-values for Case4 (CEAM)

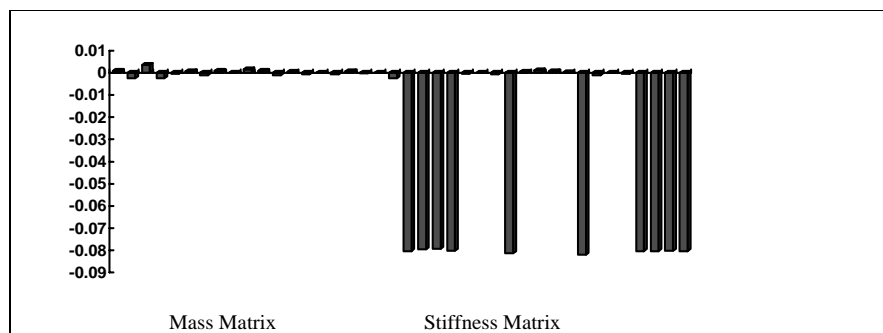


Figure 6.13: Computed p-values for Case4 (RFM)

6.5 Concluding Remarks

- The existing constrained eigenstructure assignment method has been modified so that it can deal with the updating of large-order systems. The resulting formulation is compatible with the response function and inverse eigensensitivity methods in the sense that the individual mass, stiffness and damping matrices are corrected by simple multipliers, the so-called p-values.
- The inherent difficulties associated with finite element model updating are, once again, illustrated by the case studies that are undertaken. Using a correction factor formulation, the model can only be corrected in a global sense without particular emphasis on the actual sources of discrepancy between the theoretical and experimental models. However, the response obtained from globally-updated models is a better match to the measured ones in most cases.
- Numerical case studies seem to indicate that the updating of the damping matrix becomes an easier, and certainly less ill-conditioned task, by virtue of using an unconditionally stable quadratic optimisation algorithm.
- As in many other case studies, the closeness of the initial and target models is found to be a key issue for successful updating. However, in the case of the CEAM, it is possible to employ a two-stage updating procedure to partly overcome this difficulty.
- The eigenstructure assignment method yields the solution directly and hence it has a significant advantage over the response function method, its iterative counterpart. A comparative study between the two methods reveals that the RFM requires substantially more CPU power in all cases. Also, the convergence of the RFM cannot be guaranteed in cases where the measured FRFs are polluted by noise or when the discretisation differences are significant. On the other hand, the RFM seems to be able to cope better with incomplete measured data.
- Of particular note is the fact that both methods can only correct the finite

element model in a global sense since the location of specific discrepancies cannot be achieved by the present formulation based on elemental correction factors. In any case, this feature is an inherent problem in model updating studies, as illustrated by the last case study: unless the discrepancies are actually present in the model to be updated in a one-to-one fashion, it is difficult to see how they can be remedied by changing other, albeit related, parameters.

- The importance of the model closeness is clearly illustrated by the last case study. No updated model can be guaranteed for cases where the initial and updated models do not span the same set of eigenvalues and eigenvectors by virtue of belonging to the same eigen domain. This observation is general and underlines one of the fundamental problems in model updating.

Chapter 7

Model Updating Using Generic Elements ¹

7.1 Introduction

Most updating approaches are based on parameter correcting: a set of design variables (alternately, individual finite element matrix multipliers, the so-called correction factors or p-values) are considered to be the unknowns, the correct values of which are expected to yield a correct model. Such a methodology is based on the assumption that the elemental mass and stiffness matrices can be expressed as sums or products of further intermediate matrices which are governed by one or more parameters from the chosen set. However, the elemental matrices equally depend on the integration of shape functions, the matter becoming much more complicated if the element cannot be expressed in closed form. For instance, the mass and stiffness matrices can be written directly for uniform beams if all material and geometric properties are known. In this case, it is relatively straightforward to determine a number of intermediate matrices that are directly related to the design variables. On the other hand, the task is far less well defined for more complex cases, say a 20-noded brick element,

¹Presented at 1996 International Conference on Noise and Vibration Engineering, Leuven, Belgium

the mass and stiffness matrices of which result from numerical integration. Moreover, even in cases where the intermediate matrices can be defined, the required changes in the design parameters may become unrealistic. Such situations are often encountered for awkward geometries (e.g. joint modelling using springs or beams) or when the discrepancy between the initial and target models is large so that it cannot be accommodated by relatively small changes in the design parameters.

An alternative method is to find a method in which the parameter changes are part of the finite element formulation so that a degree of consistency can be maintained throughout. Such an approach, referred to as generic element or acceptable element updating (Ahmadian *et al.*, 1994a,b; Gladwell & Ahmadian, 1995), will be adopted here. In this particular technique, the elemental mass and stiffness matrices are allowed to change dynamically while retaining their physical meaning and mathematical properties (symmetric, positive-definite, etc.) by virtue of belonging to a same consistent family of such matrices. The idea is somewhat reminiscent of adaptive meshing techniques that are routinely used in computational fluid dynamics applications.

The main purpose of this Chapter is to adapt the generic element formulation to any case where the mass and stiffness matrices are numerically known and to provide a benchmark against other more established updating methods which are based on direct parameter correction. It is further proposed to use a response function based objective function, though a sensitivity based formulation is also possible.

7.2 Basic Theory

Let us consider the stiffness and mass matrices, $[K^e]$ and $[M^e]$, of a typical finite element. It is possible to seek an eigensolution at the elemental level:

$$([K^e] - \lambda[M^e]) [\Phi] = 0 \quad (7.1)$$

If the element has n degrees of freedom and r rigid body modes ($r \leq 6$) then $[\Phi]$ can

be written as:

$$[\Phi] = [[\Phi_R], [\Phi_S]] \quad (7.2)$$

Because of the relationship between the rigid body modes and the stiffness matrix, one can write:

$$[K^e][\Phi_R] = 0 \quad (7.3)$$

Since $[K^e]$ and $[M^e]$ are positive semi-definite and positive definite respectively, it is possible to write them in a diagonal form as:

$$\begin{aligned} [K^e] &= [U][\Theta][U]^T = \sum_{i=r+1}^n \theta_i u_i u_i^T \\ [M^e] &= [V][\Sigma][V]^T = \sum_{i=1}^n \sigma_i v_i v_i^T \end{aligned} \quad (7.4)$$

where $[U]$ and $[V]$ are orthogonal element decomposition matrices and $[U]^T[\Phi_R] = 0$.

The proposed way of constructing a family of generic elements is to consider some initial $[K_0^e]$ and $[M_0^e]$ matrices, usually the standard FE matrices, and find their corresponding constituent matrices $[U_0]$ and $[V_0]$. In some simple cases, it is possible to relate $[K_0^e]$ and $[M_0^e]$ directly to material and geometric properties of the element (Ahmadian *et al.*, 1994b). However, this particular approach requires those matrices to be available in parametric form and hence it is not applicable to the general case where the matrices can only be derived numerically.

In any case, a second set of constituent matrices can then be defined by:

$$\begin{aligned} [U] &= [U_0][R] \\ [V] &= [V_0][T] \end{aligned} \quad (7.5)$$

Where $[R]$ and $[T]$ are two orthogonal matrices, the choice of which is arbitrary. Using equations (7.4) and (7.5), a new set of elemental mass and stiffness matrices can be written as:

$$\begin{aligned} [K^e] &= [U_0] [R] [\Theta] [R]^T [U_0]^T \\ [M^e] &= [V_0] [T] [\Sigma] [T]^T [V_0]^T \end{aligned} \tag{7.6}$$

In equations (7.6), the diagonal elements of matrices $[\Theta]$ and $[\Sigma]$, where θ_i ($i = r + 1, \dots, n$) and σ_i ($i = 1, \dots, n$), can also take some arbitrary values, thus increasing the number of possible updating parameters. Remembering that most model updating methods are based on minimising some objective function between the reference and the target models, an iterative solution involving matrix building over equations (7.6) is somewhat undesirable.

In order to reduce the number of unknowns in the symmetric matrix products $[R] [\Theta] [R]^T$ and $[T] [\Sigma] [T]^T$, it is possible to update just the dominant modes of each matrix and keep the remaining ones unchanged. This can be achieved by considering the singular values σ_i and θ_i of the mass and stiffness matrices. Ross (1971) has indicated the importance of accurate representation of the mass contributions at the high frequencies and of the stiffness contributions at lower frequencies. This observation will have implications for both selecting and computing the σ_i and θ_i parameters.

Some more restrictions can be applied on diagonal matrices $[R]$ and $[T]$. For instance, the number of rigid body modes remain the same in both old and new system and the new rigid body modes are linear combinations of the original ones. This causes the matrices $[R]$ and $[T]$ to be in block form.

A further reduction is also possible by considering the symmetry of the elemental matrices. For example, the symmetric eigenvectors are a linear combination of initial symmetric eigenvectors and the same can be applied to the anti-symmetric eigenvectors.

Therefore equations (7.6) are the main equations for constructing a generic family. In the following, the mass and stiffness matrices for rod, 2D beam and 4-nodes plate element will be described.

7.3 Rod Elements

Consider the longitudinal vibration of a straight, thin rod of length L . The mass and stiffness matrices for the lumped mass model of a uniform element are:

$$[K_0^e] = k_0 \begin{bmatrix} 1 & -1 \\ -1 & 1 \end{bmatrix} \quad (7.7)$$

$$[M_0^e] = m_0 \begin{bmatrix} 1/2 & 0 \\ 0 & 1/2 \end{bmatrix} \quad (7.8)$$

where $m_0 = \rho AL$, $k_0 = EA/L$ and ρ , E , A and L are density, module of elasticity, cross section and the length of the rod.

The initial mass and stiffness matrices $[M_0^e]$ and $[K_0^e]$ can be decomposed to find $[U]$, $[\Theta]$, $[V]$ and $[\Sigma]$ matrices:

$$[K_0^e] = k_0 \begin{bmatrix} -\frac{1}{\sqrt{2}} & -\frac{1}{\sqrt{2}} \\ -\frac{1}{\sqrt{2}} & \frac{1}{\sqrt{2}} \end{bmatrix} \begin{bmatrix} 0 & 0 \\ 0 & 2 \end{bmatrix} \begin{bmatrix} -\frac{1}{\sqrt{2}} & -\frac{1}{\sqrt{2}} \\ -\frac{1}{\sqrt{2}} & \frac{1}{\sqrt{2}} \end{bmatrix}^T \quad (7.9)$$

$$[M_0^e] = m_0 [I] \begin{bmatrix} \frac{1}{2} & 0 \\ 0 & \frac{1}{2} \end{bmatrix} [I] \quad (7.10)$$

Let's first consider the stiffness matrix. Since the system possesses one rigid mode which remains the same in the new system, the orthogonal matrix $[R]$ should be equal to identity matrix. Therefore, the new stiffness matrix, $[K^e]$, can be constructed as:

$$[K_0^e] = k_0 \begin{bmatrix} -\frac{1}{\sqrt{2}} & -\frac{1}{\sqrt{2}} \\ -\frac{1}{\sqrt{2}} & \frac{1}{\sqrt{2}} \end{bmatrix} \begin{bmatrix} 0 & 0 \\ 0 & \theta_1 \end{bmatrix} \begin{bmatrix} -\frac{1}{\sqrt{2}} & -\frac{1}{\sqrt{2}} \\ -\frac{1}{\sqrt{2}} & \frac{1}{\sqrt{2}} \end{bmatrix}^T \quad (7.11)$$

After some manipulations:

$$[K_0^e] = k \begin{bmatrix} 1 & -1 \\ -1 & 1 \end{bmatrix} \quad (7.12)$$

where $k = \frac{1}{2}k_0\theta_1$. It is noticeable that $[K^e]$ does not change its form and is specified by one parameter, i.e. k .

Now consider the elemental mass matrix $[M_0^e]$. By considering a general form for the orthogonal matrix $[T]$, the new $[M^e]$ can be defined as:

$$[M^e] = m_0 [I] \begin{bmatrix} \cos \zeta & \sin \zeta \\ -\sin \zeta & \cos \zeta \end{bmatrix} \begin{bmatrix} \sigma_1 & 0 \\ 0 & \sigma_2 \end{bmatrix} \begin{bmatrix} \cos \zeta & \sin \zeta \\ -\sin \zeta & \cos \zeta \end{bmatrix}^T [I] \quad (7.13)$$

After some simplifications, one gets:

$$[M^e] = \begin{bmatrix} m_1 & m_{12} \\ m_{12} & m_2 \end{bmatrix} \quad (7.14)$$

where

$$\begin{aligned} m_1 &= \sigma_1 \cos^2 \zeta + \sigma_2 \sin^2 \zeta \\ m_2 &= \sigma_1 \sin^2 \zeta + \sigma_2 \cos^2 \zeta \\ m_{12} &= (\sigma_2 - \sigma_1) \cos \zeta \sin \zeta \end{aligned} \quad (7.15)$$

The mass matrix is symmetric and is determined by three parameters. If one considers

the element symmetry about its centre, then $\zeta = 45^\circ$ and $m_1 = m_2$ and the number of parameters will be reduced to two parameters per each elemental mass matrix.

Thus, there are three parameters for each rod element, one for the stiffness and two for the mass matrix, and for the purpose of updating the derivatives of $[K^e]$ and $[M^e]$ matrices with respect to the unknown parameters should be calculated.

7.4 Beam Elements

Let's consider a simple Euler Bernoulli beam. We assume a lumped-mass model for mass matrix and a stiffness matrix with cubic shape functions. Then, for a uniform beam element :

$$[K_0^e] = k_0 \begin{bmatrix} 12 & 6 & -12 & 6 \\ 6 & 4 & -6 & 2 \\ -12 & -6 & 12 & -6 \\ 6 & 2 & -6 & 4 \end{bmatrix} \quad (7.16)$$

$$[M_0^e] = m_0 \begin{bmatrix} 1/2 & 0 & 0 & 0 \\ 0 & 1/24 & 0 & 0 \\ 0 & 0 & 1/2 & 0 \\ 0 & 0 & 0 & 1/24 \end{bmatrix} \quad (7.17)$$

Where $m_0 = \rho AL$, $k_0 = EI/L^3$ and the displacement vector is $\{w_{i-1}, Lw'_i, w_i, Lw'_i\}$.

The stiffness matrix may be written in the form of:

$$[K_0^e] = k_0 \begin{bmatrix} \frac{1}{\sqrt{2}} & -\frac{1}{\sqrt{3}} & 0 & \frac{2}{\sqrt{10}} \\ 0 & \frac{1}{\sqrt{3}} & \frac{1}{\sqrt{2}} & \frac{1}{\sqrt{10}} \\ \frac{1}{\sqrt{2}} & 0 & 0 & -\frac{2}{\sqrt{10}} \\ 0 & \frac{1}{\sqrt{3}} & -\frac{1}{\sqrt{2}} & \frac{1}{\sqrt{10}} \end{bmatrix} \begin{bmatrix} 0 & 0 & 0 & 0 \\ 0 & 0 & 0 & 0 \\ 0 & 0 & 2 & 0 \\ 0 & 0 & 0 & 30 \end{bmatrix} \begin{bmatrix} \frac{1}{\sqrt{2}} & -\frac{1}{\sqrt{3}} & 0 & \frac{2}{\sqrt{10}} \\ 0 & \frac{1}{\sqrt{3}} & \frac{1}{\sqrt{2}} & \frac{1}{\sqrt{10}} \\ \frac{1}{\sqrt{2}} & 0 & 0 & -\frac{2}{\sqrt{10}} \\ 0 & \frac{1}{\sqrt{3}} & -\frac{1}{\sqrt{2}} & \frac{1}{\sqrt{10}} \end{bmatrix}^T$$

Since the rigid body modes remain unchanged for both systems, therefore the matrices $[\Theta]$ and $[R]$ will be:

$$[\Theta] = \begin{bmatrix} 0 & 0 & 0 & 0 \\ 0 & 0 & 0 & 0 \\ 0 & 0 & \theta_1 & 0 \\ 0 & 0 & 0 & \theta_2 \end{bmatrix} \quad (7.18)$$

$$[R] = \begin{bmatrix} 1 & 0 & 0 & 0 \\ 0 & 1 & 0 & 0 \\ 0 & 0 & \cos \zeta & \sin \zeta \\ 0 & 0 & -\sin \zeta & \cos \zeta \end{bmatrix} \quad (7.19)$$

After some calculations, the most general stiffness matrix will obtain as:

$$[K^e] = \begin{bmatrix} 0 & \frac{2}{\sqrt{10}} \\ \frac{1}{\sqrt{2}} & \frac{1}{\sqrt{10}} \\ 0 & -\frac{2}{\sqrt{10}} \\ -\frac{1}{\sqrt{2}} & \frac{1}{\sqrt{10}} \end{bmatrix} \begin{bmatrix} x_1 & x_{12} \\ x_{21} & x_2 \end{bmatrix} \begin{bmatrix} 0 & \frac{1}{\sqrt{2}} & 0 & -\frac{1}{\sqrt{2}} \\ \frac{2}{\sqrt{10}} & \frac{1}{\sqrt{10}} & -\frac{2}{\sqrt{10}} & \frac{1}{\sqrt{10}} \end{bmatrix} \quad (7.20)$$

where

$$\begin{aligned} x_1 &= \theta_1 \cos^2 \zeta + \theta_2 \sin^2 \zeta \\ x_{12} &= (\theta_2 - \theta_1) \sin \zeta \cos \zeta \\ x_2 &= \theta_1 \sin^2 \zeta + \theta_2 \cos^2 \zeta \end{aligned} \quad (7.21)$$

There are two rigid body modes and two strain modes for this system. Two of these modes are symmetric and the other two modes are antisymmetric about the centre of element. If the symmetry property for the element is preserved then matrix $[T]$ will be in the form of:

$$[T] = \begin{bmatrix} \cos \eta & 0 & \sin \eta & 0 \\ 0 & \cos \gamma & 0 & \sin \gamma \\ -\sin \eta & 0 & \cos \eta & 0 \\ 0 & -\sin \gamma & 0 & \cos \gamma \end{bmatrix} \quad (7.22)$$

If one writes $[\Sigma] = \text{diag}\{\sigma_1, \sigma_2, \sigma_3, \sigma_4\}$, the final result for the mass matrix will be:

$$[M^e] = m_0[V_0] \begin{bmatrix} s_1 & 0 & s_{13} & 0 \\ 0 & s_2 & 0 & s_{24} \\ s_{13} & 0 & s_3 & 0 \\ 0 & s_{24} & 0 & s_4 \end{bmatrix} [V_0]^T \quad (7.23)$$

where s_1, \dots, s_4 are functions of $\sigma_1, \dots, \sigma_4, \eta$ and γ .

Thus, in this family, there are six unknown parameters for mass matrix, namely $s_1, s_2, s_3, s_4, s_{13}$ and s_{24} and three unknown parameters for stiffness matrix, namely x_1, x_{12} and x_2 . As mentioned by Gladwell & Ahmadian (1995), different types of 2D beam elements belong to this family. For instance, the Timoshenko beam element mass and stiffness matrices. Again, for the purpose of updating the derivatives of $[K^e]$ and $[M^e]$ matrices with respect to each parameter should be calculated.

7.5 Plate Elements

In this section, the bending of rectangular plates will be considered. The family consists of 12 degree-of-freedom elements, with two axis of symmetry (See Fig. 7.6). Each node has three degrees of freedom namely, deflection in Z direction and rotation around X and Y axis. This element has three rigid body modes and nine strain modes. For the latter case when $a/b = 2$ and $\nu = .3$, there are four symmetric modes around XZ and YZ planes, labelled as u_1, u_5, u_8 and u_9 . There are also two modes, u_2 and u_7 , which are symmetric around Z axis. The element has two symmetric modes

around x axis namely, u_4 and u_6 and one around y axis, u_3 . By considering such a symmetry, the generic family for the stiffness matrix can be constructed as:

$$[U] = \begin{bmatrix} u_1 & u_5 & u_8 & u_9 & u_2 & u_7 & u_3 & u_4 & u_6 \end{bmatrix} \begin{bmatrix} [R_1] & & & \\ & [R_2] & & \\ & & 1 & \\ & & & [R_3] \end{bmatrix} \quad (7.24)$$

where $[R_1]$ is a 4×4 orthogonal matrix while $[R_2]$ and $[R_3]$ are 2×2 orthogonal matrices. The family for the stiffness matrix contains 17 parameters. In general case all nine eigenvalues may change, i.e. $\lambda_i (i = 1, \dots, 9)$. The matrices $[R_1]$, $[R_2]$ and $[R_3]$ have six, one and one parameters respectively. If we assume that the effects of the three highest modes u_7 , u_8 and u_9 are negligible, the orthogonal matrices $[R_1]$, $[R_2]$ and $[R_3]$ can be written as:

$$[R_1] = \begin{bmatrix} \cos \zeta & \sin \zeta & 0 & 0 \\ -\sin \zeta & \cos \zeta & 0 & 0 \\ 0 & 0 & 1 & 0 \\ 0 & 0 & 0 & 1 \end{bmatrix} \quad (7.25)$$

$$[R_2] = \begin{bmatrix} 1 & 0 \\ 0 & 1 \end{bmatrix} \quad (7.26)$$

and

$$[R_3] = \begin{bmatrix} \cos \eta & \sin \eta \\ -\sin \eta & \cos \eta \end{bmatrix} \quad (7.27)$$

Now, the family specifies by 8 parameters namely, ζ , η and $\lambda_i (i = 1, \dots, 6)$. The above process can be applied for the mass matrix as well. Having constructed the

family of stiffness and mass matrices, the derivatives of $[K^e]$ and $[M^e]$ with respect to the selected parameters can be calculated. The next step is the selection of updating procedure which will be discussed in the next section.

7.6 Model Updating

Once the (unknown) correction parameters are selected, $[K^e]$ and $[M^e]$ can be expressed as a function of those parameters, i.e.

$$\begin{aligned} [K^e] &= [K^e(\alpha_1, \alpha_2, \dots, \alpha_k)] \\ [M^e] &= [M^e(\beta_1, \beta_2, \dots, \beta_m)] \end{aligned} \quad (7.28)$$

where $\alpha_1, \alpha_2, \dots, \alpha_k$ are the updating parameters for the element stiffness matrix while $\beta_1, \beta_2, \dots, \beta_m$ are the updating parameters for the element mass matrix.

In any case, the global stiffness and mass matrices may be written as:

$$\begin{aligned} [K] &= \sum_{i=1}^N [K_i^e] \\ [M] &= \sum_{i=1}^N [M_i^e] \end{aligned} \quad (7.29)$$

For simplicity of notation, it has been assumed that both global matrices have N elements.

Defining a vector $\{p\}$ of the unknown updating parameters as:

$$\{p\} = \{\alpha_1^1, \dots, \alpha_k^1, \dots, \alpha_1^N, \dots, \alpha_k^N; \beta_1^1, \dots, \beta_m^1, \dots, \beta_1^N, \dots, \beta_m^N\}$$

one can write ²:

²see Chapter 3

$$\{\epsilon(\{p\})\} = \{I\}_j - [Z^{Red}(\{p\})] \{H_X\}_j \quad (7.30)$$

where $\{\epsilon\}$ is a complex-valued vector of residuals, $[Z^{Red}]$ and $\{H_X\}_j$ are the reduced dynamic stiffness matrix and the vector of measured receptance respectively. The unknown parameters are contained in $[Z^{Red}]$ as the full dynamic stiffness matrix is given by:

$$[Z] = \sum_{i=1}^N ([K_i^e] - \omega^2[M_i^e]) \quad (7.31)$$

Because of the mathematical non-linearities involved in computing the α and β values of the elemental stiffness and mass matrices, equation (7.30) may or may not have a solution. In any case, $[Z^{Red}]$ can be expressed as a truncated Taylor series:

$$[Z^{Red}(\{p\})] = [Z^{Red}(\{p\}^0)] + \sum_i \frac{\partial[Z^{Red}]}{\partial p_i} \Delta p_i + O(\Delta p_i)^2 \quad (7.32)$$

By substituting equation (7.32) into equation (7.30) and assuming null residual vector, one obtains:

$$\{I\}_j - [Z^{Red}(\{p\}^0)] \{H_X\}_j = \left(\sum_i \frac{\partial[Z^{Red}]}{\partial p_i} \Delta p_i \right) \{H_X\}_j \quad (7.33)$$

Calculating the derivatives of $[Z^{Red}]$ with respect to the unknown parameters and writing equation (7.33) at different frequency points gives:

$$[A] \times \{p\} = \{b\} \quad (7.34)$$

Equation (7.34) can now be solved iteratively to obtain the unknown vector $\{p\}$. In most cases, $[A]$ will not be a square matrix and hence a generalised inverse will need to be used.

7.7 Case Studies

7.7.1 Uniform Rod

This case study deals with a uniform rod which is fixed in one end and free to vibrate at the other end (Fig. 7.1).

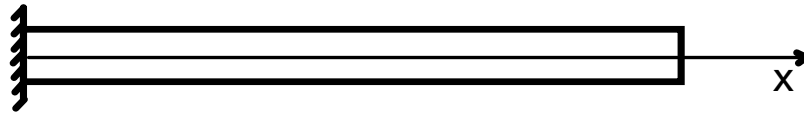


Figure 7.1: Uniform rod

The length of the rod is 1 meter, its circular cross section has a diameter of 1 cm. The rod is made of steel with modulus of elasticity of $207 \frac{GN}{m^2}$ and density of 2.700 Kg/m .

The experimental data are based on an analytical solution taken from Bishop & Johnson (1960). The rod is modelled by a 10-DOF mass-spring system in which the individual masses ($.254 \text{ Kg}$) and springs ($6.28 \times 10^8 \text{ N/m}^2$) are the initial generic elements for the system. The analytical model contains errors in the form of 10% mass decrease as well as discretisation errors due to the modelling of a continuous rod with a mass-spring system.

Fig. (7.2) shows the receptances in X direction at node 1, located at 10 cm from the fixed end of the bar, all obtained from a X direction excitation at node 1. Using a frequency resolution of 20 Hz, the receptances are evaluated for the 0-20,000 Hz frequency range.

In this case the number of unknowns is $3 \times 10 = 30$, as there are two unknowns for the mass matrix and one for the stiffness matrix of each element. Using 10 frequency points in the frequency range of interest, the modelling errors are identified and the discretisation errors are somewhat compensated for as there is good agreement at the response level (Fig. 7.2).

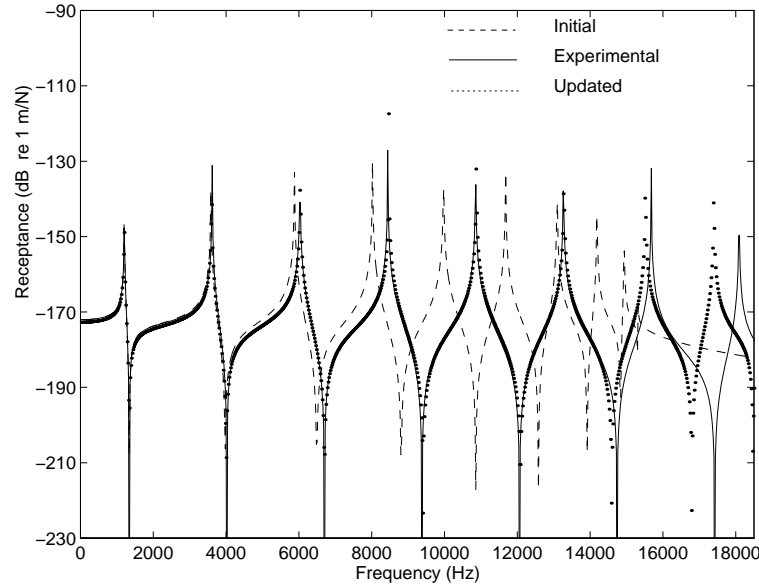


Figure 7.2: Initial, target and updated FRFs
Rod example

7.7.2 Uniform Beam

The second case study is a 2D uniform beam with a rectangular cross section (Fig. 7.3). The FE model consists of 10 elements which have lumped mass matrices while the stiffness matrices have cubic shape functions. Two cases will be considered here.

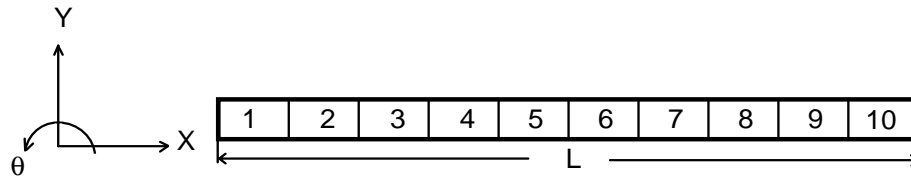


Figure 7.3: Uniform Beam

Case A. The experimental model, which contains no errors, consists of 11 Y direction receptances, all obtained for an excitation in the same direction at node 1. The analytical model contains errors in the form of 10% height decrease in all of its elements, which corresponds to a 27.1% decrease in moment of inertia. Ten frequency points, namely 500, 690, 900, 1000, 1145, 1600, 1700, 1883, 2200 and 2750 Hz, were selected from the range of 0-3000 Hz and equation (7.34) was used for calculating

the generic element parameters α and β . The point receptance at node 1 is depicted in Fig. (7.4) for the initial, experimental and updated cases. The success of the generic element formulation in updating this particular model is evident from the FRF overlays.

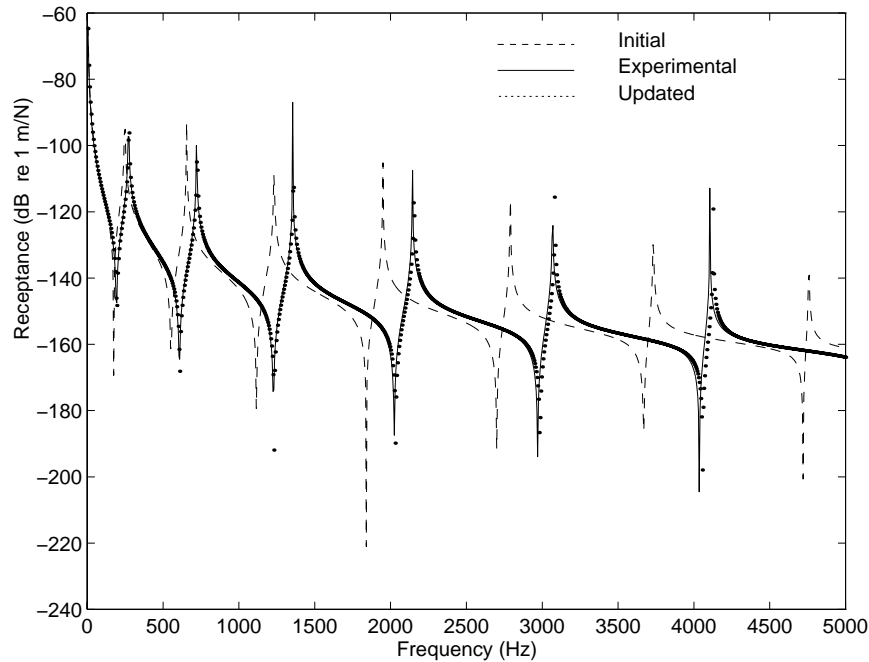


Figure 7.4: Initial, target and updated FRFs
Beam example - case A

Case B. The purpose of Case B is to investigate the effect of discretisation errors and hence the reference data are obtained from the closed-form expressions provided by Bishop & Johnson (1960). In this particular case, the FE model has discretisation errors only, since it uses the same nominal dimensions and material properties as the closed-form beam solution. As before, the experimental model consists of 11 Y direction receptances, all obtained for an excitation in the same direction at node 1. For this case, 17 frequency points were selected from the 0-4600 Hz frequency range (500, 690, 900, 1000, 1145, 1600, 1700, 1883, 2200, 2750, 3290, 3710, 3900, 4000, 4100, 4200 and 4600 Hz).

The FRFs obtained from the updated model are compared to the initial and experimental (i.e. closed-form solution) ones in Fig. (7.5). Although the experimental

and updated FRFs are not completely coincident, the results still show a good improvement over the initial model. More significantly, other formulations (p-value or actual design parameter) were unable to produce a converged solution for the same case, the objective function being still based on the difference of the response functions. Therefore, it appears that the generic element formulation is somehow able to compensate for discretisation errors as well as correcting parametric differences.

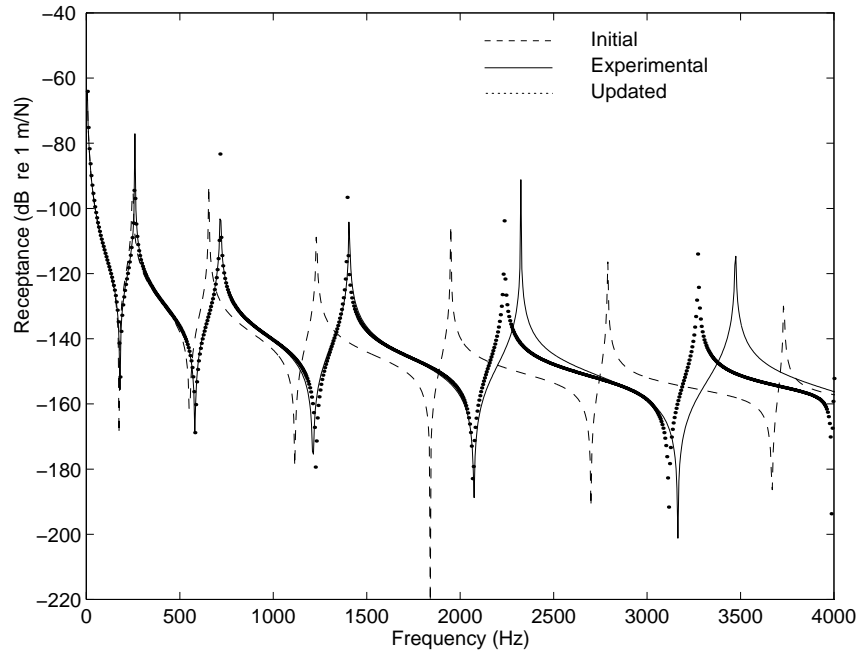


Figure 7.5: Initial, target and updated FRFs
Beam example - case B

7.7.3 Uniform Plate

The generic element formulation was applied to the case of a 4-nodded 12 DOF shell element next (Fig. 7.6). A free-free uniform plate, shown in Fig. (7.7), was analysed in two different configurations. In order to maintain compatibility with existing finite element programs, it was decided to import the elemental mass and stiffness matrices from the FE code ANSYS and to use them as the initial generic

elements. In this example, $[R]$ and $[T]$ were kept constant by assigning them a unit matrix throughout the updating process. Thus, only the singular values of the elemental mass and stiffness matrices were used as correction parameters and hence the number of unknowns was reduced to 21. Three cases will be studied here:

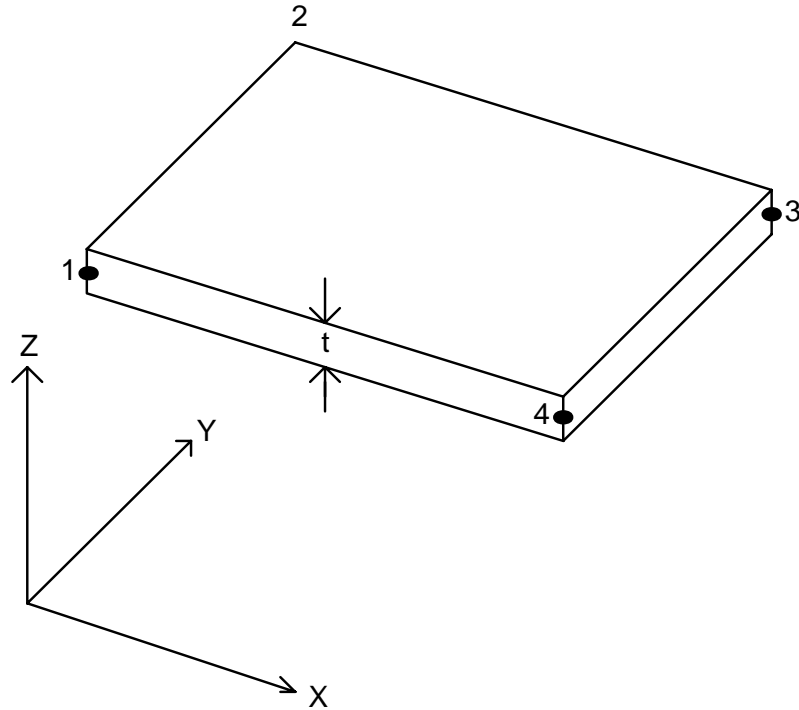


Figure 7.6: A four-node rectangular 2D plate element

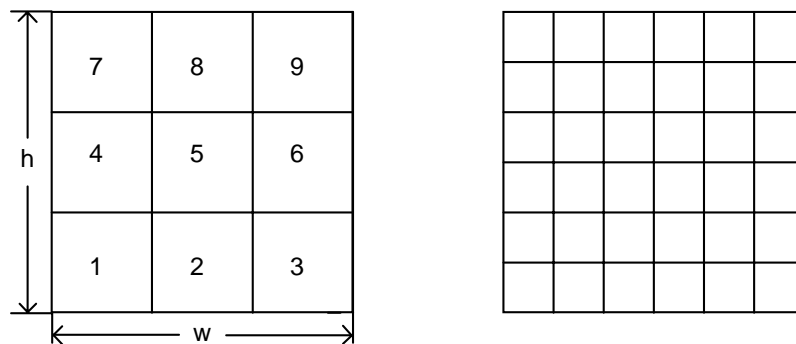


Figure 7.7: The two mesh configurations for the plate example
 ($E = 207GN/m^2$, $\rho = 7800Kg/m^3$, width= height=
 .15 m, thickness= .001m)

Case A. The plate was divided into nine elements, thus yielding $16 \times 3 = 48$ degrees of freedom. The analytical model contains errors in the form of 10% overall decrease in the mass matrix (elements 1, 3, 5, 7 and 9) and 10% overall increase in the stiffness matrix (elements 2, 4, 6 and 8). Here it should be noted that the chosen error configuration (direct matrix multiplier) does not correspond to a physical change in the structure. The experimental model, which contains no errors, consists of all Z direction receptances, obtained for a Z direction excitation at node 1. Ten frequency points, namely 50, 110, 170, 230, 300, 350, 450, 500, 600 and 700 Hz, were selected from the range of 0-800 Hz and equation (7.34) was used to compute the required generic element parameters. The initial, experimental and updated FRFs corresponding to this case are shown in Fig. (7.8). The results clearly show the capability of the generic element formulation for the identification of proportional errors in both the mass and stiffness matrices.

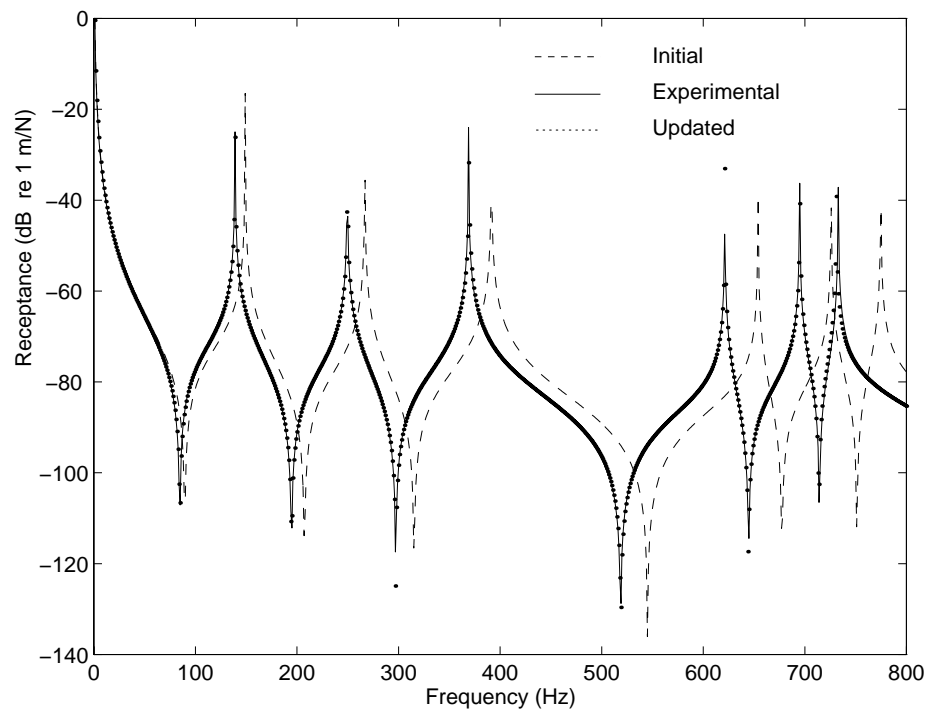


Figure 7.8: Initial, target and updated FRFs
Plate example - Case A

Case B. As before, the purpose of Case B is to investigate the effect of discretisation errors and reference data, same as Case A, were obtained from a refined FE model with a 6×6 the mesh (Fig. 7.7). The FE model to be corrected used the previous 3×3 mesh but had the same geometry and the material properties as the 6×6 mesh. The results of this case study is plotted in Fig. (7.9) in the form of initial, experimental and updated FRFs. As expected, the discretisation errors are more prominent after the first few modes but, nevertheless, they are corrected with remarkable success by the generic element formulation.

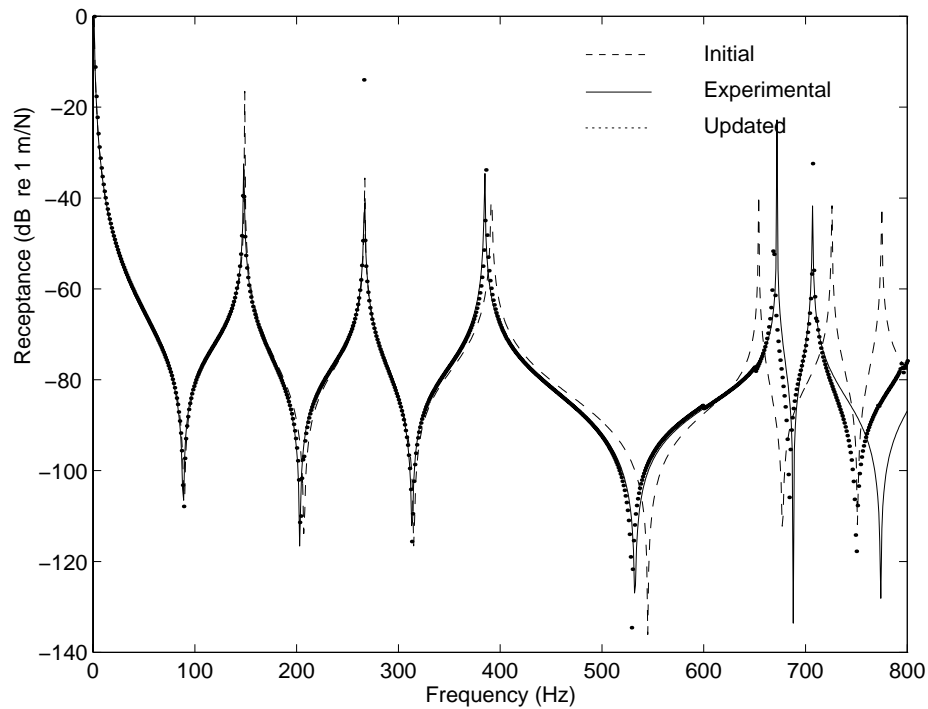


Figure 7.9: Initial, target and updated FRFs
Plate example - Case B

Case C. It was decided to investigate the effects of using experimental data polluted by noise and Case B was repeated by adding 1% random noise to the measured FRFs. The results are shown in Fig. (7.10) and it is immediately seen that noise has a relatively minor effect on the results.

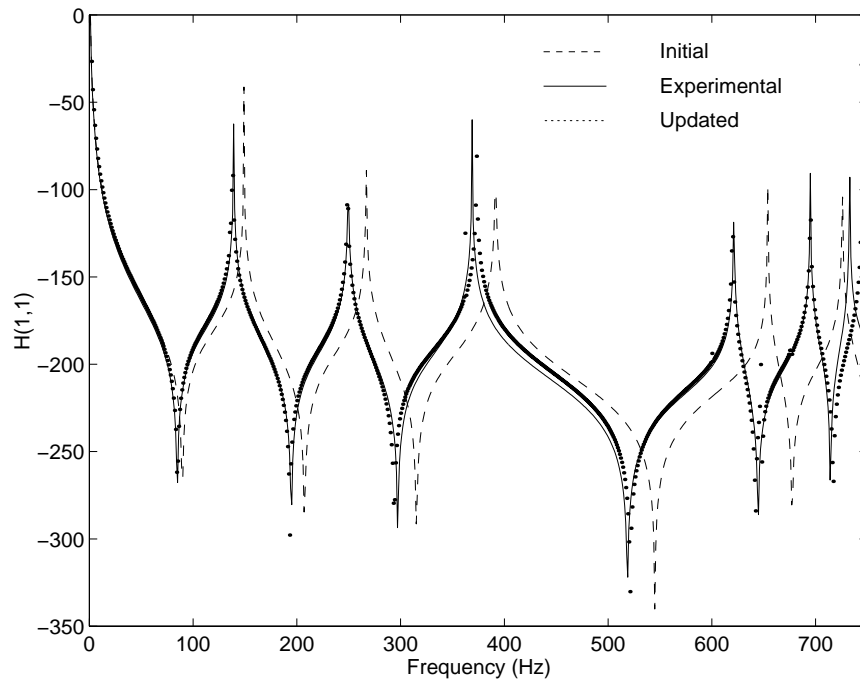


Figure 7.10: Initial, target and updated FRFs
Plate example - Case C

7.7.4 Computational Considerations

From the outset, it must be stressed that the generic element formulation is computationally very expensive and its application to large models requires careful optimisation of the existing formulation. This is the main reason of using small-size 2D elements in the numerical case studies. For instance, the beam generic element of the first study had 8 parameters per element (6 for the mass and 2 for the stiffness matrix)

while the plate generic element had 21 parameters per element (12 for the mass and 9 for the stiffness matrix). A 3D brick element with 8 nodes may well require over 30 parameters, depending on the details of a particular implementation. In any case, any finite element can be used to derive a corresponding family of generic elements, provided the finite element is known to full numerical accuracy.

Table 7.1: Computational effort for generic element and p-value formulations (CPU seconds are for an IBM RS/6000 model 540 computer)

Case Study	Generic element formulation		p-value formulation	
	9 correction factors/beam element 21 correction factors/plate element		2 correction factors/element	
	No of iterations	Seconds/iteration	No of iterations	Seconds/iteration
Beam - Case A	4	52	3	12
Beam - Case B	5	161	No convergence	N/A
Plate - Case A	3	2067	2	349
Plate - Case B	5	2067	No convergence	N/A
Plate - Case C	7	2067	-	-

7.8 Concluding Remarks

- A generic element formulation, together with a response function based objective function, has been used to update a number of small FE models. The results show that the approach can deal with both physical parameter and discretisation errors. The extension of the work to include a sensitivity-based objective function is believed to be straightforward.
- Although the generic element formulation can be based on the use of true design parameters such as material and geometric properties, this particular technique can only be applied to a small number of elements since the analytical formulation must be known.
- In the general case, where compatibility with existing FE programs is essential, it is possible to generate a family of generic elements for any given finite element.

In such situations, the correction parameters become the element singular values and/or the orthogonal constituent matrices and hence their physical meaning is lost.

- The main disadvantage of the method is the large amount of CPU effort that is needed for the solution a feature that arises from the number of unknowns per element and the nonlinear form of the objective function. However, the latter is not a specific generic element problem.

Chapter 8

Model Updating based on Physical Parameters

8.1 Introduction

When correcting mass and stiffness matrices via p-values, a correction in Young's modulus and density is inherently implied for most elements. The aim here is to extend the method of Chapter 3 to consider model updating through changes in physical parameters such as moment of inertia, Poisson's ratio, thickness and so on. Using such parameters, the model is likely to be adjusted more accurately and its connectivities will be preserved.

Sections (8.2) and (8.4) discuss a 3D beam element and a 2D plate element respectively, while an exact 3D beam element is addressed in Section (8.6).

8.2 Three Dimensional Beam Element

A general vibration analysis of a prismatic bar requires simultaneous consideration of its motion in all six directions and such an approach will be employed here.

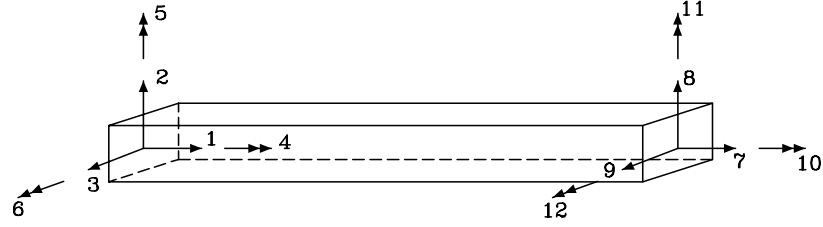


Figure 8.1: Spatial coordinates of beam element

Consider the case of a three-dimensional Euler-Bernoulli beam element where the degrees of freedom are ordered as:

$$[v_{x1} \ v_{y1} \ v_{z1} \ \theta_{x1} \ \theta_{y1} \ \theta_{z1} \ v_{x2} \ v_{y2} \ v_{z2} \ \theta_{x2} \ \theta_{y2} \ \theta_{z2}]$$

The subscripts 1 and 2 refer to the two nodes of the element, and v and θ denote the displacement and rotation fields, respectively. The elemental stiffness matrix is given by Przemieniecki (1968):

$$[K^e] = \begin{bmatrix} \frac{\alpha}{l} & 0 & 0 & 0 & 0 & 0 & -\frac{\alpha}{l} & 0 & 0 & 0 & 0 & 0 \\ 0 & \frac{12\gamma_z}{l^3} & 0 & 0 & 0 & \frac{6\gamma_z}{l^2} & 0 & -\frac{12\gamma_z}{l^3} & 0 & 0 & 0 & \frac{6\gamma_z}{l^2} \\ 0 & 0 & \frac{12\gamma_y}{l^3} & 0 & -\frac{6\gamma_y}{l^2} & 0 & 0 & 0 & -\frac{12\gamma_y}{l^3} & 0 & -\frac{6\gamma_y}{l^2} & 0 \\ 0 & 0 & 0 & \frac{\beta}{l} & 0 & 0 & 0 & 0 & 0 & -\frac{\beta}{l} & 0 & 0 \\ 0 & 0 & -\frac{6\gamma_y}{l^2} & 0 & \frac{4\gamma_y}{l} & 0 & 0 & 0 & \frac{6\gamma_y}{l^2} & 0 & \frac{2\gamma_y}{l} & 0 \\ 0 & \frac{6\gamma_z}{l^2} & 0 & 0 & 0 & \frac{4\gamma_z}{l} & 0 & -\frac{6\gamma_z}{l^2} & 0 & 0 & 0 & \frac{2\gamma_z}{l} \\ -\frac{\alpha}{l} & 0 & 0 & 0 & 0 & 0 & \frac{\alpha}{l} & 0 & 0 & 0 & 0 & 0 \\ 0 & -\frac{12\gamma_z}{l^3} & 0 & 0 & 0 & -\frac{6\gamma_z}{l^2} & 0 & \frac{12\gamma_z}{l^3} & 0 & 0 & 0 & -\frac{6\gamma_z}{l^2} \\ 0 & 0 & -\frac{12\gamma_y}{l^3} & 0 & \frac{6\gamma_y}{l^2} & 0 & 0 & 0 & \frac{12\gamma_y}{l^3} & 0 & \frac{6\gamma_y}{l^2} & 0 \\ 0 & 0 & 0 & -\frac{\beta}{l} & 0 & 0 & 0 & 0 & 0 & \frac{\beta}{l} & 0 & 0 \\ 0 & 0 & -\frac{6\gamma_y}{l^2} & 0 & \frac{2\gamma_y}{l} & 0 & 0 & 0 & \frac{6\gamma_y}{l^2} & 0 & \frac{4\gamma_y}{l} & 0 \\ 0 & \frac{6\gamma_z}{l^2} & 0 & 0 & 0 & \frac{2\gamma_z}{l} & 0 & -\frac{6\gamma_z}{l^2} & 0 & 0 & 0 & \frac{4\gamma_z}{l} \end{bmatrix} \quad (8.1)$$

where:

$$\begin{aligned}\alpha &= A \times E \\ \beta &= G \times J \\ \gamma_y &= E \times I_y \\ \gamma_z &= E \times I_z\end{aligned}$$

and the elemental mass matrix is given by:

$$[M^e] = \kappa \begin{bmatrix} \frac{1}{3} & 0 & 0 & 0 & 0 & 0 & \frac{1}{6} & 0 & 0 & 0 & 0 & 0 \\ 0 & a_z & 0 & 0 & 0 & b_z & 0 & c_z & 0 & 0 & 0 & d_z \\ 0 & 0 & a_y & 0 & -b_y & 0 & 0 & 0 & c_y & 0 & -d_y & 0 \\ 0 & 0 & 0 & \frac{\epsilon}{3} & 0 & 0 & 0 & 0 & 0 & \frac{\epsilon}{6} & 0 & 0 \\ 0 & 0 & -b_y & 0 & e_y & 0 & 0 & 0 & d_y & 0 & f_y & 0 \\ 0 & b_z & 0 & 0 & 0 & e_z & 0 & -d_z & 0 & 0 & 0 & f_z \\ \frac{1}{6} & 0 & 0 & 0 & 0 & 0 & \frac{1}{3} & 0 & 0 & 0 & 0 & 0 \\ 0 & c_z & 0 & 0 & 0 & -d_z & 0 & a_z & 0 & 0 & 0 & -b_z \\ 0 & 0 & c_y & 0 & d_y & 0 & 0 & 0 & a_y & 0 & b_y & 0 \\ 0 & 0 & 0 & \frac{\epsilon}{6} & 0 & 0 & 0 & 0 & 0 & \frac{\epsilon}{3} & 0 & 0 \\ 0 & 0 & -d_y & 0 & f_y & 0 & 0 & 0 & b_y & 0 & e_y & 0 \\ 0 & d_z & 0 & 0 & 0 & f_z & 0 & -b_z & 0 & 0 & 0 & e_z \end{bmatrix} \quad (8.2)$$

where:

$$\begin{aligned}a_z &= \frac{13}{35} + 6 \frac{\gamma_z}{5\alpha l^2} \\ b_z &= \frac{11l}{210} + \frac{\gamma_z}{10\alpha l} \\ c_z &= \frac{9}{70} - \frac{6\gamma_z}{5\alpha l^2} \\ d_z &= -\frac{13l}{420} + \frac{\gamma_z}{10\alpha l} \\ e_z &= \frac{l^2}{105} + \frac{2\gamma_z}{15\alpha}\end{aligned}$$

$$\begin{aligned}
f_z &= -\frac{l^2}{140} - \frac{\gamma_z}{30\alpha} \\
a_y &= \frac{13}{35} + 6\frac{\gamma_y}{5\alpha l^2} \\
b_y &= \frac{11l}{210} + \frac{\gamma_y}{10\alpha l} \\
c_y &= \frac{9}{70} - \frac{6\gamma_y}{5\alpha l^2} \\
d_y &= -\frac{13l}{420} + \frac{\gamma_y}{10\alpha l} \\
e_y &= \frac{l^2}{105} + \frac{2\gamma_y}{15\alpha} \\
f_y &= -\frac{l^2}{140} - \frac{\gamma_y}{30\alpha} \\
\kappa &= \rho A l \\
\epsilon &= \frac{J}{A}
\end{aligned}$$

It is now proposed to use a sensitivity based updating method given by:

$$\{I\}_j - [Z^{Red}(\{p\}_0)] \{H_X\}_j = \left(\sum_{i=1} \frac{\partial [Z^{Red}]}{\partial p_i} \Delta p_i \right) \{H_X\}_j \quad (8.3)$$

We must now choose our physical parameters, say α , β , γ_y , γ_z , κ and ϵ , and express the element sensitivity matrices with respect to these parameters. For a given element, the stiffness and mass sensitivity matrices will have the same pattern as $[K^e]$ and $[M^e]$. Only the coefficients α , β , \dots need to be redefined, as done in Appendix A.

After assembling the global $[K]$ and $[M]$ matrices, the reduced dynamic stiffness matrix, $[Z^{Red}]$, and its derivatives with respect to the unknown parameters need to be calculated. Writing equation (8.3) at different frequency points at each iteration step yields:

$$[A]\{p\} = \{b\} \quad (8.4)$$

Equation (8.3) can now be solved iteratively together with equation (8.4) until convergence solution to a prescribed tolerance is obtained.

8.3 Case Study

Let us now consider model FE2 of Section (3.4). As before, the X and Y moments of inertia for eight elements were increased by 30%, the reference structure remaining X1. A p-value approach has already been used to update model FE2 in Chapters 3 and 6. Although convergence was obtained in some cases, the results were found to be non-unique and did not match the experimental results identically. The idea here is to update this structure using physical parameters and to show that it is possible to have a unique solution which will also show the exact errors locations.

A computer program BEAM3D-P was developed in MATLAB for the case of the 3D beam element described by equations (8.1) and (8.2). The sensitivity based algorithm of equation (8.3) was also programmed. An initial test case was carried out using noise-free FRF data. All elements of the FRF vector (rotations as well as translations) were assumed to be known. Nine frequency points, namely 20, 40, 75, 80, 135, 142, 190, 210 and 245, were selected in the frequency range 0-250 Hz. The solution converged after 4 iterations. All elements in error were correctly identified (Fig. 8.2) and the computed parameters were used to update the model. It was observed that the experimental and the updated FRFs were identical.

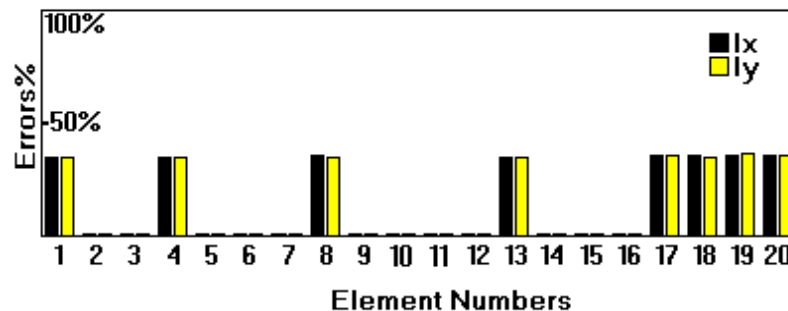


Figure 8.2: Error location for structure FE2

In the case of incomplete FRF data, no convergence was achieved for noise levels of 1% to 5% in spite of using different sets of frequency points. This can be explained by the non-linear behaviour of the objective function. Since the dynamic stiffness

matrix is no longer a linear function of the updating parameters, the FRF incompleteness, coupled with noise, can cause major errors in calculating the derivatives of the objective function and hence no convergence can be obtained.

8.4 Plate Element

A 2D plate element was considered next. Its degrees of freedom are ordered as:

$$[v_{z1} \ \theta_{x1} \ \theta_{y1} \ v_{z2} \ \theta_{x2} \ \theta_{y2} \ v_{z3} \ \theta_{x3} \ \theta_{y3} \ v_{z4} \ \theta_{x4} \ \theta_{y4}]$$

The subscripts 1, 2, 3 and 4 refer to the four nodes of the element, and v and θ denote the displacement and rotation fields, respectively. The elemental stiffness matrix is given by Mansfield (1964):

$$[K^e] = \kappa \begin{bmatrix} F & H & -G & L & N & M & O & Q & P & I & K & -J \\ H & V & -Z & -N & X & 0 & -Q & Y & 0 & K & W & 0 \\ -G & -Z & R & M & 0 & T & -P & 0 & U & J & 0 & S \\ L & -N & M & F & -H & -G & I & -K & -J & O & -Q & P \\ N & X & 0 & -H & V & Z & -K & W & 0 & Q & Y & 0 \\ M & 0 & T & -G & Z & R & J & 0 & S & -P & 0 & U \\ O & -Q & -P & I & -K & J & F & -H & G & L & -N & -M \\ Q & Y & 0 & -K & W & 0 & -H & V & -Z & N & X & 0 \\ P & 0 & U & -J & 0 & S & G & -Z & R & -M & 0 & T \\ I & K & J & O & Q & -P & L & N & -M & F & H & G \\ K & W & 0 & -Q & Y & 0 & -N & X & 0 & H & V & Z \\ -J & 0 & S & P & 0 & U & -M & 0 & T & G & Z & R \end{bmatrix} \quad (8.5)$$

where

$$\begin{aligned}
\kappa &= \frac{E h}{180(1-\nu^2)} \\
\beta &= \frac{a}{b} \\
F &= (42 - 12\nu + 60\beta^2 + \frac{60}{\beta^2}) \frac{h^2}{ab} \\
G &= (30\beta + \frac{3}{\beta} + \frac{12\nu}{\beta}) \frac{h^2}{b} \\
H &= (\frac{30}{\beta} + 3\beta + 12\nu\beta) \frac{h^2}{a} \\
I &= (-42 + 12\nu - 60\beta^2 + \frac{30}{\beta^2}) \frac{h^2}{ab} \\
J &= (30\beta + \frac{3(1-\nu)}{\beta}) \frac{h^2}{b} \\
K &= (\frac{15}{\beta} - 3\beta - 12\nu\beta) \frac{h^2}{a} \\
L &= (-42 + 12\nu - \frac{60}{\beta^2} + 30\beta^2) \frac{h^2}{ab} \\
M &= (-15\beta + \frac{3}{\beta} + \frac{12\nu}{\beta}) \frac{h^2}{b} \\
N &= (\frac{30}{\beta} + 3(1-\nu)\beta) \frac{h^2}{a} \\
O &= (42 - 12\nu - 30\beta^2 - \frac{30}{\beta^2}) \frac{h^2}{ab} \\
p &= (-15\beta + \frac{3(1-\nu)}{\beta}) \frac{h^2}{b} \\
Q &= (\frac{15}{\beta} - 3(1-\nu)\beta) \frac{h^2}{a} \\
R &= (20\beta + \frac{4(1-\nu)}{\beta}) h^2 \\
S &= (10\beta - \frac{1-\nu}{\beta}) h^2 \\
T &= (10\beta - \frac{4(1-\nu)}{\beta}) h^2 \\
U &= (5\beta + \frac{1-\nu}{\beta}) h^2 \\
V &= (\frac{20}{\beta} + 4(1-\nu)\beta) h^2 \\
W &= (\frac{10}{\beta} - 4(1-\nu)\beta) h^2 \\
X &= (\frac{10}{\beta} - (1-\nu)\beta) h^2 \\
Y &= (\frac{5}{\beta} + (1-\nu)\beta) h^2 \\
Z &= 15\nu h^2
\end{aligned} \tag{8.6}$$

The elemental mass matrix is given by:

$$[M^e] = C_o [\alpha] [m] [\alpha] \tag{8.7}$$

where:

$$[m] = \begin{bmatrix} 3454 & 461 & -461 & 1226 & -274 & -199 & 394 & -116 & 116 & 1226 & 199 & 274 \\ 461 & 80 & -63 & 274 & -60 & -42 & 116 & -30 & 28 & 199 & 40 & 42 \\ -461 & -63 & 80 & -199 & 42 & 40 & -116 & 28 & -30 & -274 & -42 & -60 \\ 1226 & 274 & -199 & 3454 & -461 & -461 & 1226 & -199 & 274 & 394 & 116 & 116 \\ -274 & -60 & 42 & -461 & 80 & 63 & -199 & 40 & -42 & -116 & -30 & -28 \\ -199 & -42 & 40 & -461 & 63 & 80 & -274 & 42 & -60 & -116 & -28 & -30 \\ 394 & 116 & -116 & 1226 & -199 & -274 & 3454 & -461 & 461 & 1226 & 274 & 199 \\ -116 & -30 & 28 & -199 & 40 & 42 & -461 & 80 & -63 & -274 & -60 & -42 \\ 116 & 28 & -30 & 274 & -42 & -60 & 461 & -63 & 80 & 199 & 42 & 40 \\ 1226 & 199 & -274 & 394 & -116 & -116 & 1226 & -274 & 199 & 3454 & 461 & 461 \\ 199 & 40 & -42 & 116 & -30 & -28 & 274 & -60 & 42 & 461 & 80 & 63 \\ 274 & 42 & -60 & 116 & -28 & -30 & 199 & -42 & 40 & 461 & 63 & 80 \end{bmatrix}$$

$$C_o = \frac{h \rho a b}{25200} \quad (8.8)$$

$$[\alpha] = \begin{bmatrix} [\alpha_1] & 0 & 0 & 0 \\ 0 & [\alpha_1] & 0 & 0 \\ 0 & 0 & [\alpha_1] & 0 \\ 0 & 0 & 0 & [\alpha_1] \end{bmatrix} \quad (8.9)$$

and

$$[\alpha_1] = \begin{bmatrix} 1 & 0 & 0 \\ 0 & a & 0 \\ 0 & 0 & b \end{bmatrix} \quad (8.10)$$

For this case the design variables are thickness h , Poisson's ratio ν , density ρ and Young's modulus E . The derivatives of the mass and stiffness matrices with respect to these variables are given in Appendix A. The same procedure described in Section

(8.2) can also be applied for this case.

8.5 Case Study

The rectangular plate of Section (3.5.4) was used again to carry out the sensitivity analysis of Section (8.4).

The plate was divided into 45 elements, the total number of DOFs being $60 \times 3 = 180$. The initial mass and stiffness matrices were calculated from the equations given in Section (8.4).

Here, the finite element model was assumed to be undamped. In this case, there will be four parameters for each finite element, a feature which will increase the number of unknowns substantially. The analytical model had errors in the form of 15 % increase in the height of elements 1, 4, 7, ..., 40, 43 and 8% increase in the modulus of elasticity of elements 1, 5, 9, ..., 41, 45. Nine known errors of 10% were also introduced into the density of some elements namely, 1, 6, 11, ..., 36, 41. Finally a 12 % increase in the Poisson's ratio of fifteen elements, 2, 5, 8, ..., 44, was also introduced to the analytical model. The experimental data consisted all Z direction receptances of the corresponding uniform error-free plate.

The errors were identified with good accuracy and it was seen that the updated FRFs were almost identical to the measured ones. A typical FRF, α_{33} , is depicted in Fig. (8.3) for the initial, reference and updated models.

Since physical parameter updating requires substantially more CPU time, it was decided to use macro-elements to reduce the computational effort. Several elements which have the same physical parameters were grouped together into one element. Four macro elements were introduced initially. The first macro element consisted of all elements with 15% increased height. The second, third and fourth macro elements were grouped according to modulus of elasticity, density and Poisson's ratio changes. The computation was carried out with the macro elements and convergence achieved

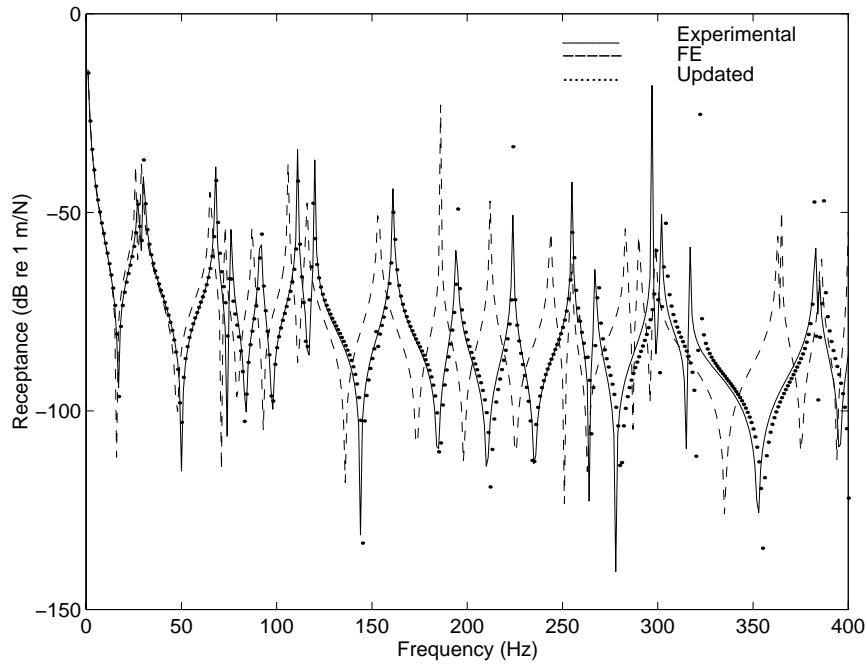


Figure 8.3: Comparison of the measured, analytical and updated receptance FRF, α_{1Z1Z}

after a few iterations. The updated parameters were found to be very close to those obtained from the previous run, i.e. without the macro elements (Table 8.1). However, it was observed that the CPU requirement was reduced by about 90%.

In any case, further runs, not reported here, showed that the choice of the macro elements was crucial to obtain convergence. However, as the grouping of the elements was based a-priori knowledge of the errors, the use of macro elements is unlikely to be straightforward in practice.

Table 8.1: Computational effort for macro elements

Macro	Elements in Macro	Parameter	Change Introduced	Prediction	CPU time (Sec)
1	[1, 4, ..., 43]	h	[+15 %]	[+14.91 %]	110
2	[1, 5, ..., 45]	E	[+8 %]	[+8.1 %]	
3	[1, 6, ..., 41]	ρ	[+10 %]	[+9.6 %]	
4	[2, 5, ..., 44]	ν	[+12 %]	[+10.8 %]	
1	[1][4] ... [43]	h	[+15 %]	[+14.33 %] ^a	1190
2	[1][5] ... [45]	E	[+8 %]	[+7.7 %]	
3	[1][6] ... [41]	ρ	[+10 %]	[+8.7 %]	
4	[2][5] ... [44]	ν	[+12 %]	[+11.9 %]	
1	[1][2] ... [45] ^b	h	[+15 %]	[+14.98 %] ^c	4274
2	[1][2] ... [45]	E	[+8 %]	[+7.9 %]	
3	[1][2] ... [45]	ρ	[+10 %]	[+9.7 %]	
4	[1][2] ... [45]	ν	[+12 %]	[+11.8 %]	

^aAveraged over macros

^bInitial (without the macro elements)

^cAveraged over non-zero macros

8.6 Updating of Exact elements Using Design Parameters

8.6.1 Introduction

For a limited number of geometries, such as uniform beam and discs, the vibration properties of the corresponding structures can be expressed in an exact fashion, based on available analytical solutions. In such cases, there is no need to use many elements for better spatial discretisation, the requirement to use additional elements being dictated by geometrical considerations, such as changes in beam's cross section. We propose to call these analytically-derived elements as exact elements and we propose to update, as before, a number of selected design parameters that correspond directly to the physical properties of the structure.

Here it is proposed to use a beam structure as the demonstration vehicle. 3D Timoshenko beams (Timoshenko, 1935), vibrating in flexure, coupled with simultaneous longitudinal vibration and torsional vibration will be used for this case study.

8.6.2 Spatial Vibration of a Prismatic Bar

The equation of motion of a prismatic bar including rotary inertia effects, can be expressed as (Timoshenko & Young, 1945):

$$EI \frac{\partial^4 v}{\partial x^4} + \rho A \frac{\partial^2 v}{\partial t^2} - \rho I \frac{\partial^4 v}{\partial x^2 \partial t^2} = 0 \quad (8.11)$$

If the effects of shear deformation are also added, the Timoshenko equation for the flexural vibrations of uniform, prismatic bar will be obtained (Huang, 1967):

$$EI \frac{\partial^4 v}{\partial x^4} + \rho A \frac{\partial^2 v}{\partial t^2} - \rho I \left(1 + \frac{E}{\kappa G}\right) \frac{\partial^4 v}{\partial x^2 \partial t^2} + \frac{\rho^2 I}{\kappa G} \frac{\partial^4 v}{\partial t^4} = 0 \quad (8.12)$$

where

EI = flexural rigidity

A = cross sectional area

ρ = material density

κ = shearing constant

G = modulus of rigidity in shear

I = second moment of area of the beam's cross section

The constant κ is based on the shape of the section and is usually less than unity. (for example, $\kappa_{rectangular} = .85$ and $\kappa_{circular} = .9$)

The equation of motion in longitudinal direction is given by (Den Hartog, 1956):

$$EA \frac{\partial^2 u}{\partial x^2} - \rho A \frac{\partial^2 u}{\partial t^2} = 0 \quad (8.13)$$

where

E = modulus of elasticity

A = area of cross section

ρ = density

u = axial displacement

Since longitudinal and transverse vibrations of beam elements can take place simultaneously, an exact analysis should consider the two motions together. It can be shown that the resulting motion can be expressed as a linear superposition of the separate motions considered previously (Afolabi, 1978).

When a beam is subjected to torsional vibration only, the equation of motion is given by (Den Hartog, 1956):

$$GJ \frac{\partial^2 \theta}{\partial x^2} - \rho J \frac{\partial^2 \theta}{\partial t^2} = 0 \quad (8.14)$$

where

G = shear modulus

ρ = density

J = torsional constant

For circular cross sections, J is equal to the polar moment of inertia. For rectangular cross section, a list of torsional constants is given by Roark (1954).

For a free-free Timoshenko beam, the complete equation of motion can be obtained by a linear superposition of the in-plane and out-of-plane motions. By solving the equations (8.12), (8.13) and (8.14) with free-free boundary conditions and using the principle of superposition, one can obtain the dynamic stiffness matrix for a 3D beam element as (Afolabi, 1978):

$$[Z_{ij}] = \begin{bmatrix} G_1 & 0 & 0 & 0 & 0 & 0 & G_2 & 0 & 0 & 0 & 0 & 0 \\ 0 & -f_1 & 0 & 0 & 0 & -f_2 & 0 & f_3 & 0 & 0 & 0 & f_4 \\ 0 & 0 & -g_1 & 0 & -g_2 & 0 & 0 & 0 & g_3 & 0 & g_4 & 0 \\ 0 & 0 & 0 & G_3 & 0 & 0 & 0 & 0 & 0 & G_4 & 0 & 0 \\ 0 & 0 & -g_2 & 0 & g_5 & 0 & 0 & 0 & -g_4 & 0 & g_6 & 0 \\ 0 & -f_2 & 0 & 0 & 0 & f_5 & 0 & -f_4 & 0 & 0 & 0 & f_6 \\ G_2 & 0 & 0 & 0 & 0 & 0 & G_1 & 0 & 0 & 0 & 0 & 0 \\ 0 & f_3 & 0 & 0 & 0 & -f_4 & 0 & -f_1 & 0 & 0 & 0 & f_2 \\ 0 & 0 & g_3 & 0 & -g_4 & 0 & 0 & 0 & -g_1 & 0 & g_2 & 0 \\ 0 & 0 & 0 & G_4 & 0 & 0 & 0 & 0 & 0 & G_3 & 0 & 0 \\ 0 & 0 & g_4 & 0 & g_6 & 0 & 0 & 0 & g_2 & 0 & g_5 & 0 \\ 0 & f_4 & 0 & 0 & 0 & f_6 & 0 & f_2 & 0 & 0 & 0 & f_5 \end{bmatrix} \quad (8.15)$$

where:

$$\begin{aligned} \nu^2 &= \rho\omega^2/G \\ \psi^2 &= \rho\omega^2/E \\ G_1 &= EA\psi \cot(\psi\ell) \\ G_2 &= -EA\psi \csc(\psi\ell) \\ G_3 &= GJ\nu \cot(\nu\ell) \\ G_4 &= -GJ\nu \csc(\nu\ell) \\ \epsilon_1 &= \sqrt{[\rho^2\omega^4(\frac{1}{\kappa G} - \frac{1}{E})^2 + \frac{4\rho\omega^2 A}{EI}]} \\ \epsilon_3 &= \rho\omega^2(\frac{1}{\kappa G} + \frac{1}{E}) \\ \alpha &= \sqrt{\frac{\epsilon_1 + \epsilon_3}{2}} \\ \beta &= \sqrt{\frac{\epsilon_1 - \epsilon_3}{2}} \\ \gamma_1 &= \alpha^2 - \frac{\rho\omega^2}{\kappa G} \\ \gamma_2 &= \beta^2 + \frac{\rho\omega^2}{\kappa G} \\ \epsilon_2 &= \frac{\gamma_1 \gamma_2}{\alpha \beta} \\ \delta &= 2\epsilon_2(\cos(\alpha\ell) \cosh(\beta\ell) - 1) + (\frac{\gamma_1^2}{\alpha^2} - \frac{\gamma_2^2}{\beta^2}) \sin(\alpha\ell) \sinh(\beta\ell) \\ K &= \frac{EI}{\delta} \end{aligned} \quad (8.16)$$

$$\begin{aligned}
f1 &= K\epsilon_1\epsilon_2 \left[\frac{\gamma_1}{\alpha} \sin(\alpha\ell) \cosh(\beta\ell) + \frac{\gamma_2}{\beta} \cos(\alpha\ell) \sinh(\beta\ell) \right] \\
f2 &= K\gamma_1\gamma_2 \left[\left(\frac{\gamma_1}{\alpha^2} + \frac{\gamma_2}{\beta^2} \right) \sin(\alpha\ell) \sinh(\beta\ell) + \frac{\gamma_2 - \gamma_1}{\alpha\beta} (\cos(\alpha\ell) \cosh(\beta\ell) - 1) \right] \\
f3 &= K\epsilon_1\epsilon_2 \left[\frac{\gamma_1}{\alpha} \sin(\alpha\ell) + \frac{\gamma_2}{\beta} \sinh(\beta\ell) \right] \\
f4 &= K\epsilon_1\epsilon_2 [\cos(\alpha\ell) - \cosh(\beta\ell)] \\
f5 &= K\epsilon_1 \left[\frac{\gamma_1}{\alpha} \cos(\alpha\ell) \sinh(\beta\ell) - \frac{\gamma_2}{\beta} \sin(\alpha\ell) \cosh(\beta\ell) \right] \\
f6 &= K\epsilon_1 \left[\frac{\gamma_2}{\beta} \sin(\alpha\ell) - \frac{\gamma_1}{\alpha} \sinh(\beta\ell) \right]
\end{aligned} \tag{8.17}$$

ω is the excitation frequency and g_1, \dots, g_6 are the same as f_1, \dots, f_6 when I_y replaced by I_z .

There are seven physical parameters per element, namely, ρ, A, E, G, J, I_y and I_z . For updating purpose, the derivatives of $[Z_{ij}]$ with respect to these parameters should be calculated (See Appendix A).

8.7 Case Study

As before, equation (8.3) will be used for updating the analytical model against some reference data. Model X1¹ of Section (3.4), consisting of 19 nodes, will also be used as reference model here. Table (8.2) lists the errors that were introduced to the analytical model.

Table 8.2: Details of the errors in the analytical model

Properties	Perturbed elements	Description
Density	1, 5, 9, 13, 17	10% decrease
Elasticity Modulus	1, 2, 3, 4, 8, 13, 17, 18, 19, 20	10% increase
Shear Modulus	5, 6, 7, 8, 12, 13, 19, 20	10% increase
Width	1, 6, 11, 16	10% increase

To make the study more realistic, 2% structural damping was introduced by making the Young's modulus complex, i.e.:

¹ $E = 207 \text{ GN/m}^2, G = 79.6 \text{ GN/m}^2, \rho = 7850 \text{ Kg/m}^3, b = 1 \text{ cm}, h = 10 \text{ cm}$

$$\bar{E} = E(1 + i\eta) \quad (8.18)$$

The case of noise-free FRF data was investigated first, and all elements of the measured FRF vector were assumed to be known. Eight frequency points, namely 30, 70, 110, 135, 155, 180, 210 and 2305 Hz, were selected in the frequency range of 0-250 Hz. The solution converged after a few iterations and all errors were identified correctly.

The computed parameters were used to compute a new set of FRFs. It was observed that the experimental and the updated FRFs were almost coincident (Fig. 8.4).

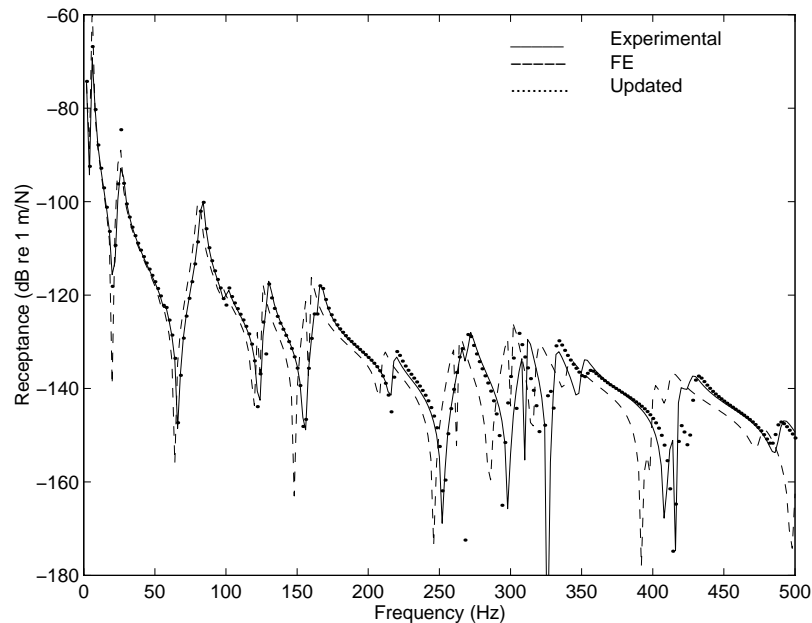


Figure 8.4: Comparison of the measured, analytical and updated receptance FRF, α_{1Z1Z}

The updating process needed not only more iterations but also significantly more CPU time per iteration than the other updating approaches such as p-values or 3D beam element of section (8.2). This is mainly due to the presence of trigonometric and hyperbolic functions in the dynamic stiffness matrix which increase the computational time. It was also noticed that by increasing the perturbations of some of the elements, the convergence became slower and could not be obtained in all cases. This can be

explained by the linearisation of the dynamic stiffness matrix up to the first term only. However, the problem can probably be alleviated by considering the higher terms in the Taylor series expansion of the dynamic stiffness matrix.

8.8 Concluding Remarks

- The use of physical parameters, instead of elemental p-values, is introduced into the FRF-based updating technique. The approach has been investigated for 3D beams and plate elements on a number of case studies, namely the FE2 structure and a plate structure.
- In the general case, modelling errors cannot be expressed as a linear combination of the individual mass and stiffness matrices, as assumed by the p-value approach. So, by using physical parameters it is possible to adjust the model more accurately without losing the connectivity information.
- In common with many other updating techniques, the incompleteness and noise in the experimental data remains a major problem. Noise makes the process of convergence unstable while incompleteness restricts the updating range.
- Since the objective function is highly non-linear respect to local minima, the solution may again not be unique.
- The physical parameter method needs more CPU time and more iterations than the more conventional p-value. However, this disadvantage can partly be offset by the use of macro elements.
- An exact element based updating approach was also reported in this chapter. The derivatives of the dynamic stiffness matrix with respect to design parameters were derived using exact closed-form expressions. The basic idea is to start from an initial model that is free from discretisation errors. Such a route is possible for some simple beam systems, such as pipingworks, space frames, etc.

It is expected that the technique can also be applied to the updating of joints in such structures.

Chapter 9

Experimental Case Study

9.1 The Two Plate Structures

The overall aim of this Chapter is to investigate the applicability of the introduced model updating techniques to a simple but representative engineering structure such as a uniform rectangular plate subjected to some design modification. The first structure to be studied is the uniform plate of Fig. (9.1), hereafter referred to as Structure A. The second one is a derivative of Structure A, re-enforced by two crossing strips which were spot welded on both side of the plate, called hereafter as Structure B (Fig. 9.2).

The nominal dimensions of the base plate are $665 \times 455 \times 2.5\text{mm}$ and the material properties are estimated to be $E = 206\text{GN}/\text{m}^2$ and $\rho = 7860\text{Kg}/\text{m}^3$. The strips have the same properties as the base plate and are welded to both sides of Structure B by 12 equally-spaced and nominally-identical spot-welds.

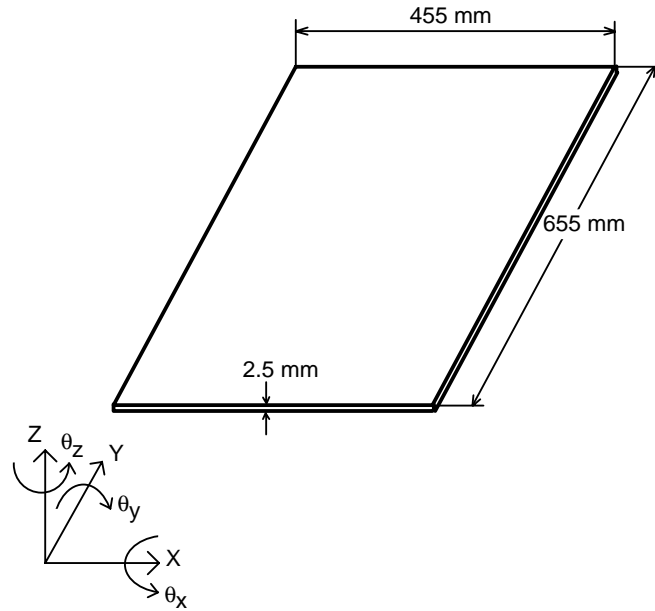


Figure 9.1: Structure A

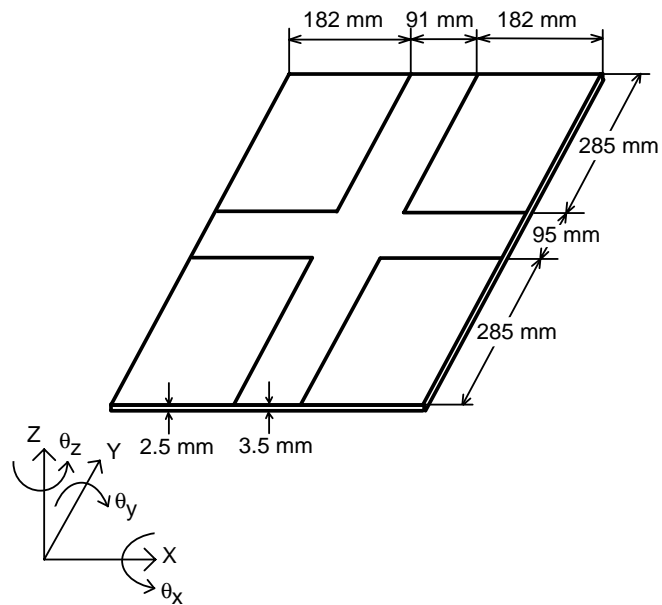


Figure 9.2: Structure B

9.2 Experimental Data

The structures were suspended by two soft strings and tested in free-free conditions (Fig. 9.3). The experimental data were obtained via hammer testing using a B&K analyser connected to an IBM compatible PC running data acquisition program MODACQ. A B&K piezoelectric accelerometer model 2222c (0.5g) was attached to the structure by using wax.

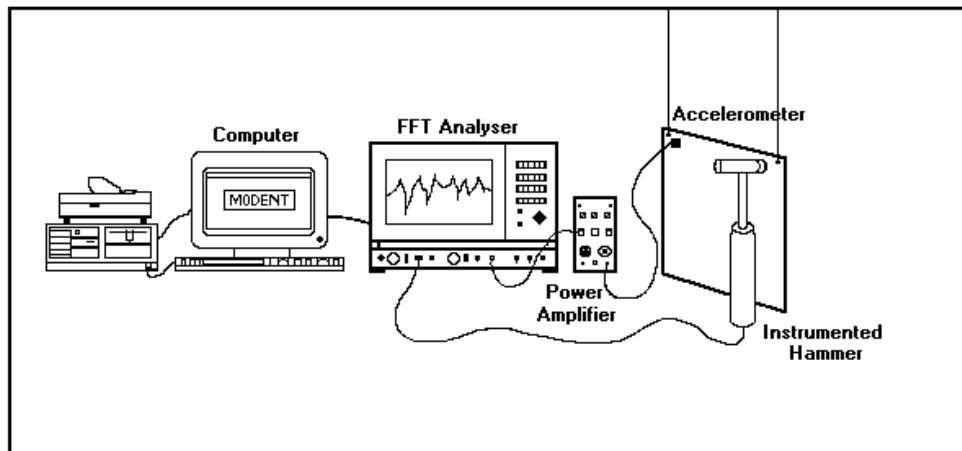


Figure 9.3: Experimental set-up

Forty eight Z-direction inertance FRFs were measured for Structure A (Fig. 9.4).

Seventy two inertance FRF measurements were made for Structure B. The extra twenty four measurements were carried out to check the effect of the location of accelerometer near the edges of the strips. The accelerometer positions are shown in Fig. (9.5). The responses were measured at 801 frequencies between 8 and 408 Hz and the number of averages was set to 5.

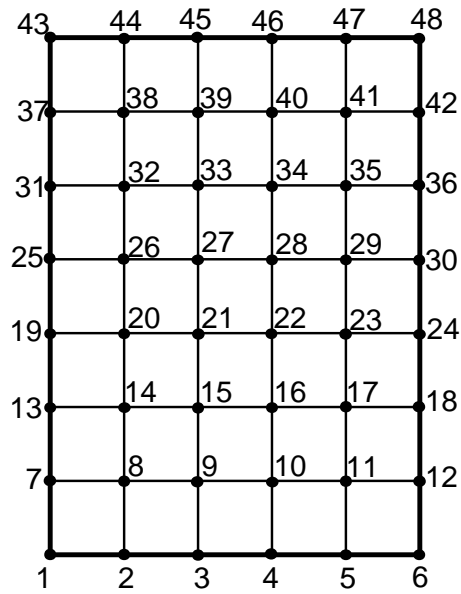


Figure 9.4: Measurement points for Structure A

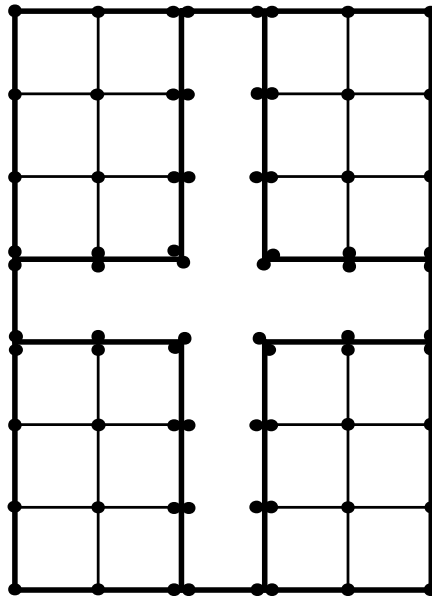


Figure 9.5: Measurement points for Structure B

9.3 The FE Models

Both structures were modelled using 4-node plate elements which were described in Chapter 8. It should be noted that there is only one FE model as the aim is to detect the cross-shape stiffeners from the measurements. Fig. (9.6) shows the FE mesh consisting of 35 plate elements and having $48 \times 3 = 144$ DOFs.

Individual mass and stiffness matrices, together with the connectivity information, were read into Program Update, written in MATLAB language. The global mass and stiffness matrices were assembled internally and the derivatives of the unknown parameters were calculated by the program to formulate the sensitivity matrix at each iteration.

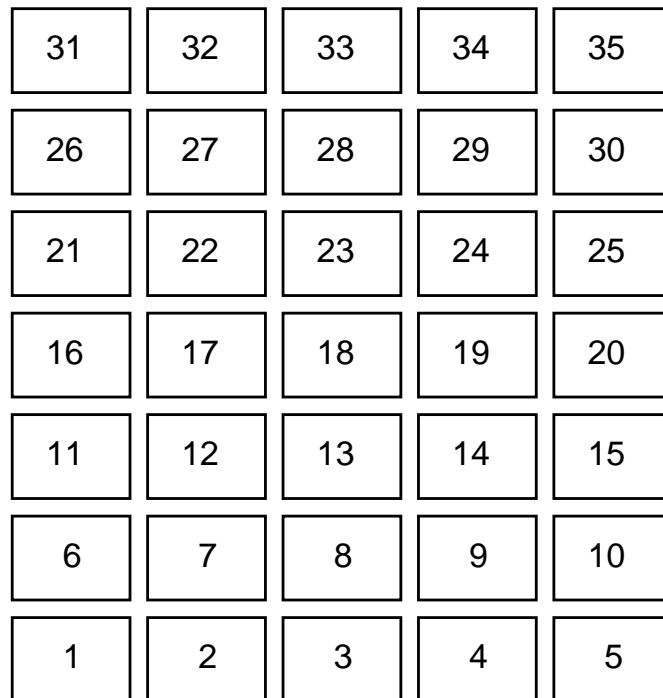


Figure 9.6: The FE model for both Structures A and B

9.4 Correlation of Experimental and Predicted Results for Structure A

Prior to updating the FE model of Structure A, a comparison of the experimental and FE data sets was carried out in several stages. Measured and predicted FRFs were overlaid first, as shown in Fig. (9.7). There is good agreement between two sets for the lower part of the frequency range, the discrepancies increasing with increasing frequency. It seems that the experimental model is stiffer than the analytical model.

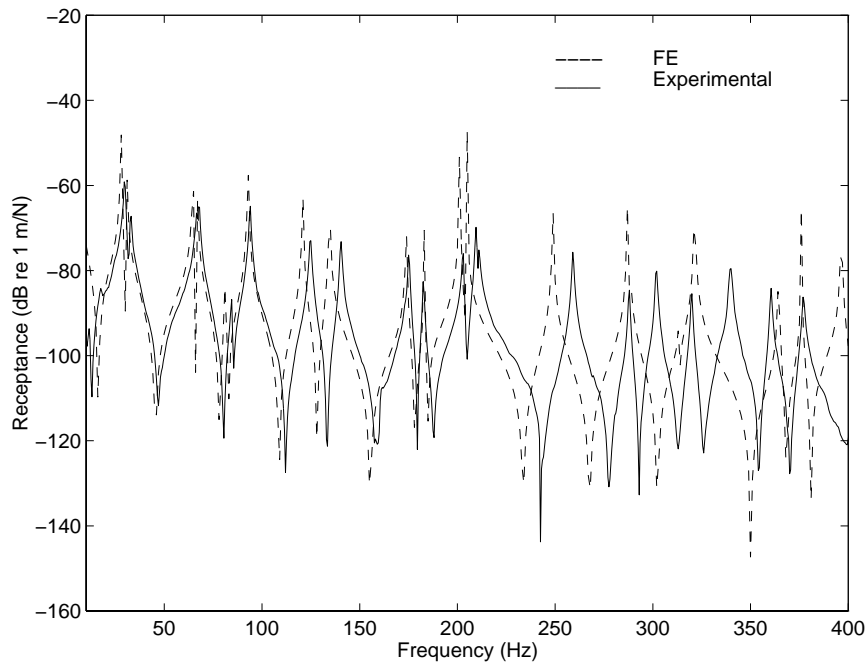


Figure 9.7: Experimental and analytical receptance FRFs, α_{1z1z} - Structure A

In a second stage, the experimental FRF data were analysed using the MODENT suite, a modal analysis package running on IBM compatible PCs. A global multi-FRF analysis method called GLOBAL-M was used. GLOBAL-M is based on complex singular value decomposition of a system matrix expressed in terms of measured FRFs and then on a complex eigensolution which extracts the required modal properties. This particular algorithm was chosen because of its ability in detecting close modes.

Each measured data set contained 48 individual FRFs in the appropriate file format for MODENT. The data were analysed by applying 5 GLOBAL-M runs to several frequency windows, thus covering the entire frequency range. The most consistent results were saved in a modal data set.

After the modal analysis, the natural frequencies obtained from the FE model and those extracted from modal analysis were compared. It is obvious from Table (9.1) that there are good agreement between two sets, the maximum natural frequency discrepancy being less than 6% and the MAC values showing a very good correlation.

Table 9.1: Measured and predicted natural frequencies of Structure A

Measured (Hz)	FE (Hz)	Relative ^a Error %	Damping %	MAC
29.6	27.9	5.7	3.1	98.5
32.5	30.8	5.2	3.1	89.1
66.6	66.7	.15	1.1	97.7
67.7	64.7	4.4	1.3	97.2
84.5	81.3	3.8	.78	98.9
93.9	92.8	1.2	.95	99.6
124.7	120.8	3.1	.78	99.3
140.4	134.6	4.1	.67	99.8
175.2	173.8	.80	.43	99.5
182.6	183.1	.27	.41	99.2
202.9	201.0	.90	.39	98.6
209.5	205.0	2.2	.38	95.6
210.9	201.3	4.6	.38	96.2
259.1	248.8	3.9	.31	99.7
287.8	288.2	.15	.27	99.6
301.7	286.9	4.9	.30	99.3
319.9	313.4	2.0	.27	92.6
339.7	321.4	5.4	.45	91.9
360.4	364.4	1.1	.27	98.6
376.9	376.0	.24	.35	99.0

$$^a\text{Relative Error} = \frac{ABS(\text{Measured}-\text{Predicted})}{\text{Measured}} \times 100$$

A further comparison was made by plotting the natural frequencies of the experimental and predicted data sets (Fig. 9.8).

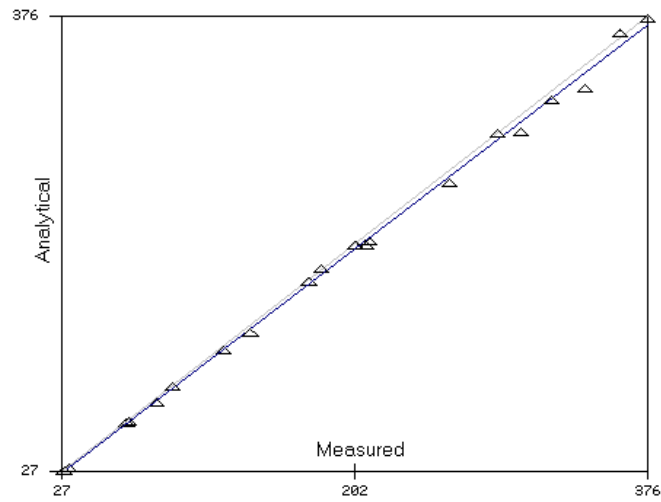


Figure 9.8: 45 Degree lines for natural frequencies of Structure A

The MAC values between the experimental and analytical modes were calculated next (Fig. 9.9 and Table 9.1). The correlation is very good since there is a one-to-one correspondence between the two data sets.

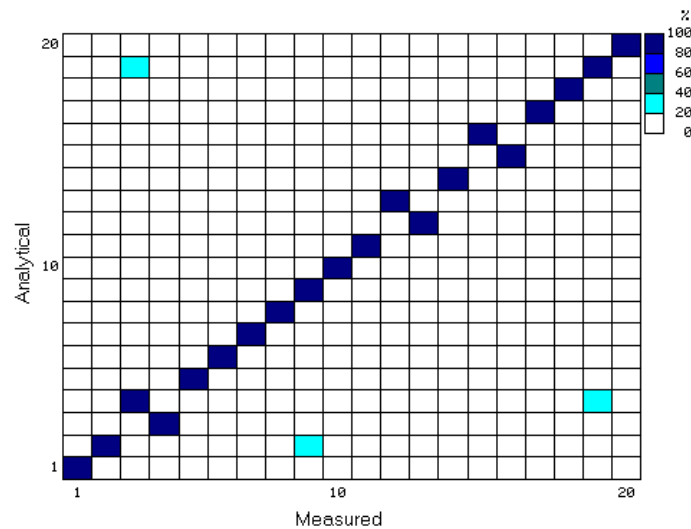


Figure 9.9: MAC values for Structure A

The COMAC values were calculated using the 20 correlated mode shape pairs of Fig. (9.9) and are plotted in Fig. (9.10). Again, the results indicate very good agreement.

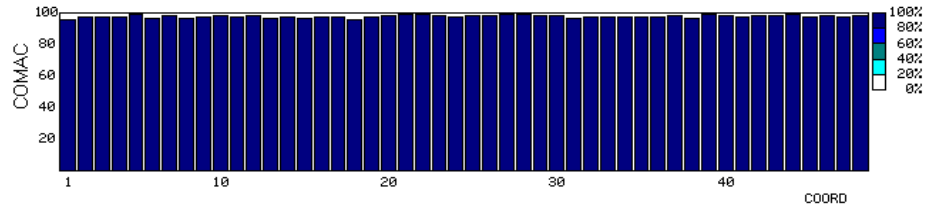


Figure 9.10: COMAC values for Structure A

Finally, 45 degree lines were plotted for mode shapes 1 and 9 (Fig. 9.11). Once again the results confirm the basic agreement between two data sets.

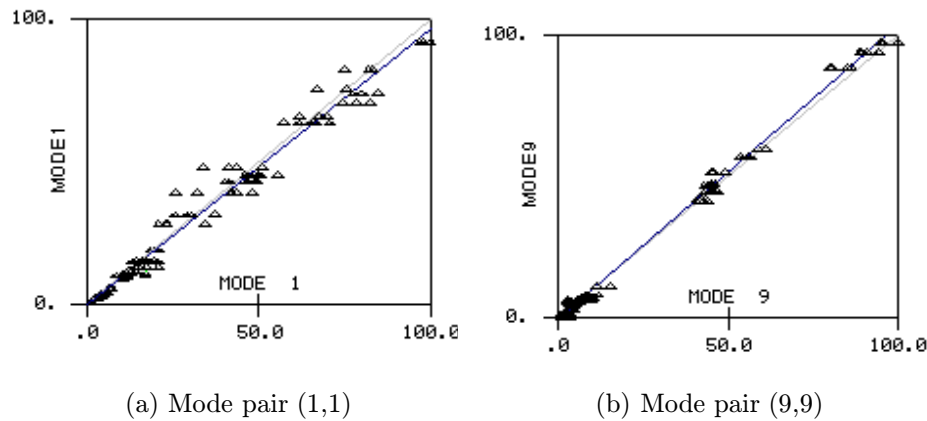


Figure 9.11: 45 degree plots for selected mode shapes

The correlation results indicate that there is good agreement between the two models, an essential requirement for successful model updating.

9.5 Model Updating for Structure A

The previously-described FE model will now be updated using the experimentally obtained FRFs of Structure A. In this particular case, there are no obvious modelling errors and the task is to make the experimental and theoretical models as close as possible. To this end, it is proposed to use a physical parameter based updating technique. Damping was ignored initially as the modal analysis showed that Structure A was lightly damped, most modes having a structural damping values of less than 0.4%.

In order to reduce the effects of measurement noise and other experimental inconsistencies, it was decided to use synthesised FRFs which were regenerated using the identified modal parameters. However, such a treatment cannot solve the problem of consistent bias errors in the experimental data. A typical FRF curve, here α_{1z1z} , is plotted in Fig. (9.12) for both raw and synthesised FRFs.

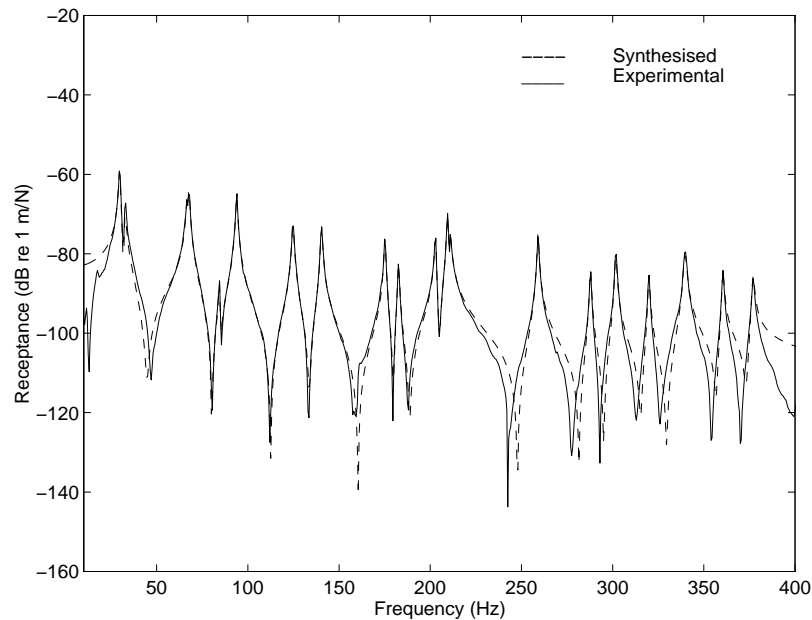


Figure 9.12: Measured and synthesised receptance FRF α_{1z1z} - Structure A

As it mentioned before, the updating will be based on the physical parameter version

of frequency response function method, as discussed in Chapter 8. The unknown physical parameters for each plate element are thickness, modulus of elasticity, density and Poisson's ratio, giving a total of $4 \times 35 = 140$.

It was decided to focus on the frequency in the range of 10-260 Hz which contained 14 modes. The frequency points were selected in accordance with the recommendations made in Chapter 3. A total of 20 frequency points, namely 20, 25, 35, 40, 60, 70, 90, 100, 105, 115, 126, 145, 150, 165, 170, 177, 184, 191, 195 and 215 were used in this particular case.

As the structure was assumed to be lightly damped, the imaginary part of the measured FRFs were set to zero. All plate elements were included in the updating of finite element model. A converged solution was obtained after 7 iterations. The physical parameter values were saved and used for the calculation of updated mass and stiffness matrices. The FRFs of the updated model were then computed via the direct inversion of the updated mass and stiffness matrices. After some runs with different sets of frequency points, it was found that different sets of physical parameters were obtained in each case but the corresponding FRFs were almost indistinguishable. Fig. (9.13) illustrates a typical convergence path of the design parameters with respect to iteration number for elements 1 and 30.

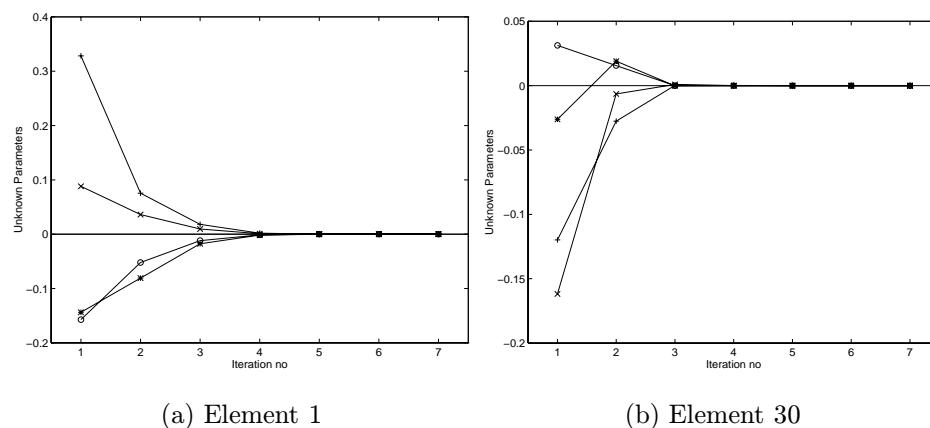


Figure 9.13: Convergence of the physical parameters - Structure A (* p_h , x p_ν , o p_e , + p_ρ)

Having updated the finite element model of Structure A, it was decided to overlay the point FRF obtained from the updated models together with the corresponding measured and initially-predicted FRFs for several co-ordinate locations (Fig. 9.14). A marked improvement is achieved by the updated model over the initially one.

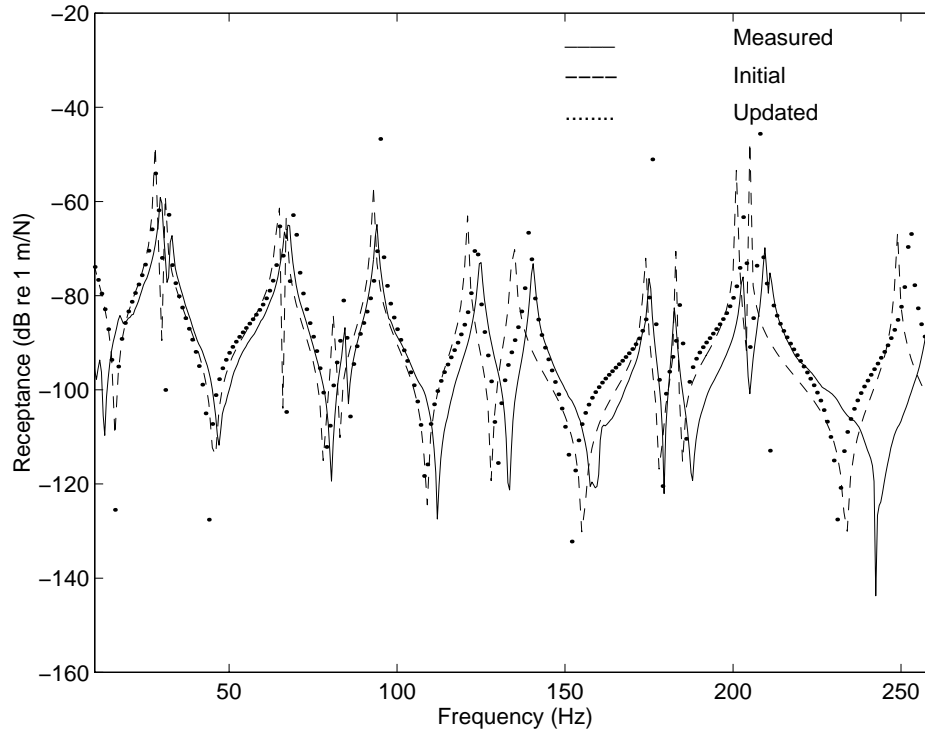


Figure 9.14: Experimental, initially-predicted and updated receptance FRF α_{1z1z} - Structure A

In order to assess the success of the updated model, the frequencies obtained from the updated model are presented in Table (9.2) together with the initially-predicted and measured ones. It is immediately seen that the average error is almost halved.

Table 9.2: Measured, initially-predicted and updated natural frequencies of Structure A

Measured (Hz)	Initially predicted (Hz)	Relative ^a Error %	Updated (Hz)	Relative ^b Error %
29.6	27.9	5.7	28.3	4.4
32.5	30.8	5.2	31.8	2.2
66.6	66.7	.15	64.5	3.1
67.7	64.7	4.4	69.3	2.3
84.5	81.3	3.8	84.4	.19
93.9	92.8	1.2	94.9	1.0
124.7	120.8	3.1	123.5	.96
140.4	134.6	4.1	139.5	.64
175.2	173.8	.80	175.9	.40
182.6	183.1	.27	184.1	.82
202.9	201.0	.90	203.1	.10
209.5	205.0	2.2	208.2	.62
210.9	201.3	4.6	211.1	.10
259.1	248.8	3.9	252.6	2.5
287.8	288.2	.15	292.0	1.4
301.7	286.9	4.9	295.5	2.1
319.9	313.4	2.0	320.4	.16
339.7	321.4	5.4	322.5	5.1
Ave. Error	-	2.70	-	1.56

$$^a\text{Relative Error} = \frac{ABS(\text{Measured}-\text{Predicted})}{\text{Measured}} \times 100$$

$$^b\text{Relative Error} = \frac{ABS(\text{Measured}-\text{Updated})}{\text{Measured}} \times 100$$

9.6 Correlation of Experimental and Predicted Results for Structure B

Prior to updating the FE model, a comparison of the experimental and initial FE models was carried out. Here, it is appropriate to remind the reader that the FE model used remains the same as the previous section but the measured FRFs now belong to Structure B which is a modified version of Structure A.

The measured and predicted FRFs were overlaid first (Fig. 9.15).

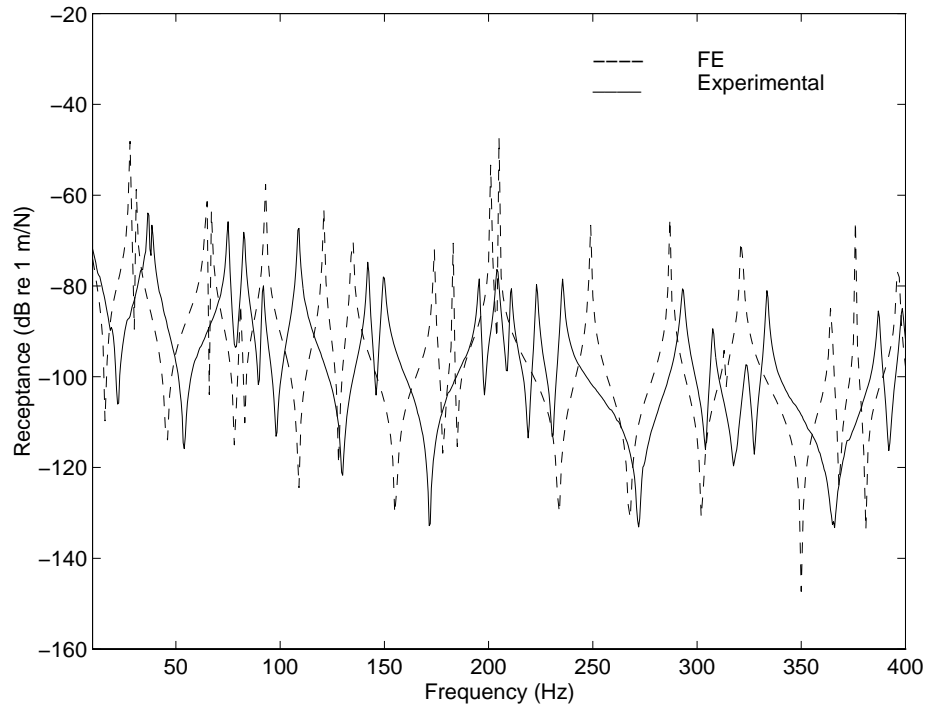


Figure 9.15: Experimental and initially-predicted receptance FRF α_{1z1z} - Structure B

In this second case, there is no good response agreement, even for the lower frequency range. This can be explained by the expected effect of the stiffeners in the physical structure.

A modal analysis was performed next and a MAC comparison is given in Table (9.3).

Table 9.3: Comparison of experimental model with initially-predicted model - Structure B

Measured (Hz)	Initially predicted (Hz)	Relative ^a Error %	MAC value
36.8	27.9	24.2	99.5
38.5	30.8	20.0	97.5
75.0	64.7	13.7	98.7
82.6	66.7	19.2	95.3
91.8	81.3	11.4	96.5
108.8	92.8	14.7	96.1
142.2	120.8	15.5	91.8
149.7	134.6	10.0	87.4
195.5	173.8	11.1	85.5
204.2	183.1	10.3	95.6
210.7	201.0	4.6	97.6
223.1	201.3	9.8	89.2
235.4	205.0	12.9	91.8

$$^a\text{Relative Error} = \frac{ABS(\text{Measured}-\text{Predicted})}{\text{Measured}} \times 100$$

The COMAC values were also calculated using the correlated mode shape pairs above and the results are shown in Fig. (9.16).

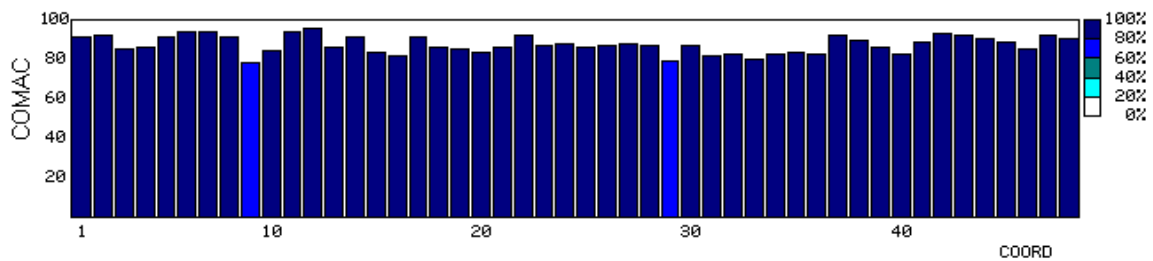


Figure 9.16: COMAC values between experimental and FE data - Structure B

It is seen the contribution from all measurement points is about the same, a feature

that suggests that there are no obvious test errors.

9.7 Model Updating for Structure B

It is clear from Table (9.3) that there is significant stiffness mismatch since all MAC values are above 85 % but the relative natural frequency errors are high (max. = 24 %).

Once again, the structure was assumed to be undamped and the imaginary part of the measured FRFs was set to zero. The incompleteness of the measured data was dealt with the exact reduction method of Chapter 3.

9.7.1 Updating Using Simulated Experimental Data

To assess the feasibility of the proposed updating exercise, it was decided to use simulated experimental data first. The simulated data were noise-free and, like the experimental data, they consisted of 48 FRFs for an excitation at node 1 in the Z direction. Convergence was achieved after 5 iterations. Although the error locations were not correct, the updated FRFs showed a remarkable improvement over the initially-predicted ones (Fig. 9.17). The reason for this may be explained by the non-linear nature of the algorithm. The objective function is a highly non-linear function of the unknown parameters and the optimisation algorithm may not be able to capture the true minimum. In such cases, convergence towards local minima is a very likely possibility.

The same test case was repeated for different levels of added random noise. Convergence was achieved for low noise levels (up to 1%) but more iterations were needed to achieve convergence. Again error localisation was poor but the updated FRFs were in a good agreement with the original simulated experimental receptances for the cases converged. Further studies, not reported here, indicated that increasing the number

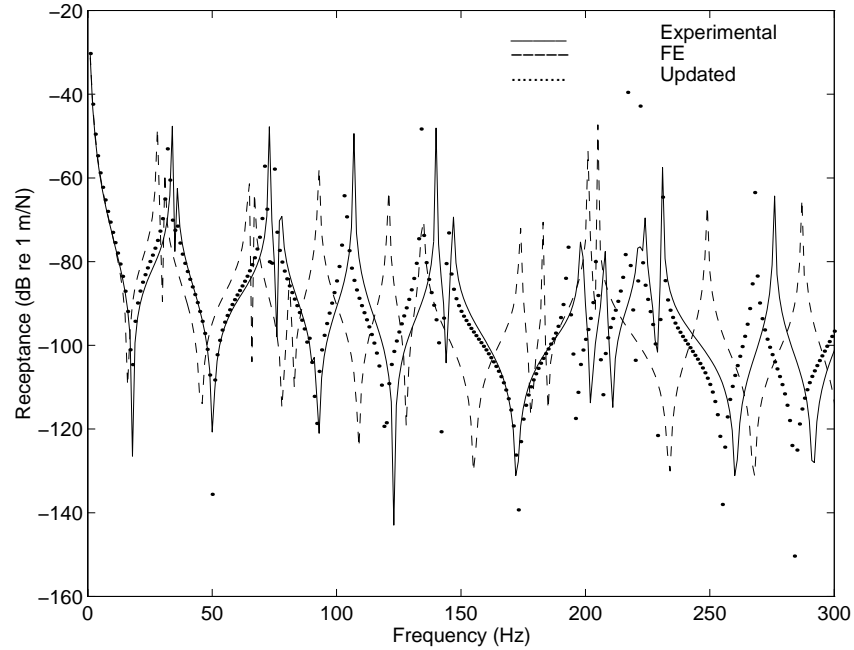


Figure 9.17: Experimental, initially-predicted and updated receptance FRF α_{1z1z} - Structure B

of measurement co-ordinates or reducing the noise levels improved the convergence and made the updated response model closer to the simulated experimental FRFs. The findings, once again, highlight the difficulty of updating FE models. A particular solution is not only non-unique but does not necessarily have a physical meaning. In spite of this, better predictive models can be found in a "best match" sense but their use for further analysis remains questionable as long as a full validation is not carried out.

9.7.2 Updating Using Measured FRF Data

Earlier studies indicated that convergence could not be achieved when raw measured FRFs were used directly. Therefore synthesised FRF data were used instead of raw measured data in order to reduce the effects of random noise and other inconsistencies. The Z-direction FRF set was computed using modal analysis results and a typical FRF is plotted in Fig. (9.18) in both original (raw) and synthesised form. The discrepancy is seen to be minimal for updating purpose.

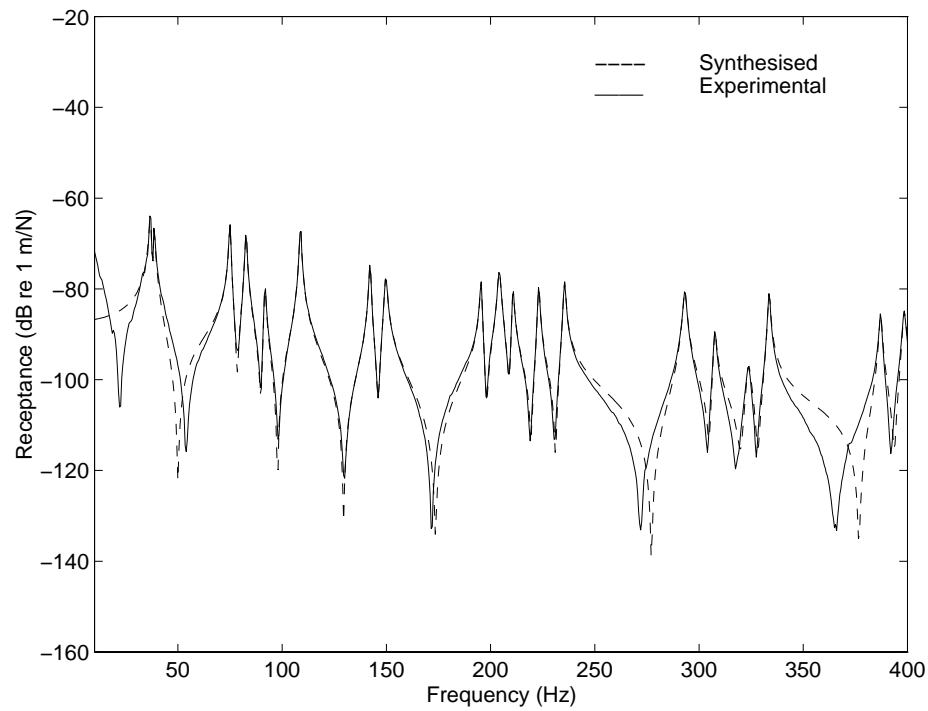


Figure 9.18: Experimental and synthesised FRF α_{1z1z} - Structure B

Here, one is confronted with another problem. In the FE model, it is possible to generate a response function at a node that is situated exactly on the stiffener line. However, the accelerometer has a finite contact area and can be placed on one or the other side of this thickness change line. In other words, it is either on the extra metal strip, or the base plate. The response that is measured in each case is plotted in Fig. (9.19).

Although the difference is small, it can be a source of error which can affect the updating procedure adversely. After some deliberation, it was decided to compute the average FRFs at the thickness line and use these in updating procedure.

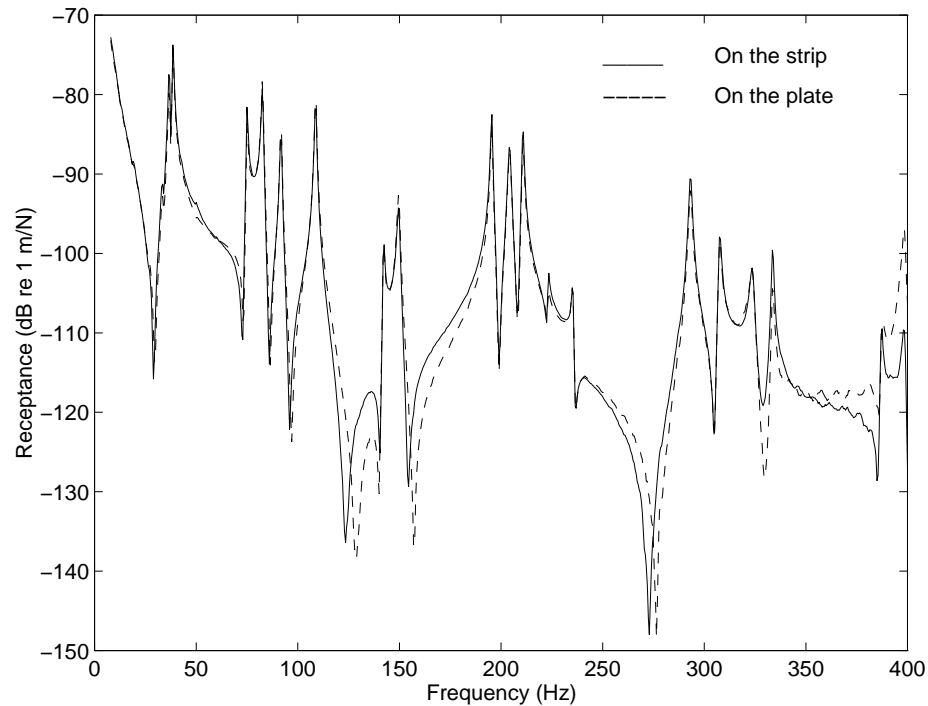


Figure 9.19: Measured FRF α_{1z9z} - Structure B

As before, several sets of physical parameters were obtained by selecting different frequency point sets, convergence being achieved in most cases tried. The best results were obtained for 24 frequency points selected from the 0-240 Hz frequency range, these being at 21, 25, 27, 40, 43, 54, 61, 70, 76, 85, 95, 105, 115, 125, 140, 152, 165,

180, 190, 200, 210, 221, 230 and 240 Hz. Although the updated parameters were not representative of the thickness errors, the natural frequency difference of Table (9.3) was improved by 60.4 %. The results are summarised in Table (9.4).

Table 9.4: Measured, initially-predicted and updated natural frequencies of Structure B

Measured (Hz)	Initially Predicted (Hz)	Relative ^a Error %	Updated (Hz)	Relative ^b Error %
36.8	27.9	24.2	31.3	14.9
38.5	30.8	20.0	33.2	13.7
74.9	64.7	13.6	71.2	4.9
82.6	66.7	19.2	79.5	3.8
91.7	81.3	11.3	89.7	2.2
108.7	92.8	14.7	104.9	3.5
142.1	120.8	14.9	135.6	4.5
149.6	134.6	10.0	143.5	4.1
195.4	173.8	11.1	185.8	4.9
204.1	183.1	10.3	199.4	2.3
202.9	201.0	.90	203.1	.10
210.7	201.3	4.6	210.3	.19
223.1	205.0	8.2	212.9	4.9
235.4	248.8	5.7	230.5	2.3
Ave. Error	-	12.90	-	5.09

$$^a\text{Relative Error} = \frac{ABS(\text{Measured}-\text{Predicted})}{\text{Measured}} \times 100$$

$$^b\text{Relative Error} = \frac{ABS(\text{Measured}-\text{Updated})}{\text{Measured}} \times 100$$

The MAC values either stayed the same or decreased slightly after updating (Table 9.3). The measured, initially-predicted and updated receptance FRF α_{1Z1Z} is plotted in Fig. (9.20), from which it is seen that updating has been successful in bringing the FE model closer to the experimental model. However, once again, this has been achieved in a "curve-fitting" sense rather than "error-correction" sense.

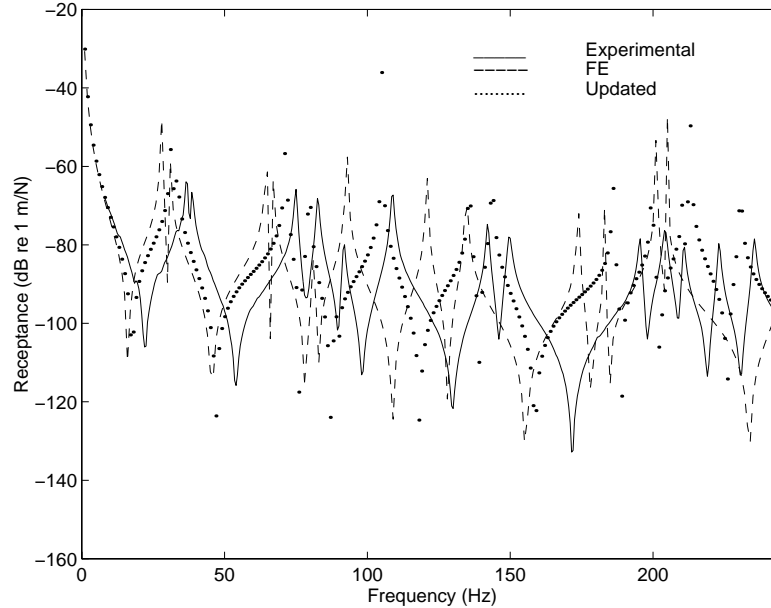


Figure 9.20: Experimental, initially-predicted and updated FRF α_{1z1z} - Structure B

9.8 Concluding Remarks

- As expected, the model updating quality depend heavily on the quality of experimental FRFs, noise and systematic errors causing both instability and multiple solutions. The effects of random noise were reduced by using synthesised FRFs but consistent bias errors are still present in the updating process.
- The procedure based on physical parameters seems to be more effective than its p-values based counterpart. However, the algorithm has a non-linear objective function with many local minima. It also needs more CPU time than the conventional RFM using p-values.
- It is concluded that response function based updating procedures demand a degree of accuracy which may not be available from the conventional measurement techniques. This is in line with the results from Chapter 4 of this thesis.

Chapter 10

Conclusions and Recommendations for Further Work

10.1 Conclusions

- (i) In spite of extensive research over the past fifteen years, the state-of-the-art in finite element model updating is far from maturing and no reliable and generally applicable procedures have been formulated so far. Despite a wealth of updating algorithms, success seems to be case-dependent and applicability appears to be bounded by the skill of the analyst in choosing a correct set of parameters.
- (ii) The response function method, based on forced vibration testing, was investigated in some detail. It was shown that the elements of the reduced dynamic stiffness matrix were smooth functions of the design parameters and of the excitation frequency up to the first natural frequency of the partially-grounded system clamped at the measurement points. However, this limit is a sufficient but not necessary condition and the updating range may be increased, subject to other considerations.
- (iii) A new p-value formulation was introduced and implemented in the RFM algorithm. The results show that the modified algorithm is more stable and

converges faster.

- (iv) Different approaches to include damping in the FE models were described and the effect of damping on the solution stability was investigated. It was found that damping made the convergence process numerically more stable.
- (v) A strategy for the selection of updating frequency points was introduced. The quality of the selection was checked via a singular value decomposition of the FRF matrix formed by the selected measurement points.
- (vi) Numerical ill-conditioning, associated with the minimisation of force balance residue, was avoided by pre-multiplying the residue vector by the dynamic flexibility matrix of the analytical model. Such an approach was found to reduce the sensitivity of the method to measurement errors.
- (vii) In most cases, incomplete and noisy data result in non-unique solutions. However, the incompleteness problem of the experimental model was overcome by introducing an exact reduction technique, albeit by reducing the updating frequency range.
- (viii) Measurement noise has a significant adverse effect on model updating if the FRF data are used directly. However, an acceptable and potentially more accurate solution can be found by using regularisation techniques. Some popular techniques, namely truncated SVD, Tikhonov method, linear-least-squares (LLS) method, total-least-squares (TLSQ) method and entropy method were discussed. The numerical experiments have shown that the solution quality substantially deteriorates for TLSQ and LLS in case of large noise variance. However, such noise variances are unlikely to be encountered in updating problems. By increasing the number of equations, the accuracy of TSVD and TLSQ solutions increases faster than that for LLS. The maximum entropy method was then applied to the solution of the updating equations. The results showed that the method required significantly more computational effort without yielding any increased accuracy.

-
- (ix) The determination of the required experimental accuracy that must be attained when updating finite element models with use of measured vibration test data was investigated in detail. Starting from a response function based updating technique, it has been possible to develop a mathematical formulation in the form of a simple relationship between the system's properties, the correction matrices and the amount of experimental noise. It was shown that the proposed formulation can be used to assess the threshold of maximum allowable experimental error.
 - (x) A further use of the characteristic function lies in its ability to yield the optimum excitation frequency points that must be provided to the updating algorithm. This feature can be used for either relaxing the error threshold or for improving the numerical stability. The present study suggests that the maximum allowable error is small, say within the 0.10% - 0.25% range. This finding is likely to have implications on the acquisition and processing of vibration test data which are going to be used in the updating of mathematical models.
 - (xi) The existing constrained eigenstructure assignment method was modified to deal with the updating of large-order systems. The resulting formulation is compatible with the response function and inverse eigensensitivity methods in the sense that the individual mass, stiffness and damping matrices are corrected by simple multipliers, the so-called p-values. The eigenstructure assignment method yields the solution directly and hence it has a significant advantage over its iterative counterparts such as RFM and IESM. A comparative study reveals that the RFM requires substantially more CPU power in all cases. Also, the convergence of the RFM cannot be guaranteed in cases where the measured FRFs are polluted by noise or when the discretisation differences are significant. On the other hand, the RFM seems to be able to cope better with incomplete measured data.
 - (xii) The existing generic elements formulation was extended to include some 2D and 3D finite elements and a number of case studies were presented to investigate the effect of various modelling errors as well as experimental noise. A generic

element formulation, together with a response function based objective function, has been used to update a number of small FE models. The results showed that the approach can deal with both physical parameter and discretisation errors. The performance of the generic element method was compared to the other popular updating methods. The main disadvantage of the method is the excessive computational effort that is required in comparison with the other finite element updating techniques.

- (xiii) The use of physical parameters, instead of elemental p-values, is introduced into the FRF-based updating technique. The approach has been investigated for 3D beam and plate elements on a number of case studies. The use of design parameters in exact 3D beam elements was also introduced. In common with many other updating techniques, the incompleteness and noise in the experimental data remains a major problem. Noise makes the process of convergence unstable while incompleteness restricts the updating range. The method also needs more CPU time and more iterations than the more conventional p-value approach. However, this disadvantage can partly be offset by the use of macro elements.
- (xiv) An exact element based updating approach, where the derivatives of the dynamic stiffness matrix with respect to the design parameters are calculated, was also reported. The basic idea was to start from an initial model that is free of discretisation errors. Such a route is possible for some simple beam systems, such as pipingworks, space frames, etc. It is expected that the technique can also deal with the updating of joints in such structures.
- (xv) Two experimental case studies using actual measured data on two real structure were carried out. The updating procedure was based on physical parameters, as this approach was judged to be more effective than the use of p-values. Although the convergence achieved in both cases and improvement was obtained in FRF overlays, the location of the errors could not be determined correctly. It was concluded that systematic updating procedures demanded an experimental degree of accuracy which was not readily available from the conventional

measurement techniques.

10.2 Suggestions for Further Work

(i) On the required experimental accuracy

The present calculations, as well as other numerical studies, suggest that the maximum allowable error is small. This finding is likely to have implications on the acquisition and processing of vibration test data which are going to be used in the updating of mathematical models. Therefore, the success of model updating depends on the accuracy of the experimental data and the development of appropriate data acquisition techniques are of primary importance. This requirement is particularly important for the rotational degrees of freedom as current techniques are particularly limited.

(ii) Development of new techniques

The use of the boundary elements method (BEM) for constructing the initial model can be a promising avenue to explore. Using BEM, only the external points have to be modelled, thus providing a natural compatibility with experimental response points.

(iii) Further considerations

- There is a need to define the number of measurement locations for successful model updating.
- The uniqueness and existence aspects of the updating problem are still not fully understood and should be investigated more.
- When physical or exact parameters, the linearisation of the dynamic stiffness matrix up to the first term may not be adequate and the inclusion of higher order terms in the formulation is necessary.

The use of the updated model for further analysis remains an important but unaddressed aspect since updating is not an end in itself.

10.3 Summary of Contributions of Present Work

- All major state-of-the-art updating techniques were classified on the basis of their approach and were presented in a consistent notation. A survey on regularisation techniques was carried out and the most popular methods were applied to incomplete and noisy model updating problems.
- Problems with forced vibration testing based updating methods were illustrated. Some recommendations for the selection of updating frequencies and of the initial damping matrix were proposed.
- The required experimental accuracy for updating finite element models was determined using an analytical approach.
- The existing constrained eigenstructure assignment method was modified to deal with large-order systems.
- The existing generic element method was extended to include some 2D and 3D finite elements and a number of case studies were presented to investigate the effect of various modelling errors as well as experimental noise.
- The use of physical parameters was introduced into the FRF-based updating technique. An updating approach, referred as 'exact method', was also developed.
- Practical problems encountered during physical parameters updating were demonstrated on two true experimental test cases.

10.4 Closure

The initial aim of this study was to develop a practical approach to update mathematical structural dynamics models using measured test data. Although a number of contributions were made, it is recognised that the problem is far from being solved

in the general case. A 1000-fold increase in computing power and a corresponding increase in experimental accuracy might make some of today's engineering models updatable in a global sense. However, a true improvement will probably come from a thorough re-evaluation for current modelling methodologies.

Appendix A

Derivatives of the Sensitivity Matrices with Respect to the Updating Parameters

A.1 3D Beam Element

Updating parameters: E , A , G , J , I_y , I_z and ρ

Coefficient of sensitivity matrices with respect to E:

$$\begin{aligned} \frac{\partial \alpha}{\partial E} &= A & , & & \frac{\partial \beta}{\partial E} &= 0 & , & & \frac{\partial \gamma_y}{\partial E} &= I_y \\ \frac{\partial \gamma_z}{\partial E} &= I_z & , & & \frac{\partial \kappa}{\partial E} &= 0 & , & & \frac{\partial \epsilon}{\partial E} &= 0 \end{aligned} \quad (\text{A.1})$$

Coefficient of sensitivity matrices with respect to A:

$$\begin{aligned} \frac{\partial \alpha}{\partial A} &= E & , & & \frac{\partial \beta}{\partial A} &= 0 & , & & \frac{\partial \gamma_y}{\partial A} &= 0 \\ \frac{\partial \gamma_z}{\partial A} &= 0 & , & & \frac{\partial \kappa}{\partial A} &= \rho \ell & , & & \frac{\partial \epsilon}{\partial A} &= -\frac{J}{A^2} \end{aligned} \quad (\text{A.2})$$

Coefficient of sensitivity matrices with respect to G:

$$\begin{aligned} \frac{\partial \alpha}{\partial G} &= 0 & , & & \frac{\partial \beta}{\partial G} &= J & , & & \frac{\partial \gamma_y}{\partial G} &= 0 \\ \frac{\partial \gamma_z}{\partial G} &= 0 & , & & \frac{\partial \kappa}{\partial G} &= 0 & , & & \frac{\partial \epsilon}{\partial G} &= 0 \end{aligned} \quad (\text{A.3})$$

Coefficient of sensitivity matrices with respect to J:

$$\begin{aligned} \frac{\partial \alpha}{\partial J} &= 0 & , & & \frac{\partial \beta}{\partial J} &= G & , & & \frac{\partial \gamma_y}{\partial J} &= 0 \\ \frac{\partial \gamma_z}{\partial J} &= 0 & , & & \frac{\partial \kappa}{\partial J} &= 0 & , & & \frac{\partial \epsilon}{\partial J} &= \frac{1}{A} \end{aligned} \quad (\text{A.4})$$

Coefficient of sensitivity matrices with respect to I_y :

$$\begin{aligned} \frac{\partial \alpha}{\partial I_y} &= 0 & , & & \frac{\partial \beta}{\partial I_y} &= 0 & , & & \frac{\partial \gamma_y}{\partial I_y} &= E \\ \frac{\partial \gamma_z}{\partial I_y} &= 0 & , & & \frac{\partial \kappa}{\partial I_y} &= 0 & , & & \frac{\partial \epsilon}{\partial I_y} &= 0 \end{aligned} \quad (\text{A.5})$$

Coefficient of sensitivity matrices with respect to I_z :

$$\begin{aligned} \frac{\partial \alpha}{\partial I_z} &= 0 & , & & \frac{\partial \beta}{\partial I_z} &= 0 & , & & \frac{\partial \gamma_y}{\partial I_z} &= 0 \\ \frac{\partial \gamma_z}{\partial I_z} &= E & , & & \frac{\partial \kappa}{\partial I_z} &= 0 & , & & \frac{\partial \epsilon}{\partial I_z} &= 0 \end{aligned} \quad (\text{A.6})$$

Coefficient of sensitivity matrices with respect to ρ :

$$\begin{aligned} \frac{\partial \alpha}{\partial \rho} &= 0 & , & & \frac{\partial \beta}{\partial \rho} &= 0 & , & & \frac{\partial \gamma_y}{\partial \rho} &= 0 \\ \frac{\partial \gamma_z}{\partial \rho} &= 0 & , & & \frac{\partial \kappa}{\partial \rho} &= A\ell & , & & \frac{\partial \epsilon}{\partial \rho} &= 0 \end{aligned} \quad (\text{A.7})$$

A.2 2D Plate Element

Updating parameters: h , ν , ρ and E

Coefficient of sensitivity matrices with respect to h :

$$\begin{aligned}
 \frac{\partial \kappa}{\partial h} &= \frac{\kappa}{h} & , & & \frac{\partial C_o}{\partial h} &= \frac{C_o}{h} & , & & \frac{\partial F}{\partial h} &= \frac{2F}{h} \\
 \frac{\partial G}{\partial h} &= \frac{2G}{h} & , & & \frac{\partial H}{\partial h} &= \frac{2H}{h} & , & & \frac{\partial I}{\partial h} &= \frac{2I}{h} \\
 \frac{\partial J}{\partial h} &= \frac{2J}{h} & , & & \frac{\partial K}{\partial h} &= \frac{2K}{h} & , & & \frac{\partial L}{\partial h} &= \frac{2L}{h} \\
 \frac{\partial M}{\partial h} &= \frac{2M}{h} & , & & \frac{\partial N}{\partial h} &= \frac{2N}{h} & , & & \frac{\partial O}{\partial h} &= \frac{2O}{h} \\
 \frac{\partial P}{\partial h} &= \frac{2P}{h} & , & & \frac{\partial Q}{\partial h} &= \frac{2Q}{h} & , & & \frac{\partial R}{\partial h} &= \frac{2R}{h} \\
 \frac{\partial S}{\partial h} &= \frac{2S}{h} & , & & \frac{\partial T}{\partial h} &= \frac{2T}{h} & , & & \frac{\partial U}{\partial h} &= \frac{2U}{h} \\
 \frac{\partial V}{\partial h} &= \frac{2V}{h} & , & & \frac{\partial W}{\partial h} &= \frac{2W}{h} & , & & \frac{\partial X}{\partial h} &= \frac{2X}{h} \\
 \frac{\partial Y}{\partial h} &= \frac{2Y}{h} & , & & \frac{\partial Z}{\partial h} &= \frac{2Z}{h} & , & & &
 \end{aligned} \tag{A.8}$$

Coefficient of sensitivity matrices with respect to ν :

$$\begin{aligned}
 \frac{\partial \kappa}{\partial \nu} &= -\frac{2\nu E h}{180(1-\nu^2)^2} & , & & \frac{\partial C_o}{\partial \nu} &= 0 & , & & \frac{\partial F}{\partial \nu} &= -\frac{h^2}{ab} \\
 \frac{\partial G}{\partial \nu} &= \frac{12h^2}{\beta b} & , & & \frac{\partial H}{\partial \nu} &= \frac{12\beta h^2}{a} & , & & \frac{\partial I}{\partial \nu} &= \frac{12h^2}{ab} \\
 \frac{\partial J}{\partial \nu} &= \frac{3h^2}{\beta b} & , & & \frac{\partial K}{\partial \nu} &= -\frac{12\beta h^2}{a} & , & & \frac{\partial L}{\partial \nu} &= \frac{12h^2}{ab} \\
 \frac{\partial M}{\partial \nu} &= \frac{12h^2}{\beta b} & , & & \frac{\partial N}{\partial \nu} &= -\frac{3\beta h^2}{a} & , & & \frac{\partial O}{\partial \nu} &= -\frac{12h^2}{ab} \\
 \frac{\partial P}{\partial \nu} &= -\frac{3h^2}{\beta b} & , & & \frac{\partial Q}{\partial \nu} &= \frac{3\beta h^2}{a} & , & & \frac{\partial R}{\partial \nu} &= -\frac{4h^2}{\beta} \\
 \frac{\partial S}{\partial \nu} &= \frac{h^2}{\beta} & , & & \frac{\partial T}{\partial \nu} &= \frac{4h^2}{\beta} & , & & \frac{\partial U}{\partial \nu} &= -\frac{h^2}{\beta} \\
 \frac{\partial V}{\partial \nu} &= -4\beta h^2 & , & & \frac{\partial W}{\partial \nu} &= 4\beta h^2 & , & & \frac{\partial X}{\partial \nu} &= \beta h^2 \\
 \frac{\partial Y}{\partial \nu} &= -\beta h^2 & , & & \frac{\partial Z}{\partial \nu} &= 15h^2 & , & & &
 \end{aligned} \tag{A.9}$$

Coefficient of sensitivity matrices with respect to ρ :

$$\begin{aligned}
 \frac{\partial \kappa}{\partial \rho} &= 0 & , & & \frac{\partial C_o}{\partial \rho} &= \frac{C_o}{\rho} & , & & \frac{\partial F}{\partial \rho} &= 0 \\
 \frac{\partial G}{\partial \rho} &= 0 & , & & \frac{\partial H}{\partial \rho} &= 0 & , & & \frac{\partial I}{\partial \rho} &= 0 \\
 \frac{\partial J}{\partial \rho} &= 0 & , & & \frac{\partial K}{\partial \rho} &= 0 & , & & \frac{\partial L}{\partial \rho} &= 0 \\
 \frac{\partial M}{\partial \rho} &= 0 & , & & \frac{\partial N}{\partial \rho} &= 0 & , & & \frac{\partial O}{\partial \rho} &= 0 \\
 \frac{\partial P}{\partial \rho} &= 0 & , & & \frac{\partial Q}{\partial \rho} &= 0 & , & & \frac{\partial R}{\partial \rho} &= 0 \\
 \frac{\partial S}{\partial \rho} &= 0 & , & & \frac{\partial T}{\partial \rho} &= 0 & , & & \frac{\partial U}{\partial \rho} &= 0 \\
 \frac{\partial V}{\partial \rho} &= 0 & , & & \frac{\partial W}{\partial \rho} &= 0 & , & & \frac{\partial X}{\partial \rho} &= 0 \\
 \frac{\partial Y}{\partial \rho} &= 0 & , & & \frac{\partial Z}{\partial \rho} &= 0 & & & &
 \end{aligned} \tag{A.10}$$

Coefficient of sensitivity matrices with respect to E :

$$\begin{aligned}
 \frac{\partial \kappa}{\partial E} &= \frac{\kappa}{E} & , & & \frac{\partial C_o}{\partial E} &= 0 & , & & \frac{\partial F}{\partial E} &= 0 \\
 \frac{\partial G}{\partial E} &= 0 & , & & \frac{\partial H}{\partial E} &= 0 & , & & \frac{\partial I}{\partial E} &= 0 \\
 \frac{\partial J}{\partial E} &= 0 & , & & \frac{\partial K}{\partial E} &= 0 & , & & \frac{\partial L}{\partial E} &= 0 \\
 \frac{\partial M}{\partial E} &= 0 & , & & \frac{\partial N}{\partial E} &= 0 & , & & \frac{\partial O}{\partial E} &= 0 \\
 \frac{\partial P}{\partial E} &= 0 & , & & \frac{\partial Q}{\partial E} &= 0 & , & & \frac{\partial R}{\partial E} &= 0 \\
 \frac{\partial S}{\partial E} &= 0 & , & & \frac{\partial T}{\partial E} &= 0 & , & & \frac{\partial U}{\partial E} &= 0 \\
 \frac{\partial V}{\partial E} &= 0 & , & & \frac{\partial W}{\partial E} &= 0 & , & & \frac{\partial X}{\partial E} &= 0 \\
 \frac{\partial Y}{\partial E} &= 0 & , & & \frac{\partial Z}{\partial E} &= 0 & & & &
 \end{aligned} \tag{A.11}$$

A.3 Exact 3D Beam Element

Updating parameters: $E, A, \rho, J, G, I_y, I_z$

Let's define a vector X as:

$$\{X\} = \{E, A, \rho, J, G, I_y, I_z\} \quad (\text{A.12})$$

The Derivatives of G_1 with respect to x_i :

$$\begin{aligned} \frac{\partial \psi}{\partial E} &= \frac{\psi}{-2E} \\ \frac{\partial \psi}{\partial \rho} &= \frac{\psi}{2\rho} \\ \frac{\partial G_1}{\partial \rho} &= EA (\cot(\psi\ell) - \psi\ell(1 + \cot^2(\psi\ell))) \frac{\partial \psi}{\partial \rho} \\ \frac{\partial G_1}{\partial A} &= E\psi \cot(\psi\ell) \\ \frac{\partial G_1}{\partial E} &= A\psi \cot(\psi\ell) + EA (\cot(\psi\ell) + \psi\ell(1 + \cot^2(\psi\ell))) \frac{\partial \psi}{\partial E} \\ \frac{\partial G_1}{\partial J} &= 0 \\ \frac{\partial G_1}{\partial G} &= 0 \\ \frac{\partial G_1}{\partial I_y} &= 0 \\ \frac{\partial G_1}{\partial I_z} &= 0 \end{aligned} \quad (\text{A.13})$$

The Derivatives of G_2 with respect to x_i :

$$\begin{aligned} \frac{\partial G_2}{\partial \rho} &= -EA \left(\csc(\psi\ell) - \ell \frac{\cos(\psi\ell)}{\sin^2(\psi\ell)} \right) \frac{\partial \psi}{\partial \rho} \\ \frac{\partial G_2}{\partial A} &= -E\psi \csc(\psi\ell) \\ \frac{\partial G_2}{\partial E} &= -A\psi \csc(\psi\ell) - EA \left(\csc(\psi\ell) - \psi\ell \frac{\cos(\psi\ell)}{\sin^2(\psi\ell)} \right) \frac{\partial \psi}{\partial E} \\ \frac{\partial G_2}{\partial J} &= 0 \\ \frac{\partial G_2}{\partial G} &= 0 \\ \frac{\partial G_2}{\partial I_y} &= 0 \\ \frac{\partial G_2}{\partial I_z} &= 0 \end{aligned} \quad (\text{A.14})$$

The Derivatives of G_3 with respect to x_i :

$$\begin{aligned}
\frac{\partial \nu}{\partial G} &= \frac{\nu}{-2G} \\
\frac{\partial \nu}{\partial \rho} &= \frac{\nu}{2\rho} \\
\frac{\partial G_3}{\partial \rho} &= GJ (\cot(\nu\ell) - \nu\ell(1 + \cot^2(\nu\ell))) \frac{\partial \nu}{\partial \rho} \\
\frac{\partial G_3}{\partial A} &= 0 \\
\frac{\partial G_3}{\partial E} &= 0 \\
\frac{\partial G_3}{\partial J} &= G\nu \cot(\nu\ell) \\
\frac{\partial G_3}{\partial G} &= J\nu \cot(\nu\ell) + GJ (\cot(\nu\ell) + \nu\ell(1 + \cot^2(\nu\ell))) \frac{\partial \nu}{\partial G} \\
\frac{\partial G_3}{\partial I_y} &= 0 \\
\frac{\partial G_3}{\partial I_z} &= 0
\end{aligned} \tag{A.15}$$

The Derivatives of G_4 with respect to x_i :

$$\begin{aligned}
\frac{\partial G_4}{\partial \rho} &= -GJ \left(\csc(\nu\ell) - \ell \frac{\cos(\nu\ell)}{\sin^2(\nu\ell)} \right) \frac{\partial \nu}{\partial \rho} \\
\frac{\partial G_4}{\partial A} &= 0 \\
\frac{\partial G_4}{\partial E} &= 0 \\
\frac{\partial G_4}{\partial J} &= -G\nu \csc(\nu\ell) \\
\frac{\partial G_4}{\partial G} &= -J\nu \csc(\nu\ell) - GJ \left(\csc(\nu\ell) - \nu\ell \frac{\cos(\nu\ell)}{\sin^2(\nu\ell)} \right) \frac{\partial \nu}{\partial G} \\
\frac{\partial G_4}{\partial I_y} &= 0 \\
\frac{\partial G_4}{\partial I_z} &= 0
\end{aligned} \tag{A.16}$$

Now, let's define the following variables for the sake of simplicity:

$$\begin{aligned}
T_1 &= \frac{\rho\omega^2 A}{EI} \\
T_2 &= \rho\omega^2 \left(\frac{1}{\kappa G} - \frac{1}{E} \right) \\
T_3 &= \rho\omega^2 \left(\frac{1}{\kappa G} + \frac{1}{E} \right) \\
T_4 &= \frac{\rho\omega^2 A}{\kappa G} \\
T_5 &= EI
\end{aligned} \tag{A.17}$$

Now, we are going to calculate the derivatives of T_1, \dots, T_5 with respect to the ele-

ments of vector X .

The derivatives of T_1, \dots, T_5 with respect to E :

$$\begin{aligned} \frac{\partial T_1}{\partial E} &= \frac{T_1}{E} \quad , \quad \frac{\partial T_2}{\partial E} = \frac{\rho\omega^2}{E^2} \quad , \quad \frac{\partial T_3}{\partial E} = -\frac{\rho\omega^2}{E^2} \\ \frac{\partial T_4}{\partial E} &= 0 \quad , \quad \frac{\partial T_5}{\partial E} = I \end{aligned} \quad (\text{A.18})$$

The derivatives of T_1, \dots, T_5 with respect to A :

$$\begin{aligned} \frac{\partial T_1}{\partial A} &= \frac{T_1}{A} \quad , \quad \frac{\partial T_2}{\partial A} = 0 \quad , \quad \frac{\partial T_3}{\partial A} = 0 \\ \frac{\partial T_4}{\partial A} &= 0 \quad , \quad \frac{\partial T_5}{\partial A} = 0 \end{aligned} \quad (\text{A.19})$$

The derivatives of T_1, \dots, T_5 with respect to ρ :

$$\begin{aligned} \frac{\partial T_1}{\partial \rho} &= \frac{T_1}{\rho} \quad , \quad \frac{\partial T_2}{\partial \rho} = \frac{T_2}{\rho} \quad , \quad \frac{\partial T_3}{\partial \rho} = \frac{T_3}{\rho} \\ \frac{\partial T_4}{\partial \rho} &= \frac{T_4}{\rho} \quad , \quad \frac{\partial T_5}{\partial \rho} = 0 \end{aligned} \quad (\text{A.20})$$

The derivatives of T_1, \dots, T_5 with respect to J :

$$\begin{aligned} \frac{\partial T_1}{\partial J} &= 0 \quad , \quad \frac{\partial T_2}{\partial J} = 0 \quad , \quad \frac{\partial T_3}{\partial J} = 0 \\ \frac{\partial T_4}{\partial J} &= 0 \quad , \quad \frac{\partial T_5}{\partial J} = 0 \end{aligned} \quad (\text{A.21})$$

The derivatives of T_1, \dots, T_5 with respect to G :

$$\begin{aligned} \frac{\partial T_1}{\partial G} &= 0 \quad , \quad \frac{\partial T_2}{\partial G} = -\frac{\rho\omega^2}{\kappa G^2} \quad , \quad \frac{\partial T_3}{\partial G} = -\frac{\rho\omega^2}{\kappa G^2} \\ \frac{\partial T_4}{\partial G} &= -\frac{\rho\omega^2}{\kappa G^2} \quad , \quad \frac{\partial T_5}{\partial G} = 0 \quad , \end{aligned} \quad (\text{A.22})$$

The derivatives of T_1, \dots, T_5 with respect to I_y :

$$\begin{aligned} \frac{\partial T_1}{\partial I_y} &= -\frac{T_1}{I_y} \quad , \quad \frac{\partial T_2}{\partial I_y} = 0 \quad , \quad \frac{\partial T_3}{\partial I_y} = 0 \\ \frac{\partial T_4}{\partial I_y} &= 0 \quad , \quad \frac{\partial T_5}{\partial I_y} = E \end{aligned} \quad (\text{A.23})$$

The derivatives of T_1, \dots, T_5 with respect to I_z :

$$\begin{aligned} \frac{\partial T_1}{\partial I_z} &= -\frac{T_1}{I_z} & , & & \frac{\partial T_2}{\partial I_z} &= 0 & , & & \frac{\partial T_3}{\partial I_z} &= 0 \\ \frac{\partial T_4}{\partial I_z} &= 0 & , & & \frac{\partial T_5}{\partial I_z} &= E \end{aligned} \quad (\text{A.24})$$

Then,

$$\begin{aligned} \epsilon_1 &= \sqrt{T_2^2 + 4T_1} \\ \epsilon_3 &= T_3 \\ \alpha &= \sqrt{\frac{\epsilon_1 + \epsilon_3}{2}} \\ \beta &= \sqrt{\frac{\epsilon_1 - \epsilon_3}{2}} \\ \gamma_1 &= \alpha^2 - T_4 \\ \gamma_2 &= \beta^2 + T_4 \\ \epsilon_2 &= \frac{\gamma_1 \gamma_2}{\alpha \beta} \\ \delta &= 2\epsilon_2 (\cos(\alpha \ell) \cosh(\beta \ell) - 1) + \left(\frac{\gamma_1^2}{\alpha^2} - \frac{\gamma_2^2}{\beta^2} \right) \sin(\alpha \ell) \sinh(\beta \ell) \\ K &= \frac{T_5}{\delta} \end{aligned}$$

If we assumed that x_i ($i = 1, \dots, 7$) is an element of vector X:

$$\begin{aligned} \frac{\partial \epsilon_1}{\partial x_i} &= T_2/\epsilon_1 \frac{\partial T_2}{\partial x_i} + 2/\epsilon_1 \frac{\partial T_1}{\partial x_i} \\ \frac{\partial \epsilon_3}{\partial x_i} &= \frac{\partial T_3}{\partial x_i} \\ \frac{\partial \alpha}{\partial x_i} &= \frac{1}{4\alpha} \left(\frac{\partial \epsilon_1}{\partial x_i} + \frac{\partial \epsilon_3}{\partial x_i} \right) \\ \frac{\partial \beta}{\partial x_i} &= \frac{1}{4\beta} \left(\frac{\partial \epsilon_1}{\partial x_i} - \frac{\partial \epsilon_3}{\partial x_i} \right) \\ \frac{\partial \gamma_1}{\partial x_i} &= 2\alpha \frac{\partial \alpha}{\partial x_i} - \frac{\partial T_4}{\partial x_i} \\ \frac{\partial \gamma_2}{\partial x_i} &= 2\beta \frac{\partial \beta}{\partial x_i} + \frac{\partial T_4}{\partial x_i} \\ \frac{\partial \epsilon_2}{\partial x_i} &= 1/(\alpha\beta) \left[\gamma_1 \frac{\partial \gamma_2}{\partial x_i} + \gamma_2 \frac{\partial \gamma_1}{\partial x_i} - (\gamma_1 \gamma_2 / \beta) \frac{\partial \beta}{\partial x_i} - (\gamma_1 \gamma_2 / \alpha) \frac{\partial \alpha}{\partial x_i} \right] \\ \frac{\partial \delta}{\partial x_i} &= 2 \frac{\partial \epsilon_2}{\partial x_i} [\cos(\alpha \ell) \cosh(\beta \ell) - 1] + 2\epsilon_2 \ell \left[-\frac{\partial \alpha}{\partial x_i} \sin(\alpha \ell) \cosh(\beta \ell) + \frac{\partial \beta}{\partial x_i} \cos(\alpha \ell) \sinh(\beta \ell) \right] \\ &\quad + 2 \left[(\gamma_1 / \alpha^2) \frac{\partial \gamma_1}{\partial x_i} - (\gamma_1^2 / \alpha^3) \frac{\partial \alpha}{\partial x_i} - (\gamma_2 / \beta^2) \frac{\partial \gamma_2}{\partial x_i} + (\gamma_2^2 / \beta^3) \frac{\partial \beta}{\partial x_i} \right] \sin(\alpha \ell) \sinh(\beta \ell) \\ &\quad + \ell (\gamma_1^2 / \alpha^2 - \gamma_2^2 / \beta^2) \left[\cos(\alpha \ell) \sinh(\beta \ell) \frac{\partial \alpha}{\partial x_i} + \sin(\alpha \ell) \cosh(\beta \ell) \frac{\partial \beta}{\partial x_i} \right] \\ \frac{\partial K}{\partial x_i} &= (1/\delta) \frac{\partial T_5}{\partial x_i} - (T_5/\delta^2) \frac{\partial \delta}{\partial x_i} \end{aligned}$$

The derivatives of f_1 with respect to x_i :

$$\begin{aligned}
f_1 &= F_1 (F_2 + F_3) \\
F_1 &= K \epsilon_1 \epsilon_2 \\
F_2 &= (\gamma_1 / \alpha) \sin(\alpha \ell) \cosh(\beta \ell) \\
F_3 &= (\gamma_2 / \beta) \cos(\alpha \ell) \sinh(\beta \ell) \\
\frac{\partial F_1}{\partial x_i} &= \epsilon_1 \epsilon_2 \frac{\partial K}{\partial x_i} + K \epsilon_2 \frac{\partial \epsilon_1}{\partial x_i} + K \epsilon_1 \frac{\partial \epsilon_2}{\partial x_i} \\
\frac{\partial F_2}{\partial x_i} &= \frac{1}{\alpha} \left[\sin(\alpha \ell) \cosh(\beta \ell) \frac{\partial \gamma_1}{\partial x_i} + \ell \gamma_1 \cos(\alpha \ell) \cosh(\beta \ell) \frac{\partial \alpha}{\partial x_i} + \ell \gamma_1 \sin(\alpha \ell) \sinh(\beta \ell) \frac{\partial \beta}{\partial x_i} \right] \\
&\quad - (\gamma_1 / \alpha^2) \sin(\alpha \ell) \cosh(\beta \ell) \frac{\partial \alpha}{\partial x_i} \\
\frac{\partial F_3}{\partial x_i} &= \frac{1}{\beta} \left[\cos(\alpha \ell) \sinh(\beta \ell) \frac{\partial \gamma_2}{\partial x_i} - \ell \gamma_2 \sin(\alpha \ell) \sinh(\beta \ell) \frac{\partial \alpha}{\partial x_i} + \ell \gamma_2 \cos(\alpha \ell) \cosh(\beta \ell) \frac{\partial \beta}{\partial x_i} \right] \\
&\quad - (\gamma_2 / \beta^2) \cos(\alpha \ell) \sinh(\beta \ell) \frac{\partial \beta}{\partial x_i} \\
\frac{\partial f_1}{\partial x_i} &= (F_2 + F_3) \frac{\partial F_1}{\partial x_i} + F_1 \left(\frac{\partial F_2}{\partial x_i} + \frac{\partial F_3}{\partial x_i} \right)
\end{aligned}$$

The derivatives of f_2 with respect to x_i :

$$\begin{aligned}
f_2 &= F_4 (F_5 F_6 + F_7 F_8) \\
F_4 &= K \gamma_1 \gamma_2 \\
F_5 &= \frac{\gamma_1}{\alpha^2} + \frac{\gamma_2}{\beta^2} \\
F_6 &= \sin(\alpha \ell) \sinh(\beta \ell) \\
F_7 &= \frac{\gamma_2 - \gamma_1}{\alpha \beta} \\
F_8 &= \cos(\alpha \ell) \cosh(\beta \ell) - 1 \\
\frac{\partial F_4}{\partial x_i} &= \gamma_1 \gamma_2 \frac{\partial K}{\partial x_i} + K \gamma_2 \frac{\partial \gamma_1}{\partial x_i} + K \gamma_1 \frac{\partial \gamma_2}{\partial x_i} \\
\frac{\partial F_5}{\partial x_i} &= (1 / \alpha^2) \frac{\partial \gamma_1}{\partial x_i} - 2(\gamma_1 / \alpha^3) \frac{\partial \alpha}{\partial x_i} + (1 / \beta^2) \frac{\partial \gamma_2}{\partial x_i} - 2(\gamma_2 / \beta^3) \frac{\partial \beta}{\partial x_i} \\
\frac{\partial F_6}{\partial x_i} &= \ell \cos(\alpha \ell) \sinh(\beta \ell) \frac{\partial \alpha}{\partial x_i} + \ell \sin(\alpha \ell) \cosh(\beta \ell) \frac{\partial \beta}{\partial x_i} \\
\frac{\partial F_7}{\partial x_i} &= \frac{1}{\alpha \beta} \left(\frac{\partial \gamma_2}{\partial x_i} - \frac{\partial \gamma_1}{\partial x_i} \right) - \frac{\gamma_2 - \gamma_1}{\alpha^2 \beta^2} \left(\beta \frac{\partial \alpha}{\partial x_i} - \alpha \frac{\partial \beta}{\partial x_i} \right) \\
\frac{\partial F_8}{\partial x_i} &= -\ell \sin(\alpha \ell) \cosh(\beta \ell) \frac{\partial \alpha}{\partial x_i} + \ell \cos(\alpha \ell) \sinh(\beta \ell) \frac{\partial \beta}{\partial x_i} \\
\frac{\partial f_2}{\partial x_i} &= (F_5 F_6 + F_7 F_8) \frac{\partial F_4}{\partial x_i} + F_4 \left(F_6 \frac{\partial F_5}{\partial x_i} + F_5 \frac{\partial F_6}{\partial x_i} + F_8 \frac{\partial F_7}{\partial x_i} + F_7 \frac{\partial F_8}{\partial x_i} \right)
\end{aligned}$$

The derivatives of f_3 with respect to x_i :

$$\begin{aligned}
 f_3 &= F_1 (F_9 + F_{10}) \\
 F_9 &= \frac{\gamma_1}{\alpha} \sin(\alpha\ell) \\
 F_{10} &= \frac{\gamma_2}{\beta} \sinh(\beta\ell) \\
 \frac{\partial F_9}{\partial x_i} &= (1/\alpha) \left[\sin(\alpha\ell) \frac{\partial \gamma_1}{\partial x_i} + \ell \gamma_1 \cos(\alpha\ell) \frac{\partial \alpha}{\partial x_i} \right] - (\gamma_1/\alpha^2) \sin(\alpha\ell) \frac{\partial \alpha}{\partial x_i} \\
 \frac{\partial F_{10}}{\partial x_i} &= (1/\beta) \left[\sinh(\beta\ell) \frac{\partial \gamma_2}{\partial x_i} + \ell \gamma_2 \cosh(\beta\ell) \frac{\partial \beta}{\partial x_i} \right] - (\gamma_2/\beta^2) \sinh(\beta\ell) \frac{\partial \beta}{\partial x_i} \\
 \frac{\partial f_3}{\partial x_i} &= (F_9 + F_{10}) \frac{\partial F_1}{\partial x_i} + F_1 \left(\frac{\partial F_9}{\partial x_i} + \frac{\partial F_{10}}{\partial x_i} \right)
 \end{aligned}$$

The derivatives of f_4 with respect to x_i :

$$\begin{aligned}
 f_4 &= F_1 (\cos(\alpha\ell) - \cosh(\beta\ell)) \\
 \frac{\partial f_4}{\partial x_i} &= (\cos(\alpha\ell) - \cosh(\beta\ell)) \frac{\partial F_1}{\partial x_i} - \ell F_1 \left(\sin(\alpha\ell) \frac{\partial \alpha}{\partial x_i} + \sinh(\beta\ell) \frac{\partial \beta}{\partial x_i} \right)
 \end{aligned}$$

The derivatives of f_5 with respect to x_i :

$$\begin{aligned}
 f_5 &= F_{11} (F_{12} F_{14} - F_{13} F_{15}) \\
 F_{11} &= K \epsilon_1 \\
 F_{12} &= \frac{\gamma_1}{\alpha} \\
 F_{13} &= \frac{\gamma_2}{\beta} \\
 F_{14} &= \cos(\alpha\ell) \sinh(\beta\ell) \\
 F_{15} &= \sin(\alpha\ell) \cosh(\beta\ell) \\
 \frac{\partial F_{11}}{\partial x_i} &= \epsilon_1 \frac{\partial K}{\partial x_i} + K \frac{\partial \epsilon_1}{\partial x_i} \\
 \frac{\partial F_{12}}{\partial x_i} &= (1/\alpha) \frac{\partial \gamma_1}{\partial x_i} - (\gamma_1/\alpha^2) \frac{\partial \alpha}{\partial x_i} \\
 \frac{\partial F_{13}}{\partial x_i} &= (1/\beta) \frac{\partial \gamma_2}{\partial x_i} - (\gamma_2/\beta^2) \frac{\partial \beta}{\partial x_i} \\
 \frac{\partial F_{14}}{\partial x_i} &= \ell \left[-\sin(\alpha\ell) \sinh(\beta\ell) \frac{\partial \alpha}{\partial x_i} + \cos(\alpha\ell) \cosh(\beta\ell) \frac{\partial \beta}{\partial x_i} \right] \\
 \frac{\partial F_{15}}{\partial x_i} &= \ell \left[\cos(\alpha\ell) \cosh(\beta\ell) \frac{\partial \alpha}{\partial x_i} + \sin(\alpha\ell) \sinh(\beta\ell) \frac{\partial \beta}{\partial x_i} \right] \\
 \frac{\partial f_5}{\partial x_i} &= (F_{12} F_{14} - F_{13} F_{15}) \frac{\partial F_{11}}{\partial x_i} + F_{11} \left(F_{14} \frac{\partial F_{12}}{\partial x_i} + F_{12} \frac{\partial F_{14}}{\partial x_i} - F_{15} \frac{\partial F_{13}}{\partial x_i} - F_{13} \frac{\partial F_{15}}{\partial x_i} \right)
 \end{aligned}$$

The derivatives of f_6 with respect to x_i :

$$\begin{aligned} f_6 &= F_{11} (F_{13} \sin(\alpha\ell) - F_{12} \sinh(\beta\ell)) \\ \frac{\partial f_6}{\partial x_i} &= (F_{13} \sin(\alpha\ell) - F_{12} \sinh(\beta\ell)) \frac{\partial F_{11}}{\partial x_i} \\ &\quad + F_{11} \left(\sin(\alpha\ell) \frac{\partial F_{13}}{\partial x_i} + \ell F_{13} \cos(\alpha\ell) \frac{\partial \alpha}{\partial x_i} - \sinh(\beta\ell) \frac{\partial F_{12}}{\partial x_i} - \ell F_{12} \cosh(\beta\ell) \frac{\partial \beta}{\partial x_i} \right) \end{aligned}$$

Bibliography

- J. B. Abbiss. Regularized iterative and noniterative procedures for object restoration from experimental data. *Optica Acta*, 107–124, 1983.
- H. O. Afolabi. *The Vibration of Turbine Blade Packets*. PhD thesis, Imperial College of Science, Technology and Medicine, London, UK, 1978.
- H. Ahmadian and G. Gladwell. Extracting real modes from complex measured modes. *Proc. of the 13th IMAC*, 507–510, Nashville, Tennessee, 1995.
- H. Ahmadian, G. Gladwell, and F. Ismail. Families of finite element models for updating procedures. *Proc. of the 12th IMAC*, 898–905, Honolulu, Hawaii, 1994a.
- H. Ahmadian, F. Ismail, and G. Gladwell. Acceptable element matrices for finite element model updating. *Proc. of 2nd Int. Symp. on Inverse Problems in Engineering*, 209–213, 1994b.
- K. Alexiou and J. R. Wright. Determination of force distribution in multi point resonance testing using various direct methods. *2nd International Symposium on Aeroelasticity and Structural Dynamics*, 553–564, 1985.
- K. Alexiou and J. R. Wright. Multi-point resonance test methods. *MOD contract 2607*, 1987.
- R. J. Allemang and L. D. Brown. A correlation coefficient for modal vector analysis. *Proc. of the 1st IMAC*, 110–116, Orlando, Florida, 1982.
- U. Amato and W. Hughes. Maximum entropy regularization of Fredholm integral equations of the first kind. *Inverse Problems*, 793–808, 1991.

- A. N. Andry and J. C. Chung. Eigenstructure assignment for linear systems. *IEEE Transactions on Aerospace and Electronic Systems*, **19**(5), 711–729, 1983.
- P. Avitabile and J. O’Callahan. Model correlation and orthogonality criteria. *Proc. of 6th IMAC*, 1039–1047, Kissimmee, Florida, 1988.
- M. Baruch and Y. Bar Itzhac. Optimisation weighted orthogonalisation of measured modes. *AIAA Journal*, **16**(4), 346–351, 1978.
- M. Baruch. Optimization procedure to correct stiffness and flexibility matrices using vibration test data. *AIAA Journal*, **16**(1), 1208–1210, 1978.
- M. Baruch. Optimal correction of mass and stiffness matrices using measured modes. *AIAA Journal*, **20**(11), 1623–1626, 1982.
- K. J. Bathe. *Finite Element Procedures in Engineering Analysis*. Prentice-Hall, Englewood Cliffs, New Jersey, 1982.
- Adi. Ben-Israel. *Generalize Inverses: Theory and Applications*. Thomas N.E. Greville, 1974.
- A. Berman and E. J. Nagy. Improvement of a large analytical model using test data. *AIAA Journal*, **21**(8), 1168–1173, 1983.
- A. Berman. Mass matrix correction using an incomplete set of measured modes. *AIAA Journal*, **17**(1), 1147–1148, 1979.
- R. E. D. Bishop and D. C. Johnson. *The Mechanics of Vibration*. Cambridge University Press, 1960.
- L. Boltzmann. *Vorlesungen Uber Gastheorie*. Johann Ambrosius Barth: Leipzig, 1910.
- H. Brakhage. On ill-posed problems and the method of conjugate gradients. *Inverse and Ill-Posed Problems*, 165–176, 1987.
- L. P. Bugeat and G. Lallement. Methods of matching calculated and identified eigen-solutions. *Storjnicky Casopis*, **32**(5), 162–167, 1976.

- B. Caesar. Update and identification dynamic mathematical models. *Proc. of the 4th IMAC*, 394–401, Los Angeles, California, 1986.
- B. Caesar. Updating system matrices using modal test data. *Proc. of the 5th IMAC*, 453–459, London, England, 1987.
- M. K. Chargin and H. Miura. An implementation of modal update based on Larsson's formulation. *Proc. of the 11th IMAC*, 379–389, Kissimmee, Florida, 1993.
- J. C. Chen and J. A. Garba. Analytical model improvement using modal test results. *AIAA Journal*, **18**(6), 684–690, 1980.
- S. Y. Chen and Y. G. Tsuei. A simple method for extraction of normal modes. *Vibration, Shock, Damage, and Identification of Mechanical System*, 1–8, 1993.
- D. F. Chu and J. M. DeBroy. Pitfalls of mass orthogonality check. *Proc. of the 7th IMAC*, 822–829, Las Vegas, Nevada, 1989.
- Y. Chu and C. S. Rudisill. Numerical methods for evaluating the derivatives of eigenvalues and eigenvectors. *AIAA Journal*, 834–837, 1975.
- J. D. Collins and J. Young. Methods and applications of system identification in shock and vibration. *Presented at Winter Annual Meeting of the ASME*, 1972.
- J. E. Cooper and J. R. Wright. Experimental evaluation of normal mode force appropriation methods using a rectangular plate. *Proc. of the 10th IMAC*, 1327–1333, San Diego, California, 1992.
- N. Cottin, M. Felgenhauer, and H. G. Natke. On the parameter identification of elastomechanical systems using input and output residual. *Ingenieur Archive*, **40**(2), 378–387, 1984.
- E. Dascotte and P. Vanhonacker. Development of an automatic model updating program. *Proc. of the 7th IMAC*, 596–602, Las Vegas, Nevada, 1989.
- E. Dascotte. Practical applications of finite element tuning using experimental modal data. *Proc. of the 8th IMAC*, 1032–1037, Kissimmee, Florida, 1990.

- E. Dascotte. Material identification of composite structure from combined use of finite element analysis and experimental modal analysis. *Proc. of the 10th IMAC*, 1274–1280, San Diego, California, 1992.
- J. P. Den Hartog. *Mechanical Vibration*. McGraw-Hill, New York, 1956.
- C. S. Desai and J. F. Abel. *Introduction to the Finite Element Method*. Van Nostrand Reinhold, New York, 1972.
- H. W. Engl and J. Gfrerer. A posteriori parameter choice for general regularisation methods for solving linear ill-posed problems. *Applied Numerical Mathematics*, **4**(2), 395–417, 1988.
- H. W. Engl and G. Landl. Convergence rates for maximum entropy regularization. *Report No. 445, Institute for Mathematics, University of Linz, Austria*, 1991.
- D. J. Ewins. *Modal Testing: Theory and Practice*. Research Studies Press, 1984.
- P. J. Eykhoff. *System Identification: Parameters and State Estimation*. John Wiley, 1980.
- E. Fissette and S. Ibrahim. Error location and updating of analytical dynamic models using a force balance method. *Proc of the 6th IMAC*, 1063–1070, Kissimmee, Florida, 1988.
- C. A. J. Fletcher. *Computational Galerkin Methods*. Springer-Verlag, New York, 1984.
- C. D. Foster and J. E. Mottershead. A method of improving finite element models by using experimental data: Application and implications for vibration monitoring. *International Journal of Mechanical Science*, **32**(3), 191–203, 1990.
- R. L. Fox and M. P. Kapoor. Rate of change of eigenvalues and eigenvectors. *AIAA Journal*, **12**(6), 2426–2429, 1968.
- A. Fregolent. Dynamic model updating using input residual. *To be Published*, 1996.

- M. I. Friswell and J. E. Mottershead. *Finite Element Model Updating in Structural Dynamics*. Kluwer Academic publishers, 1995.
- M. I. Friswell and J. E. T. Penny. Updating model parameters from frequency domain data via reduced order model. *Mechanical system and Signal Processing*, **4**(5), 377–391, 1990.
- M. I. Friswell. The adjustment of structural parameters using a minimum variance estimator. *Mechanical system and Signal Processing*, **3**(2), 143–155, 1989.
- C. P. Fritzen and Zhu. Updating of finite element models by means of measured information. *Computer and Structure*, **40**(2), 475–486, 1991.
- C. P. Fritzen. Identification of mass, damping and stiffness matrices of mechanical systems. *ASME, Journal of Vibration, Acoustics, Stress and Reliability in Design*, **108**(4), 9–16, 1986.
- G. E. Frolythe, M. A. Malcolm, and C. B. Moler. *Computer Methods For Mathematical Computations*. Prentice-Hall, 1977.
- J. S. Fuh and S. Y. Chen. System identification of analytical models of damped structures. *AIAA Journal*, **30**(2), 384–392, 1984.
- G.M.L Gladwell and H. Ahmadian. Generic element matrices for finite element model updating. *Journal of Sound and Vibration*, 601–614, 1995.
- G. H. Golub and C. F. Van Loan. *Matrix Computations*. North Oxford Academic, 1983.
- G. H. Golub and C. Vanloan. Total least squares in smoothing techniques for curve estimation. *Numerical Mathematics*, 69–76, 1979.
- G. H. Golub and C. Vanloan. An analysis of the total least squares problem. *SIAM Journal of Numerical Analysis*, 883–893, 1980.
- R. J. Guyan. Reduction of stiffness and mass matrices. *AIAA Journal*, 380, 1965.

- H. P. Gysin. Critical application of the error matrix method for localisation of finite element modelling inaccuracies. *Proc. of the 4th IMAC*, 1339–1351, Los Angeles, California, 1986.
- H. P. Gysin. Comparison of expansion method for FE modelling error localisation. *Proc. of the 8th IMAC*, 195–204, Kissimmee, Florida, 1990.
- P. C. Hansen. The truncated SVD as a method of regularization. *BIT* 72, 534–553, 1987.
- P. C. Hansen. The discrete Picard condition for discrete ill-posed problems. *BIT*, 30, 658–672, 1990.
- P. C. Hansen. Numerical tools for analysis and solution of Fredholm integral equation of the first kind. *Inverse Problems*, 849–872, 1992.
- G. C. Hart and J. P. Yao. System identification in structural dynamics. *American Society of Civil Engineers, Journal of engineering Mechanics Division*, 1089–1104, 1977.
- J. He and D. J. Ewins. Location of damping elements in a vibration structure. *Proc. of the 11th International Seminar on Modal Analysis*, Paper No. A2–4, Leuven, Belgium, 1986.
- J. He and M. Imregun. Different forms of orthogonality for MDOF systems. *Int. J. of Analytical and Experimental Modal Analysis*, 131–141, 1995.
- W. E. Heinz and A. Neubauer. Optimal parameter choice for ordinary and iterated Tikhonov regularization. *Inverse and Ill-posed Problems*, 97–125, 1987.
- W. Heylen and P. Sas. Review of model optimisation techniques. *Proc. of the 5th IMAC*, 1177–1182, London, England, 1987.
- P. S. Holmes and J. E. Cooper. Optimum exciter placement for normal mode force appropriation using an a priori model. *Proc. of the 14th IMAC*, 1–7, Dearborn, Michigan, 1996.

- C. Hsu and Y. G. Tsuei. Extraction of normal modes from experimental data. *Proc. of the 11th IMAC*, 1612–1617, Kissimmee, Florida, 1993.
- T. C. Huang. On precession and critical speeds of two-bearing machines with overhung weight. *Trans. ASME*, 713, 1967.
- P. Ibanez and K. D. Blakely. Automatic force appropriation - A review and suggested improvements. *Proc. of the 2nd IMAC*, 903–907, Orlando, Florida, 1984.
- S. R. Ibrahim and U. Fullekrug. Investigation into exact normalisation of incomplete complex modes by decomposition transformation. *Proc. of the 8th IMAC*, 205–212, Kissimmee, Florida, 1990.
- S.R. Ibrahim and A.A. Saafan. Correlation of analysis and test in modelling of structures assessment and review. *Proc. of the 5th IMAC*, 1651–1660, London, England, 1987.
- S. R. Ibrahim and A. Sestieri. Existence and normalisation of complex modes in post experimental use in modal analysis. *Proc. of the 13th IMAC*, 483–489, Nashville, Tennessee, 1995.
- S. R. Ibrahim. Computation of normal modes from identified complex modes. *AIAA Journal*, 446–451, 1983a.
- S. R. Ibrahim. Dynamic modelling of structures from measured complex modes. *AIAA Journal*, 898–901, 1983b.
- S. R. Ibrahim. Correlation and updating methods: Finite element dynamic model and vibration test data. *International Conference on Structural Dynamics Modelling, Test, Analysis and Correlation*, 323–347, 1993.
- M. Imregun and D. J. Ewins. Realisation of complex mode shapes. *Proc. of the 11th IMAC*, 1303–1309, Kissimmee, Florida, 1993.
- M. Imregun and D. J. Ewins. Complex modes - origins and limits. *Proc. of the 13th IMAC*, 496–506, Nashville, Tennessee, 1995.

- M. Imregun and D. J. Ewins. On the self-consistency of modal analysis results and measured FRFs data. *Proc. of the 14th IMAC*, 1593–1599, Dearborn, Michigan, 1996.
- M. Imregun and W. J. Visser. A technique to update finite element models using frequency response data. *Proc of the 9th IMAC*, 462–468, Florence, Italy, 1991.
- M. Imregun and W. J. Visser. A review of model updating techniques. *The Shock and Vibration Digest*, 9–20, 1991.
- M. Imregun, D. J. Ewins, I. Hagiwara, and T. Ichikawa. Updating of the finite element model of a box-like structure using the response function method. *Proc of the 11th IMAC*, 434–443, Kissimmee, Florida, 1993.
- M. Imregun, K. Y. salniturk, and D. J. Ewins. FE model updating using the response function method, part II: Case study on a medium size finite element model. *Journal of Mechanical System and Signal Processing*, 187–202, 1995a.
- M. Imregun, W. J. Visser, and D. J. Ewins. FE model updating using the response function method, part I: Theory and initial investigation. *Journal of Mechanical System and Signal Processing*, 203–214, 1995b.
- M. Imregun. Three case studies in finite element model updating. *Journal of Shock and Vibration*, 119–131, 1995.
- D. J. Inman and C. Minas. Matching finite element models to modal data. *Transactions of the ASME, Journal of Vibration and Acoustics*, 84–92, 1990.
- J. Juang and J. R. Wright. A multi-point force appropriation method based upon a singular value decomposition approach. *Proc. of the 9th IMAC*, 317–323, Florence, Italy, 1991.
- D. C. Kammer. Test-analysis-model development using an exact model reduction. *The International Journal of Analytical and Experimental Modal Analysis*, 174–179, 1987.

- D. C. Kammer. A hybrid approach to test analysis model development for large space structures. *Transaction of the American Society of Mechanical Engineers, Journal of Vibration and Acoustics*, **113**(3), 93–97, 1991.
- W. J. Kammerer and M. Z. Nashed. On the convergence of the conjugate gradient method for singular linear operator equations. *SIAM Journal of Numerical Analysis*, 165–181, 1972.
- R. L. Kidder. Reduction of structural frequency equations. *AIAA Journal*, 892, 1973.
- J. T. King. A minimal error conjugate gradient method for ill-posed problems. *Journal of Optimisation: Theory and Application*, 297–304, 1989.
- J. T. King. *Multilevel Iterative Method for Ill-Posed Problems*. VSP Scientific, 1992.
- M. Klaus and R. Smith. A Hilbert space approach to maximum entropy reconstruction. *Mathematical Methods in applied science*, 397–406, 1988.
- C. P. Kuo and B. K. Wada. Nonlinear sensitivity coefficient and correction in system identification. *American Institute of Aeronautics and Astronautics Journal*, 1463–1468, 1987.
- S. Lammens. Model updating using experimental frequency response functions: Case studies. *Proc. of the 11th IMAC*, 449–455, Kissimmee, Florida, 1993.
- L. Landweber. An iteration formula for fredholm integral equations of the first kind. *American Journal of Mathematics*, 615–624, 1951.
- P. O. Larsson and P. Sas. Model updating based on force vibrations. *Proc. of the 4th Conf. on Recent Advances in Structural Dynamics*, 95–108, 1991.
- P. O. Larsson and P. Sas. Modal updating based on force vibration testing using numerically stable formulations. *Proc. of the 10th IMAC*, 966–974, Sandiego, California, 1992b.
- C. Lawrence. Identification of difference between finite element analysis and experimental vibration data. *Proc. of the 5th IMAC*, 1681–1691, London, England, 1987.

- F. Lembregts and M. Brughmans. Estimation of real modes from FRFs via direct parameter identification. *Proc. of the 7th IMAC*, 631–636, Las Vegas, Nevada, 1989.
- F. Lembregts, J Leurdian, and H. V. Brussel. Frequency domain direct parameter identification for modal analysis: State space formulation. *Proc. of the 7th IMAC*, 1271–1277, Las Vegas, Nevada, 1989.
- M. Levine-West and A. Kissil. Evaluation of mode shape expansion techniques on the micro-precision interferometer truss. *Proc. of the 12th IMAC*, 212–218, Honolulu, Hawaii, 1994.
- N. A. J. Lieven and D. J. Ewins. Spatial correlation of mode shapes, the coordinate modal assurance criterion (COMAC). *Proc. of the 6th IMAC*, 690–695, Kissimmee, Florida, 1988.
- N. A. J. Lieven and D. J. Ewins. Error location and updating finite element models using singular value decomposition. *Proc. of the 8th IMAC*, 768–773, Kissimmee, Florida, 1990.
- N. A. J. Lieven and D. J. Ewins. Effect of incompleteness and noise on error matrix calculations. *Proc. of the 10th IMAC*, 1406–1413, San Diego, California, 1992.
- K. B. Lim. Re-examination of eigenvector derivatives. *AIAA Journal of Guidance, Control and Dynamics*, **10**(6), 581–587, 1987.
- R. M. Lin and D. J. Ewins. Modal updating using FRF data. *Proc. of the 15th International Seminar on Modal Analysis*, 141–162, Leuven, Belgium, 1990.
- M. Link. Identification and correction of errors in analytical model using test data - theoretical and practical bounds. *Proc. of the 8th IMAC*, 570–578, Kissimmee, Florida, 1990.
- M. Link, M. Weiland, and J. M. Bassagan. Direct physical matrix identification as compared to phase resonance testing: An assessment based on practical application. *Proc. of the 5th IMAC*, 804–811, London, England, 1987.

- M. Link. Theory of a method for identifying incomplete system matrices from vibration test. *Zeitschrift fur Flugwiss Weltraumforsch*, **10**(9), 76–82, 1985.
- L. Ljung. *System Identification-Theory for the User*. Englewood Cliffs, 1987.
- A. K. Louis. Convergence of the conjugate gradient method for compact operator. *Inverse and Ill-Posed Problems*, 177–183, 1987.
- Y. W. Luk. Identification of physical mass, stiffness and damping matrices. *Proc. of the 5th IMAC*, 679–685, London, England, 1987.
- A. Madansky. The fitting of straight lines when both variables are subject to error. *Journal of American Statistical Association*, 173–205, 1959.
- M. Maia. An introduction to the singular value decomposition technique. *Proc. of the 7th IMAC*, 335–339, Las Vegas, Nevada, 1989.
- E. H. Mansfield. *The Bending and Stretching of Plates*. Pergamon Press, 1964.
- C. Minas and D. J. Inman. Correcting finite element models with measured modal results using eigenstructure assignment methods. *Proc. of the 6th IMAC*, 583–587, Kissimmee, Florida, 1988.
- B. C. Moore. On the flexibility offered by state feedback in multivariable system beyond closed loop eigenvalue assignment. *IEEE Transactions on Automatic Control*, 689–692, 1976.
- J. E. Mottershead and C. D. Foster. On the treatment of ill-conditioning in spatial parameter estimation from measured vibration data. *Mechanical System and Signal Processing*, **5**(1), 139–154, 1991.
- J. E. Mottershead and M. I. Friswell. Model updating in structural dynamics: A survey. *Journal of Sound and Vibration*, **167**(2), 347–375, 1993.
- J. E. Mottershead and A. W. Lees. A linear frequency domain filter for parameter identification of vibrating structure. *Trans. ASME Journal of Journal of Vibration, Acoustics, Stress, and Reliability in Design*, **109**(4), 262–269, 1987.

- J. E. Mottershead and W. Shao. On the tuning of analytical models by using experimental vibration data. *Proc. 4th Int. Conf. on Recent Advances in Structural Dynamics, Southampton, England*, 432–443, 1991.
- J. E. Mottershead, M. I. Friswell, and G. H. T. NG. Experience in mechanical joint model updating. *Proc. of the 19th International Seminar on Modal Analysis, Katholieke Universiteit, Leuven, Belgium*, 1994.
- J. E. Mottershead. A unified theory of recursive, frequency domain filters with application to system identification in structural dynamics. *Trans. ASME Journal of Vibration, Acoustics, Stress, and Reliability in Design*, **110**(2), 360–365, 1988.
- J. E. Mottershead. Theory for the estimation of structural vibration parameters from incomplete data. *AIAA Journal*, **28**(2), 1326–1328, 1990.
- N. G. Nalitolela. A frequency domain technique for structural parameter updating. *Proc. of the 11th IMAC*, 676–682, Kissimmee, Florida, 1993.
- M. Nash. Use of principal force vectors with the multivariable mode indicator function. *Proc. of the 9th IMAC*, 688–693, Florence, Italy, 1991.
- B. Nath. *Fundamental of Finite Elements for Engineers*. Athlone Press, London, 1974.
- H. G. Natke. Updating computational models in the frequency domain based on measured data: A survey. *Probabilistic Engineering Mechanics*, 28–35, 1988.
- N. Niedbal. Analytical determination of real normal modes from measured complex responses. *25th Structures, Structural Dynamics and Material Conference*, 292–295, 1984.
- A. Nobari, M. Imregun, and S. Ziaei Rad. On the uniqueness of updated model. *Proc. of the 19th International Seminar on Modal Analysis*, 151–163, Leuven, Belgium, 1994.
- J. C. O’Callahan and P. Li. A non smoothing SEREP process for modal expansion. *Proc. of the 8th IMAC*, 232–238, Kissimmee, Florida, 1990.

- J. C. O'Callahan and P. Li. SEREP expansion. *Proc. of the 13th IMAC*, 1258–1264, Nashville, Tennessee, 1995.
- J. C. O'Callahan. A procedure for an improved reduced system (IRS). *Proc. of the 7th IMAC*, 17–21, Las Vegas, Nevada, 1989.
- J. C. O'Callahan. Development of a general pseudo orthogonality correlation procedure. *Proc. of the 13th IMAC*, 1013–1021, Nashville, Tennessee, 1995.
- J. C. O'Callahan, P. Avitabile, Madden, and Lieu. An efficient method of determining rotational degrees of freedom from analytical and experimental data. *Proc. of the 4th IMAC*, Los Angeles, California, 1986.
- I. U. Ojalvo and D. Pilon. A second order iteration procedure for correlation of analysis frequencies with test data. *Proc. of the 9th IMAC*, 499–502, Florence, Italy, 1991.
- I. U. Ojalvo, T. Ting, D. Pilon, and W. Twomey. Practical suggestions for modifying math models to correlate with actual modal test results. *Proc. of the 7th IMAC*, 347–354, Las Vegas, Nevada, 1989.
- I. U. Ojalvo. Efficient computation of mode shape derivatives for large dynamic systems. *AIAA Journal*, 1386–1390, 1987.
- D. Otte. Enhanced force vector appropriation methods for normal mode testing. *Proc. of the 11th IMAC*, 1310–1317, Kissimmee, Florida, 1993.
- H. N. Ozguven and M. Imregun. Complex modes arising from linear identification of nonlinear systems. *Proc. of the 9th IMAC*, 644–650, Florence, Italy, 1991.
- Y. S. Park and S. S. Lee. Weighted error matrix application to detect stiffness damage by dynamic characteristic measurement. *International Journal of Analytical and Experimental Modal Analysis*, **3**(3), 101–107, 1988.
- G. R. Parker and B. H. Ujihara. Calculating cross-orthogonality with expanded test data. *AIAA Journal*, **20**(3), 1310–1316, 1982.

- B. N. Parlett. *The Symmetric Eigenvalue Problem*. Prentice Hall, Englewood Cliffs, New Jersey, 1980.
- R. Pascual, J. C. Golinval, and M. Razeto. Testing of FRF based model updating methods using a general finite element program. *Proc. of the 21st International Seminar on Modal Analysis, 1933–1945*, Leuven, Belgium, 1996.
- M. Paz. Dynamic condensation. *AIAA Journal*, **22**(22), 724–727, 1984.
- N. Petersman. Calculation of eigenvalues using sub-structures and dynamic condensation. *Proc. Second Int. Conf. on Recent Advances in Structural Dynamics*, 211–219, 1984.
- B. Porter and R. Crossley. *Modal Control Theory and Applications*. London: Taylor and Francis, 1972.
- J. S. Przemieniecki. *Theory of Matrix Structural Analysis*. McGraw-Hill Book Company, 1968.
- R. J. Roark. *Formulas for Stress and Strain*. McGraw Hill, 1954.
- R.G. Ross. Synthesis of stiffness and mass matrices from experimental vibration modes. In *National Aeronautics and Space Engineering and Manufacturing Meeting*, 2627–2635, 1971. Society of Automotive Engineers.
- A. Sestieri and S. R. Ibrahim. Analysis of errors and approximations in the use of modal coordinates. *Proc. of the 11th IMAC*, 425–433, Kissimmee, Florida, 1993.
- M. J. Shulz and D. J. Inman. Model updating using constrained eigenstructure assignment. *Journal of Sound and Vibration*, **178**(1), 113–130, 1994.
- J. Sidhu and D. J. Ewins. Correlation of finite element and modal test studies of a practical structure. *Proc. of the 2nd IMAC*, 756–762, Orlando, Florida, 1984.
- R. C. Smith and W. T. Grandy. *Maximum-Entropy and Bayesian Methods in Inverse Problems*. Reidel, Boston, 1985.

- R. Snoeys, P. Sas, W. Heylen, and Van der Auweraer. Trends in experimental modal analysis. *Mechanical Systems and Signal Processing*, **1**(1), 5–27, 1987.
- S. Srinathkumar. Eigenvalue/eigenvector assignment using output feedback. *IEEE Transaction on Automatic Control*, 79–81, 1978.
- R. C. E. Tan and A. L. Andrew. Computing derivatives of eigenvalues and eigenvectors by simultaneous iteration. *Institute of Mathematics and its Application, Journal of Numerical Analysis*, **9**(1), 111–122, 1989.
- W. P. Targoff. Orthogonality check and correction of measured modes. *AIAA Journal*, **14**(2), 164–167, 1976.
- M. Thomas. Identification of system physical parameters from force appropriation technique. *Proc. of the 4th IMAC*, 1098–1103, Los Angeles, California, 1986.
- A. R. Thoren. Derivation of mass and stiffness matrices from dynamic test data. *AIAA Conference Paper*, **1**(72), 346, 1972.
- S. Timoshenko and D. H. Young. *Theory of Structures*. McGraw-Hill, New York, 1945.
- S. Timoshenko. *Elements of Strength of Materials*. Van Nostrand, New York, 1935.
- S. Van Huffel and J. Vandewalle. The use of total linear least squares techniques for identification and parameter estimation. *IFAC Identification and System Parameter*, 1167–1172, 1985.
- G. N. Vanderplaats. *Numerical Optimisation Techniques for Engineering Design with Applications*. McGraw Hill, 1984.
- J. W. Visser and M. Imregun. A technique to update finite element model using frequency response data. *Proc. of the 9th IMAC*, Florence, Italy, 1991.
- J. W. Visser. *Updating Structural Dynamics Models Using Frequency Response Data*. PhD thesis, Imperial College of Science, Technology and Medicine, London, UK, 1992.

- C. R. Vogel. Optimal choice of a truncation level for the truncated SVD solution of linear first kind integral equations when data are noisy. *SIAM Journal of Numerical Analysis*, **23**(1), 109–117, 1986.
- B. K. Wada. Correlation of modal and test analysis. *Technical Report Jet Propulsion Laboratory*, 1980.
- M. L. Wei and Q. Zhang. A time domain subspace iteration method for the normalization of measured complex modes. *Proc. of the 12th International Seminar on Modal Analysis*, Paper No. S2–3, Leuven, Belgium, 1987.
- J. C. Wei. Correction of finite element model via selected physical parameters. *Proc. of the 7th IMAC*, 1231–1238, Las Vegas, Nevada, 1989.
- M. L. Wei, R. J. Allemang, and D. L. Brown. Real-normalization of measured complex modes. *Proc. of the 5th IMAC*, 708–712, London, England, 1987.
- F. S. Wei. Structural dynamic model improvement using vibration test data. *AIAA Journal*, **28**(1), 1686–1688, 1990.
- R. Williams and J. Crowley. The multivariable mode indicator function in modal analysis. *Proc. of the 4th IMAC*, 66–70, Los Angeles, California, 1986.
- K. Zaveri. *Modal Analysis of Large Scale Structure - Multiple Exciter Systems*. Bruel and Kjaer Publications, 1984.
- Q. Zhang and G. Lallement. New method of determining the eigensolution of the associated conservative structure from the identified eigensolutions. *Proc. of the 3rd IMAC*, 322–328, Orlando, Florida, 1985.
- G. Zhang and G. Lallement. Dominant error localisation in a finite element model of a mechanical structure. *Mechanical System and Signal Processing*, **1**(2), 141–149, 1987.
- K. Zhou and C. K. Rushforth. Image restoration using multigrid methods. *Applied Optics*, **30**(3), 2906–2912, 1991.

-
- S. Ziaei Rad and M. Imregun. Use of generic elements for model updating. *Proc. of the 21st International Seminar on Modal Analysis*, 1895–1906, Leuven, Belgium, 1996.
- S. Ziaei Rad and M. Imregun. A modified eigenstructure assignment technique for finite element model updating. *Journal of Shock and Vibration*, **3**(4), 247–258, 1996a.
- S. Ziaei Rad and M. Imregun. On the accuracy required of experimental data for finite element model updating. *Journal of Sound and Vibration*, **196**(3), 323–336, 1996b.
- O. C. Zienkiewicz and R. L. Taylor. *The Finite Element Method*. McGraw Hill, 1989.
- O. C. Zienkiewicz. *The Finite Element Method in Engineering Science*. McGraw Hill, 1971.
- D. C. Zimmerman and M. Widengren. Correcting finite element models using a symmetric eigenstructure assignment technique. *AIAA Journal*, **28**(9), 1670–1676, 1990.